

THE BEHAVIOR AND STRUCTURE OF THE  
BAND 3 ANION TRANSPORT SITE:  
A  $^{35}\text{Cl}$  AND  $^{37}\text{Cl}$  NMR STUDY

Thesis by  
Joseph John Falke

In Partial Fulfillment of the Requirements  
for the Degree of  
Doctor of Philosophy

California Institute of Technology  
Pasadena, California

1985  
(Submitted September 28, 1984)

To the memory of a special grandfather,  
Joseph E. Greenwood, Sr.

## ACKNOWLEDGEMENTS

This thesis marks a noteworthy occasion in the career of Professor Sunney Chan: it is the fiftieth Ph.D. thesis produced by his students. I have known many of these students and their work: clearly, Sunney should feel great pride in bringing so much good science -- and so many good scientists -- into the world. Sunney is an excellent example of a true mentor: an advisor who places the interests of his students above his own. In particular, Sunney patiently encourages the intellectual development of his students so that by the time they leave, they are ready to be independent. Sunney also cares a great deal about his students as people; in short, I feel very fortunate to have had Sunney as an advisor.

Many people have contributed directly to the work in this thesis. Discussions with Sunney were always helpful due to his sound thinking and his firm grasp of the big picture; my collaboration with Ron Pace during the early phases of this project was educational and fruitful; Kathy Kanen learned quickly and contributed to the later phases of the project; Janos Lanyi taught me about halorhodopsin and about scientific writing; Howard Berg, Jean-Paul Revel and Pat Cowan provided microscopy facilities and training; Kevin Ott and Doug Meinhardt kept the JEOL FX-90Q in constant working order; Valerie Purvis artfully and quickly drew the illustrations; Sharon Vigario was always patient when typing for deadlines; and Debbie Chester skillfully typed much of this thesis at a furious pace. The experiments presented here would not have been possible without the L. A. Chapter of the American Red

Cross and: Dr. C. L. Spurling, Morris Rippey, Carol Bray and Fred Williams.

My family has indirectly but significantly contributed to this work. They have always accepted my interests and encouraged my pursuit of them. I would particularly like to thank Les for too many things to list, and I thank my whole family for being themselves: I am lucky to have them.

Finally, and very importantly, my friends made my stay here at Caltech a very special time and I will always warmly remember. Each of them knows how much I value their friendship: past, present and future. I wish them all the best.

Funding for this work was provided by a NSF predoctoral fellowship to JJF, and an NIH General Medical Sciences grant to SIC. I am grateful for this support, which in part made this thesis possible.

## ABSTRACT

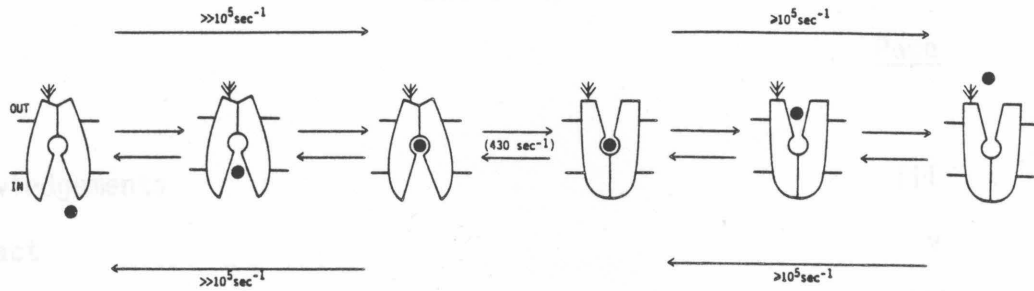
The transport of ions across cellular and organelar membranes is a widespread and fundamental process in biology. The goal of the present work is a molecular picture describing the ion translocation event in band 3, the most heavily used ion transport protein in typical vertebrate systems. The strategy employed involves  $^{35}\text{Cl}$  NMR, which is shown both theoretically and experimentally to be a sensitive probe of two microscopic events: 1) the migration of  $\text{Cl}^-$  from solution to the vicinity of a macromolecular binding site, and 2) the binding of  $\text{Cl}^-$  to the site. The technique reveals  $^{35}\text{Cl}^-$  linebroadening due to two classes of  $\text{Cl}^-$  binding sites on isolated, native red cell membranes. One class is composed solely of low affinity  $\text{Cl}^-$  binding sites of unknown function ( $K_D \gg 0.5 \text{ M}$ ), while the other class is composed solely of band 3 transport sites ( $K_D = 80 \pm 20 \text{ mM}$ ) which are identified by their affinity for substrate ( $\text{Cl}^-$ ), competing substrates ( $\text{HCO}_3^-$ ,  $\text{F}^-$ ,  $\text{Br}^-$ ,  $\text{I}^-$ ) and inhibitor (4,4'-dinitrostilbene-2,2'-disulfonate, or DNDS). A  $^{35}\text{Cl}$  NMR method is developed to ascertain the sidedness of  $\text{Cl}^-$  binding sites relative to a compartment barrier such as a membrane: this approach shows that the low-affinity and transport sites are each found on both surfaces of the membrane.

The sequence of events in the  $\text{Cl}^-$  transport cycle is investigated by monitoring the behavior of the transport sites when the concentration of DNDS, p-nitrobenzenesulfonate (pNBS),  $\text{Cl}^-$ ,  $\text{Br}^-$ , or  $\text{H}^+$  is varied. DNDS and pNBS, which are known to bind to outward-facing transport sites, each recruit all of the transport sites on both sides of the membrane to the inhibited outward-facing conformation, indicating that the inward- and outward-facing transport sites observed in the absence of inhibitor are merely different conformations of a single site. In addition, the transport sites on both sides of the membrane together behave like a homogeneous population of sites when  $[\text{Cl}^-]$ ,  $[\text{Br}^-]$ , or pH is varied. These results are quantitatively consistent with the ping-pong model for the transport cycle (Gunn and Frolich (1979) J. Gen. Physiol. 74, 351-374), in which a single transport site alternates between the inward- and outward-facing states and can only change states when occupied by bound anion. The rates of  $\text{Cl}^-$  binding and dissociation at both inward- and outward-facing transport sites are investigated

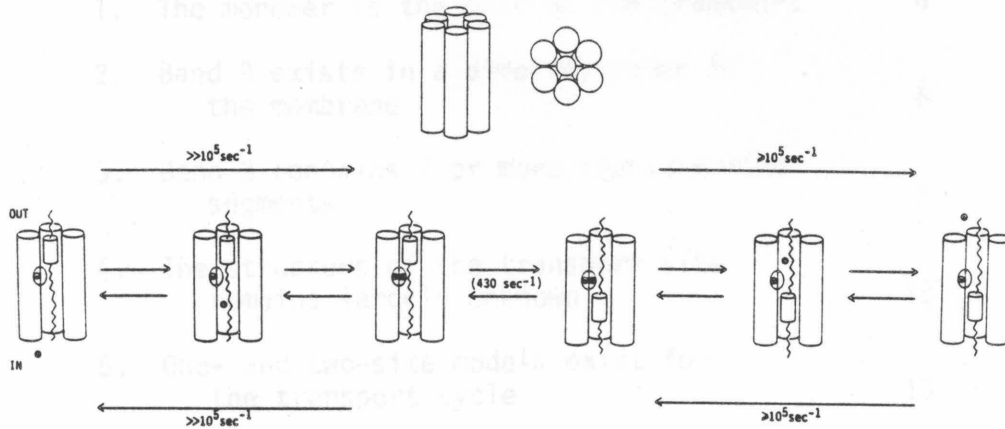
with  $^{35}\text{Cl}$  and  $^{37}\text{Cl}$  NMR, and it is shown that each of these rates exceeds  $10^5$  events  $\text{sec}^{-1}\text{site}^{-1}$  --much faster than the known turnover rate of the chloride transport cycle (430 events  $\text{sec}^{-1}\text{site}^{-1}$ ,  $0^\circ\text{C}$ ). Assuming that the rates of the influx and efflux half-turnovers of the transport cycle differ by  $10^2$  or less, it follows that the translocation of the chloride\*transport site complex is the rate-limiting step in both half-turnovers (see Figure).

The structure of the transport machinery is investigated using transport inhibitors and proteases. The reversible inhibitor niflumic acid (NIF) has no effect on the transport site linebroadening: this inhibitor slows the translocation of bound  $\text{Cl}^-$  in both the influx and efflux half-turnovers. The covalent, arginine-specific reagents phenylglyoxal (PG) and 1,2-cyclohexanedione (CHD) each eliminate the transport site linebroadening: PG modifies an essential residue in the transport site and CHD slows the migration of  $\text{Cl}^-$  between the site and solution. The observed PG-sensitivity and pH-dependence of the transport site linebroadening ( $\text{pK}_A = 11.1 \pm 0.1$ ,  $[\text{Cl}^-] = 250$  mM) indicate that an arginine residue provides the positive charge in at least one conformation of the transport site. A search is conducted for the minimal structure containing the intact transport site: this search begins with the removal of an inessential part of the transport domain, followed by monitoring of the transport site linebroadening for change. A variety of treatments leave some or all of the transport site linebroadening intact, including: 1) removal of the red cell membrane nonintegral proteins, 2) proteolytic removal of the soluble N-terminal domain of band 3, or 3) extensive proteolysis of band 3 by papain, which reduces band 3 to its transmembrane peptides (3-9 kDa). These results indicate that the essential arginine, as well as all other residues essential for  $\text{Cl}^-$  migration and binding to the transport site, are located on the papain-generated transmembrane peptides. The structural data presented here strongly support a picture in which the transport site, including the essential arginine, is buried in the membrane where it is resistant to proteolysis; and access of the buried site to solution  $\text{Cl}^-$  is provided by a channel that can be blocked by CHD. In summary, the minimal sequence of events in the  $\text{Cl}^-$  transport cycle can

be schematically illustrated by



A model is also presented that describes the molecular details of the ion translocation event: the translocation is proposed to begin when the transport site positive charge is neutralized by anion binding, so that a sliding hydrophobic barrier can move past the site and thereby expose the site to the opposite solution, as illustrated by



A sliding barrier model could explain the translocation event in many other membrane transport systems as well.

## TABLE OF CONTENTS

	<u>Page</u>
Acknowledgements	iii
Abstract	v
Table of Contents	viii
List of Tables and Figures	xvii
I. INTRODUCTION	1
A. THE FUNCTION OF BAND 3	2
B. THE STRUCTURE OF BAND 3	6
1. The monomer is the unit of ion transport	6
2. Band 3 exists in a dimer-tetramer in the membrane	6
3. Band 3 contains 7 or more transmembrane segments	9
4. The structure of the transport site remains largely unknown	12
5. One- and two-site models exist for the transport cycle	13
C. THE PRESENT STRATEGY	14
D. REFERENCES	15
II. $^{35}\text{Cl}$ AND $^{37}\text{Cl}$ NMR	17
A. ABSTRACT	18
B. INTRODUCTION	19
C. QUALITATIVE ASPECTS OF $^{35}\text{Cl}$ NMR IN THE ABSENCE OF CHEMICAL EXCHANGE	21
1. The oriented crystal case	21
2. The solution case	25
3. The membrane-bound case	26

	<u>Page</u>
D. $^{35}\text{Cl}$ NMR WITH CHEMICAL EXCHANGE BETWEEN A SITE AND SOLUTION	28
1. The effect of chemical exchange on the $^{35}\text{Cl}$ NMR spectrum	28
2. The transverse relaxation rate of chloride undergoing exchange	31
3. The slow exchange case	34
4. The rapid exchange case.	36
E. THE QUANTITATIVE RELATIONSHIP BETWEEN THE $^{35}\text{Cl}^-$ AND $^{37}\text{Cl}^-$ LINEBROADENING	42
1. Comparison of the $^{35}\text{Cl}^-$ and $^{37}\text{Cl}^-$ linebroadenings.	42
2. The slow exchange limit	43
3. The rapid exchange limit	45
F. APPLICATIONS OF $^{35}\text{Cl}$ AND $^{37}\text{Cl}$ NMR TO MACROMOLECULAR ANION BINDING SITES	49
G. REFERENCES	52
III. IDENTIFICATION OF THE BAND 3 TRANSPORT SITE	53
A. ABSTRACT	54
B. INTRODUCTION	55
C. MATERIALS AND METHODS	57
1. Reagents	57
2. Preparation of ghost membranes	57
3. NMR sample preparation	58
4. $^{35}\text{Cl}$ NMR spectroscopy	59
5. NMR sample analysis	60
6. Statistics	60

	<u>Page</u>
D. RESULTS	61
1. The $^{35}\text{Cl}^-$ NMR resonance	61
2. Identity of the chloride ions that give rise to the observed $^{35}\text{Cl}^-$ NMR resonance	61
3. Further analysis of the observed $^{35}\text{Cl}^-$ resonance	66
4. The information contained in the $^{35}\text{Cl}^-$ linebroadening	68
5. Experimental justification of the $^{35}\text{Cl}^-$ linebroadening assay for chloride binding sites	72
6. DNDS binds to band 3 transport sites and thereby inhibits the $^{35}\text{Cl}^-$ linebroadening	75
7. The DNDS-sensitive sites are high affinity chloride binding sites.	79
8. The high affinity sites are band 3 transport sites	82
E. DISCUSSION	85
F. REFERENCES	90
IV. THE SIDEDNESS AND RECRUITMENT OF THE BAND 3 TRANSPORT SITE	93
A. ABSTRACT	94
B. INTRODUCTION	96
C. MATERIALS AND METHODS	100
1. Materials	100
2. Preparation of leaky ghost membranes	100
3. Crushed ghost membranes	100
4. Sonicated ghost membranes	101

	<u>Page</u>
5. Sealed right-side-out vesicles	101
6. Intact red cells	102
7. Preparation of $^{35}\text{Cl}$ NMR samples	103
8. The $^{35}\text{Cl}^-$ linebroadening assay	105
9. Analysis of $^{35}\text{Cl}$ NMR samples	106
10. Enzyme assays	107
11. Leaky ghost hole size	108
12. Microscopy	108
13. Statistics	109
D. RESULTS	
1. Strategy of sidedness resolution	109
2. Rapid intercompartmental exchange	110
3. Slow intercompartmental exchange	111
4. Red cell membrane systems	111
5. Leaky ghost membranes	116
6. Sonicated ghost membranes	118
7. Intact red cells	118
8. Sealed right-side-out vesicles	122
9. Crushed ghost membranes	124
10. p-Nitrobenzenesulfonate inhibits the $^{35}\text{Cl}^-$ linebroadening due to band 3 transport sites on both sides of the membrane	127
E. DISCUSSION	128
F. REFERENCES	138

	<u>Page</u>
V. THE TRANSPORT SITE AND THE CHEMICAL EQUATION FOR TRANSPORT	142
A. ABSTRACT	143
B. INTRODUCTION	145
C. MATERIALS AND METHODS	147
D. THE $^{35}\text{Cl}$ NMR ASSAY	148
E. THE PING-PONG MODEL	151
F. INTRODUCTION	151
1. Definitions	151
2. Conditions	151
3. Fundamental characteristics of a ping-pong transporter	151
G. THE $^{35}\text{Cl}$ - LINEBROADENING DUE TO A PING-PONG TRANSPORTER: DEPENDENCE ON $[\text{Cl}^-]^{-1}$	152
1. Useful relationships and assumptions	153
2. The concentration of occupied transport sites	153
3. The transport site linebroadening	155
H. THE $^{35}\text{Cl}$ - LINEBROADENING DUE TO A PING-PONG TRANSPORTER: EFFECTS OF REVERSIBLE INHIBITORS	156
1. Useful relationships and assumptions	156
2. Dependence of the fractional inhibition on the inhibitor concentration	157
3. Competing substrates	159
4. Side-specific inhibitors	159

	<u>Page</u>
I. THE $^{35}\text{Cl}^-$ LINEBROADENING DUE TO A PING-PONG TRANSPORTER: EFFECTS OF pH	160
1. Useful relationships and assumptions	160
2. Dependence of the fractional inhibition on pH	162
J. RESULTS	
1. Leaky ghosts: linebroadening vs. $[\text{Cl}^-]^{-1}$	164
2. Leaky ghosts: linebroadening vs. $[\text{Br}^-]$	169
3. Leaky ghosts: linebroadening vs. pH	173
4. Crushed ghosts: dissociation of chloride from the outward-facing transport site	178
K. DISCUSSION	181
L. REFERENCES	188
VI. THE TRANSPORT SITE AND THE KINETIC EQUATION FOR TRANSPORT	190
A. ABSTRACT	191
B. INTRODUCTION	193
C. MATERIALS AND METHODS	194
1. Reagents	194
2. NMR samples containing red cell membranes	195
3. $^{35}\text{Cl}$ , $^{37}\text{Cl}$ NMR spectroscopy	195
4. NMR sample analysis	195
5. Calculation of the $^{35}\text{Cl}^-/^{37}\text{Cl}^-$ linebroadening ratio	195
6. Statistics	196

	<u>Page</u>
D. RESULTS	
1. The kinetic information contained in the $^{35}\text{Cl}^-$ or $^{37}\text{Cl}^-$ linebroadening	196
2. The kinetics of chloride binding and dissociation at the band 3 transport site as revealed by the $^{35}\text{Cl}^-$ linebroadening	199
3. The kinetics of chloride binding and dissociation at the band 3 transport site as revealed by the $^{35}\text{Cl}^-/^{37}\text{Cl}^-$ linebroadening ratio	201
4. The $^{35}\text{Cl}/^{37}\text{Cl}$ linebroadening ratio for the low-affinity chloride binding sites	208
5. Positive controls for the $^{35}\text{Cl}^-/^{37}\text{Cl}^-$ linebroadening ratio	209
E. DISCUSSION	209
F. REFERENCES	216
VII. INHIBITORS OF TRANSPORT A. TRANSPORT SITE INHIBITORS; B. CHANNEL BLOCKERS; C. TRANSLOCATION INHIBITORS	217
A. ABSTRACT	218
B. INTRODUCTION	220
C. MATERIALS AND METHODS	221
1. Reagents	221
2. Membrane preparation	221
3. NMR sample preparation	221
4. $^{35}\text{Cl}$ NMR spectroscopy	221

	<u>Page</u>
5. NMR sample analysis	221
6. Statistics	222
D. RESULTS	
1. The $^{35}\text{Cl}$ NMR technique	222
2. Linebroadening inhibitors: phenylglyoxal is a transport site inhibitor and 1,2-cyclohexanedione is a channel blocker	225
3. Niflumic acid leaves the linebroadening intact and is a translocation inhibitor	228
E. DISCUSSION	233
F. REFERENCES	240
VIII. PROTEOLYTIC DISSECTION OF THE TRANSPORT SITE	241
A. ABSTRACT	242
B. INTRODUCTION	244
C. MATERIALS AND METHODS	248
1. Reagents	248
2. $\text{H}_2\text{DIDS}$ labeling of red cells	249
3. Preparation of ghost membranes	249
4. Phenylglyoxal labeling of ghost membranes	249
5. Proteolysis of ghost membranes	250
6. High pH stripping of ghost membranes	250
7. High-salt washing of ghost membranes	250
8. NMR sample preparation	251
9. $^{35}\text{Cl}$ NMR spectroscopy	251
10. NMR sample analysis	251

	<u>Page</u>
11. Preparation of electrophoresis samples	252
12. Electrophoresis	253
D. RESULTS	
1. Observation of band 3 transport sites by $^{35}\text{Cl}$ NMR	254
2. The effect of nonintegral proteins on the transport site	255
3. The effect of the cytoskeletal domain on the transport site	261
4. The effect of proteolytic cleavage within the transport domain on the transport site	264
5. The peptides produced by extensive papain digestion of leaky ghosts	270
6. The effect of extensive papain digestion on the transport site	272
7. Verification of the identity of the transport site following extensive papain digestion	273
8. The effect of nonintegral protein removal and proteolysis on the low-affinity chloride binding sites	279
E. DISCUSSION	282
F. REFERENCES	287
IX. CONCLUSIONS, AND A MODEL FOR THE ION TRANSLOCATION EVENT	291
A. INTRODUCTION	292
B. CONCLUSIONS OF THE PRESENT WORK	292

	<u>Page</u>
C. COMPARISON OF MODELS FOR THE ION TRANSLOCATION EVENT	295
1. The choice of models to be discussed	295
2. Large scale conformational change	296
3. The anionic gate	296
4. The swinging arm model	301
5. The hydrophobic barrier model	305
6. Generalizable implications of the hydrophobic barrier model	318
7. Concluding remarks	319
D. REFERENCES	320

## LIST OF TABLES AND FIGURES

		<u>Page</u>
CHAPTER I		
Figure 1	The role of the red blood cell in CO <sub>2</sub> transport	3
Figure 2	The structure of DNDS	7
Figure 3	The transmembrane structure of the band 3 monomer	10
CHAPTER II		
Figure 1	The effect of the quadrupolar interaction on the nuclear energy levels of the <sup>35</sup> Cl or <sup>37</sup> Cl nucleus	22
Figure 2	The <sup>35</sup> Cl NMR spectrum in three different environments	29
CHAPTER III		
Figure 1	The effect of ghost membranes on the <sup>35</sup> Cl <sup>-</sup> NMR spectrum	62
Figure 2	The lineshape of the <sup>35</sup> Cl <sup>-</sup> NMR spectra	64
Figure 3	The relationship between the <sup>35</sup> Cl <sup>-</sup> linebroadening and the ghost membrane concentration	73
Figure 4	The effect of DNDS on the ghost membrane <sup>35</sup> Cl <sup>-</sup> broadening	76
TABLE 1	Apparent Dissociation Constants for Substrate and Inhibitor Binding to DNDS-Sensitive Sites on Ghost Membranes	78
Figure 5	The effect of chloride concentration on the ghost membrane <sup>35</sup> Cl <sup>-</sup> linebroadening	80
Figure 6	The effect of competing anions on the <sup>35</sup> Cl <sup>-</sup> NMR spectrum	83
TABLE 2	Apparent Dissociation Constants for Anion Binding to Band 3 Sites	86

## CHAPTER IV

Figure 1	Exchange of chloride between compartments	98
Figure 2	Sidedness of the red cell membrane $^{35}\text{Cl}^-$ linebroadening	114
TABLE 1	The escape of glyceraldehyde-3-phosphate dehydrogenase from holes in leaky ghost membranes prepared for $^{35}\text{Cl}^-$ NMR	117
Figure 3	Effect of intact red cells on the size of the $^{35}\text{Cl}$ NMR-invisible chloride population	120
TABLE 2	Sealing and sidedness in different red cell membrane systems	123
Figure 4	Morphology of leaky ghosts and crushed ghosts	125
TABLE 3	Comparison of the effects of DNDS and pNBS on leaky ghost membranes and crushed ghost membrane	129
Figure 5	Three general models for band 3-catalyzed anion exchange	132
Figure 6	Schematic alternating site model observed for band 3	135

## CHAPTER V

Figure 1	The $^{35}\text{Cl}^-$ linebroadening due to inward- and outward-facing band 3 transport sites	165
Figure 2	The effect of $\text{Br}^-$ on the $^{35}\text{Cl}^-$ linebroadening due to inward- and outward-facing band 3 transport sites	170
Figure 3	The effect of pH on the $^{35}\text{Cl}^-$ linebroadening due to inward- and outward-facing band 3 transport sites	174
TABLE I	Reversibility of the High pH Inhibition of Transport Site Linebroadening in the Sonicated Ghost System	176

	<u>Page</u>
Figure 4	182
Figure 5	186
CHAPTER VI	
TABLE I	200
Figure 1	203
Figure 2	206
Figure 3	210
Figure 4	213
CHAPTER VII	
Figure 1	226
Figure 2	229
Figure 3	231
Figure 4	234
TABLE I	236
Figure 5	238

		<u>Page</u>
CHAPTER VIII		
Figure 1	Summary of the stripping and proteolytic treatments employed	246
Figure 2	Removal of nonintegral red cell membrane proteins and removal of the band 3 cytoskeletal domain	257
Figure 3	The effect on band 3 transport sites of removal of nonintegral proteins	259
Figure 4	The effect on band 3 transport sites of removal of the cytoskeletal domain	262
Figure 5	Cleavage of the band 3 transport domain by chymotrypsin and papain	266
Figure 6	The effect on band 3 transport sites of chymotrypsin cleavage within the transport domain	268
Figure 7	The effect on band 3 transport sites of extensive papain cleavage of the transport domain	274
Figure 8	The effect of H <sub>2</sub> DIDS on the papain-modified band 3 transport site	277
Figure 9	The effect of phenylglyoxal on the papain-modified band 3 transport site	280
TABLE I	Effect of Nonintegral Protein Removal and Protease Treatment on Low-Affinity Chloride Binding Sites	283
CHAPTER IX		
Figure 1	A model for ion translocation involving a large scale conformational change	297
Figure 2	The anionic gate model	299
Figure 3	The swinging arm model	302
Figure 4	The hydrophobic barrier model	306
TABLE I	Transport Data for Different Anions	309
Figure 5	Transport site inhibitors and the hydrophobic barrier model	311

		<u>Page</u>
Figure 6	Channel blockers and the hydrophobic barrier model	314
Figure 7	Translocation inhibitors and the hydrophobic barrier model	316

CHAPTER I  
INTRODUCTION

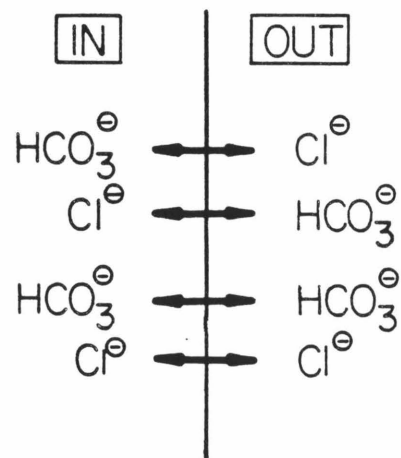
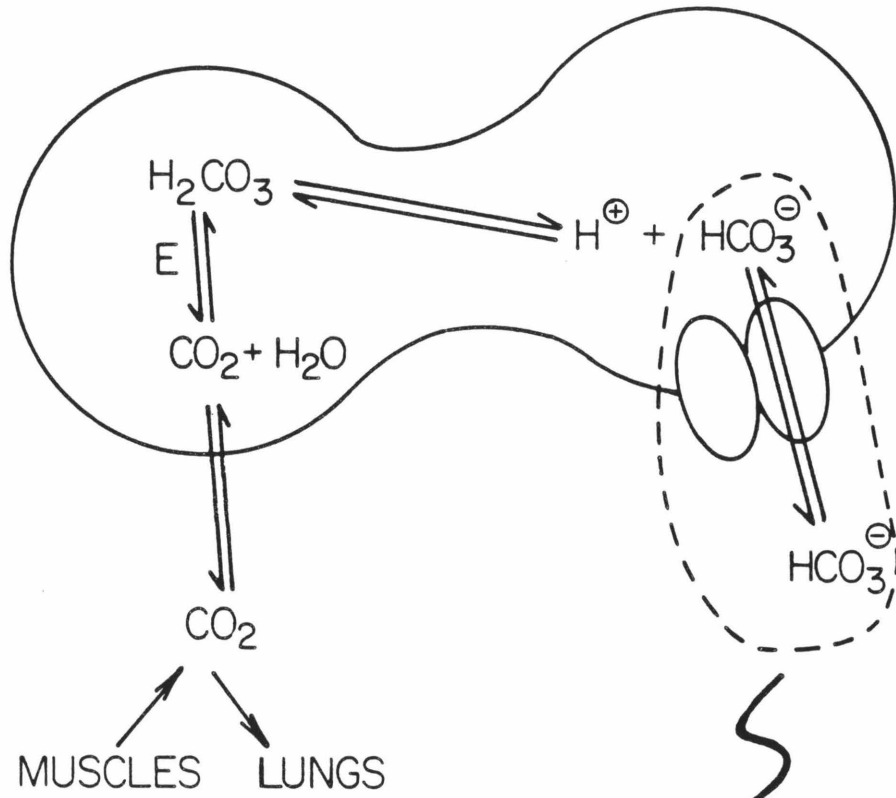
Ion transport across biological membranes is a fundamental molecular event in biological systems. Ion transport proteins are found in the plasma and organelle membranes of every type of cell, and these proteins are required for energy production, sensory transduction, neural transmission, muscle contraction, metabolite transport, and nearly all other biological processes. Yet at the present time there exists no molecular picture of the key event in ion transport: the translocation of a bound ion from one side of the membrane to the other. The object of the present thesis work has been to shed light on this translocation event by understanding the structure and mechanism of a particular ion transport protein -- band 3. More specifically, this work has utilized  $^{35}\text{Cl}$  and  $^{37}\text{Cl}$  NMR to monitor chloride binding to the anion transport site of band 3, in order to ascertain the behavior and structure of the site.

#### THE FUNCTION OF BAND 3

The band 3 protein of red blood cell membranes is the most heavily used ion transport protein in typical vertebrate animals: a simple calculation (1) shows that this protein transports one to two orders of magnitude more ions/(animal·unit time) than the  $\text{H}^+$ -ATPase, through which flows most of the chemical energy generated and used by biological systems. The reason for the surprisingly large capacity of the band 3 ion transport system is the role of this protein in the respiration of  $\text{CO}_2$  (Figure 1). In order to transport  $\text{CO}_2$  from its site of production to its site of expulsion,

Figure 1

The role of the red blood cell in CO<sub>2</sub> transport. Shown is the hydration of dissolved CO<sub>2</sub> as catalyzed by carbonic anhydrase (E), and the physiological anion exchange reactions catalyzed by band 3 (expanded view).



animals have evolved an efficient, reversible system in which  $\text{CO}_2$  gas is enzymatically hydrated inside the red cell; then the resulting bicarbonate ion is transported by band 3 to the extracellular solution which is thereby able to carry most of the dissolved  $\text{CO}_2$  in the form of bicarbonate (2). Large numbers of ions are transported by band 3 during this process, and if the band 3 transport cycle were to catalyze net ion transport a prohibitively large electrical gradient would quickly build up across the membrane. To avoid this buildup band 3 exchanges an anion in the opposite direction for every anion transported: thus the band 3 transport cycle results in the passive, electroneutral, one-for-one exchange of two monovalent anions across the red cell membrane. The two physiological anions for band 3 are bicarbonate and chloride, but the protein is also able to transport a variety of other monovalent anions in in vitro hetero- and self-exchange experiments (3). Band 3 is also an important example of a single protein possessing multiple functions: this protein serves as the attachment point on the membrane for the extensively studied red cell cytoskeleton (Figure 2, (4,5)), and recent studies indicate that 1) band 3 contains an aqueous pore distinct from its anion transport domain that may help the red cell adjust its volume while moving through small capillaries (6); 2) the carbohydrate moiety on the external surface of band 3 is altered as the red cell ages and may play a role in recognition of older cells (7) and 3) band 3 is phosphorylated,

methyated, and binds cytoplasmic proteins such as hemoglobin and glyceraldehyde-3-dehydrogenase (8), although the functions of these characteristics is not yet known. Due to its role in ion transport and other processes, band 3 is found in high concentration in the red cell membrane ( $10^6$  copies per cell). In fact band 3 is the most abundant protein in these membranes (9), and when the nonintegral proteins are stripped from the membranes, band 3 comprises 70% of the total membrane protein (8). Thus band 3 provides an important and practical system in which to study the molecular details of ion translocation across a biological membrane.

#### THE STRUCTURE OF BAND 3

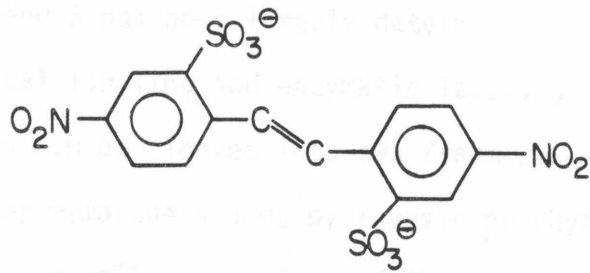
The monomer is the unit of ion transport. Band 3 is a single polypeptide chain of 90-100 kDa. The monomer independently catalyzes ion transport, since each monomer possesses one binding site for a variety of stilbene disulfonates (Figure 2), and these di-anions inhibit transport in a linear fashion such that 100% inhibition is reached when one molecule of inhibitor is bound per monomer (3).

Band 3 exists in a dimer-tetramer in the membrane.. Band 3 has long been known to exist as a stable, noncovalent dimer in the membrane and in non-ionic detergents (3). More recently, tetramers have also been observed in non-ionic detergents by electrophoretic and centrifugation techniques (8). In the membrane, quantitation of the number of intramembrane particles by freeze-fracture EM indicates that both dimers and tetramers are present (8). These

Figure 2

The structure of DNDS. Other stilbene disulfonates have the same core structure with the  $-\text{NO}_2$  functions replaced by other groups such as  $-\text{N}=\text{C}=\text{S}$  (DIDS).

TRANS-4,4'-DINITROSTILBENE-2,2'-DISULFONATE (DNDS)

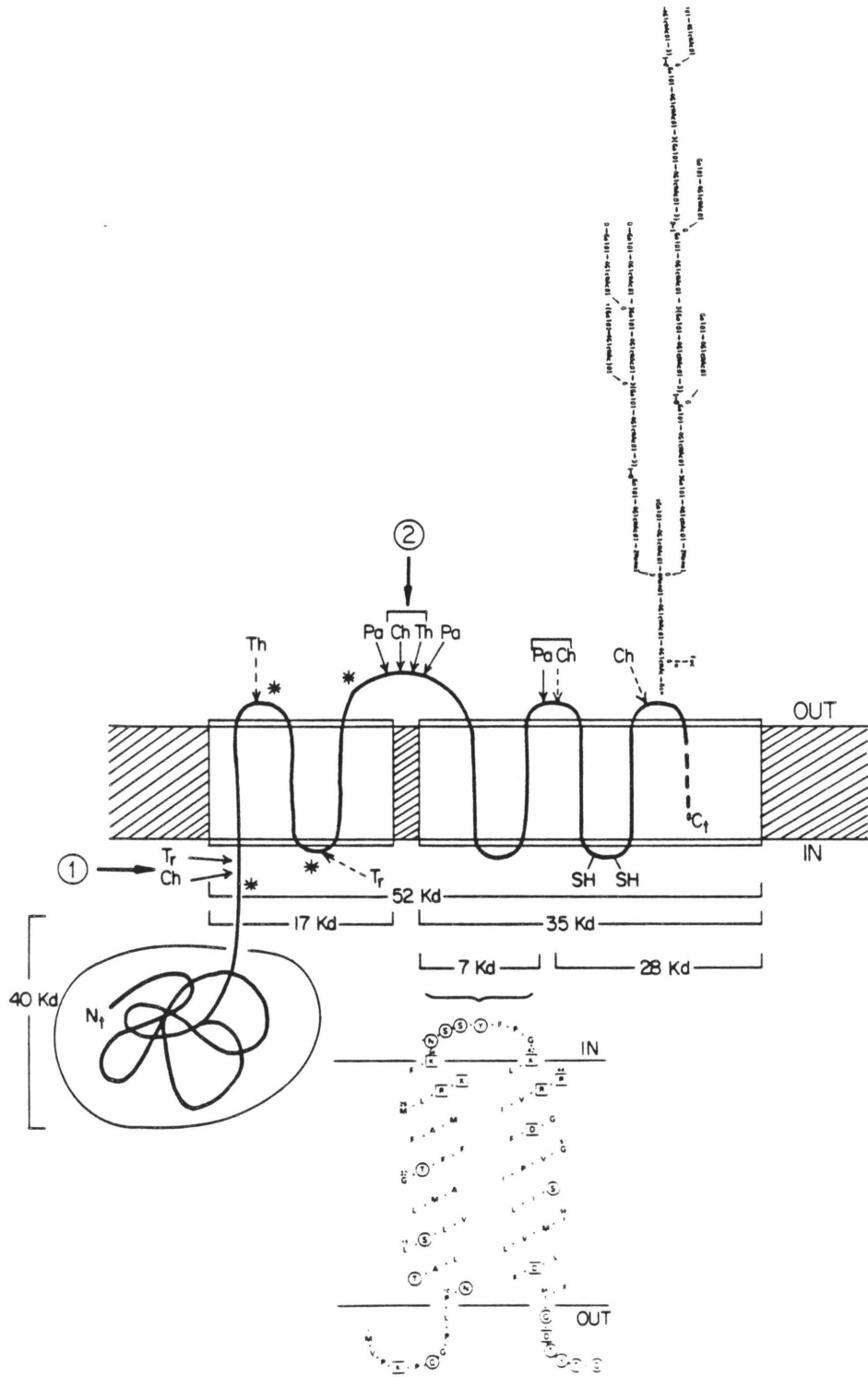


multimeric structures give rise to certain detectable interactions between monomers: the stilbene disulfonate binding sites on different monomers in the dimer are sufficiently close to interact, since larger stilbene disulfonates exhibit a higher affinity for the first monomer in the dimer than for the second monomer (8). In contrast, when only one of the monomers in the dimer is labeled with a large stilbene disulfonate, transport of sulfate by the other monomer proceeds normally. Similarly, no interactions between monomers have been detected for the binding of smaller stilbene disulfonates (8,1). Thus the transport sites on the different monomers in a multimer are close to each other but do not interact during the transport of substrate inorganic anions.

Band 3 contains 7 or more transmembrane segments. The transmembrane structure of band 3 has been largely determined by extensive proteolytic, chemical labeling and enzymatic labeling studies (Figure 3). The protein can be cleaved into two fragments, one cytoplasmic and the other membrane bound, by trypsin or chymotrypsin applied at the intracellular surface of the membrane. The isolated 40 kDa cytoplasmic fragment forms a one-to-one complex with ankyrin and thus contains the binding site for the red cell cytoskeleton (10): the sequence of the first 201 residues of this fragment have recently been determined (11). The 52 kDa membrane bound fragment retains anion transport activity, and a 7.5 kDa region of this fragment as well as several smaller regions have

Figure 3

The transmembrane structure of the band 3 monomer. Shown are the proteolytic cleavage sites and the chemical labeling sites that define the currently known transmembrane segments. Proteolytic cleavage at site 1 (heavy arrow) releases the cytoskeletal domain (circled) from the transport domain (boxed). Proteolytic cleavage at site 2 (heavy arrow) cuts the transport domain into two fragments. Within the transport domain, the major (solid arrow) and minor (broken arrow) proteolytic cleavage sites are indicated for chymotrypsin (Ch(20)), trypsin (Tr(18)), papain (Pa(13)), and thermolysin (Th(18)). Chemical labeling sites (\*(19)) are indicated for labeling with 1)  $^{125}\text{I}$  by peroxidase, 2)  $^{32}\text{P}_i$  by endogenous kinase, 3) p-nitrophenyl-N,N,N,-trimethyl[ $^{125}\text{I}$ ]iodotyrosinate, or 4) diazotized [ $^{35}\text{S}$ ]sulfanilate. The sidedness of all of these cleavage and labeling sites has been determined, as indicated. Also shown are two sulfhydryls that can be labeled only from the intracellular side of the membrane (20). Included are the sequence and proposed structure of a peptide fragment that contains the 7 kDa papain fragment (12,13). The carbohydrate shown is the core sequence of the carbohydrate moiety on mature red cells (7).



been sequenced (12,8). The membrane bound fragment also possesses the attachment site(s) for the heterogeneous carbohydrate moiety (13,7). Within the next 1-2 years more structural details of the membrane bound fragment will become available, since work is currently under way to clone and sequence the band 3 gene (8).

The structure of the transport site remains largely unknown.

The transport site must contain at least one positive charge which binds monovalent anions, but the essential residues in the transport site have not yet been identified in the primary structure. The essential positive charge in the outward-facing site is provided by arginine, since the titration with external base yields a  $pK_A = 12.1$  for inhibition of anion transport; thus the outward-facing site cannot contain an essential lysine residue (14). However, the transport site residues could be different in the inward- and outward-facing conformations of the site, and the existence of an essential lysine in the inward-facing site cannot be disproven. Both arginine-specific and lysine-specific reagents are known to inhibit transport (8), but it is not known whether these reagents act at the transport site or elsewhere in the transport unit. The characterization of transport site structure has been hampered by the lack of a direct assay for substrate binding to the site: the observation of transport inhibition is generally difficult to interpret because an inhibitor could act at one of several fundamental steps in the transport process, including substrate binding, translocation, and dissociation.

One- and two-site models exist for the transport cycle. The models that have been proposed for the electroneutral, one-for-one exchange of anions by band 3 fall into two classes: simultaneous transport and alternate transport models (3,16). In simultaneous transport models, the two anions to be exchanged each bind to different transport sites on opposite sides of the membrane; then they are simultaneously transported in opposite directions. In alternate transport models, a single transport pocket containing one or two transport sites is exposed first to one side of the membrane, then, following anion binding, to the other side. An important distinguishing feature of alternate transport is that the transport sites can all be recruited to the same side of the membrane because the transport cycle proceeds in two distinct half-turnovers. Such half-turnovers have been observed: when sealed membranes containing radioactive chloride are suspended in a chloride-free medium, the inward-facing transport sites bind and translocate an internal chloride ion to the extracellular space. Following release of the ion, the transport site halts in the outward-facing conformation due to lack of substrate, so that the release of radioactive chloride into the extracellular space stops (17). This result is highly suggestive; however, to verify the alternate transport model, and to ascertain whether one or two sites are involved in the transport cycle, it is necessary to directly monitor transport sites, including their distribution between the inward- and outward-facing conformations.

## THE PRESENT STRATEGY

The approach utilized here to study the molecular events underlying ion translocation has been to use  $^{35}\text{Cl}$  and  $^{37}\text{Cl}$  NMR to directly observed chloride binding to band 3 transport sites. The study begins with an examination of the mechanism of anion transport: the product of this initial study is a conceptual picture of the transport cycle. This conceptual picture is then used to help ascertain the structural elements central to the translocation event. The results presented here indicate that the transport unit contains a single transport site, which is alternately exposed to opposite sides of the membrane during the transport cycle; and the translocation of the chloride transport site complex across the membrane is the rate limiting step of the transport cycle. The transport site is buried within the membrane, and access to the buried site is provided by a channel leading from the site to solution. The site is composed of residues from one or more of the papain-generated transmembrane segments of band 3, and contains at least one essential arginine residue. Finally, a model is presented which summarizes a plausible molecular picture for ion translocation by band 3.

This thesis is essentially a collection of papers, many of which were written to stand alone. For the convenience of the reader, the abstract of each chapter has been rewritten to provide an overview which builds upon the preceding chapters and leads into the following chapters.

REFERENCES

1. Falke, J. J., Pace, R. J., and Chan, S. I. (1984) J. Biol. Chem. 259, 6472-6480.
2. Lowe, A. G. and Lambert, A. (1983) Biochem. Biophys. Acta 694, 353-374.
3. Knauf, P. A. (1979) Curr. Top. Memb. Transp. 12, 249-363.
4. Bennett, V. and Stenbuck, P. J. (1979) Nature 280, 486-473.
5. Hargraves, W. R., Gield, K. M., Verkly, A. and Branton, D. (1980) J. Biol. Chem. 255, 11965-11972.
6. Solomon, A. K., Clausen, B., Dix, J. A., Lukacovic, M. F., Toon, M. R. and Verkman, A. S. (1983) Ann. N. Y. Acad. Sci. 414, 97-125.
7. Fukuda, M., Dell, A., Oates, J. E. and Fukuda, M. N. (1984) J. Biol. Chem. 259, 8260-8273.
8. Macara, I. G. and Cantley, L. C. (1983) Cell Memb. 1, 41-87.
9. Haest, C. W. M. (1982) Biochem. Biophys. Acta 694, 331-352.
10. Bennett, V. and Stenbuch, P. J. (1980) J. Biol. Chem. 255, 6424-6432.
11. Kaul, R. J., Murthy, S. N. P., Reddy, A. G., Steck, T. L., and Kohler, H. (1983) J. Biol. Chem. 258, 7981-7990.
12. Brock, C. J., Tanner, M. J. A., and Kempf, C. (1983) Biochem. J. 213, 577-586.

13. Jennings, M. L., Adams-Lackey, M., and Denney, G. H. (1984) J. Biol. Chem. 259, 4652-4660.
14. Wieth, J. O. and Bjerrum, P. J. (1982) J. Gen. Physiol. 253-282.
15. Salhaney J. M. and Rauenbeuhler, P. B. (1983) J. Biol. Chem. 258, 245-249.
16. Falke, J. J., Pace, R. J., and Chan, S. I. (1984) J. Biol. Chem. 259, 6481-6491.
17. Jennings, M. L. (1982) J. Gen. Physiol. 79, 169-185.
18. Tanner, M. J. A., Williams, D. G., and Jenkins, R. E. (1980) Ann. N. Y. Acad. Sci. 341, 455-464.
19. Drickamer, K. (1980) Ann. N. Y. Acad. Sci. 341, 419-432.
20. Ramjeesingh, M., Gaarn, A., and Rothstein, A. (1983) Biochem. Biophys. Acta 729, 150-160.
- 21 Gunn, R. and Frolich, O. (1979) J. Gen Physiol. 74, 351-374.

CHAPTER II  
 $^{35}\text{C1}$  AND  $^{37}\text{C1}$  NMR

ABSTRACT

The  $^{35}\text{Cl}$  NMR technique provides a sensitive probe of two important microscopic events in macromolecular systems: 1) the migration of a chloride ion from solution to the vicinity of a macromolecular binding site, which may be buried within the macromolecule, and 2) the binding of the ion to the site. The physical basis of this technique is the large spectral width of chloride bound to a macromolecular site; the bound chloride spectral width is typically  $\geq 10^4$  times larger than the linewidth of chloride in solution (Figure 1, p. 22). As a result, when solution chloride samples a binding site sufficiently rapidly, the site can cause measurable broadening of the solution chloride linewidth (Figure 2, p. 29). As shown in the present chapter, this increase in linewidth, or linebroadening, contains information on 1) the concentration of chloride bound to the site, 2) the structure and motions of the site, and 3) the rate of chloride migration between the site and solution. In the work that follows, the  $^{35}\text{Cl}$  NMR technique is used to monitor chloride binding to band 3 anion transport sites. In addition,  $^{35}\text{Cl}$  and  $^{37}\text{Cl}$  NMR are used to assign lower limits to the rate of exchange of chloride between the site and solution. The results of this approach reveal many key elements of the mechanism and structure of the band 3 ion transport domain.

## INTRODUCTION

The first  $^{35}\text{Cl}$  NMR study of chloride binding to a biological macromolecule, hemoglobin, was conducted in 1966 by Stengle and Baldeschwieler (1). Since that time  $^{35}\text{Cl}$  and  $^{37}\text{Cl}$  NMR have been used to investigate chloride binding to a wide variety of soluble proteins containing anion binding sites in their active centers, such as metabolic enzymes that bind either phosphorylated intermediates or inorganic phosphorous (reviewed in (2)). The first membrane protein to be investigated using this approach was band 3, which was shown in 1977 to bind chloride in a study by Shami, Carver, Ship and Rothstein (3). Band 3 remains the membrane protein most extensively studied by  $^{35}\text{Cl}$  and  $^{37}\text{Cl}$  NMR: in the the present thesis this technique is used to characterize the anion transport sites of band 3, and to resolve transport sites on opposite sides of the membrane so that the distribution of sites between the two sides of the membrane can be monitored. The success of the technique in the band 3 system indicates that  $^{35}\text{Cl}$  and  $^{37}\text{Cl}$  NMR will become an important probe of structure and function for membrane-bound proteins possessing anion transport or binding sites. Recently I demonstrated the generality of this approach in a study of halorhodopsin, the light-driven chloride pump of the halobacterium membrane (4).

In order to successfully apply the  $^{35}\text{Cl}$  and  $^{37}\text{Cl}$  NMR technique to the study of chloride binding sites on membrane proteins or any other type of macromolecule, it is important to understand the limitations as well as the power of the technique. Thus in the

present chapter a theoretical treatment of the physical processes that underly the technique is described. As a qualitative introduction to the physical processes important in  $^{35}\text{Cl}$  and  $^{37}\text{Cl}$  NMR, the limiting cases of chloride in a crystal and chloride freely rotating in solution are first considered; then the experimentally important case of chloride exchange between a macromolecular binding site and solution is examined. In each of these cases the shape of the  $^{35}\text{Cl}$  NMR resonance as well as the important transverse relaxation processes are described. Finally, I also derive a quantitative relationship between the NMR relaxation processes of the  $^{35}\text{Cl}$  and the  $^{37}\text{Cl}$  nuclei in the presence of chloride exchange which can be used to study the rate of chloride exchange between a site and solution. The present theoretical treatment draws heavily on previous treatments of  $^{35}\text{Cl}$  and  $^{37}\text{Cl}$  NMR by Forsen and Lindmann (2,5), as well as on the NMR theories of chemical exchange derived by McConnell (6) and specialized for the relevant case by Swift and Connick (7). However, the present treatment includes previously unconsidered relaxation processes and is the most complete treatment heretofore described for the binding of chloride to a macromolecule.

QUALITATIVE ASPECTS OF  $^{35}\text{Cl}$  NMR IN THE ABSENCE OF CHEMICAL EXCHANGE

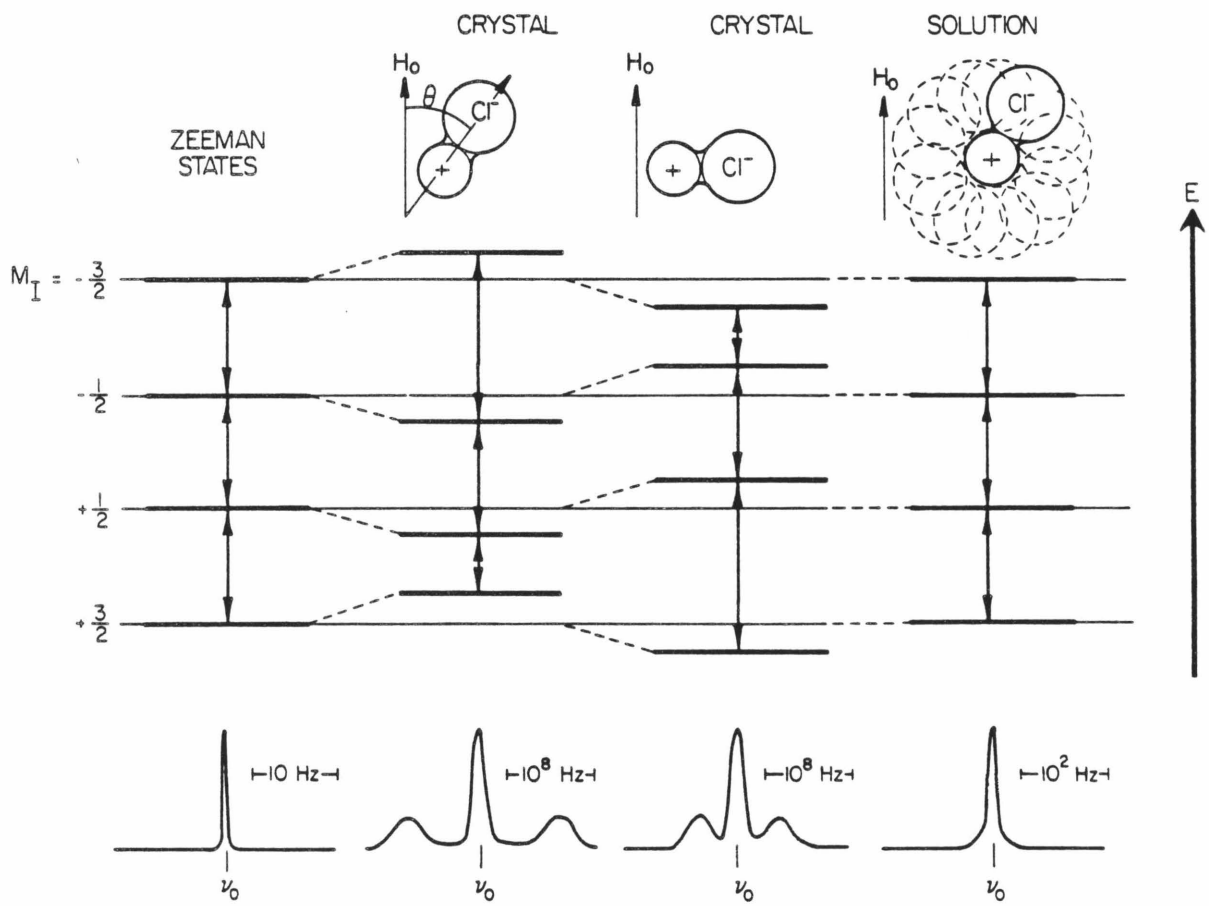
The oriented crystal case. Both  $^{35}\text{Cl}$  and  $^{37}\text{Cl}$  are  $S=3/2$  nuclei and have electric quadrupole moments; thus the following discussion of  $^{35}\text{Cl}$  NMR applies equally well to  $^{37}\text{Cl}$  NMR. The discussion begins with an examination of the oriented crystal case, which best illustrates the range of features that can be exhibited by a  $^{35}\text{Cl}$  NMR spectrum.

An  $S=3/2$  nucleus such as  $^{35}\text{Cl}$  possesses four nuclear energy levels which become nondegenerate in the presence of an applied magnetic field, giving rise to three allowed transitions (Figure 1). Here the middle transition ( $+1/2 \rightarrow -1/2$ ) will be termed the central transition, and the upper ( $-1/2 \rightarrow -3/2$ ) and lower ( $+1/2 \rightarrow +3/2$ ) transitions will be termed the flanking transitions. In the  $^{35}\text{Cl}$  NMR spectrum, the central transition gives rise to 40% of the total integrated intensity, while the flanking transitions each give rise to 30%.

The shape of the observed spectrum is largely determined by quadrupolar effects. When no electric field gradient exists at the nucleus, as in the case of chloride ion in a vacuum where the chloride electron cloud is spherically symmetric, the three transitions have the same resonance frequency and linewidth. As a result, a single Lorentzian line is observed in the  $^{35}\text{Cl}$  NMR spectrum for the overlapping three transitions. In contrast, the nuclear energy levels are perturbed when the electron cloud surrounding the nucleus has

Figure 1

The effect of the quadrupolar interaction on the nuclear energy levels of the  $^{35}\text{Cl}$  or  $^{37}\text{Cl}$  nucleus. In a vacuum, the chloride electron cloud is spherically symmetric so that no electric field gradient exists at the nucleus and the three resonances due to the  $^{35}\text{Cl}$  NMR transitions overlap to give a simple Lorentzian line. When the electron cloud is polarized, for instance by a positive charge, an electric field gradient is created at the nucleus. This field gradient interacts with the nuclear electric quadrupole so that the Zeeman energy levels are perturbed, where this perturbation is a function of the orientation of the electric field gradient relative to the applied magnetic field. In the case of an oriented crystal, the three allowed transitions lose their degeneracy and three distinct resonances are observed. In solution, the rapid tumbling of the electric field gradient averages the quadrupolar interaction to zero, so that the three transitions again exhibit the same resonance frequency.



a symmetry lower than cubic; in this a case a nonzero electric field gradient exists at the nucleus, and the nuclear electric quadrupole interacts with this field gradient. At high magnetic fields, the nucleus remains quantized along the magnetic field director and the quadrupolar interaction can be treated as a first order perturbation. This quadrupolar perturbation shifts the nuclear energy levels (Figure 1) such that the following expressions hold:

$$E(m_I, \theta) = -V_Z m_I + \frac{V_Q}{4} (m_I^2 - \frac{5}{4}) (3 \cos^2 \theta - 1) \quad (1)$$

$$\Delta = |V_Q (3 \cos^2 \theta - 1)| \quad (2)$$

$$V_Q = \frac{e^2 q Q}{h} \quad (3)$$

where  $E(m_I, \theta)$  is the energy level for the magnetic quantum number  $m_I$ ,  $V_Z$  is the original Zeeman splitting,  $\theta$  is the angle between the static magnetic field and the electric field gradient,  $\Delta$  is the observed quadrupolar splitted,  $V_Q$  is the maximum possible quadrupolar splitting ( $\theta=0$ ),  $eq$  is the electric field gradient which is assumed to have cylindrical symmetry, and  $eQ$  is the nuclear quadrupole moment. The different energy levels are perturbed by the same magnitude but not the same direction, so that for an arbitrary orientation of the crystal the three transitions no longer have identical resonance frequencies. The central transition retains the same frequency it possessed in the absence of the quadrupolar interaction, but the frequencies of the flanking transitions are symmetrically split in

frequency about the central transition. The resonances observed for the flanking transitions are the same width, but are broader than the central resonance for two reasons. First, static heterogeneity in the crystal causes spatial variation in  $\Theta$  so that different crystal regions exhibit different quadrupole splittings (Equation 2). Less importantly, lattice vibrations in the crystal alter both  $\Theta$  and the NMR frequencies of the flanking transitions (Equation 2), and the fluctuating NMR frequencies give rise to a transverse relaxation pathway that is unavailable to the central transition. In summary, then, for the oriented crystal case a central resonance (40% of the integrated intensity) and two broader flanking transitions (each 30% of the integrated intensity) are each observed in the  $^{35}\text{Cl}$  NMR spectrum (Figure 1).

The solution case. In solution the complexity of the oriented crystal spectrum is lost due to rapid tumbling of the electric field gradient relative to the static magnetic field. If this tumbling is sufficiently rapid, the quadrupolar perturbation averages to zero and the energy levels return to their unperturbed energies. Similarly, the resonance frequency and linewidths of the three transitions become identical, and the observed spectrum is a simple Lorentzian line (Figure 1). The condition for this rapid motion limit is  $\omega\tau_c \ll 1$  where  $\omega$  is the NMR frequency and  $\tau_c$  is the correlation time for isotropic reorientation of the field gradient. When this condition is satisfied, the time-averaged resonance frequencies are the same, and the longitudinal relaxa-

tion ( $1/T_1$ ) and the transverse relaxation ( $1/T_2$ ) rates are also the same for the central (c) and flanking (f) transitions (2);

$$\frac{1}{T_{1c}} = \frac{1}{T_{1f}} = \frac{1}{T_{2c}} = \frac{1}{T_{2f}} = \frac{2\pi^2 V_Q^2}{5} \tau_c \quad (4)$$

The observed relaxation rate is enhanced by the instantaneous fluctuation in the energy levels caused by the effect of tumbling on the quadrupolar interaction; thus the observed Lorentzian resonance is significantly broader than in the absence of the quadrupolar interaction.

The membrane bound case. The spectrum of chloride bound to membrane-associated protein binding sites combines elements of both the crystal and solution chloride cases. A membrane protein tumbles sufficiently slowly that a specific binding site orientation gives rise to a bound chloride spectrum similar to that of the oriented crystal case (Figure 1). However, motional averaging, restricted to certain directions, may also be present. Restricted but rapid local motions in chloride binding sites have been proposed to explain unexpectedly small quadrupolar effects in a variety of protein systems (2). When such motions are present, they reduce the quadrupolar splitting (Equation 2) observed for a particular average orientation of the binding site. Thus, the quadrupolar splitting becomes

$$\Delta = |V_Q(3 \cos^2\theta - 1)S| \quad (5)$$

where the order parameter  $S$  can have the values  $0 \leq |S| \leq 1$ . Equation 5 can be applied, for instance, to chloride binding to sites on ghost membranes. In this system the chloride binding sites are randomly oriented so that the spectrum of membrane-bound chloride is a superposition of spectra for all average orientations. The resulting spectrum is a powder pattern (Figure 2) where the splitting  $\Delta$  is given by:

$$\Delta = |V_Q S| \quad (6)$$

The maximum splitting is achieved only when the order parameter  $|S|$  attains its maximum value of unity. If the bound chloride experiences local motion, the order parameter becomes  $0 \leq S \leq 1$ . For local motion that is sufficiently isotropic, the longitudinal and transverse relaxation rates can be described by simple expressions (2):

$$\frac{1}{T_{1c}} = \frac{2\pi^2}{5} V_Q^2 (1-S)^2 \left( \frac{\tau_c}{1+4\omega^2 \tau_c^2} \right) \quad (7)$$

$$\frac{1}{T_{1f}} = \frac{2\pi^2}{5} V_Q^2 (1-S)^2 \left( \frac{\tau_c}{1+\omega^2 \tau_c^2} \right) \quad (8)$$

$$\frac{1}{T_{2c}} = \frac{\pi^2}{5} V_Q^2 (1-S)^2 \left( \frac{\tau_c}{1+4\omega^2 \tau_c^2} + \frac{\tau_c}{1+\omega^2 \tau_c^2} \right) \quad (9)$$

$$\frac{1}{T_{2f}} = \frac{\pi^2}{5} V_Q^2 (1-S)^2 \left( \tau_c + \frac{\tau_c}{1+\omega^2 \tau_c^2} \right) \quad (10)$$

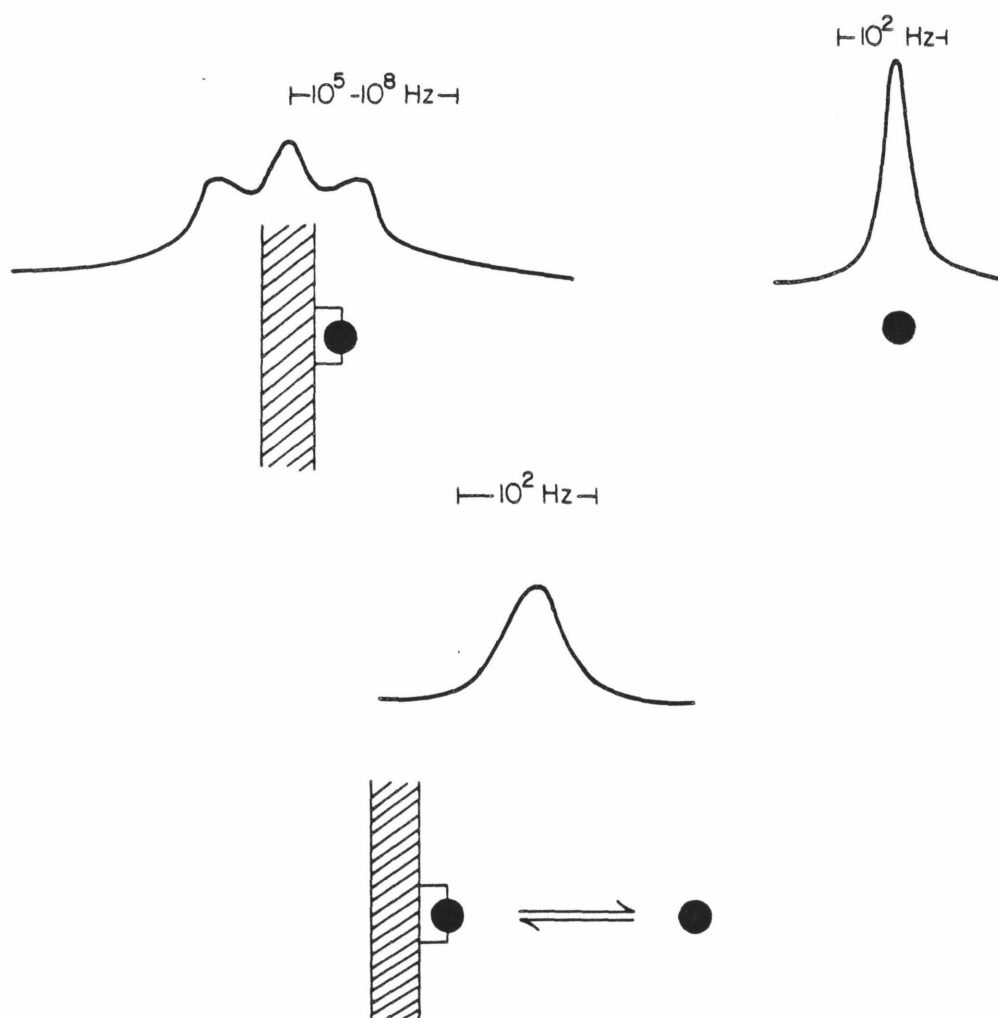
These expressions indicate that two processes contribute to the NMR relaxation. First, all of the relaxation rates contain contributions from spin lattice relaxation induced by instantaneous fluctuations in the energy levels as the electric field gradient tumbles (Equations 7-10). Second, the transverse relaxation of the flanking transitions contains a contribution from the modulation of the NMR frequency stemming from tumbling of the electric field gradient (Equation 10). In summary, chloride bound to a membrane-associated site generally exhibits a reduced quadrupolar splitting due to a powder pattern with local motion, and the flanking transitions are broader than the central transition.

### <sup>35</sup>Cl NMR WITH CHEMICAL EXCHANGE BETWEEN A SITE AND SOLUTION

The effect of chemical exchange on the <sup>35</sup>Cl NMR spectrum. In the applications of <sup>35</sup>Cl NMR presented in this thesis, the observed <sup>35</sup>Cl NMR spectra have simple Lorentzian shapes within experimental error (Chapter II). This simplicity, which at first glance is surprising due to the presence of membrane binding sites in the samples, can be easily explained. For all samples used here, the solution chloride concentration is  $\geq 10^3$  times larger than the concentration of bound chloride; thus the Lorentzian shape of the solution chloride resonance dominates the spectrum. In general, however, the binding sites can cause broadening of the observed spectrum (Figure 2). This linebroadening results from the large discrepancy between the spectral widths of solution and bound chloride: the linewidth of

Figure 2

The  $^{35}\text{Cl}$  NMR spectrum in three different environments. The spectral width ( $10^5$ - $10^8$  Hz) of chloride bound to a membrane protein is larger than the spectral width ( $10^4$ - $10^7$  Hz) of chloride bound to a soluble protein, since the membrane bound chloride a) tumbles more slowly and b) is in a hydrophobic environment that increases the covalency of the chloride-ligand bond. The bound chloride spectrum is a powder pattern, while the solution chloride spectrum is a Lorentzian line. When chloride exchanges between solution and a small number of binding sites, the solution chloride resonance is broadened but retains an essentially Lorentzian shape.



solution chloride is on the order of 10 Hz; while for chloride bound to a site on a soluble protein the spectral width is  $10^4$ - $10^6$  Hz (2); and for chloride bound to a membrane associated site the spectral width will be even larger since 1) the chloride electric field gradient exhibits slower, more restricted tumbling in a membrane-bound site; and/or 2) the chloride electron cloud is more polarized in the hydrophobic environment of a membrane-bound site. Thus even a small concentration of sites, particularly membrane-associated sites, can give rise to measurable linebroadening of the solution chloride resonance when chloride exchanges between the site and solution. The NMR relaxation processes that underly this linebroadening are examined in the following discussion of transverse relaxation rates.

The transverse relaxation rate of chloride undergoing exchange.

The transverse relaxation rate ( $1/T_2$ ) of an NMR transition is the rate at which its transverse (perpendicular to the static magnetic field) magnetization decays to the equilibrium value of zero. This relaxation process determines the linewidth of the transition and thus measurably affects the shape of the NMR spectrum. For the application at hand, the linebroadening of the observed  $^{35}\text{Cl}^-$  resonance is best understood in terms of the effect of binding sites on the transverse relaxation rates of the three distinct  $^{35}\text{Cl}^-$  NMR transitions.

The  $^{35}\text{Cl}^-$  NMR resonance is dominated by the contribution from solution chloride ions in all of the experiments conducted here.

Using McConnell's modified Bloch equations for chemical exchange (6), Swift and Connick have treated the exchange problem for the case in which the unbound species is in vast molar excess relative to the bound species (7). If the process of exchange between the bound and free states does not itself induce transitions between spin states, then the Swift and Connick results can be applied to the three  $^{35}\text{Cl}^-$  NMR transitions by treating each transition separately. Consider a set of heterogeneous binding sites. For the  $n$ 'th transition, the transverse relaxation rate observed for solution chloride ions in the presence of the binding sites is:

$$\frac{1}{T_{2n}} = \frac{1}{T_{2F}} + \sum_j R_{EXj} \quad (11)$$

where  $1/T_{2F}$  is the transverse relaxation rate of free chloride and  $R_{EX}$  is the contribution of the  $j$ 'th type of site to the excess relaxation rate. A central feature of this relationship is the additivity of the contributions from different types of sites, so that the contribution of each type of site is independent of all others. Hereafter for simplicity a single type of site will be considered, so that the sum over  $j$  is unnecessary:

$$\frac{1}{T_{2n}} = \frac{1}{T_{2F}} + R_{EX} \quad (12)$$

In this case, for a set of identical sites that have different

average orientations and therefore different average values of the angle  $\theta$ , the transverse relaxation rate is given by

$$\frac{1}{T_{2n}} = \frac{1}{T_{2F}} + \frac{1}{\tau_{FB}} \cdot \sum_{\theta} p_{\theta} \cdot \frac{\left(\frac{1}{T_{2Bn}} + \Delta\omega_{n,\theta}^2\right) + \frac{1}{T_{2Bn} \cdot \tau_{BF}}}{\left(\frac{1}{T_{2Bn}} + \Delta\omega_{n,\theta}^2\right) + \frac{2}{T_{2Bn} \cdot \tau_{BF}} + \frac{1}{\tau_{BF}^2}} \quad (13)$$

where  $1/T_{2B}$  is the transverse relaxation rate of bound chloride;  $\tau_{xy}$  is the lifetime of chloride in state x before returning to state y;  $p_{\theta}$  is the fraction of sites that have a particular value of  $\theta$ ; and  $\Delta\omega_{\theta}$ , which depends upon  $\theta$ , is the difference between the resonance frequencies of free and bound chloride. Equation 13 assumes that the only pathway available to the bound species is dissociation from the site and return to the solution. As shown in Chapter V, this assumption is reasonable in the band 3 system.

It is convenient to recast Equation 13 in terms of familiar rate constants and concentrations. First note that the characteristic time ( $\tau_{FB}$ ) spent by a chloride ion in solution before it binds, which can be expressed in terms of the on-rate for binding, can also be related to the off-rate via detailed balancing:

$$\frac{1}{\tau_{FB}} = \frac{\text{ON-RATE}}{[Cl]_F} = \frac{\text{OFF-RATE}}{[Cl]_B} = k_{\text{OFF}} \cdot \frac{[E \cdot Cl]}{[Cl]_F} = \frac{p_B}{\tau_{\text{OFF}}} \quad (14)$$

Here  $[Cl]_F$  is the free chloride concentration,  $[E \cdot Cl]$  is the bound chloride concentration, and  $k_{OFF}$  is the rate constant for dissociation. The quantity  $p_B = [ECl]/[Cl]_F$  is essentially the fraction of total chloride which is bound to the site, since it is assumed  $[Cl]_F \approx [Cl]_T$ , where  $[Cl]_T$  is the total stoichiometric chloride concentration. Similarly, the characteristic time ( $\tau_{BF}$ ) spent by a chloride ion in the binding site before it leaves can be expressed in terms of the off-rate:

$$\frac{1}{\tau_{BF}} = \frac{\text{OFF-RATE}}{[E \cdot Cl]} = k_{OFF} = \frac{1}{\tau_{OFF}} \quad (15)$$

Substitution of Equations 14 and 15 into 13 yields the desired expression:

$$\frac{1}{T_{2n}} = \frac{1}{T_{2F}} + \frac{p_B}{\tau_{OFF}} \sum_{\theta} p_{\theta} \frac{\left( \frac{1}{T_{2B_n}^2} + \Delta\omega_{n,\theta}^2 \right) + \frac{1}{T_{2B_n} \cdot \tau_{OFF}}}{\left( \frac{1}{T_{2B_n}^2} + \Delta\omega_{n,\theta}^2 \right) + \frac{2}{T_{2B_n} \cdot \tau_{OFF}} + \frac{1}{\tau_{OFF}^2}} \quad (16)$$

This expression defines the linewidth ( $=1/\pi T_{2n}$ ) of the n'th transition and is easily examined in the limits of slow and rapid exchange.

The slow exchange case. Here the bound and free chloride each give rise to separate spectra. In general, only the free chloride spectrum is observed due to the small concentration and large spectral width bound chloride, yet the binding sites can have an effect on the linewidth of the free chloride spectra. In order for the slow ex-

change limit to pertain, complete dephasing of the transverse magnetization must occur during a single visit by a chloride ion to a binding site. Moreover, this condition must be satisfied for all three transitions.

Complete dephasing of the transverse magnetization will occur upon binding if the intrinsic transverse relaxation time of the bound chloride ( $T_{2B_n}$ ) is small compared to the lifetime of the chloride ion in the site. When this condition holds so that terms containing  $1/\tau_{OFF}$  can be neglected in Equation 16, one obtains

$$\frac{1}{T_{2_n}} = \frac{1}{T_{2F}} + \frac{p_B}{\tau_{OFF}} = \frac{1}{T_{2F}} + R_{EX} \quad (17)$$

where  $R_{EX}$  is the additional or excess relaxation rate relative to that of free chloride. When  $T_{2B_n} \ll \tau_{OFF}$  so that Equation 17 holds for each transition, the binding equilibrium is in the slow exchange limit.

Since for the slow exchange complete dephasing occurs during a single visit to a binding site, the excess relaxation rate is simply a consequence of the on-reaction. Thus, it is not surprising that the excess relaxation rate from Equation 17 is the same as the on-rate for the binding of a chloride ion to a binding site ( $1/\tau_{FB} = p_B/\tau_{OFF}$ , Equation 14). Note that  $R_{EX}$  is the same for all three transitions so that in the slow exchange limit the transitions have the same linewidth ( $=1/(\pi T_{2_n})$ ). In order for the linewidth of the free chloride to be measurably increased, Equation 17

indicates that  $R_{EX}$  must be at least of the same magnitude as the relaxation rate of pure solution chloride ( $1/T_{2F}$ ). Since we have just shown  $R_{EX} = 1/\tau_{FB}$ , the required condition for measurable line-broadening can be restated: sufficient probability must exist that a free chloride ion in solution will visit a binding site before complete dephasing occurs in solution.

These results allow description of the form of the observed  $^{35}\text{Cl}^-$  NMR spectrum for the slow exchange case. As in the case of pure solution chloride the three transitions have identical linewidths. Moreover, since bound chloride does not contribute to the observed spectrum, there is no quadrupolar splitting nor any shift in the resonance frequency. Instead, the observed spectrum is a single Lorentzian line centered at the pure solution chloride resonance frequency. If the on-rate for binding is sufficiently large, then the observed linewidth will be larger than the pure solution chloride linewidth by the amount  $p_B/(\pi \cdot \tau_{OFF}) = k_{OFF} \cdot [E \cdot \text{Cl}^-] / ([\text{Cl}^-]_T \cdot \pi)$ .

The rapid exchange case. In the rapid exchange limit each chloride ion visits a large number of binding sites before complete dephasing of the transverse magnetization occurs. The binding sites that a chloride ion visits have different but random average orientations. Thus, one feature of the rapid exchange limit is that the quadrupolar splitting (Figure 2, Equation 5) is essentially averaged to zero, due to the rapid sampling of different binding site orientations that occurs upon successive visits to different sites (pseudo-tumbling).

The observed resonance frequency in the rapid exchange limit is typically similar to, but not identical to, the resonance frequency of solution chloride. If a chemical shift occurs upon binding, all three of the bound chloride resonances are shifted by the same amount and in the same direction. Due to the rapid exchange of chloride ion between the bound and free states, the ion experiences an average environment. As a result, each transition gives rise to a single exchange-averaged resonance rather than separate resonances for bound and free chloride. The three different transitions give rise to three different exchange-averaged resonances that have the same resonance frequency, since pseudo-tumbling averages the quadrupolar splitting to zero. However, the observed exchange-averaged resonance frequency is the weighted average of the central frequencies of the bound and solution chloride spectra. In particular, the difference between the central frequencies of the exchange-averaged and solution chloride spectra is given by

$$\Delta\sigma_{\text{OBS}} = p_{\text{B}} \cdot \Delta\sigma \quad (18)$$

where  $\Delta\sigma$  is the difference between the central frequencies of the bound and solution chloride spectra. Equation 18 assumes that the fraction of the total chloride which is bound at any moment satisfies  $p_{\text{B}} \ll 1$ . This condition is satisfied in the experiments presented here since  $p_{\text{B}} \lesssim 10^{-3}$ . The quantity  $\Delta\sigma$  is typically in the range 100-200 Hz (assuming a resonance frequency of 10 MHz and a chemical shift of 10-20 ppm, which has been observed for chloride

binding to micelles of alkylammonium ions (2)). For such a case, Equation 18 indicates that the central frequency of the exchange-averaged  $^{35}\text{Cl}^-$  NMR spectrum will be essentially the same as that of solution chloride.

The transverse relaxation rate for the rapid exchange case can be derived from Equation 16 using the condition  $1/\tau_{\text{OFF}}^2 \gg 1/T_{2\text{B}_n}^2, (\Delta\omega_{n,\theta})^2$ , which states that for each transition the off-rate of a bound chloride ion is much larger than both a) the bound chloride transverse relaxation rate, and b) the resonance frequency shift that occurs upon binding. In this limit, Equation 16 becomes

$$\frac{1}{T_{2n}} = \frac{1}{T_{2F}} + p_B \cdot \tau_{\text{OFF}} \cdot \overline{(\Delta\omega_{n,\theta})^2} + \frac{1}{T_{2\text{B}_n} \cdot \tau_{\text{OFF}}} = \frac{1}{T_{2F}} + R_{\text{EX}} \quad (19)$$

where the quantity  $\overline{(\Delta\omega_{n,\theta})^2}$  has been averaged over all  $\theta$  using the weighting function  $p_\theta$ . According to Equation 19, the excess relaxation rate can be dominated either by  $1/T_{2\text{B}_n}$  or  $\Delta\omega_{n,\theta}$ .

In the case  $1/T_{2\text{B}_n}^2 \gg \overline{(\Delta\omega_{n,\theta})^2}$  the excess relaxation rate becomes

$$R_{\text{EX}} = \frac{p_B}{T_{2\text{B}_n}} \quad (20)$$

where the intrinsic binding site transverse relaxation rate  $1/T_{2\text{B}_n}$  is dominant. Note that when this relationship holds, the transverse rate ( $=1/T_{2F} + p_B/T_{2\text{B}_n}$ ) is simply the weighted average of the intrinsic relaxation rates of free and bound chloride ( $p_F \cong 1$  due to the vast excess of free chloride). The value of  $1/T_{2\text{B}_n}$  is the same for

the flanking transitions but the central transition can have a  $1/T_{2B_n}$  that is smaller. This difference in  $1/T_{2B_n}$  between different transitions vanishes in the limit  $\omega_n \tau_c \ll 1$  (the extreme narrowing limit) where  $\omega_n$  is the resonance frequency of the n'th transition and  $\tau_c$  is the correlation time for isotropic tumbling.

In the case  $\overline{(\Delta\omega_{n,\theta})^2} \gg 1/(T_{2B_n} \cdot \tau_{OFF})$ , the excess relaxation rate becomes

$$R_{EX} = p_B \cdot \tau_{OFF} \cdot \overline{(\Delta\omega_{n,\theta})^2} \quad (21)$$

where the resonance frequency shift that occurs upon binding is dominant. For the flanking transitions,  $\Delta\omega_{f,\theta} = \Delta\sigma \pm \Delta_1$ , where  $\Delta\sigma$  is the resonance frequency shift that occurs upon binding, and  $\Delta_1$  is the quadrupolar splitting defined in Equation 9. The quantity of interest  $\overline{(\Delta\omega_{f,\theta})^2}$  can be calculated by averaging over a uniform distribution of  $\theta$  to yield

$$\overline{(\Delta\omega_{f,\theta})^2} = \Delta\sigma^2 + \frac{4}{5}(2\pi V_Q S)^2 \quad (22)$$

The central transition is unaffected by quadrupolar splitting so that  $\overline{(\Delta\omega_{c,\theta})^2} = \Delta\sigma^2$ . Thus, the quantity  $\overline{(\Delta\omega_{n,\theta})^2}$ , which is the same for the flanking transitions, is generally larger for the flanking transitions than for the central transition. However, when the order parameter  $S$  becomes zero, the three transitions have the same value of  $\overline{(\Delta\omega_{n,\theta})^2}$ .

It is interesting to note that the intrinsic binding site relaxation rate  $1/T_{2B_n}$  dominates the excess relaxation rate even when  $1/T_{2B_n}^2 = (\Delta\omega_{n,\theta})^2$  (Equation 20). The basis for this dominance becomes obvious when the decay of the transverse magnetization is described in terms of a one-dimensional random walk. The decay of the transverse magnetization is due to fluctuations that, to a first approximation, can be described as random walks in resonance frequency. The intrinsic transverse relaxation of bound chloride is caused by fluctuations in the length and orientation of chloride-ligand bonds. These fluctuations are fast; thus a large number of random walk steps occur during a single binding site visit. In contrast, in the random walk due to  $\Delta\omega_n$  each binding site visit is only a single step. Thus, relaxation due to  $\Delta\omega_n$  tends to occur more slowly than that due to the intrinsic  $1/T_{2B_n}$ .

A measurable increase in the solution chloride linewidth will occur only if the excess relaxation rate is at least the same order of magnitude as the transverse relaxation rate of pure solution chloride (Equation 19). When the inherent binding site transverse relaxation dominates (Equation 20), this condition becomes

$$\frac{1}{T_{2F}} \lesssim \frac{P_B}{T_{2B_n}} = \frac{\tau_{OFF}}{T_{2B_n}} \cdot \left( \frac{[E \cdot Cl] \cdot k_{OFF}}{[Cl]_F} \right) \quad (23)$$

When the frequency shift that occurs upon binding dominates (Equation 21), the condition becomes

$$\frac{1}{T_{2F}} \lesssim p_B \cdot \tau_{OFF} \cdot \overline{(\Delta\omega_{n,\theta})^2} = \tau_{OFF}^2 \cdot \overline{(\Delta\omega_{n,\theta})^2} \cdot \left( \frac{[E \cdot Cl]}{[Cl]_F} \cdot k_{OFF} \right) \quad (24)$$

Recall that in the rapid exchange limit the conditions  $\tau_{OFF}^2/T_{2B_i}^2$ ,  $\tau_{OFF}^2 \overline{(\Delta\omega_{n,\theta})^2} \ll 1$  both hold. Thus, measurable broadening is observed only when each chloride ion makes a large number of binding site visits on the timescale of  $T_{2F}$ . This is necessary because each binding site visit only slightly dephases the transverse magnetization of the spin.

In summary, the presence of binding sites can significantly alter the  $^{35}\text{Cl}$  NMR resonance of solution chloride when the exchange of chloride between binding sites and solution is in the rapid exchange limit. In this limit the three transitions have the same exchange-averaged resonance frequency which differs negligibly from the resonance frequency of solution chloride. However, the linewidths  $(\pi \cdot T_{2n})^{-1}$  of the three transitions can be significantly different; in particular, the linewidths of the flanking transitions can be larger than that of the central transition. As a result the exchange-averaged  $^{35}\text{Cl}^-$  NMR resonance is generally a superposition of two Lorentzians: the broader one stems from the flanking transitions and possesses 60% of the total integrated intensity, while the narrower one stems from the central transition and possesses 40% of the total integrated intensity. In the experiments presented here the difference in linewidth between the two Lorentzians is insignificant so that the observed resonance is well approximated

by a Lorentzian curve with a single linewidth. Then, from Equations 20 and 21 the linebroadening is:  $p_B \cdot (\pi \cdot T_{2B})^{-1}$  when the intrinsic binding site transverse relaxation dominates; or  $p_B \cdot \tau_{OFF} \cdot \Delta\omega^2 / \pi$  when the binding site frequency shift dominates.

#### THE QUANTITATIVE RELATIONSHIP BETWEEN THE $^{35}\text{Cl}^-$ AND $^{37}\text{Cl}^-$ LINE-BROADENING

Comparison of the  $^{35}\text{Cl}^-$  and  $^{37}\text{Cl}^-$  linebroadenings. The linebroadening is defined as the increase in the  $^{35}\text{Cl}^-$  or  $^{37}\text{Cl}^-$  NMR linewidth due to the presence of chloride binding sites. Such linebroadening is observed only when chloride exchanges sufficiently rapidly between the site and solution; as a result, both the  $^{35}\text{Cl}^-$  and  $^{37}\text{Cl}^-$  linebroadenings contain information on the rate of chloride exchange between the two environments.

Both  $^{35}\text{Cl}$  and  $^{37}\text{Cl}$  are spin 3/2 nuclei with essentially identical NMR properties so that the same NMR relaxation processes are important for both nuclei. However, the quadrupole moments of  $^{35}\text{Cl}$  and  $^{37}\text{Cl}$  are measurably different, and this difference can be exploited to ascertain whether the chloride exchange between the site and solution is slow or rapid on the NMR timescale. In particular, in the slow exchange limit the linebroadening is insensitive to the difference between the quadrupole moments, while in the rapid exchange limit the linebroadening is sensitive to this difference. As a result, the ratio of the  $^{35}\text{Cl}^-$  and  $^{37}\text{Cl}^-$  linebroadenings is unity for slowly exchanging sites but deviates from unity for

rapidly exchanging sites. In fact, the  $^{35}\text{Cl}^-/^{37}\text{Cl}^-$  linebroadening ratio can be used to characterize a site as slowly or rapidly exchanging site on the appropriate NMR timescale, and once the characterization has been made the maximum information on chloride exchange rates can be extracted from the linebroadening. For a slowly exchanging site, the linebroadening completely specifies the chloride binding and dissociation rate constants ( $k_{\text{ON}}$  and  $k_{\text{OFF}}$ ) and the chloride dissociation constant ( $K_{\text{D}} = k_{\text{OFF}}/k_{\text{ON}}$ ), while for a site in the rapid exchange limit lower limits can be placed on these rate constants.

The slow exchange limit. A simple derivation will show that a site in the slow exchange limit has a  $^{35}\text{Cl}^-/^{37}\text{Cl}^-$  linebroadening ratio of unity. This limit occurs when each of the three  $^{35}\text{Cl}^-$  or  $^{37}\text{Cl}^-$  NMR transitions fulfills the condition

$$\tau_{\text{OFF}} = 1/k_{\text{OFF}} \gg T_{2\text{B}_n} \quad (25)$$

where  $\tau_{\text{OFF}}$  is the length of time a chloride ion typically remains in the site, and  $T_{2\text{B}_n}$  is the intrinsic NMR relaxation time for the  $n^{\text{th}}$  transition when chloride is bound to the site. In this case, complete dephasing of the transverse magnetization occurs for a bound chloride ion before it can leave the site, and the  $^{35}\text{Cl}^-$  or  $^{37}\text{Cl}^-$  linebroadening ( $\delta = R_{\text{EX}}/\pi$ ) for each transition is given by Equation 17.

$$\delta = k_{\text{OFF}} p_{\text{B}}/\pi \quad (26)$$

where  $p_B$  is the fraction of total chloride in the sample that is bound to the site. The quantity  $p_B$  can be rewritten when the free chloride concentration ( $[Cl^-]_F$ ) is essentially equal to the total chloride concentration ( $[Cl^-]_T$ ):

$$p_B = \frac{[EC]}{[Cl^-]_T} = \left( [E]_T \frac{[Cl^-]_F}{[Cl^-]_F + K_D} \right) / [Cl^-]_T \cong \frac{[E]_T}{[Cl^-]_T + K_D} \quad (27)$$

where  $EC$  is bound chloride,  $[E]_T$  is the stoichiometric concentration of site  $E$ , and  $K_D$  is the dissociation constant for chloride at site  $E$ . Combining Equations 26 and 27 yields the desired result:

$$\delta = \frac{[E]_T}{\pi} \cdot \frac{k_{OFF}}{[Cl^-]_T + K_D} = \frac{[E]_T}{\pi} \cdot \frac{k_{OFF}}{[Cl^-]_T + (k_{OFF}/k_{ON})} \quad (28)$$

The quantities  $k_{ON}$  and  $k_{OFF}$  are essentially the same for  $^{35}Cl^-$  and  $^{37}Cl^-$  since ions of such relatively large mass exhibit a negligible kinetic isotope effect. Thus, for a given  $[E]_T$  and  $[Cl^-]_T$  the  $^{35}Cl^-/^{37}Cl^-$  linebroadening ratio is simply

$$^{35}\delta / ^{37}\delta = 1 \quad (29)$$

This value of unity is diagnostic for the slow exchange case.

Once a site has been shown by its  $^{35}Cl^-/^{37}Cl^-$  linebroadening ratio to be in the slow exchange limit, then (assuming that  $[E]_T$  is known) Equation 28 can be used to determine the values of  $k_{ON}$  and  $k_{OFF}$ . In particular, a plot of  $\delta$  vs.  $[Cl^-]_T$  will yield best-fit values of both  $k_{ON}$  and  $k_{OFF}$ . It is interesting to note that

when the site is far from saturation ( $[Cl^-]_T \ll K_D$ ), the linebroadening is controlled by the on-reaction (Equation 28):

$$\delta = [E]_T k_{ON} / \pi \quad (30)$$

In contrast, when the site approaches saturation ( $[Cl^-]_T \gg K_D$ ) the off-reaction dominates (Equation 28):

$$\delta = [E]_T k_{OFF} / (\pi [Cl^-]_T) \quad (31)$$

These simple limiting behaviors stem from the fact that in the slow exchange limit the linebroadening is equal to the rate that a chloride in solution becomes bound to the site. When the site is far from saturation, the on-reaction is rate-limiting and controls the binding rate, whereas, when the site is near saturation, the off-reaction is rate-limiting and controls the binding rate.

The rapid exchange limit. Here it will be shown that a site in the rapid exchange limit exhibits a  $^{35}Cl^- / ^{37}Cl^-$  linebroadening ratio of 1.6. This limit occurs when each of the  $^{35}Cl$  or  $^{37}Cl$  NMR transitions fulfills the condition

$$\tau_{OFF}^{-2} \gg T_{2B_n}^{-2}, \overline{(\Delta\omega_{\Theta,n}^2)} \quad (32)$$

where  $\Delta\omega_{\Theta,n}$  is the frequency shift for the  $n^{th}$  transition that occurs upon chloride binding, which depends upon the orientation ( $\Theta$ ) of the electric-field gradient at the nucleus relative to the direction of the magnetic field. In this limit a chloride ion can visit many sites before complete dephasing of the transverse

magnetization occurs, and the  $^{35}\text{Cl}^-$  or  $^{37}\text{Cl}^-$  linebroadening of the  $n^{\text{th}}$  transition is given by:

$$\delta = \frac{P_B}{\pi k_{\text{OFF}}} \left( \overline{(\Delta\omega_{\theta,n}^2)} + \frac{k_{\text{OFF}}}{T_{2B_n}} \right) \quad (33)$$

It is important to examine  $\overline{(\Delta\omega_{\theta,n}^2)}$ , which can be explicitly written

$$\overline{(\Delta\omega_{\theta,n}^2)} = \begin{cases} \overline{(\sigma^2)} & \text{for } +\frac{1}{2} \rightarrow -\frac{1}{2} \text{ transition} \\ \overline{(\sigma \pm 2\pi V_Q (3 \cos^2\theta - 1)S)^2} & \text{for } -\frac{1}{2} \rightarrow -\frac{3}{2} \text{ transition and} \\ & +\frac{3}{2} \rightarrow +\frac{1}{2} \text{ transition} \end{cases} \quad (34)$$

where  $\sigma$  is the frequency shift of the central transition that occurs upon binding,  $V_Q$  is the quadrupole coupling constant, and  $S$  is the order parameter associated with the motional averaging of the nuclear electric quadrupolar interaction experienced by the bound chloride during its lifetime at the site. The quantity  $\sigma$  complicates the analysis of the line-broadening ratio because the central frequency shift is independent of the quadrupole moment, while the quantities  $V_Q$  and  $T_{2B_n}$  are each dependent upon the quadrupole moment. Fortunately, in the experimental system employed here, the  $\sigma$  term contributes at most 0.5% of the observed linebroadening due to band 3 transport sites (Table 1) so that this term can be neglected and the linebroadening becomes

$$\delta = \begin{cases} \frac{P_B}{\pi T_{2B_n}} & \text{for } +\frac{1}{2} \rightarrow -\frac{1}{2} \text{ transition} \\ \frac{P_B}{\pi k_{OFF}} \left( \frac{(2\pi V_Q(3\cos^2\theta - 1)S)^2}{T_{2B_n}} + k_{OFF} \right) & \text{for } -\frac{1}{2} \rightarrow -\frac{3}{2} \text{ transition and} \\ & +\frac{3}{2} \rightarrow +\frac{1}{2} \text{ transition} \end{cases} \quad (35)$$

or, when the  $\theta$  term is averaged over a uniform distribution of  $\theta$

$$\delta = \begin{cases} \frac{P_B}{\pi T_{2B_n}} & \text{for } +\frac{1}{2} \rightarrow -\frac{1}{2} \text{ transition} \\ \frac{P_B}{\pi k_{OFF}} \left( \frac{4}{5}(2\pi V_Q S)^2 + \frac{k_{OFF}}{T_{2B_n}} \right) & \text{for } -\frac{1}{2} \rightarrow -\frac{3}{2} \text{ transition and} \\ & +\frac{3}{2} \rightarrow +\frac{1}{2} \text{ transition} \end{cases} \quad (36)$$

The quantities  $V_Q$  and  $T_{2B_n}$  each are related to the quadrupole moment (Q):

$$V_Q = C_1 Q \quad \text{and} \quad 1/T_{2B_n} = C_2 Q^2 \quad (39)$$

where  $C_1$  and  $C_2$  are constants that are the same for  $^{35}\text{Cl}$  and  $^{37}\text{Cl}$ , assuming that the dependence of  $T_{2B_n}$  on the NMR frequency is not important because the  $^{35}\text{Cl}$  and  $^{37}\text{Cl}$  NMR frequencies are quite similar

(8.8 MHz and 7.3 MHz, respectively, in the present study). Noting that the kinetic isotope effect is small so that the value of  $k_{\text{OFF}}$  and  $p_B$  are the same for  $^{35}\text{Cl}^-$  and  $^{37}\text{Cl}^-$ , the desired final result is obtained by combining Equations 35 and 36:

$$^{35}\delta/^{37}\delta = (^{35}\text{Q})^2/(^{37}\text{Q})^2 = 1.6 \quad (38)$$

This value is measurable larger than unity and thus may be used to distinguish the rapid exchange limit from the slow exchange limit.

In general,  $k_{\text{ON}}$  and  $k_{\text{OFF}}$  cannot be determined from the line-broadening in the rapid exchange limit unless the quantities  $p_B$ ,  $V_Q$ ,  $S$ , and  $T_{2B_n}$  are all known. Yet a lower limit still can be placed on  $k_{\text{ON}}$  and  $k_{\text{OFF}}$  because Equation 33 can be rewritten as

$$\delta = (k_{\text{OFF}} p_B/\pi) \left\{ (\overline{\Delta\omega_{n,\theta}^2}) \tau_{\text{OFF}}^2 + \tau_{\text{OFF}}/T_{2B_n} \right\} \quad (39)$$

and from Equation 32 the bracketed quantity is  $\ll 1$ . Thus, in rapid exchange limit

$$\delta \ll k_{\text{OFF}} p_B/\pi . \quad (40)$$

By analogy with Equations 30 and 31, Equation 39 can be rewritten for the case  $[\text{Cl}^-] \ll K_D$  where the site is far from saturation

$$\delta \ll [\text{E}]_T k_{\text{ON}}/\pi \quad (41)$$

or, for the case  $[\text{Cl}^-]_T \gg K_D$  where the site is near saturation

$$\delta \ll [E]_T k_{OFF} / ([Cl^-]_T \pi) \quad (42)$$

These equations provide lower limits on  $k_{OFF}$  and  $k_{ON}$  when  $[E]_T$  and  $[Cl^-]_T$  are known. Such lower limits can be quite useful for certain applications, as in the determination of the rate-limiting step in a reaction that involves chloride binding and/or dissociation.

#### APPLICATIONS OF $^{35}Cl$ AND $^{37}Cl$ NMR TO MACROMOLECULAR ANION BINDING SITES

A variety of information about an anion binding site can be obtained using the  $^{35}Cl$  and  $^{37}Cl$  NMR technique. In general there is not sufficient information to allow determination of the concentration of sites; however, the work presented in this thesis uses  $^{35}Cl$  and  $^{37}Cl$  NMR: 1) to determine the chloride dissociation constant of a chloride binding site; 2) to determine the affinities of anions other than chloride for the site by competing those anions with chloride for binding to the site; 3) to resolve sites on opposite sides of a membrane; 4) to place lower limits on the rate of exchange of chloride between a site and solution; 5) to investigate the identity of essential amino acids in the site by monitoring chloride binding as a function of varying pH, covalent modification of transport site residues, or proteolytic removal of peptides unnecessary for transport site structure; and 6) to study inhibitors that leave chloride binding to a site intact but hinder the migration of chloride between the site and solution. Thus the  $^{35}Cl$  and

$^{37}\text{Cl}$  NMR technique can be used to characterize many of the structural and functional aspects of a chloride transport or binding site.

There is one potential source of serious misinterpretation in  $^{35}\text{Cl}$  and  $^{37}\text{Cl}$  NMR studies. Many applications of the  $^{35}\text{Cl}$  and  $^{37}\text{Cl}$  NMR technique are based on the observation of linebroadening inhibition. Historically, when a linebroadening due to a chloride binding site is inhibited, it has virtually always been assumed that the site itself can no longer be occupied by chloride ( $p_B = 0$ , Equation 16). This is a dangerous assumption, since an equally plausible explanation<sup>1</sup> for linebroadening inhibition is that the exchange of chloride between the intact site and solution is hindered ( $\tau_{\text{OFF}} = \infty$ , Equation 16). Thus when linebroadening inhibition is observed, an attempt must be made to determine whether the locus of inhibition is the binding site itself, or the pathway that chloride transverses when migrating between the site and solution. In practice, these two possibilities are easily resolved; binding site inhibitors compete with chloride for binding to the site, such that the affinity of this inhibitor for the site depends on the chloride concentration (and vice-versa). In contrast, channel blockers occupy a substrate channel leading from the substrate site to the solution, and if the blocking site is sufficiently far from the substrate site, the affinity of the inhibitor will be independent of the chloride concentration. Alternatively, an inhibitor could lock bound chloride into the substrate site so that the exchange between the site and solution is slow;

in this case the affinity of the inhibitor will increase as the chloride concentration increases. The importance of this type of analysis is emphasized by the fact that at least two of these types of linebroadening inhibitors have now been observed (Chapter VII).

---

<sup>†</sup>Another explanation, which is much less plausible, is that the structure of the site is altered so that  $\alpha$  decreases while chloride binding and migration to the site are unaffected.

## REFERENCES

1. Stengle, T.R. and Baldeschwieler, J.D. (1966) Proc. Natl. Acad. Sci. USA. 55, 1020-1026.
2. Forsen, S. and Lindman, P. (1981) Meth. Bioch. Anal. 27, 209-486.
3. Shami, Y., Carver, J., Ship, S. and Rothstein, A. (1977) Biochem. Biophys. Res. Comm. 76, 429-436.
4. Falke, J. J., Chan, S.I., Steiner, M., Oesterhelt, P., Townes, P., and Lanyi, J.K. (1984) J. Biol. Chem. 259, 2185-2189.
5. Lindman, B. and Forsen, S. (1976) in NMR: Basic Principles and Progress (Diehl, P., Fluch, E., Kosfeld, R., eds.) 12. pp. 1-368, Springer-Verlag, NY.
6. McConnell, H.M. (1958) J. Chem. Phys. 28, 430-431.
7. Swift, T.J. and Connick, R.E. (1962) J. Chem. Phys. 37, 307-320.

CHAPTER III  
IDENTIFICATION OF THE BAND 3  
TRANSPORT SITE

ABSTRACT

The first step in the use of  $^{35}\text{Cl}$  NMR to study a  $\text{Cl}^-$  binding site is the identification of the  $^{35}\text{Cl}^-$  linebroadening due to that site. The membrane systems used throughout the present thesis are isolated red cell membranes that retain all of their native membrane lipids and proteins. These membranes rigorously maintain band 3 in its functional state, but they possess an unknown number of irrelevant  $\text{Cl}^-$  binding sites in addition to band 3 transport sites; thus, the transport sites must be resolved from a background of other sites. Here it is shown that  $^{35}\text{Cl}$  NMR enables direct and specific observation of substrate  $\text{Cl}^-$  binding to band 3 transport sites, which are identified by a variety of criteria: 1) the sites are inhibited by 4,4'-dinitrostilbene-2-2'-disulfonate or DNDS, which is known to inhibit competitively  $\text{Cl}^-$  binding to band 3 transport sites; 2) the sites have affinities for DNDS and  $\text{Cl}^-$  that are quantitatively similar to the known affinities of band 3 transport sites for these anions; and 3) the sites have relative affinities for  $\text{Cl}^-$ ,  $\text{HCO}_3^-$ ,  $\text{F}^-$  and  $\text{I}^-$  that are quantitatively similar to the known relative affinities of band 3 transport sites for these anions. The  $^{35}\text{Cl}$  NMR assay also reveals a class of low-affinity  $\text{Cl}^-$  binding sites ( $K_D \gg 0.5 \text{ M}$ ) that are not affected by DNDS. The function of these background low-affinity sites is unknown, but they may be responsible for the inhibition of band 3 catalyzed anion transport that has been previously observed at high anion concentrations. In the following chapter, the distribution of transport sites between the inward- and outward-facing conformations is investigated, thereby enabling tests of the mechanism of anion transport.

## INTRODUCTION

Band 3 is an integral membrane protein in human erythrocyte membranes. The protein consists of a single polypeptide chain (MW = 95,000) and although the catalytic unit is thought to be the monomer (1), the protein exists in the membrane as a dimer (2). Band 3 has at least two functions, one structural and the other physiological. The cytoplasmic portion of this protein contains the site to which the red cell cytoskeleton binds and thereby is anchored to the membrane (3,4). Completely unrelated to this structural function is the role of band 3 in the respiratory system, where it facilitates the transport of  $\text{CO}_2$  by the bloodstream. As the central component of the Hamburger (or chloride) shift, band 3 exchanges  $\text{HCO}_3^-$ , which is produced from  $\text{CO}_2$  and  $\text{H}_2\text{O}$  by carbonic anhydrase inside the cell, for  $\text{Cl}^-$  on the other side of the membrane (5-7). This exchange process allows the serum to carry the bulk of the dissolved  $\text{CO}_2$  in the form of  $\text{HCO}_3^-$ . The physiological importance of this exchange process is illustrated by the fact that the band 3 system is the most heavily used ion transport system in a typical vertebrate animal such as man. I believe that an important current goal of membrane biochemistry should be to understand, in molecular terms, the anion transport event which occurs within this relatively simple and easily obtainable band 3 protein.

The mechanism of band 3-catalyzed anion exchange has been extensively studied in kinetic experiments; for a review, see (1). These kinetic studies have stimulated the development of a variety of models (1,8-15) for the exchange process, all of which postulate the existence of one or more transport sites that bind substrate anion during the transport event.

The existence of transport sites is suggested by the saturation kinetics that are observed at high concentrations of substratum anion (1); however, saturation kinetics are also exhibited by ion channels that require single-file passage of ions (16). Thus, I have attempted to observe directly transport sites using an assay for substrate (chloride) binding to band 3.

Chloride binding to protein binding sites has been studied in a large number of water-soluble protein systems using  $^{35}\text{Cl}$  NMR, and the theory and practice of this approach have been the subject of extensive reviews by Forsen and Lindman (17,18). Rothstein and his co-workers (19) first showed that  $^{35}\text{Cl}$  NMR can be used to study the binding of chloride to band 3; the work presented here and in the following chapters improves upon this technique and extends its application. In the chapter at hand  $^{35}\text{Cl}$  NMR is used to observe two classes of chloride binding sites on leaky red cell membranes. One class is composed of low-affinity sites that may include nonspecific chloride binding sites, while the other class is composed of high-affinity chloride binding sites. The high affinity sites can be identified as band 3 transport sites by studying their affinity for a variety of anions: chloride, fluoride, iodide and bicarbonate, as well as the inhibitor of anion exchange 4,4'-dinitrostilbene-2,2'-disulfonate (or DNDS). Surprisingly, no evidence is seen of an inhibitory chloride binding site termed the modifier site (20) which has been thought to be present on band 3.

## MATERIALS AND METHODS

Reagents. 4,4'-dinitrostilbene-2,2'-disulfonic acid, disodium salt (DNDS, Pfaltz and Bauer) was recrystallized one time as follows: 10 g DNDS was dissolved in 200 ml boiling H<sub>2</sub>O; 100 ml saturated NaCl in H<sub>2</sub>O (24° C) was added; the suspension was cooled (4° C) overnight; and the crystals were isolated and washed with 60% saturated NaCl in H<sub>2</sub>O (0° C). When the crystals were redissolved in H<sub>2</sub>O, they gave a single absorption maximum at 353 nm and the A<sub>353</sub>/A<sub>310</sub> ratio was 2.25, indicating pure or nearly pure trans isomer (22). Used without further purification were: D<sub>2</sub>O (Aldrich); phenylmethylsulfonyl fluoride (PMSF, Sigma); and dithiothreitol (DTT, Calbiochem). All other chemicals used were reagent grade or better.

Preparation of Ghost Membranes. Freshly outdated human blood (packed red cells) was a kind gift of the Los Angeles Chapter of the American Red Cross. Two units of any type were mixed and ghost membranes were prepared essentially as described previously (23,24). The following modifications were necessary to produce large quantities of leaky ghost membranes (~100 ml of pellet) which were not crushed by the forces of centrifugation (see following paper (21)). The entire preparation was carried out at 0° to 4° C using a Sorvall GSA rotor, and the efficiency of all washes was maximized by filling the centrifuge bottles to maximum capacity. The packed red cells were aliquoted into six 250 ml centrifuge bottles and suspended in PBS (150 mM NaCl, 10 mM NaH<sub>2</sub>PO<sub>4</sub>, pH to 8 with NaOH). The cells were pelleted by centrifugation at 8000 rpm (10,400 x g<sub>max</sub>) for 20 min; then the supernatant and buffy coat were removed by aspiration. The cells were washed twice more by resuspending each time in PBS, then pelleting (10 min at 3000 rpm

or  $1500 \times g_{\max}$ ), then aspirating away the supernatant. Following the washes the cells were lysed. The pellets were resuspended in 5P8(+) (or 5 mM  $\text{NaH}_2\text{PO}_4$ , pH to 8 with NaOH, 130  $\mu\text{M}$  dithiothreitol and 10  $\mu\text{M}$  PMSF) then the membranes were pelleted by centrifugation at 11,000 rpm ( $19,700 \times g_{\max}$ ) for 20 min. The supernatant and the dense pellet underlying the membranes were removed by aspiration. This wash cycle in 5P8(+) was repeated six or seven times until the supernatant was colorless. The resulting leaky ghost membranes possessed the typically observed range of shapes from biconcave to spherical, and few (~5%) crushed ghosts are produced (see following paper (21)). The membranes were used within four days and were stored at  $4^\circ\text{C}$ .

NMR Sample Preparation. In all experiments samples were made on ice by diluting the ghost membrane pellet from the above preparation with an equal volume of ice cold 2 x NMR buffer (see figure and table legends for final buffer compositions). Samples that were compared to each other, for instance those plotted in the same figure, were always made using aliquots of the same membrane suspension. Samples were always prepared and stored on ice and were assayed using  $^{35}\text{Cl}$  NMR the same day, within 10 hrs of preparation.

For experiments with added DNDS, a sufficiently large volume of ghosts in NMR buffer was aliquoted to give identical samples; then an appropriate volume of inhibitor (in  $\text{H}_2\text{O}$ ) stock solution was added to each sample to give the desired final inhibitor concentration. The same total volume (50  $\mu\text{l}$  per ml sample) of inhibitor stock plus  $\text{H}_2\text{O}$  was added to all the related samples so that they were identical except (when appropriate) for the inhibitor concentration. Due to the light-sensitive nature of DNDS, the DNDS stock solution was stored in darkness

and was used only if it satisfied the conditions  $A_{353}/A_{310} \geq 2.20$  (or, more than 95% trans isomer, the cis isomer being inactive (22)). Also, for routine assays excess DNDS (1.0 mM total, which gives ~0.9 mM unbound) was used so that full inhibition of the DNDS-sensitive linebroadening was ensured even if some degradation occurred.

Samples containing different amounts of the anions chloride, bicarbonate, fluoride, or iodide (Figures 5 and 6) were prepared by diluting 1 vol. of membranes with 1 vol. of a different 2 X NMR buffer stock for each anion concentration. The ionic strength was held constant in all samples by including a sufficient amount of citric acid (pH to 8.0 with NaOH). Thus, enough citrate was added to make the ionic strength the same as that of the sample containing the highest concentration (500 mM, Figure 5, or 200 mM, Figure 6) of the varying anion. No citrate was added to the latter sample.

$^{35}\text{Cl}$  NMR Spectroscopy. The spectra were obtained using one of two NMR spectrometers: a JEOL FX-90 ( $^{35}\text{Cl}$  resonance frequency is 8.8 MHz) or a Varian XL-200 ( $^{35}\text{Cl}$  resonance frequency is 19.6 MHz). The standard parameters for spectral acquisition were as follows. The spectral width was 1000 Hz, containing 256 data points and centered on the solution chloride peak in the  $^{35}\text{Cl}$  NMR spectrum. Using 5 mm or 10 mm sample tubes, from 1000 to 3000 pulses were accumulated for up to 6.4 minutes (3000 pulses) at 3° C without sample spinning. An extra linebroadening of precisely 10.0 Hz was added to all samples during data processing to improve signal/noise, and the number of Fourier-transform points was zero-filled to over 8000 to smooth the spectrum (see (25)). The central 500 Hz of the spectrum was plotted and the linewidth of the  $^{35}\text{Cl}$  peak at half height

hand measured. For all experiments the same acquisition parameters were used for samples that were compared to each other, for instance, those plotted in the same figure.

NMR Sample Analysis. After NMR spectra were obtained, samples were stored overnight at 4<sup>o</sup> C before chemical analysis. Total ghost protein was determined using the modified (26) Lowry protein assay (27) that has been developed for use with membrane samples. The concentration of nonmembrane-bound DNDS was determined essentially as described elsewhere (28,29). The membranes were pelleted by centrifugation for 45 min at 15,000 rpm (29,000 x g<sub>max</sub>) in a Sorvall SS-34 rotor, 3 ml tubes. The optical absorbance of the supernatant was measured and corrected for the background absorbance present in supernatants containing no inhibitor. The DNDS concentration was calculated using the molar extinction coefficient  $\epsilon_{353} = 3.0 \times 10^4$  (22).

Statistics. All confidence limits for means and for best-fit (nonlinear least-squares) parameters are given as  $\pm$  one standard deviation for  $n \geq 3$ .

## RESULTS

The  $^{35}\text{Cl}^-$  NMR resonance. For chloride in aqueous solution, the chloride  $^{35}\text{Cl}$  NMR spectrum (here termed the  $^{35}\text{Cl}^-$  NMR spectrum) contains a single resonance of Lorentzian shape (Figures 1,2). Within experimental error, the shape of the observed resonance remains Lorentzian when leaky ghost membranes are added (Figures 1,2). Note, however, that the linewidth at half height of the resonance is increased by the membranes (Figure 1). This linewidth increase is due to the presence of membrane-bound chloride binding sites. In the following the linewidth increase will be used as an assay for these sites; but first it is necessary to a) examine the characteristics of the  $^{35}\text{Cl}^-$  NMR spectrum and b) demonstrate the validity of the binding site assay in the leaky ghost system.

Identity of the Chloride Ions that Give Rise to the Observed  $^{35}\text{Cl}^-$  NMR Resonance. At a given instant in time, the chloride ions in a suspension of ghost membranes can be divided into three populations: chloride ions in the extracellular solution, chloride ions in the intracellular solution, and chloride ions bound to the membranes. The Lorentzian shape of the observed  $^{35}\text{Cl}^-$  resonance indicates that the resonance stems from a homogeneous population of chloride ions. This homogeneous population contains  $100 \pm 2\%$  of the total number of chloride ions in the sample (from integration of the spectra used to generate Figure 2). Thus the observed population is large compared to the population of chloride bound to macromolecules (total protein  $\leq 10 \mu\text{m}$ ,

Figure 1

The effect of ghost membranes on the  $^{35}\text{Cl}^-$  NMR spectrum. Shown are typical spectra obtained at 19.6 MHz and 3°C using standard  $^{35}\text{Cl}^-$  linebroadening assay parameters (see text). Upper spectrum: with leaky ghost membranes, 1.4 mg/ml total ghost protein. Lower spectrum: without ghost membranes. The linewidths at half height are 34.5 Hz and 27.1 Hz for the upper and lower spectra, respectively. Each sample contained: 250 mM  $\text{NH}_4\text{Cl}$ , 5 mM  $\text{NaH}_2\text{PO}_4$ , 20%  $\text{D}_2\text{O}$ , pH to 8.0 with  $\text{NH}_4\text{OH}$ . The two spectra are plotted at the same absolute intensity.

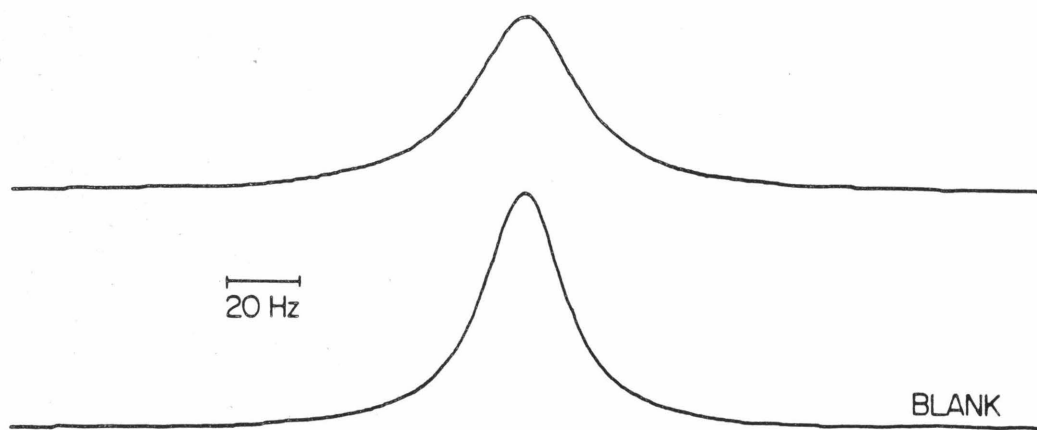
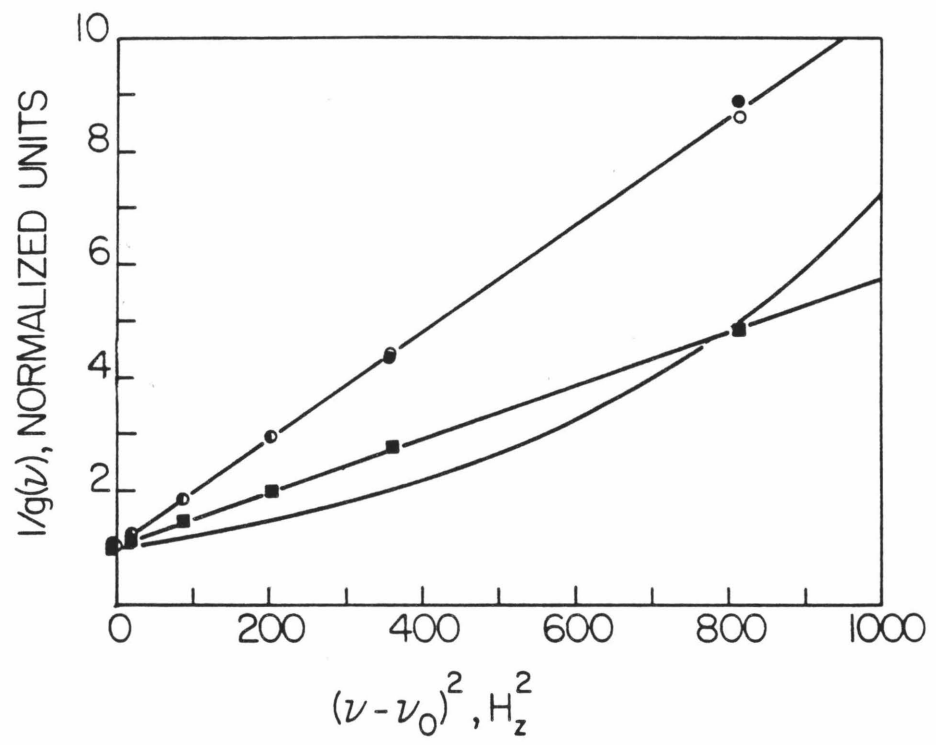


Figure 2

The lineshape of the  $^{35}\text{Cl}^-$  NMR spectra. Spectra for samples containing leaky ghosts (■), ghosts plus 1% SDS (●) and no ghosts (○) were normalized so that the absorption intensity ( $g(\nu_0)$ ) of each spectrum at the resonance frequency ( $\nu_0$ ) was 1. Then the absorption intensity ( $g(\nu)$ ) at other frequencies ( $\nu$ ) was measured and the inverse of the absorption intensity ( $1/g(\nu)$ ) was recorded in this plot which linearizes Lorentzian spectra. The solid lines are nonlinear least-squares best-fit curves. The straight lines show the best-fit Lorentzian lineshapes and the curved line shows the best-fit Gaussian lineshape for the ghost (■) points. The buffer was: 250 mM NaCl, 5 mM  $\text{NaH}_2\text{PO}_4$ , 20%  $\text{D}_2\text{O}$ , pH to 8.0 with NaOH. Spectral parameters were 19.6 MHz, 3°C and standard assay parameters (see text).



observed chloride  $250 \pm 5$  mM), and it follows that the bulk of the observed population are solution chloride ions.

Both the intracellular and extracellular populations of solution chloride contribute to the observed  $^{35}\text{Cl}^-$  resonance. The ratio of intracellular: extracellular chloride ions in these samples is ~25:75 (calculated assuming  $100 \mu\text{m}^3$  total volume and  $6 \times 10^{-10}$  mg total protein per ghost membrane). The integration data indicate that the majority of chloride ions in both compartments are visible. The fact that these two populations give rise to a  $^{35}\text{Cl}^-$  resonance due to a homogeneous population of chloride ions is not surprising, since large holes exist in these leaky ghost membranes ((30); see also following chapter (21)). These holes should allow rapid exchange of chloride ions between the intra- and extracellular compartments such that the intra- and extracellular solution chloride ions are chemically equivalent on the NMR timescale. Thus, the  $^{35}\text{Cl}^-$  NMR resonance of samples that contain ghost membranes is best described as the spectrum of a homogeneous population of solution chloride ions whose linewidth is perturbed (increased) by the presence of chloride binding sites.

Further Analysis of the Observed  $^{35}\text{Cl}^-$  Resonance. Two characteristics of the observed  $^{35}\text{Cl}^-$  NMR spectrum deserve further explanation. First, the shape of the observed spectrum is simple, despite the fact that the  $^{35}\text{Cl}$  nucleus ( $S=3/2$ ) actually gives rise to three distinct NMR transitions. Secondly, the increase in linewidth caused by ghost membranes is of interest because this effect forms the basis of the assay for chloride binding sites used here.

Both the shape and the width of the  $^{35}\text{Cl}^-$  spectrum are largely controlled by the effect of the quadrupolar interaction on the three  $^{35}\text{Cl}^-$  NMR transitions. The  $^{35}\text{Cl}$  nucleus possesses an electric quadrupole moment, which interacts with the electric field gradient at the nucleus. The magnitude of this field gradient is large when the chloride ion's electron cloud is polarized by an asymmetrical ligand environment. However, the effect of the field gradient on the  $^{35}\text{Cl}^-$  NMR spectrum is decreased when the chloride-ligand complex tumbles sufficiently rapidly to partially or completely randomize the direction of the field gradient.

The tumbling of hydrated chloride in aqueous solution is unrestricted, essentially isotropic and rapid. Under these conditions the quadrupolar interaction is averaged to zero and the three  $^{35}\text{Cl}^-$  NMR transitions have identical resonance frequencies and linewidths so that they sum to give a Lorentzian absorption (Figures 1,2). In contrast, a large quadrupolar interaction occurs when chloride binds to a slowly tumbling, asymmetric binding site on a macromolecule. The large quadrupolar interaction causes differences in the resonance frequencies and linewidths of the three transitions so that the spectrum is no longer Lorentzian. However, in the experiments presented here, free chloride in solution is present in large molar excess relative to chloride bound to macromolecules. Thus the solution chloride spectrum with its Lorentzian shape dominates the observed spectrum, even in the presence of ghost membranes (Figures 1,2).

The increase in the linewidth of the  $^{35}\text{Cl}^-$  NMR resonance in the presence of ghost membranes is due to the exchange of chloride between solution and chloride binding sites associated with the membranes (Figure 1). Due to the quadrupolar interaction and to shifts of resonance frequencies that occur upon binding, the linewidth of a  $^{35}\text{Cl}^-$  NMR transition is typically over  $10^4$  times larger for chloride bound to a macromolecule than for chloride in solution (17,18). As a result, when chloride exchanges sufficiently rapidly between binding sites and solution, the observed linewidth is larger than that of pure solution chloride. The previous chapter presents a detailed analysis of the observed  $^{35}\text{Cl}^-$  NMR resonance and of the physical processes that cause the linewidth increase.

The Information Contained in the  $^{35}\text{Cl}^-$  Linebroadening. The linewidth increase (or linebroadening) contains a variety of information about the sites that give rise to it, as shown in the following simple theoretical analysis. The  $^{35}\text{Cl}^-$  linebroadening ( $\delta$ ) is defined as

$$\delta = \Delta\nu_{\frac{1}{2}} - (\Delta\nu_{\frac{1}{2}})_F \quad (1)$$

Here  $(\Delta\nu_{\frac{1}{2}})_F$  is the linewidth (at half height) of free chloride in solution, obtained using a blank sample, and  $\Delta\nu_{\frac{1}{2}}$  is the observed linewidth when binding sites are present. In the presence of a heterogeneous population of independent sites the linebroadening may be written (Chapter II):

$$\delta = \sum_i \alpha_i \frac{[X_i Cl]}{[Cl_T^-]} \quad (2)$$

Here  $[Cl_T^-]$  is the total (stoichiometric) chloride concentration,  $[X_i Cl]$  is the concentration of chloride bound to the  $i$ 'th type of site, and  $\alpha_i$  is a proportionality constant. Two fundamental assumptions have been made during the derivation of Equation 2 (Chapter II, also (31,32)). First, it is assumed that the free chloride ions in solution are in vast molar excess relative to the bound chloride ions. This assumption is justified in the experiments presented here because the protein concentration is small: the ratio of band 3, the most abundant polypeptide in the ghost membrane (33), to the total chloride concentration is always  $<10^{-4}$ . Secondly, it is assumed that the only significant pathway available to a bound chloride ion is return to the solution. Here chloride bound to band 3 can undergo translocation as well as dissociation, but the dissociation rate is very fast (Chapter VI) relative to the translocation rate (turnover rate 400/sec at  $0^\circ C$  (22)); thus the use of Equation 2 is valid in the system at hand.

An important feature of Equation 2 is that the observed linebroadening is the sum of the additive contributions from the different types of sites:

$$\delta = \sum_i \delta_i \quad (3)$$

where  $\delta_i (= \alpha_i [X_i Cl]/[Cl_T^-])$  is directly proportional to the fraction of total chloride that is bound to the  $i$ 'th type of site. This relationship can be rewritten in terms of bulk parameters to yield the desired final result. The quantity  $[X_i Cl]$  can be replaced using the expression

$[X_iCl]/[X_{T_i}] = [Cl_F^-]/([Cl_F^-] + K_{D_i})$ , where  $[X_{T_i}]$  is the total (stoichiometric) concentration of the  $i$ 'th type of site,  $[Cl_F^-]$  is the free chloride concentration, and  $K_{D_i}$  is the chloride dissociation constant for the  $i$ 'th type of site. In addition, the quantity  $[Cl_F^-]$  is essentially equivalent to  $[Cl_T^-]$  since it is assumed that the free chloride ions are in vast molar excess to the bound chloride ions. Substitution for  $[X_iCl]$  in Equation 2 gives

$$\delta = \sum_i \alpha_i \frac{[X_{T_i}]}{[Cl^-] + K_{D_i}} \quad (4)$$

where  $[Cl_T^-]$  is now written simply  $[Cl^-]$ . Finally,  $[X_{T_i}]$  can be expressed in terms of the total ghost protein concentration  $[P]$ , using the simple proportionality  $[X_{T_i}] = Z_i [P]$

$$\delta = [P] \cdot \sum_i \alpha_i \frac{Z_i}{[Cl^-] + K_{D_i}} \quad (5)$$

where  $Z_i$  is a proportionality constant.

Equation 5 indicates that the quantity  $\delta/[P]$  contains all of the interesting information provided by the assay. (Hereafter linebroadengs will generally be expressed in the units Hz per mg/ml total ghost protein.) The information contained in the quantity  $\alpha_i$  depends on the rate of chloride exchange between the  $i$ 'th type of site and solution: in the rapid exchange limit  $\alpha_i$  depends upon the characteristics of the binding site environment, while in the slow exchange limit  $\alpha_i$  depends upon the rate constant for chloride dissociation from the site (Chapter II). The proportionality constant  $Z_i$  contains information on the number

of sites of the  $i$ 'th type. If a particular protein  $P_i$  possesses the  $i$ 'th type of site, then  $Z_i$  can be written

$$Z_i = n_i \cdot [P_{T_i}] / [P] \quad (6)$$

For the ghost membrane system the  $n_i$  have not yet been determined because the  $\alpha_i$  are presently unknown. Nevertheless the linebroadening remains a useful assay for chloride binding sites because of the linear relationship between the linebroadening and the binding site concentration (Equation 4). The linebroadening also contains information on the chloride dissociation constant of each type of site. It is convenient to recast Equation 5 in terms of the inverse chloride concentration to emphasize the high affinity chloride binding sites:

$$\frac{\delta}{[P]} = \sum_i \frac{\alpha_i \cdot Z_i}{K_{D_i}} \cdot \frac{[Cl^-]^{-1}}{[Cl^-]^{-1} + K_{D_i}^{-1}} \quad (7)$$

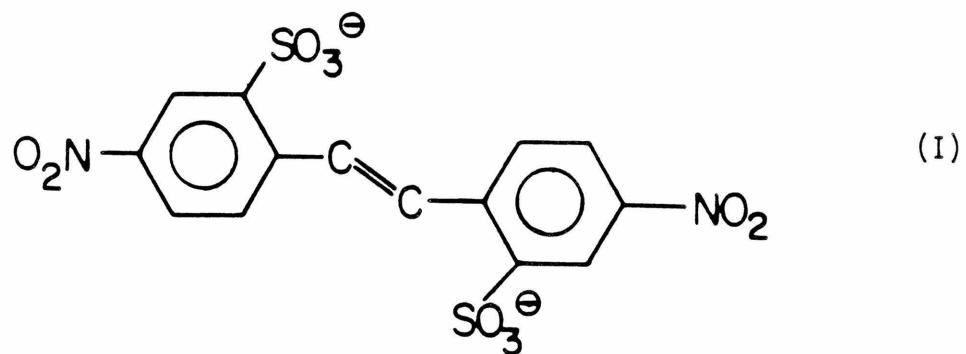
or, for a single type of site:

$$\frac{\delta_i}{[P]} = \frac{\alpha_i \cdot Z_i}{K_{D_i}} \cdot \frac{[Cl^-]^{-1}}{[Cl^-]^{-1} + K_{D_i}^{-1}} \quad (8)$$

This equation states that a high affinity site ( $K_{D_i} \leq [Cl^-]$ ) will give rise to a square hyperbola on a plot of linebroadening vs  $[Cl^-]^{-1}$ , while on the same plot the curve due to a low affinity site ( $K_{D_i} \gg [Cl^-]^{-1}$ ) collapses to a straight line of zero slope. Consequently, binding sites can be operationally defined as high- or low-affinity sites on the basis of their behavior in this type of plot.

Experimental Justification of the  $^{35}\text{Cl}^-$  Linebroadening Assay for Chloride Binding Sites. The preceding theoretical analysis of the chloride binding assay is supported experimentally by the data of Figure 3, which demonstrates that at constant  $[\text{Cl}^-]$  the  $^{35}\text{Cl}^-$  linebroadening is directly proportional to the concentration of chloride binding sites on leaky ghost membranes. This simple linear relationship enables straightforward examination of the leaky ghost system, where the assay reveals a variety of important binding site characteristics.

The Linebroadening Due to DNDS-Sensitive Sites. Multiple types of chloride binding sites exist on leaky ghost membranes, since many composite proteins are present (34,35). The  $^{35}\text{Cl}^-$  linebroadening contributions of the different types of sites are additive (Equation 3); thus the linebroadening due to band 3 transport sites can be identified using a competitive inhibitor which blocks the binding of chloride to the transport sites, for example DNDS

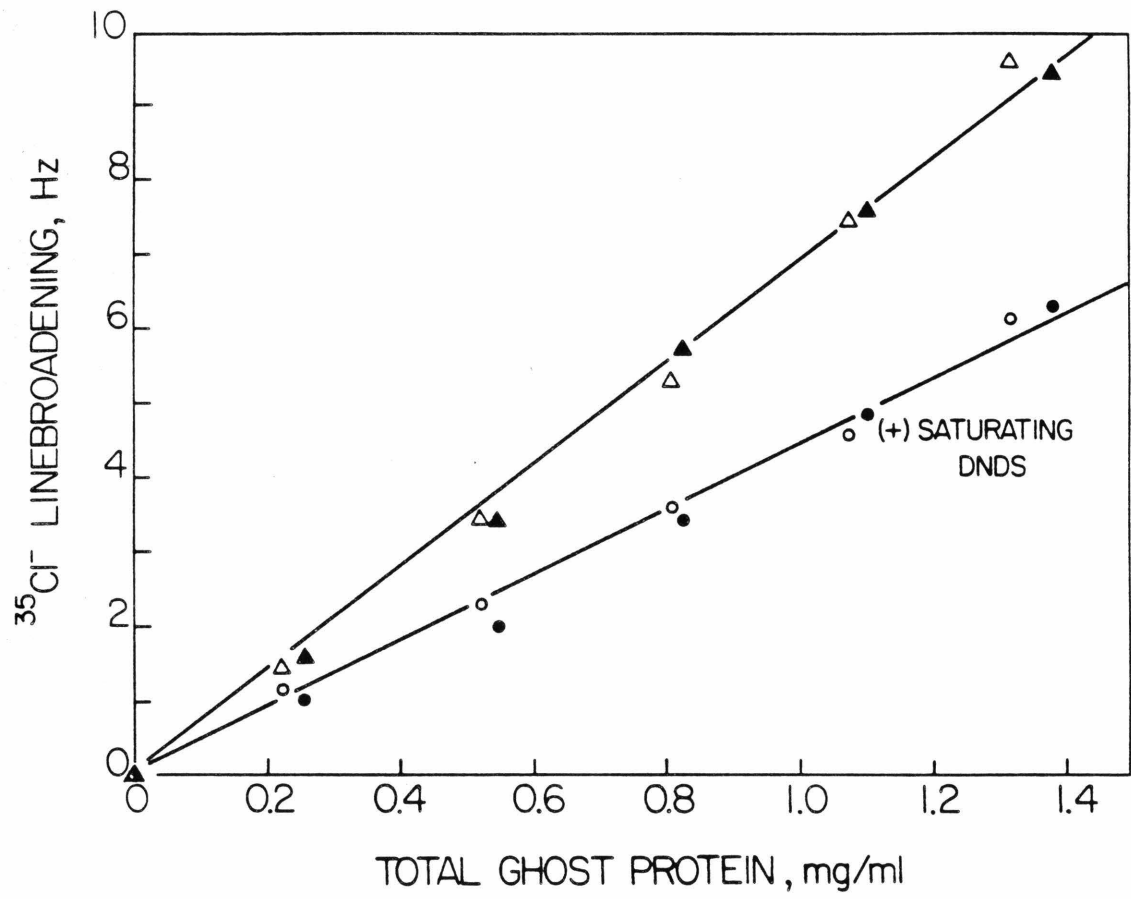


trans-4,4'-dinitrostilbene-2,2'-disulfonate (DNDS)

This molecule is a potent anion exchange inhibitor that binds reversibly to the extracellular band 3 anion transport sites in a manner that prevents chloride binding (1,36,37).

Figure 3

The relationship between the  $^{35}\text{Cl}^-$  linebroadening and the ghost membrane concentration. The  $^{35}\text{Cl}^-$  linebroadening of samples containing leaky ghost membranes with ( $\bullet, \circ$ ) or without ( $\blacktriangle, \triangle$ ) DNDS, 1 mM total concentration. The solid lines are least-squares best-fit straight lines ( $y = Mx$ ) that have slopes of  $6.87 \pm 0.04$  Hz per mg/ml total ghost protein. The buffers used were 250 mM  $\text{NH}_4\text{Cl}$ , 5 mM  $\text{NaH}_2\text{PO}_4$ , 20%  $\text{D}_2\text{O}$ , pH to 8.0 with  $\text{NH}_4\text{OH}$  ( $\blacktriangle, \bullet$ ); or 220 mM  $\text{NaCl}$ , 30 mM glycylglycine  $\text{HCl}$ , 2.5 mM  $\text{NaH}_2\text{PO}_4$ , 20%  $\text{D}_2\text{O}$ , pH to 8.0 with  $\text{NaOH}$  ( $\triangle, \circ$ ). Spectral parameters: 8.8 MHz,  $3^\circ\text{C}$  and standard assay parameters (see text).



A saturating concentration (or, a concentration sufficient to yield maximal inhibition, see Figure 4) of DNDS partially reduces the ghost linebroadening (Figure 3); the linebroadening of DNDS-saturated membranes is  $4.41 \pm .04$  Hz per mg/ml total protein, which is 36% less than the value for DNDS-free ghosts of  $6.87 \pm .04$  Hz per mg/ml. Thus, at least two types of chloride binding sites exist on ghost membranes. The sites that give rise to the DNDS-sensitive component of the linebroadening are termed the DNDS-sensitive sites, while the remaining sites are DNDS-insensitive. The additivity of linebroadening enables isolation of the DNDS-sensitive linebroadening by subtraction of the DNDS-insensitive linebroadening from the total linebroadening. This DNDS-subtraction technique will often be used in future presentations of data.

DNDS Binds to Band 3 Transport Sites and Thereby Inhibits the  $^{35}\text{Cl}^-$  Linebroadening. The linebroadening of the DNDS-sensitive sites is inhibited by DNDS binding to a class of inhibitory binding sites that are identical, since the DNDS binding is well described by a single apparent dissociation constant (Figure 4). This apparent  $K_D$  is quantitatively similar to the known apparent  $K_D$  for DNDS binding to band 3 transport sites in the presence of 250 mM chloride (Table 1). Note that because of the presence of chloride, which competes with DNDS for binding (data not shown; also (37)), the apparent  $K_D$  is larger than the true  $K_D$  for DNDS binding to the inhibitory sites (Chapter V).

DNDS is known to bind to the extracellular band 3 transport site with a stoichiometry of one molecule of DNDS per band 3 transport unit (28). When DNDS binds to this site, it inhibits the linebroadening due to one or more chloride binding sites (Figures 3 and 4). The affected sites could include: transport sites on band 3, other chloride binding sites on

Figure 4

The effect of DNDS on the ghost membrane  $^{35}\text{Cl}^-$  broadening. Samples were prepared containing leaky ghost membranes and different concentrations of unbound DNDS. The solid curve is the nonlinear least-squares best-fit curve ( $y = A - Bx/(x + K_D)$ ) for a homogeneous set of sites with an apparent  $K_D$  of  $6.4 \pm 0.5 \mu\text{M}$  for DNDS binding. The buffer was 250 mM  $\text{NH}_4\text{Cl}$ , 5 mM  $\text{NaH}_2\text{PO}_4$ , 20%  $\text{D}_2\text{O}$ , pH to 8.0 with  $\text{NH}_4\text{OH}$ . Spectral parameters: 8.8 MHz,  $3^\circ\text{C}$  and standard assay parameters (see text).



Table 1. Apparent Dissociation Constants for Substrate and Inhibitor Binding to DNDS-Sensitive Sites on Ghost Membranes

Anion	DNDS-Sensitive Site <sup>a</sup> Apparent $K_D$	Band 3 Transport Site <sup>c</sup> Apparent $K_D$
$\text{Cl}^-$	$80 \pm 30 \text{ mM}$	$67, 65 \pm 5 \text{ mM}^d$
DNDS <sup>b</sup>	$6.4 \pm .5 \text{ }\mu\text{M}$	$4.4 \text{ }\mu\text{M}^e$

a. Obtained as described in text.

b. Both values are given for  $[\text{Cl}^-] = 250 \text{ mM}$ .

c. From equilibrium chloride exchange measurements in red cells.

d. From References 20 and 38; both have been corrected for the modified effect.

e. Extrapolated from Figure 7 in Reference 37.

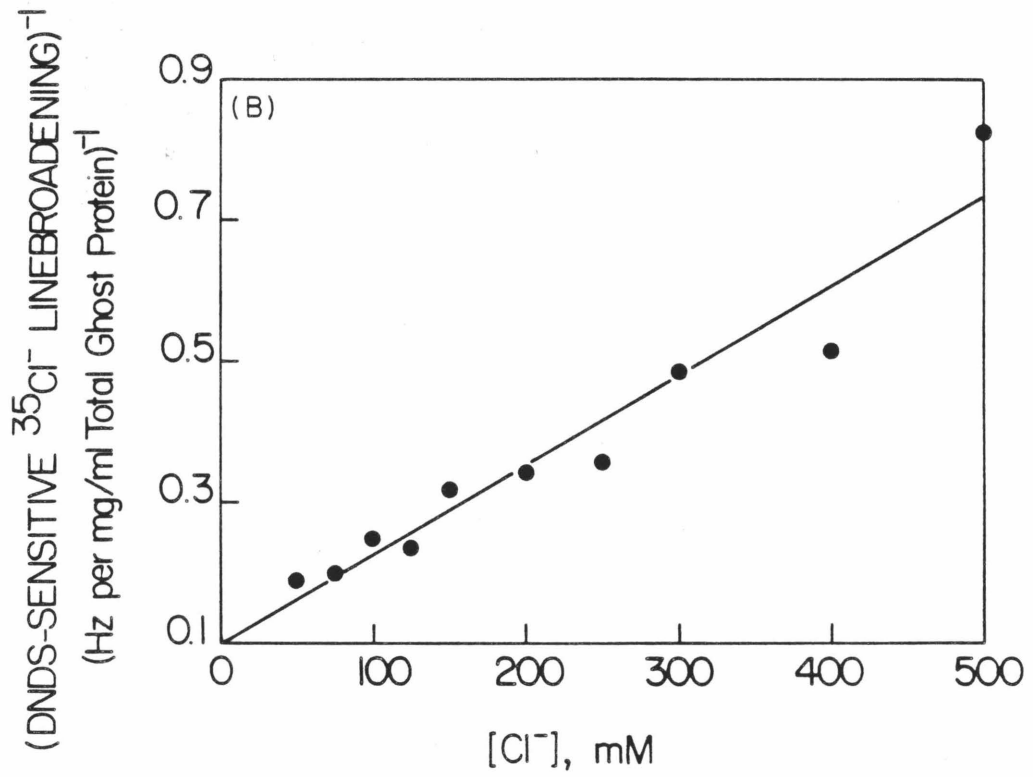
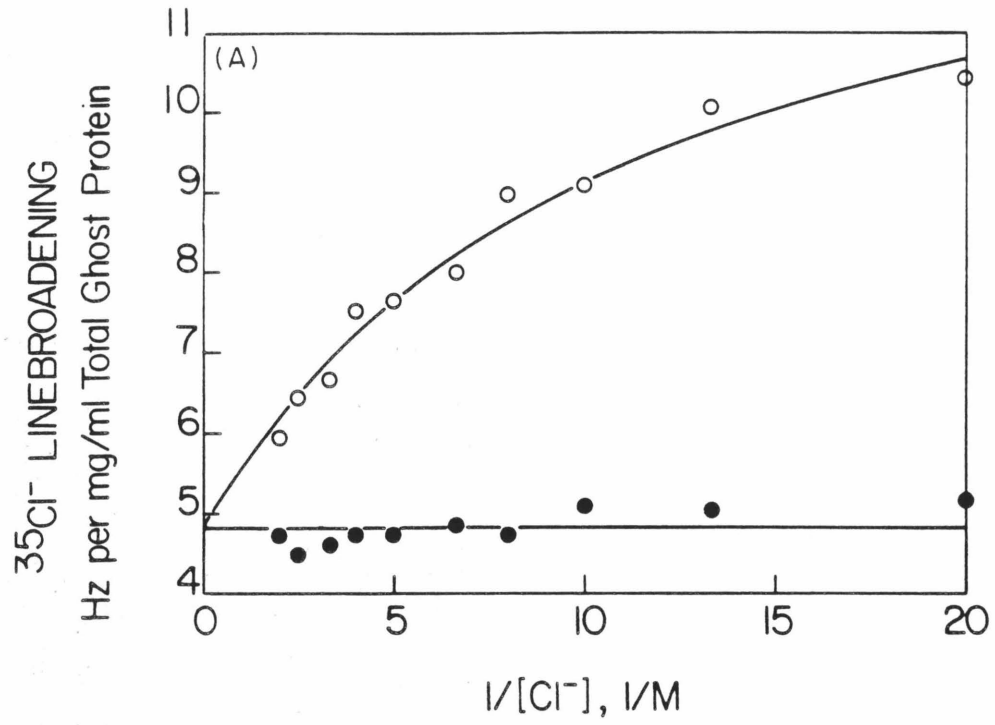
band 3, or chloride binding sites on a protein(s) other than band 3 that are allosterically coupled to the DNDS binding sites. One parameter which is useful in the identification of the DNDS-sensitive sites is the affinity of these sites for chloride.

The DNDS-sensitive Sites Are High Affinity Chloride Binding Sites. Both high affinity and low affinity chloride binding sites are observed in the leaky ghost membrane system (Fig. 5a). In the presence of a saturating concentration of DNDS, the linebroadening due to ghost membranes is well approximated by a best-fit straight line of zero slope (Figure 5a, lower curve). Thus, the DNDS-insensitive sites can be operationally defined as low-affinity sites that satisfy  $K_{D_i} \gg 0.5 \text{ M}$ . (The plot could not be extended to chloride concentrations greater than 0.5 M because DNDS becomes increasingly insoluble at such chloride concentrations). In the absence of DNDS, high-affinity sites appear (Figure 5a, upper curve). The resulting linebroadening is the sum of the contributions from both the DNDS-sensitive and insensitive sites. This linebroadening is well approximated by a best-fit curve calculated for a) a homogeneous set of high-affinity binding sites described by Equation 8, plus b) a set of low-affinity binding sites described by the best-fit straight line obtained for the DNDS-containing samples. The data indicate that saturation with DNDS completely inhibits the linebroadening of the high-affinity sites but has no effect on the low-affinity sites.

The apparent dissociation constant for chloride binding to the high-affinity sites can be determined from the best-fit curve in Figure 5a.

Figure 5

The effect of chloride concentration on the ghost membrane  $^{35}\text{Cl}^-$  linebroadening. a) The  $^{35}\text{Cl}^-$  linebroadenings of samples containing leaky ghost membranes with (●) or without (○) DNDS, 1 mM total concentration. The solid curves are nonlinear least-squares best-fit curves calculated for a set of low affinity (lower curve,  $y = A$ ,  $K_D \gg 0.5 \text{ M}$ ) chloride binding sites plus a homogeneous set of high affinity (upper curve,  $y = A + Bx/(x + K_D^{-1})$ ,  $K_D = 90 \pm 10 \text{ mM}$ ) chloride binding sites. Each sample contained the indicated  $[\text{NH}_4\text{Cl}]$  as well as 2.5 mM  $\text{NaH}_2\text{PO}_4$ , 20%  $\text{D}_2\text{O}$ , pH to 8.0 with  $\text{NH}_4\text{OH}$ . Sufficient citric acid (pH to 8.0 with  $\text{NaOH}$ ) was added to bring the ionic strength up to that of the sample containing the highest  $[\text{NH}_4\text{Cl}] = 500 \text{ mM}$ . Spectral parameters: 8.8 MHz,  $3^\circ\text{C}$  and specified assay parameters (see text). b) The DNDS-sensitive linebroadening was obtained from the data in a) by subtracting each point for a sample containing DNDS from the corresponding (same  $[\text{Cl}^-]$ ) point for a sample without DNDS. The inverse of the DNDS-sensitive linebroadening was taken. The solid line is a linear least-squares best-fit straight line calculated for a homogeneous set of chloride binding sites ( $y = A(1 + [\text{Cl}^-]/K_D)$ ,  $K_D = 80 \pm 5 \text{ mM}$ ).



Alternatively, the inverse of the DNDS-sensitive linebroadening can be plotted as a function of the chloride concentration (Figure 5b). This type of plot yields a straight line for a homogeneous set of chloride binding sites that are described by Equation 8. The extracted best-fit apparent  $K_{D_i}$ , along with the results of seven similar experiments at 19.6 MHz or 8.8 MHz, together yield an average of  $80 \pm 30$  mM for the apparent  $K_{D_i}$  for chloride binding to the DNDS-sensitive sites. This value is quantitatively similar to the known apparent  $K_D$  for chloride binding to band 3 transport sites (Table 1).

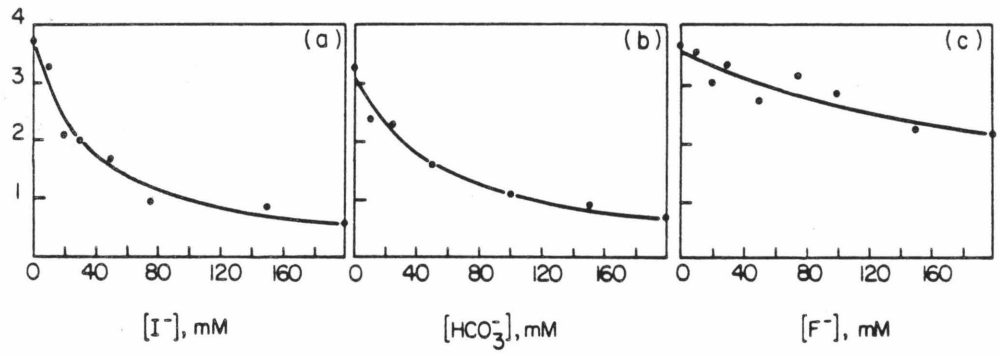
Surprisingly, no chloride binding sites are observed that have a  $K_D \approx 300$  mM, which is the predicted chloride affinity for a site termed the modifier site (1,20). The existence of a modifier site on band 3 has been proposed to explain the inhibition of chloride self-exchange across the membrane which occurs at high  $[Cl^-]$ . Such inhibition has been thought to result from chloride binding to the modifier site. Yet no evidence of this chloride binding site is seen in the experiments presented here.

The High-affinity Sites Are Band 3 Transport Sites. In order to verify the conclusion that the DNDS-sensitive sites are transport sites and are uncontaminated with modifier sites, we have studied the binding of anions other than chloride to ghost membranes. If an anion ( $A^-$ ) competes with chloride for binding to an anion binding site, then the  $^{35}Cl^-$  NMR assay can be used to study  $A^-$  binding. In such an experiment  $[Cl^-]$  is held constant, while  $[A^-]$  is varied. The resulting data (Figure 6, for the DNDS-sensitive sites) allow determination of the apparent  $K_D$  for  $A^-$  binding at the given  $[Cl^-]$  (Chapter V). The best-fit theoretical curves in Figure 6 (solid lines) were calculated

Figure 6

The effect of competing anions on the  $^{35}\text{Cl}^-$  NMR spectrum. Samples were prepared that contained different concentrations of a competing anion ( $\text{A}^-$ ) and a fixed concentration of chloride (100 mM). The linebroadening of a sample containing 1 mM DNDS was subtracted from the linebroadening of an otherwise identical DNDS-free sample to yield the linebroadening of the DNDS-sensitive sites. The solid lines are the nonlinear least-squares best-fit curves ( $y = A - Bx/(x + K_D)$ ) for a homogeneous set of sites with apparent  $K_D$ 's of: a)  $34 \pm 3$  mM for  $\text{I}^-$ , b)  $55 \pm 4$  mM for  $\text{HCO}_3^-$ , and c)  $290 \pm 30$  mM for  $\text{F}^-$ . The buffer contained the indicated concentration of NaA as well as 100 mM NaCl, 2.5 mM  $\text{NaH}_2\text{PO}_4$ , 20%  $\text{D}_2\text{O}$ , pH to 8.0 with NaOH. Citric acid (pH to 8.0 with NaOH) was added so that the ionic strength in all samples was the same as that of the  $[\text{A}^-] = 200$  mM sample. Spectral parameters: 8.8 MHz,  $3^\circ\text{C}$  and standard assay parameters (see text).

DNDS-SENSITIVE  $^{35}\text{Cl}^-$  LINEBROADENING  
Hz per mg/ml Total Ghost Protein



using the assumption that the DNDS-sensitive sites are a class of identical sites. The reasonable fit of these curves indicates that the assumption of homogeneity is consistent with the data.

The apparent  $K_D$ 's for bicarbonate, fluoride, chloride and iodide binding to the DNDS-sensitive sites are given in Table 2. Also given are the known apparent  $K_D$ 's for binding of these anions both to band 3 transport sites and to the hypothetical modifier sites. Note that the apparent  $K_D$ 's for the DNDS-sensitive sites were obtained in the presence of competing chloride (100 mM), while the other values were obtained in the absence of competing chloride. Two patterns emerge in the data of Table 2: a) the apparent  $K_D$ 's of the DNDS-sensitive sites are larger than the apparent  $K_D$ 's of band 3 transport sites. This result is expected because only the former values were obtained in the presence of competing chloride. In contrast, the apparent  $K_D$ 's of the DNDS-sensitive sites are smaller than the apparent  $K_D$ 's predicted for modifier sites, indicating that the DNDS-sensitive sites have higher affinities for anions than those expected for modifier sites. b) The relative affinities ( $I > \text{HCO}_3 \gg \text{Cl} > \text{F}$ ) exhibited by the DNDS-sensitive sites are essentially the same as those exhibited by band 3 transport sites but are different from those expected for modifier sites. Together the data of Table 2 suggest that the modifier sites do not contribute significantly to the DNDS-sensitive linebroadening. Instead the DNDS-sensitive sites behave like a homogeneous class of band 3 transport sites.

## DISCUSSION

The  $^{35}\text{Cl}^-$  NMR linebroadening assay reveals two classes of chloride binding sites associated with leaky ghost membranes. The first class

Table 2. Apparent Dissociation Constants for Anion Binding to Band 3 Sites

Anion	DNDS-Sensitive Site <sup>a</sup> Apparent $K_D$ [Cl <sup>-</sup> ] = 100 mM	Transport Site <sup>c</sup> Apparent $K_D$ [Cl <sup>-</sup> ] = 0 mM	Modifier Site <sup>c</sup> Apparent $K_D$ [Cl <sup>-</sup> ] = 0 mM
I <sup>-</sup>	34 ± 3 mM	10 mM	60 mM
HCO <sub>3</sub> <sup>-</sup>	55 ± 4 mM	16 mM	565 mM
Cl <sup>-</sup>	(190 mM) <sup>b</sup>	67, 65 ± 5 <sup>d</sup> mM	335 mM
F <sup>-</sup>	290 ± 30 mM	88 mM	337 mM

a. Measured as described in text by competing the anion with 100 mM Cl<sup>-</sup>.

b. Calculated as described in Reference 43.

c. Obtained from kinetic studies of equilibrium anion exchange in Reference 20.

d. From Reference 38.

consists of low-affinity binding sites that are unaffected by DNDS. The second class consists of band 3 transport sites. The linebroadening of these transport sites is completely inhibited by a saturating concentration of DNDS. Such linebroadening inhibition is consistent with the previous observation that DNDS competes with chloride for binding to the extracellular band 3 transport site (1,36,37).

The data presented here indicate that DNDS can be used to isolate that part of the total ghost linebroadening which is associated with band 3 transport sites. Actually, DNDS is not very specific for these sites. For instance, we have found that DNDS reduces the linebroadening associated with chloride binding to hemoglobin (data not shown). However, the molar ratio of band 3:hemoglobin in ghosts prepared at pH 8.0 is at least 10:1 (39). This molar ratio would result in a corresponding ratio of DNDS-sensitive linebroadenings of at least 100:1 (data not shown), which is a negligible interference. Another protein which could contribute to the DNDS-sensitive linebroadening is the erythrocyte  $\text{Ca}^{++}$ -ATPase, which is inhibited by DIDS (or 4,4'-diisothiocyanostilbene-2,2'-disulfonate), a structural analogue of DNDS. Again, band 3 is present in great molar excess to this protein; there are ~100 times more copies of band 3 per membrane (40). These examples stress that in the unpurified ghost membrane system, the DNDS-sensitive linebroadening could be contaminated with contributions from proteins other than band 3. Fortunately, band 3 is the most abundant polypeptide in ghost membranes (33), so these contaminating contributions could be negligible. This appears to be the case, since the DNDS-sensitive sites are homogeneous with respect to their

affinity for a variety of anions (chloride, bicarbonate, fluoride, iodide and DNDS). Moreover, the apparent affinities that are observed for chloride and DNDS are quantitatively similar to those previously measured for band 3 transport sites. The relative apparent affinities that are observed for the inorganic anions ( $I > \text{HCO}_3 \gg \text{Cl} > \text{F}$ ) are essentially the same as those previously measured for band 3 transport sites. Thus, we believe that the bulk of the sites that make up the DNDS-sensitive class are in fact band 3 transport sites.

An unexpected conclusion of the  $^{35}\text{Cl}^-$  NMR experiments is that the linebroadening assay reveals no evidence for the existence of the proposed inhibitory anion binding site on band 3, which has been termed the modifier site (20). It is possible that this site exists but is invisible to the linebroadening assay; a site will become invisible when the quantity  $\alpha_j$  in Equation 5 tends to zero. This condition occurs when the exchange of chloride between the binding site and solution is sufficiently slow or when the symmetry of the binding site is tetrahedral or higher.

Actually, we prefer a different explanation in which an inhibitory chloride binding site of the predicted ( $K_D \approx 300 \text{ mM}$ ) chloride affinity does not exist. Instead inhibition results from nonspecific chloride binding to the low-affinity ( $K_D \gg 0.5 \text{ M}$ ) chloride binding sites that are revealed by the linebroadening assay. In this model, bound chloride builds up in the vicinity of the low-affinity sites as the chloride concentration increases. The local density of bound chloride ion would in turn inhibit the transport process. The step in the transport cycle which is inhibited is the chloride transmembrane translocation step rather than the chloride

binding step, since no inhibition of chloride binding has been observed at chloride concentrations up to 500 mM (Figure 5). Previous observations indicate that the onset of transport inhibition is rapid as the chloride concentration is increased above 250 mM (41), suggesting that the mechanism of inhibition is highly cooperative.

A cooperative process which could give rise to the observed self-inhibition of anion exchange is membrane protein aggregation. Such aggregation has been observed in the erythrocyte system at large  $[\text{NaCl}^-]$  (42). Perhaps in the aggregated state band 3 cannot undergo a conformational change which is necessary for the transmembrane translocation of bound anion. If aggregation of erythrocyte membrane proteins indeed causes the modifier effect, then a comparison of different anions should show a correlation between the ability of an anion to induce inhibition of band 3 and its ability to induce aggregation of erythrocyte membrane proteins.

In this chapter the  $^{35}\text{Cl}^-$  linebroadening assay has been used to observe band 3 transport sites. However, certain questions concerning these sites have not yet been addressed. For instance, do transport sites on both sides of the membrane contribute to the linebroadening? If sites on both surfaces are indeed observed, how could DNDS inhibit transport sites on both membrane surfaces when it is thought to bind only to the external transport site? These questions are considered in the following chapter.

## REFERENCES

1. Knauf, P. A. (1979) Curr. Topics in Membranes and Transport 12, 249-363.
2. Steck, T. L. (1978) J. Supramol. Struct. 8, 311-324.
3. Bennett, V., and Stenbuck, P. J. (1979) Nature (London) 280, 468-473.
4. Branton, D., Cohen, C. M., and Tyler, J. (1981) Cell 24, 24-32.
5. Cabantchik, A. I., and Rothstein, A. (1974) J. Memb. Biol. 15, 207-226.
6. Ho, M. K., and Guidotti, G. (1975) J. Biol. Chem. 250, 675-683.
7. Passow, H., Fasold, H., Zaki, L., Schuhman, B., and Lepke, S. (1975) in Biomembranes: Structure and Function (Gárdos, G. and Szász, eds.), FEBS Symposium Series Vol. 35, pp. 197-214, North-Holland, Amsterdam.
8. Gunn, R. B., and Frohlich, O. (1980) in Membrane Transport in Erythrocytes (Larsen, V. V., Ussing, H. H., and Wieth, J. O., eds.), Vol. 14, pp. 431-449.
9. Passow, H., Kampmann, L., Fasold, H., Jennings, M., and Lepke, S., Ibid., pp. 345-372.
10. Rothstein, A., Ramjeesingh, M., and Grinstein, S., Ibid., pp. 329-344.
11. Jennings, M. L., Ibid., pp. 450-466.
12. Macara, I. G., and Cantley, L. C. (1981) Biochemistry 20, 5695-5701.
13. Wieth, J. O., and Bjerrum, P. J. (1982) J. Gen. Physiol. 79, 253-282.
14. Eidelman, O. and Cabantchik, Z. I. (1983) J. Memb. Biol. 71, 141-148.
15. Salhany, J. M., and Rauenbeuhler, P. B. (1983) J. Biol. Chem. 258, 245-249.
16. Lauger, P. (1973) Biochim. Biophys. Acta 311, 423-441.
17. Lindmann, B., and Forsén, S. (1976) Chlorine, Bromine and Iodine NMR in NMR: Basic Principles and Progress, Vol. 12 (Diehl, P., Fluck, E., Kosfeld, R., eds.), pp. 1-368, Springer-Verlag, N.Y.

18. Forsén, S., and Lindman, B. (1981) in Methods of Biochemical Analysis, Vol. 27 (Glick, D., ed.), pp. 289-486, John Wiley and Sons, N.Y.
19. Shami, Y., Carver, J., Ship, S., and Rothstein, A. (1977) Bioch. Biophys. Res. Comm. 76, 429-436.
20. Dalmark, M. (1976) J. Gen. Physiol. 67, 223-234.
21. Next paper in this journal.
22. Frölich, D., and Gunn, R. B. (1981) in Advances in Physiological Sciences (Hollán, S. R., Gárdos, G., and Sarkadi, B., eds.), Vol. 6, pp. 275-280, Pergamon and Akademia Kiado, Budapest.
23. Steck, T. L. (1974) in Methods in Membrane Biology (Korn, E. D., ed.), Vol. 2, pp. 245-381, Plenum, New York.
24. Fairbanks, G., Steck, T. J., and Wallach, D. F. H. (1971) Biochemistry 10, 2606-2616.
25. Farrar, T. C., and Becker, E. D. (1971) Pulse and Fourier Transform NMR, pp. 66-85, Academic, New York.
26. Markwell, M. A., Haas, S. M., Bieber, L. L., and Tolbert, N. E. (1978) Analytical Biochemistry 87, 206-210.
27. Lowry, O. H., Rosebrough, N. J., Farr, A. L., and Randall, R. J. (1951) J. Biol. Chem. 193, 265-275.
28. Frölich, O. (1982) J. Membr. Biol. 65, 111-123.
29. Cousin, J. L., and Motais, R. (1979) J. Membr. Biol. 46, 125-153.
30. Lieber, M. R., and Steck, T. L. (1982) J. Biol. Chem. 257, 11651-11659.
31. McConnell, H. M. (1958) J. Chem. Phys. 28, 430-431.
32. Swift, T. J., and Connick, R. E. J. Chem. Phys. 37, 307-320.
33. Jones, M. N., and Nickson, J. K. (1981) Bioch. Biophys. Acta 650, 1-20.
34. Lux, S. E. (1979) Nature 281, 426-429.

35. Haest, C. W. M. (1982) Bioch. Biophys. Acta 694, 331-353.
36. Barzilay, M., and Cabantchik, Z. I. (1979) Membr. Bioch. 2, 297-322.
37. Frölich, O. (1982) J. Membr. Biol. 65, 111-123.
38. Brazy, P. C., and Gunn, R. B. (1976) J. Gen. Physiol. 68, 583-500.
39. Shaklai, N., Yguerabide, J., and Ranney, H. M. (1977) Biochemistry 16, 5585-5592.
40. Niggli, V., Sigel, E., and Cornfoli, E. (1982) FEBS Lett. 138, 164-166.
41. Cass, A., and Dalmak, M. (1973) Nature New Biol. 244, 47-49.
42. Elgsaeter, A., and Branton, D. (1974) J. Cell. Biol. 63, 1018-1030.
43. Falke, J. J., Pace, R. J., and Chan, S. I. (1984) J. Biol. Chem. 259, 6472-6480.

CHAPTER IV  
THE SIDEDNESS AND RECRUITMENT OF THE  
BAND 3 TRANSPORT SITE

ABSTRACT

The initial objective of this thesis is to ascertain the mechanism of band 3-catalyzed anion transport. In general, the most powerful tests of transport mechanism involve the resolution of transport sites on opposite sides of the membrane. Here it is shown that  $^{35}\text{Cl}$  NMR provides such resolution. The physical basis of this sidedness resolution is simple, and the approach is easily generalized to other compartmentalized systems. The  $^{35}\text{Cl}^-$  linebroadening assay for chloride binding requires sufficiently rapid exchange of chloride between the site and solution. This rapid exchange requirement can be exploited in compartmentalized systems where the solution chloride population in each compartment gives rise to a distinct  $^{35}\text{Cl}$  NMR resonance. The chloride binding sites in a particular compartment are rapidly sampled only by the solution chloride ions in that same compartment (Figure 1, p. 98). As a result, the sites in a target compartment of interest can be specifically monitored by 1) observing the  $^{35}\text{Cl}$  NMR resonance of the solution chloride in the target compartment, and 2) quantitating the linebroadening of this resonance.

The specific strategy used here is to monitor outward-facing sites in compartmentalized systems where the internal solution chloride resonance is too weak or too broad to observe (intact red cells, sealed right-side-out vesicles, crushed ghosts). Then both inward- and outward-facing sites are monitored in a leaky ghost system where the entire solution chloride population can rapidly sample sites in each compartment (Figure 1, p. 98; leaky ghosts, sonicated ghosts). This strategy reveals that band 3 transport sites, as well as the low-

affinity sites, are found on both surfaces of the red cell membrane.

The ability to resolve the sidedness of transport sites is then used to test mechanistic models. It is shown that the di-anion 4,4'-dinitrostilbene-2-2'-disulfonate (DNDS), which is known to bind to a single outward-facing transport site on each band 3 monomer, inhibits all of the transport sites on both sides of the membrane. The same result is obtained with the mono-anion p-nitrobenzenesulfonate (pNBS), indicating that the inhibition does not stem from simultaneous occupation of inward- and outward-facing transport sites by the two negative charges on DNDS. Instead, DNDS and pNBS each recruit all of the transport sites on both sides of the membrane to the outward-facing conformation. These data strongly disfavor models proposing two sites simultaneously exposed to opposite sides of the membrane (Figure 5, p. 132). In contrast, the data are completely consistent with the alternating site model, which proposes a single transport site that is alternately exposed first to one side of the membrane, then to the other (Figure 6, p.135 ). The following paper quantitatively tests the simplest form of this alternating site model.

## INTRODUCTION

Band 3 has a transport cycle which results in the one-for-one exchange of anions across the red cell membrane. A variety of models for this transport cycle have already been described (older models reviewed in (1), newer models include (1-10)). In general, these models propose the existence of anion transport binding sites, which have now been directly observed (see the previous chapter (11)). The transport cycle models can be divided into several fundamental categories depending on the behavior of the transport sites during the cycle. These categories can be distinguished by examining the ability of transport sites to be recruited to one side of the membrane (12-16). Here I present a study of the transmembrane recruitment of band 3 transport sites that occurs in the presence of 4,4'-dinitrostilbene-2,2'-disulfonate (DNDS) or p-nitrobenzenesulfonate (pNBS). Each of these molecules inhibits band 3 catalyzed anion exchange by preferentially binding to the extracellular transport site.

In order to observe directly the transmembrane recruitment of transport sites, one must first resolve the sites on opposite sides of the membrane. The  $^{35}\text{Cl}^-$  linebroadening assay can provide such sidedness resolution. This assay measures the effect of chloride binding sites on the width of the  $^{35}\text{Cl}$  NMR resonance of solution chloride ions (see Chapters II,III) (11)). Typically, the width of this resonance is negligible compared to the much larger spectral width of chloride bound to a macromolecule. However, the exchange of chloride between binding sites and solution can cause an increase in the solution chloride linewidth, provided the exchange is sufficiently rapid. It is this rapid exchange requirement

that is exploited here to resolve the sidedness of chloride binding sites.

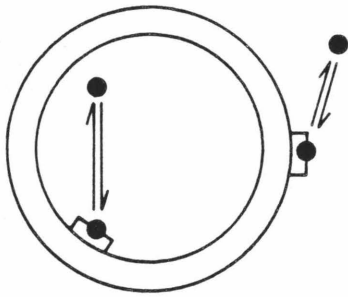
The general strategy is summarized in Fig. 1, where two populations of NMR-visible chloride binding sites are shown to be on opposite sides of the membrane and exposed to different solution compartments. When solution chloride exchanges sufficiently slowly between compartments (Fig. 1a), the internal and external solution chloride populations give rise to distinct  $^{35}\text{Cl}$  NMR resonances. The internal resonance has a linebroadening that stems solely from internal chloride binding sites; similarly, the external resonance has a linebroadening that stems solely from external sites. In contrast, when solution chloride exchanges sufficiently rapidly between compartments (Fig. 1b), a single exchange-averaged solution chloride resonance is observed. The linebroadening of this average resonance is the sum of contributions from both the internal and external sites. Thus, through proper design of the compartmentalized system, chloride binding sites that are in different compartments can be observed either separately (Fig. 1a) or simultaneously (Fig. 1b).

Using both types of compartmentalized system, I now show that the band 3 transport sites observed in the previous chapter (7) are found on both surfaces of the red cell membrane. Also described here is the first direct observation of transport site recruitment in the band 3 system. Recruitment of transport sites to the extracellular-facing conformation is achieved using either DNDS or pNBS. These results show that anion exchange by band 3 proceeds via an alternating site mechanism, in which a single functional transport site is

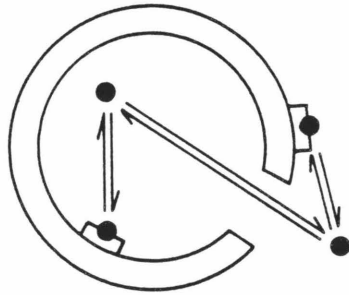
Figure 1

Exchange of chloride between compartments. a) Slow exchange: the internal and external compartments are separated by a sealed membrane. b) Rapid exchange: the same compartments are separated by a leaky membrane.

a



b



alternately exposed to opposite sides of the membrane.

#### MATERIALS AND METHODS

Materials. 4,4-dinitrostilbene-2-2'-disulfonic acid, disodium salt, was purified and analyzed as described previously (11). p-Nitrobenzenesulfonate, sodium salt (pNBS, Kodak) was prepared as follows: 10 g pNBS was dissolved in 50 ml 1 N NaOH; 25 ml H<sub>2</sub>O saturated with NaCl was added, and the solution was cooled overnight at 4° C. The resulting crystals were isolated by filtration, washed with ice cold saturated NaCl and dried in a dessicator under vacuum. Thin layer chromatography on silica gel plates (solvent n-butanol saturated with H<sub>2</sub>O, or 1-propanol:NH<sub>4</sub>OH:H<sub>2</sub>O (6:3:2)) and on n-octyl reverse phase plates (solvent MeOH:H<sub>2</sub>O:con HCl (36:23:1)) showed a single spot. When dissolved in water the product gave a single absorption maximum at 264 nm and was calculated to be ≥ 97% pure using the extinction coefficient  $\epsilon_{264} = 9310$  (17). All other chemicals used were reagent grade or better.

Preparation of leaky ghost membranes. Freshly outdated human packed red cells were a kind gift of the Los Angeles Chapter of the American Red Cross. Leaky ghost membranes were prepared exactly as described previously (11). The final pellet was stored at 4° C in 5P8(+) buffer (5 mM NaH<sub>2</sub>PO<sub>4</sub>, pH to 8 with NaOH, 130 μM dithiothreitol and 10 μM phenylmethylsulfonyl fluoride (PMSF)).

Crushed ghost membranes. The pellet from the leaky ghost prep was diluted with an equal volume of ice cold 2X NMR buffer (see below), then 8 ml aliquots were transferred to 12 ml polysulfone centrifuge

tubes (Sorvall). Some of the tubes were centrifuged at 20,000 rpm in a Sorvall SS-34 rotor ( $48,000 \times g_{\max}$ ) for 2 h to produce a pellet of crushed ghosts. The pellet was resuspended without removal of supernatant by vortexing and by drawing the suspension into a Pasteur pipet before expelling the suspension toward the bottom of the tube to free any remaining pellet. The morphology of the crushed ghosts was verified by phase contrast microscopy.

Sonicated ghost membranes. The pellet from the leaky ghost prep was diluted with an equal volume of ice cold 2X NMR buffer (see below), then 8 ml aliquots were transferred to 12 ml polysulfone centrifuge tubes. Where appropriate the membranes were crushed and resuspended as above before sonication. Samples in the specified tubes were sonicated for 10 min on ice using a Heat Systems-Ultrasonics Model W225R sonicator at output setting 7 with a 75% duty cycle. During sonication nitrogen was blown over the top of the sample to inhibit the oxidation of lipids. The membrane suspension went from opaque to semi-transparent upon sonication.

Sealed right-side-out vesicles. These vesicles (ROV) were prepared essentially as described (18) with the following modifications. All buffers were ice cold and all manipulations were on ice. Immediately after isolation of the final leaky ghost pellet, 6 ml of pellet were added to 240 ml of 0.5P8(+) (or 0.5 mM  $\text{NaH}_2\text{PO}_4$ , pH to 8 with NaOH, 130  $\mu\text{M}$  dithiothreitol and 10  $\mu\text{M}$  PMSF) in each of six or twelve 250 ml polysulfone centrifuge bottles (Sorvall). The membranes were incubated 1-2 h; then 2.4 ml of 10 mM  $\text{MgSO}_4$  was added to each bottle with a syringe, and the membranes were pelleted by centrifugation at 13,000 rpm in a

GSA rotor ( $27,000 \times g_{\max}$ ) for 35 min. The pellets were immediately pooled and diluted with 1/3 part 0.5 P8(+); then vesiculation was carried out by passing the suspension four times through a 27 gauge needle on a 2.5 ml syringe. The homogenate was stored at 4° C.

The following day the ROV were separated from contaminating membranes essentially as described (19) with the following modifications. Each 4 ml aliquot of pellet was diluted with 15 ml of 0.5P8(+), 0.1 mM  $\text{MgSO}_4$ . The resulting 19 ml volume was layered on top of 19 ml of a 4% wt/vol Dextran (avg MW = 64,000; Sigma) solution containing 0.5P8(+), 0.1 mM  $\text{MgSO}_4$  in a 40 ml cellulose nitrate ultracentrifuge tube (Beckman). Sealed vesicles were isolated by ultracentrifugation at 20,000 rpm in a Beckman SW-27 rotor ( $50,000 \times g_{\text{avg}}$ ) for 45 min. The sealed vesicles, which remain near the density interface, were removed using a Pasteur pipet from the unsealed membranes, which pellet in the bottom of the tube. The isolated ROV were pooled and stored at 4° C.

On the day they were used, the ROV were washed (net dilution 1/100) with 5P8(+), 0.1 mM  $\text{MgSO}_4$ . Each 10 ml aliquot of ROV was diluted with 40 ml buffer in a 50 ml polysulfone centrifuge bottle (Sorvall); then the ROV were pelleted at 15,000 rpm in a Sorvall SS-34 rotor ( $27,100 \times g_{\max}$ ) for 30 min, followed by removal of supernatant, resuspension in 40 ml of fresh buffer and recentrifugation. The washed pellets were pooled and used to make  $^{35}\text{Cl}$  NMR samples. Finally, after completion of the  $^{35}\text{Cl}^-$  linebroadening assay, the sealing and sidedness of the ROV were examined using the enzyme assays described below.

Intact red cells. The entire preparation was carried out at 0° to 4° C. Two units of outdated or freshly drawn packed red cells were

mixed and aliquoted into six 250 ml centrifuge bottles, then suspended in PBS (150 mM NaCl, 10 mM NaH<sub>2</sub>PO<sub>4</sub>, pH to 8 with NaOH, 2 mM D-glucose). The efficiency of this wash and all subsequent washes was maximized by filling the centrifuge bottles to maximum capacity with buffer. The cells were pelleted by centrifugation at 8000 rpm in a Sorvall GSA rotor (10,400 X g<sub>max</sub>) for 20 min; then the supernatant and buffy coat were removed by aspiration. The cells were washed twice again by resuspending each time in PBS, then pelleting at 3000 rpm (1500 X g<sub>max</sub>) for 10 min, then aspirating away the supernatant. In order to increase the intracellular chloride concentration to 250 mM, the concentration used in the NMR experiments, the cells were washed with cell buffer (250 mM NaCl, 5 mM NaH<sub>2</sub>PO<sub>4</sub>, pH to 8 with NaOH, 4 mM D-glucose). In each of three washes, the cells were resuspended in cell buffer, then pelleted at 11,000 rpm (19,700 X g<sub>max</sub>) for 20 min; then the supernatant was removed. After washing, the pellets were pooled, mixed with 3 volumes of cell buffer and stored at 4° C. The following day 25 ml aliquots of the suspension were placed in 50 ml polysulfone centrifuge bottles. In each of three washes the cells were resuspended in cell buffer, then pelleted at 2000 rpm in a SS-34 rotor (500 X g<sub>max</sub>) for 10 min, then the supernatant was removed. Finally, the washed pellets were pooled and diluted with 1/3 volume of cell buffer.

Preparation of <sup>35</sup>Cl NMR samples. Most of the experiments presented here involve comparison of leaky ghost membranes with a different type of membrane system. For each such comparison it was necessary to use only membranes prepared from the same batch of red cells since the number of band 3 molecules per cell can vary for different donors.

Thus, membranes to be compared were prepared simultaneously from the same batch of red cells and stored at 4° C for no more than two days. NMR samples to be compared were prepared simultaneously and were stored on ice until  $^{35}\text{Cl}$  NMR analysis that same day.

When crushed or sonicated ghosts were compared to leaky ghosts, NMR samples were prepared as follows. The final pellet from the leaky ghost prep was diluted with an equal volume of ice-cold 2X NMR buffer (500 mM  $\text{NH}_4\text{Cl}$ , 5 mM  $\text{NaH}_2\text{PO}_4$ , 40%  $\text{D}_2\text{O}$ , pH to 8 with  $\text{NH}_4\text{OH}$ ). The resulting suspension was aliquoted and, where appropriate, the aliquots were crushed or sonicated as above. Then to some aliquots 40 mM DNDS in  $\text{H}_2\text{O}$  or 1 M pNBS in  $\text{H}_2\text{O}$  was added to yield 1 mM DNDS or 50 mM pNBS total concentration. To the other aliquots sufficient  $\text{H}_2\text{O}$  was added so that the total volume was the same for all aliquots.

Leaky ghost membranes, prepared as just described, were also compared to ROV. The ROV were prepared by diluting the freshly washed ROV pellet with an equal volume of ice-cold 2X NMR buffer containing 0.1 mM  $\text{MgSO}_4$ , followed by incubation for 2-4 h on ice to ensure equilibration of  $\text{NH}_4\text{Cl}$  across the sealed membranes (20). The suspension was aliquoted, and  $\text{H}_2\text{O}$  or 40 mM DNDS was added as for leaky ghosts.

Leaky ghost membranes, prepared as described above, were also compared to intact red cells. Lysis of red cells releases hemoglobin, which interferes with the  $^{35}\text{Cl}^-$  linebroadening assay. This interference was minimized by using gentle inversion to suspend red cells and by prewetting all surfaces with cell buffer. First, the freshly washed suspension of red cells was diluted with an equal volume of 250 mM  $\text{NaCl}$ , 5 mM  $\text{NaH}_2\text{PO}_4$ , pH to 8 with  $\text{NaOH}$ , 40%  $\text{D}_2\text{O}$ . The resulting suspension was

stored on ice for 1 hr to ensure equilibration; then 10 ml aliquots of the suspension were placed in 12 ml polysulfone centrifuge tubes. To each aliquot either 20 mM DNDS in cell buffer or cell buffer was added to yield 1 mM DNDS or 0 mM DNDS, as appropriate. Just before taking its NMR spectrum, the aliquot was resuspended, and 4 ml was transferred to a prewetted NMR tube. The remaining aliquot was stored on ice for subsequent analysis of the supernatant. After completion of  $^{35}\text{Cl}$  NMR analysis of the cell samples, the centrifuge tubes containing the remaining aliquots were centrifuged at 2000 rpm in a SS-34 rotor ( $500 \times g_{\text{max}}$ ) for 10 min. The supernatant was transferred to a clean tube and centrifuged at 13,000 rpm ( $20,400 \times g_{\text{max}}$ ) for 20 min. An aliquot of 4 ml was removed from the resulting supernatant and placed in an NMR tube.

The final step in NMR sample preparation was to load a membrane or cell suspension into a 10 mm diameter NMR tube. A 4 ml sample was loaded into each tube; this volume was sufficient to completely fill the receiver coil in the NMR probe. In this case the effective sample size is simply the volume defined by the receiver coil so that the effective sample size is independent of small changes in the total sample volume.

The  $^{35}\text{Cl}^-$  linebroadening assay. The  $^{35}\text{Cl}^-$  linebroadening of each sample of membranes, cells, or supernatant was measured at 8.8 MHz exactly as described previously using 10 mm NMR tubes (11). The frequency of 8.8 MHz was chosen because preliminary experiments at 19.6 MHz indicated that the linebroadening due to inward-facing band 3 transport sites becomes too small to measure easily at this higher frequency. (The

frequency dependence of a particular chloride binding site depends upon the characteristics of that site (21).)

Analysis of  $^{35}\text{Cl}$  NMR samples. Samples of leaky ghosts, crushed ghosts, sonicated ghosts or ROV were stored at 4° C overnight. Then total protein concentrations were determined using the modified (22) Lowry procedure (23) developed for use with membrane proteins. These protein concentrations were used to normalize the  $^{35}\text{Cl}^-$  linebroadening to the units Hz per mg/ml total membrane protein, and the resulting linebroadenings of triplicate samples were averaged. The DNDS-insensitive linebroadening was defined as the linebroadening observed in the presence of 1 mM DNDS, while the DNDS-sensitive linebroadening was defined as the decrease in the linebroadening caused by 1 mM DNDS (11). For each membrane system, the DNDS-sensitive and DNDS-insensitive linebroadenings were determined, then were divided by the corresponding linebroadenings of leaky ghost membranes obtained in the same experiment. This division yielded DNDS-sensitive and DNDS-insensitive linebroadenings relative to leaky ghost membranes (see Fig. 2)

The use of these relative linebroadenings ensured that when leaky ghost membranes were compared to crushed ghosts, sonicated ghosts, or ROV, the same number of band 3 molecules was compared. This approach required that 1) the comparison always involve membranes prepared from the same batch of red cells, and 2) the ratio of band 3/total protein be the same for such membranes. Here the first requirement was always satisfied by experimental design. The second requirement was necessarily satisfied when leaky ghosts were compared to crushed or sonicated ghosts since these samples were always made from identical aliquots of the same

batch of leaky ghosts, and neither crushing nor sonication changed the composition of the sample. The second requirement was also satisfied when leaky ghosts were compared to ROV since the ratio of band 3/total membrane protein did not change when ROV were made from leaky ghosts (39).

Samples of intact red cells and leaky ghosts were stored at 4° C overnight. Then the number of ghosts or cells per ml was determined by counting NMR buffer dilutions of the samples using a Petroff-Hauser counting chamber and a phase-contrast microscope. The leaky ghost counts were used to convert the linebroadenings of leaky ghost samples to the units Hz per ghost/ml, and the resulting linebroadening of triplicate samples was averaged. For intact red cells, the linebroadening of each sample was first corrected for the presence of extracellular hemoglobin by subtraction of the supernatant linebroadening. Then the corrected linebroadening was converted to the units Hz per cell/ml, and the resulting linebroadenings of triplicate samples were averaged. Finally, the DNDS-sensitive and DNDS-insensitive linebroadenings of leaky ghosts and intact red cells were determined and were divided by the corresponding linebroadenings of leaky ghosts obtained in the same experiment. This procedure yielded DNDS-sensitive and DNDS-insensitive linebroadenings relative to leaky ghost membranes. The use of these relative linebroadenings ensured that the same number of band 3 molecules was compared since a leaky ghost and a red cell prepared from the same batch of cells possess the same number of band 3 molecules.

Enzyme assays. The glyceraldehyde-3-phosphate dehydrogenase and the acetylcholine esterase assays used here were exactly as previously described (18).

Leaky ghost hole size. The size of the leaky ghost holes in NMR samples was examined using the ghost membrane protein glyceraldehyde-3-phosphate dehydrogenase (G3PDH). This protein binds to the intracellular surface of the membrane but is released at high ionic strength (24). Thus, when leaky ghosts are suspended in NMR buffer containing 250 mM  $\text{NH}_4\text{Cl}$ , G3PDH is released from the membrane. If the membrane holes are sufficiently large, the G3PDH can be washed away from the membranes. If the membrane holes are instead too small, the G3PDH will be trapped in the internal space and will not be washed away. To resolve these two possibilities, 2 ml of pellet from the leaky ghost prep was brought to 250 mM  $\text{NH}_4\text{Cl}$  by addition of 4M  $\text{NH}_4\text{Cl}$ , pH 8, on ice. The resulting suspension was incubated on ice for 5 h. Approximately 60% of the volume of this suspension was intracellular volume; thus, even if the holes closed after G3PDH had diffused throughout the sample, 60% of the G3PDH would still be trapped inside the membranes. Following the incubation the membranes were washed four times by suspending the pellet to 10 ml in a 12 ml polysulfone centrifuge tube in 240 mM  $\text{NH}_4\text{Cl}$ , 5 mM  $\text{NaH}_2\text{PO}_4$ , pH 8, then pelleting at 20,000 rpm in a SS-34 rotor (48,000 X  $g_{\text{max}}$ ), then aspirating away the supernatant. For comparison, duplicate unwashed membranes were prepared and handled in parallel to the washed membranes except that supernatants were not removed nor additional buffer added in the washing steps. The washed and unwashed membranes were stored overnight at 4° C; then G3PDH activity was measured as above.

Microscopy. NMR samples were routinely diluted with NMR buffer and examined using a Nikon Optiphot phase-contrast microscope. Photographs were taken using Polaroid type 667 land film.

Electron microscopy of NMR samples was conducted using a negative stain technique. NMR samples were diluted with NMR buffer and prepared exactly as described elsewhere (25) using 4% ammonium molybdate, pH 7.0, as the stain. A Phillips EM 201 electron microscope was used, and images were recorded on 35 mm film to enable hand measurement of membrane sizes.

Statistics. For each membrane system, the linebroadening of triplicate samples was measured as described above. The resulting DNDS-sensitive and DNDS-insensitive linebroadenings, relative to leaky ghost membranes, defined a single experiment. From three to seven such experiments were carried out for each membrane system where each experiment involved a different batch of red cells and was performed on a different day from other experiments. The results of the different experiments were averaged to yield the average DNDS-sensitive and DNDS-insensitive linebroadenings relative to leaky ghost membranes (Fig. 2).

All other confidence limits for averages are given as  $\pm$  one standard deviation for  $n \geq 3$ .

## RESULTS

Strategy of sidedness resolution. The problem at hand is to resolve the chloride binding sites in the intracellular and extracellular compartments of the red cell membrane. (Here only right-side-out membrane systems are used; as a result, intracellular = internal and extracellular = external). The specific approach used is straightforward. First, the sum of the  $^{35}\text{Cl}^-$  linebroadenings due to both internal and external

sites is observed using a red cell membrane system in which intercompartmental chloride exchange is fast. Then the linebroadening due to external sites alone is observed using a red cell membrane system in which intercompartmental chloride exchange is slow. This approach utilizes both the rapid and the slow exchange limits of intercompartmental chloride exchange, where each limit is defined by the intrinsic timescale of the  $^{35}\text{Cl}$  NMR experiment.

Rapid intercompartmental exchange. The rapid exchange limit occurs when the typical solution chloride ion makes repeated visits to each compartment, and to chloride binding sites within each compartment, during the intrinsic NMR timescale. The length of this timescale depends upon the characteristics of the experiment; here it is always  $\leq 0.03$  sec (39). When chloride ion rapidly samples different compartments, the solution chloride resonance behaves as if barriers between compartments did not exist. Instead, a given ion experiences an average environment composed of contributions from each compartment it visits during the NMR timescale. Such averaging forces the multiple compartments in the rapid exchange network to give rise to a single  $^{35}\text{Cl}$  NMR resonance. The total linebroadening ( $\delta_T$ ) of this exchange-averaged resonance is

$$\delta_T = \frac{\sum_i (\alpha_i \cdot \sum_c n_c (X_i \text{Cl}))}{\sum_c n_c (\text{Cl}^-)} \quad (1)$$

where the first sum is over each type of binding site ( $i$ ) and the second sum is over each compartment ( $c$ ) within the exchange-averaged region.

The proportionality constant  $\alpha_i$  is characteristic of the  $i$ 'th type

of site,  $n_c(X_iCl)$  is the total number of chloride ions bound to that type of site in compartment  $c$ , and  $n_c(Cl^-)$  is the total, stoichiometric number of chloride ions in compartment  $c$ . Equation 1 states that when intercompartmental exchange is rapid, sites in different compartments make additive contributions to the linebroadening<sup>1</sup>.

Slow intercompartmental exchange. Chloride binding sites in a particular compartment can be uniquely observed when the solution chloride in that compartment is isolated on the NMR timescale. Complete isolation is always achieved if the typical chloride ion in the target compartment remains there for at least 0.03 sec (39).

The resulting target compartment resonance will generally overlap interfering resonances from other compartments, but a variety of approaches can be used to isolate the target resonance, which possess the linebroadening

$$\delta_c = \frac{\sum_i \alpha_i \cdot n_c(X_iCl)}{n_c(Cl^-)} \quad (2)$$

where the sum is over each type of binding site ( $i$ ) in the target compartment  $c$ . This equation states that when chloride exchanges slowly between compartments, the linebroadening is composed of the additive contributions from sites in the target compartment alone.

Red cell membrane systems. Equations 1 and 2 can be specialized for the case at hand. The sum of the  $^{35}Cl^-$  linebroadenings due to internal and external sites can be measured using a red cell membrane

system in which chloride exchanges rapidly between the internal and external compartments. Now Equation 1 is applicable, and adapting it to the situation at hand, we obtain

$$\delta_T = \delta_I + \delta_E = \frac{\sum_i (\alpha_i \cdot \sum_I n_I(X_i, Cl))}{n_E(Cl^-) + \sum_I n_I(Cl^-)} + \frac{\sum_i \alpha_i \cdot n_E(X_i, Cl)}{n_E(Cl^-) + \sum_I n_I(Cl^-)} \quad (3)$$

where one external compartment E and multiple internal compartments I exist within the exchange-averaged region, and  $n_c(S)$  is the total number of species S within compartment c. Alternatively, the linebroadening due to external sites alone can be measured using a red cell membrane system in which chloride exchanges slowly between the internal and external compartments. Here Equation 2 is applicable and we write

$$\delta_E' = \frac{\sum_i \alpha_i \cdot n_E(X_i, Cl)}{n_E(Cl^-)} \quad (4)$$

where  $n_E(S)$  is the total number of species S in the isolated external compartment E. After  $\delta_E'$  is measured, it is converted to  $\delta_E$  using the following scaling relationship, obtained by comparing Equations 3 and 4:

$$\delta_E = \delta_E' \cdot \left( \frac{n_E(Cl^-)}{n_E(Cl^-) + \sum_I n_I(Cl^-)} \right) \quad (5)$$

Finally, the results of Equations 3 and 5 are used to calculate the linebroadening due to internal sites ( $\delta_I = \delta_T - \delta_E$ ).

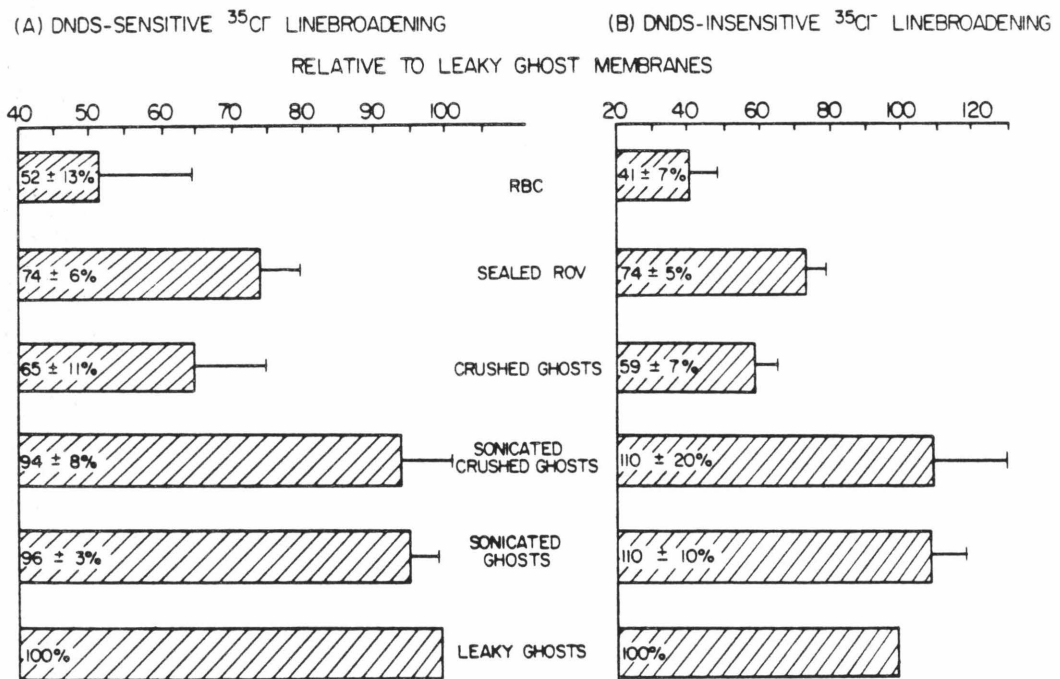
The quantities  $\delta_T$  (Equation 3) and  $\delta_E$  (Equation 5) are obtained using different red cell membrane systems, but comparison of these

quantities assumes that the corresponding terms in Equations 3 and 5 have the same value: this assumption can be tested by examining the terms  $\alpha_i$ ,  $n_E(\text{Cl}^-) + \sum_I n_I(\text{Cl}^-)$ , and  $n_E(X_i\text{Cl})$ . First, the quantity  $\alpha_i$  is always the same since the structural and exchange parameters for the  $i$ 'th type of site are independent of the red cell membrane system used. Second, the quantity  $n_E(\text{Cl}^-) + \sum_I n_I(\text{Cl}^-)$  is fixed since the samples used here all have the same total number of chloride ions. Similarly, the quantity  $n_E(X_i\text{Cl})$  is fixed since the linebroadenings used here are all normalized to the same number of band 3 molecules. Thus, the comparison of  $\delta_T$  and  $\delta_E$  to ascertain  $\delta_I$  is valid, and together Equations 3 and 5 can be employed to probe both surfaces of the red cell membrane.

The results of such an analysis are summarized in Fig. 2. In the previous chapter (11) I demonstrated that band 3 transport sites give rise to DNDS-sensitive  $^{35}\text{Cl}^-$  linebroadening, while low-affinity chloride binding sites give rise to DNDS-insensitive  $^{35}\text{Cl}^-$  linebroadening. Both types of linebroadening are presented in Fig. 2 for a variety of red cell membrane systems. In the intact red cell, ROV, and crushed ghost systems, the exchange of chloride between compartments is slow, and the linebroadenings in Fig. 2 correspond to  $\delta_E$  (Equation 5). In the sonicated crushed ghost, sonicated ghost, and leaky ghost systems the exchange of chloride between compartments is fast, and the linebroadenings in Fig. 2 correspond to  $\delta_T$  (Equation 3). In every case  $\delta_E$  is nonzero but is significantly less than  $\delta_T$ , indicating that both  $\delta_E$  and  $\delta_I$  contribute significantly to  $\delta_T$  so that chloride binding sites on both

Figure 2

Sidedness of the red cell membrane  $^{35}\text{Cl}^-$  linebroadening. Shown are a) the DNDS-sensitive linebroadening due to band 3 transport sites, and b) the DNDS-insensitive linebroadening due to low-affinity chloride binding sites. In the intact red cell (RBC), right-side-out vesicle (ROV) and crushed ghost systems, only sites on the external surface of the membrane are observed. In the sonicated crushed ghost, sonicated ghost and leaky ghost systems, sites on both sides of the membrane are observed. The upper three linebroadenings are missing the contribution from the internal sites and thus are smaller than the lower three linebroadenings.



sides of the red cell membrane are observed. In the following, these results are discussed in detail for each system of interest.

Leaky ghost membranes. These membranes retain a structure and composition essentially the same as that of the native red cell membrane (26). However, each leaky ghost membrane possesses a single large hole produced by osmotic shock during membrane isolation (27,28), and this hole controls the exchange of chloride between the internal and external compartments. In the NMR experiments presented here, the hole remains large enough to be permeable to glyceraldehyde-3-phosphate dehydrogenase. This enzyme binds to the internal surface of the membrane (24) but can be quantitatively removed even after incubation under NMR sample conditions (Table 1). The Stokes radius of this protein is  $43 \text{ \AA}$ ; thus the ghost membranes in NMR samples must possess holes that are at least this large.

These holes allow rapid exchange of chloride between the internal and external compartments so that the chloride populations in these compartments are exchange-averaged on the NMR timescale (39). The resulting DNDS-sensitive linebroadening is  $2.3 \pm .2 \text{ Hz per mg/ml}$  total ghost protein, while the DNDS-insensitive linebroadening is  $4.5 \pm .7 \text{ Hz per mg/ml}$ . (These values are the average of the leaky ghost linebroadenings used in Fig. 2). The DNDS-insensitive linebroadening has a large standard deviation due to differences between batches of membranes, since for samples from the same batch the average standard deviation was only

Table 1. The escape of glyceraldehyde-3-phosphate dehydrogenase from holes in leaky ghost membranes prepared for  $^{35}\text{Cl}^-$  NMR.

	G3PDH Activity <sup>a</sup>
Without washing	1.00 ± .03
With washing	0.00 ± .01

<sup>a</sup>Glyceraldehyde-3-phosphate dehydrogenase activity, expressed in units of  $\mu\text{moles NADH produced}/(\text{min} \cdot \text{mg total membrane protein})$

$0.14 \pm 0.05$  Hz per mg/ml. As a result, only those membrane systems from the same batch of red cells are compared in the present experiments.

Because exchange averaging occurs, the linebroadening observed in the leaky ghost system could be due to sites in either the internal or external compartments. If the exchange is very rapid, the sites in each compartment could contribute to the observed linebroadening exactly as if the barriers between compartments did not exist. In this case the observed linebroadening should not change when the intercompartmental exchange rate is increased. This prediction can be tested by comparing the linebroadenings of leaky ghost membranes and sonicated ghost membranes.

Sonicated ghost membranes. When leaky ghost membranes (diameter  $6 \mu\text{m}$ ) are sonicated, electron microscopy shows that the resulting unsealed membrane fragments have an average diameter of  $90 \pm 80$  nm (range 20-380 nm for 37 fragments). Although sonication damages the barrier between the internal and external compartments of leaky ghosts (24), no significant change in the linebroadening is observed (Fig. 2). This result indicates that exchange averaging of the internal and external compartments is essentially complete even for unsonicated samples of leaky ghosts<sup>2</sup>. Other experiments with the detergent saponin, as well as experiments with inside-out vesicles, confirm this conclusion (Appendices III, IV). In the remaining red cell-derived membrane systems, the internal and external compartments are isolated, rather than completely exchange-averaged, on the NMR timescale.

Intact red cells. These cells were always  $\geq 94\%$  intact (from measurement of supernatant hemoglobin). In intact red cells the chloride

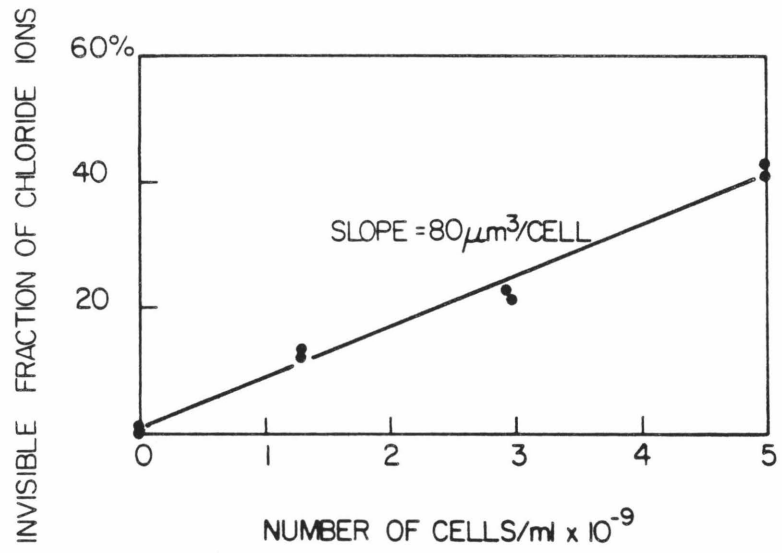
ions in the internal and external compartments are isolated on the NMR timescale despite the exchange of chloride across the membrane by band 3 (39). Thus, the internal and external solution chloride populations give rise to separate  $^{35}\text{Cl}$  NMR resonances.

Solution chloride in the external compartment can be observed without interference since the internal compartment contains a large hemoglobin concentration (4 mM). This protein binds chloride, resulting in an internal solution chloride linewidth that is  $> 300$  Hz (data not shown, also (30)). Such a broad resonance could not be observed under the conditions employed here; thus, the internal chloride ions are expected to be invisible. This prediction is confirmed by the integration data of Fig. 3, where the slope yields the invisible volume of solution chloride per red cell. The best-fit slope is  $80 \mu\text{m}^3$  invisible volume per cell, which is the entire internal volume of the red cell (31).

Thus, in this system the observed resonance stems completely from the external solution chloride population. As a result, the linebroadening specifically associated with chloride binding sites on the external surface of the red cell membrane can be measured. Both DNDS-sensitive and DNDS-insensitive linebroadenings are present (Fig. 2); therefore the external surface of the red cell membrane possesses both band 3 transport sites and low-affinity chloride binding sites. The indicated linebroadenings (Fig. 2) have been corrected for the invisible internal chloride ions to enable direct comparison with leaky ghost membranes. Both the DNDS-sensitive and the DNDS-insensitive linebroadenings are significantly smaller than the corresponding ghost membrane

Figure 3

Effect of intact red cells on the size of the  $^{35}\text{Cl}$  NMR-invisible chloride population. The  $^{35}\text{Cl}$  NMR resonance of a blank sample was integrated over a 500 Hz region centered on the resonance to yield A. Then the  $^{35}\text{Cl}$  NMR resonance of a sample containing the indicated concentration of intact red cells was integrated to yield B, and the fraction of invisible  $^{35}\text{Cl}^-$  ions was  $1-B/A$ . Since the chloride concentration was homogeneous within these samples, the invisible fraction of  $^{35}\text{Cl}^-$  ions is equivalent to the invisible fraction of sample volume. Thus, the slope is expressed as the missing volume per red cell.



linebroadenings ( $p < 0.01$  in both cases), indicating that band 3 transport sites and low-affinity chloride binding sites each reside on the internal as well as the external membrane surface.

Sealed right-side-out vesicles. Under certain conditions, ghost membranes break up to form sealed right-side-out vesicles (ROV (18)). The resonance due to external solution chloride can be specifically observed in this system due to the integrity of the ROV. Integrity can be measured with enzymatic assays utilizing glyceraldehyde-3-phosphate dehydrogenase (G3PD) or acetylcholinesterase (ACE) (18). Both enzymes are native to the red cell membrane; G3PD binds to the intracellular surface and ACE binds to the extracellular surface. The assays used here employ charged substrates that are added to the external solution and cannot cross a sealed membrane. Thus, if an enzyme is sequestered within the internal space of a sealed vesicle, the activity of that enzyme is less than that observed after the membrane is unsealed by detergent. Analysis of ROV indicates that the vesicles were  $86 \pm 7\%$  right-side-out and sealed (Table 2).

Electron microscopy shows an average ROV diameter of  $0.6 \pm 0.4 \mu\text{m}$  (range  $0.2 - 2.2 \mu\text{m}$  for 28 vesicles), yielding an external/internal volume ratio of  $> 100/1$  in the samples used here, so the observed  $^{35}\text{Cl}$  NMR resonance is essentially that of external solution chloride alone. For sealed ROV, the external solution chloride is isolated from the internal compartment on the NMR timescale, despite the exchange of chloride across the membrane by band 3 (39). Thus, the linebroadening due to sites on the external surface of the ROV can be specifically observed. Both DNDS-sensitive and DNDS-

Table 2. Sealing and sidedness in different red cell membrane systems

Membrane System	Fraction Sealed and Right-side-out <sup>a</sup>	Fraction Sealed and Inside-out <sup>b</sup>	Fraction Unsealed <sup>c</sup>
Leaky ghosts	2 ± 3%	-4 ± 1%	102%
Crushed ghosts	0 ± 6%	-2 ± 1%	102%
Sonicated ghosts	0 ± 4%	6 ± 2%	94%
Sonicated crushed ghosts	0 ± 0%	8 ± 3%	92%
Right-side-out vesicles	86% ± 7%	2 ± 4%	12%

<sup>a</sup>Determined by glyceraldehyde-3-phosphate dehydrogenase activity measurements.

<sup>b</sup>Determined by acetylcholinesterase activity measurements. Negative values stem from a small but reproducible inhibition of acetylcholinesterase by triton-X-100.

<sup>c</sup>Determined by subtraction of the left and middle columns from 100%.

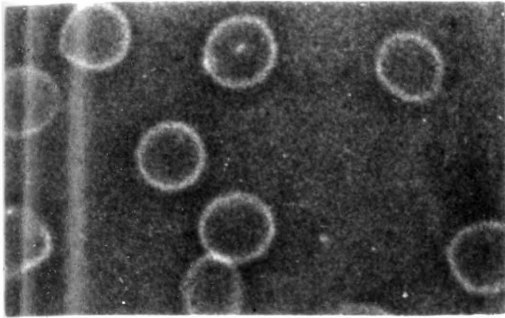
insensitive linebroadenings are present (Fig. 2), and these linebroadenings are significantly smaller than the corresponding linebroadenings due to leaky ghost membranes ( $p < 0.001$  in both cases). These results corroborate the evidence from intact cells and indicate that the internal and external red cell membrane surfaces each possess both band 3 transport sites and low-affinity chloride binding sites.

Crushed ghost membranes. The leaky ghost membranes used here exhibit a variety of shapes that range from spherical to the biconcave disk shape reminiscent of native red cells. Phase-contrast microscopy reveals that most leaky ghosts (86%) possess significant internal volume; only a minority (14%) are crushed so that the internal volume is negligible (75 membranes counted). However, when ghost membranes in NMR buffer are centrifuged with sufficient centripetal force for a sufficient period of time, nearly all of the membranes collapse to form crushed ghost membranes. After centrifugation, most membranes (91%) were crushed, while a few (9%) retained open structures (74 membranes counted). The morphology of ghost membranes before and after is shown in Fig. 4. Careful examination showed that in each case fewer than 1% of the membranes were found in aggregates.

Samples of crushed ghost membranes give rise to a solution chloride resonance that is dominated by external solution chloride since the external/internal volume ratio in such samples is  $> 100/1$  (assuming  $\text{vol ghost} > 30 \times \text{vol crushed ghost}$ , see Fig. 4). Internal chloride binding sites do not significantly contribute to the linebroadening of the observed resonance because, when leaky ghost membranes are crushed, the intercompartmental exchange rate is forced to go from the rapid exchange limit to the slow exchange limit by two factors: 1) the relevant NMR timescale is shortened by an increase in the binding site

Figure 4

Morphology of leaky ghosts and crushed ghosts. NMR samples of a) leaky ghosts and b) leaky ghosts crushed by centrifugation were prepared and then diluted with ice cold NMR buffer. The resulting membranes were photographed using phase-contrast microscopy to show the open structure of leaky ghosts (a) and the collapsed structure of crushed ghosts (b). The photographs were taken in an identical manner: the crushed membranes appear bright because two bilayers are pressed together. The measured diameter of the ghosts was 6.6  $\mu\text{m}$  in each case.



activity within the collapsed internal compartment (39) and  
2) the diffusion of chloride is slowed within the internal compartment since in crushed ghosts this compartment must be largely filled with the lattice-like network of cytoskeletal proteins that are bound to the internal membrane surface. Because the internal chloride binding sites are invisible, both the DNDS-sensitive and DNDS-insensitive chloride linebroadenings (Fig. 2) are smaller than the corresponding leaky ghost linebroadenings ( $p < 0.001$  in both cases). However, sonication of the crushed ghosts shears the membrane so that both membrane surfaces are readily accessible to the bulk solution chloride (see "Sonicated ghosts"; also (29)). As a result the DNDS-sensitive and DNDS-insensitive linebroadenings of sonicated crushed ghosts are restored to the values observed for leaky ghosts (Fig. 2). These data further corroborate the evidence from the intact red cell and sealed ROV systems, which indicate that band 3 transport sites and low-affinity chloride binding sites are each found on both the internal and external surfaces of red cell membranes.

p-Nitrobenzenesulfonate inhibits the  $^{35}\text{Cl}^-$  linebroadening due to band 3 transport sites on both sides of the membrane. The experiments presented here indicate that DNDS inhibits the  $^{35}\text{Cl}^-$  linebroadening that stems from band 3 transport sites on both membrane surfaces. Yet DNDS is known to bind to the extracellular band 3 transport site and has no effect when present on the intracellular side of the membrane (32,33). Note that DNDS has two negative charges that are spatially separated. Thus, the inhibitor could conceivably bind to band 3 with one charge occupying an extracellular

transport site and the other charge occupying an intracellular transport site.

This two-site model of linebroadening inhibition requires two negative charges on the inhibitor molecule. Like DNDS, the inhibitor p-nitrobenzenesulfonate (pNBS) is known to inhibit band 3 by binding to the extracellular transport site (Chapter VII, also (32,34)). Unlike DNDS, the pNBS molecule has only one negative charge. Yet experiments comparing the effects of DNDS and pNBS on the linebroadening of leaky ghost membranes and crushed ghost membranes indicate that these inhibitors behave in exactly the same manner (Table 3). Thus, even though pNBS possesses only a single negative charge, it still inhibits band 3 transport sites on both surfaces of the red cell membrane.

#### DISCUSSION

Comparison of the  $^{35}\text{Cl}^-$  linebroadening of a variety of red cell membrane-derived systems yields a consistent picture (Fig. 2). In exchange-averaged systems (leaky ghosts, sonicated ghosts, sonicated crushed ghosts), band 3 transport sites and low-affinity chloride binding sites on both sides of the membrane are observed. In isolated compartment systems (intact red cells, ROV, crushed ghosts), only the transport sites and low-affinity sites on the extracellular surface of the membrane are observed; the internal sites of each type are hidden. The transport sites are of primary interest here; 60-75% of the transport site linebroadening stems from outward-facing sites, while the inward-facing sites give rise to the remainder. The two orientations of transport site could differ in

Table 3. Comparison of the effects of DNDS and pNBS on leaky ghost membranes and crushed ghost membranes

	<sup>35</sup> Cl <sup>-</sup> Linebroadening, Hz per mg/ml Total Membrane Protein			
	Control	1 mM DNDS	50 mM pNBS	1 mM DNDS + 50 mM pNBS
Leaky Ghosts	5.8 ± .1	3.8 ± .1	3.7 ± .1	3.6 ± .1
Crushed Ghosts	3.5 ± .1	2.2 ± .1	2.4 ± .1	2.4 ± .1

structure (1) and/or in accessibility to solution chloride, and the constant  $\alpha_i$  (Equations 1-5) is sensitive to these parameters. Thus, the ratio of  $\alpha_i$  for the two orientations is unknown. As a result, the ratio of the internal and external transport site linebroadenings cannot be used to determine the quantitative distribution of transport sites between the two sides of the membrane (Equation 3). Still, changes in the quantitative distribution can be detected; thus, the  $^{35}\text{Cl}^-$  linebroadening assay can be used to observe directly the recruitment of transport sites from one side of the membrane to the other.

Two inhibitors that recruit transport sites to one side of the membrane are DNDS and pNBS. When present in the extracellular solution, either inhibitor can bind to the outward-facing transport site and thereby competitively inhibit chloride binding to that site (32-34). In contrast, even when present in the intracellular solution, neither molecule can bind to the inward-facing transport site ((32-34); also Chapter VII). Yet DNDS and pNBS each completely eliminate the linebroadening due to band 3 transport sites on both the inner and outer surfaces of the membrane. This simultaneous inhibition of both transport site orientations does not stem from simultaneous occupation of two anion transport sites by one inhibitor molecule since pNBS has only one negative charge. Similarly, simultaneous inhibition is not due to allosteric inhibition of the inward-facing site by an inhibitor molecule bound to the outward-facing site, since each inhibitor exhibits simple competition with substrate for binding to a single transport site on the external surface (chloride competition (33), sulfate competition (32)). Instead, simultaneous inhibition arises from simultaneous recruitment of all band 3 transport sites to

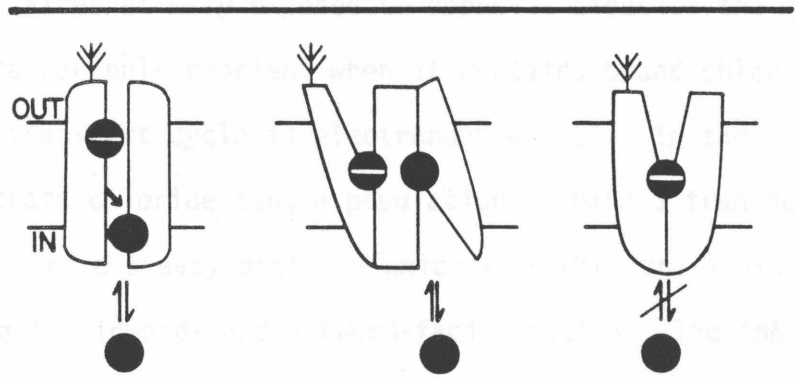
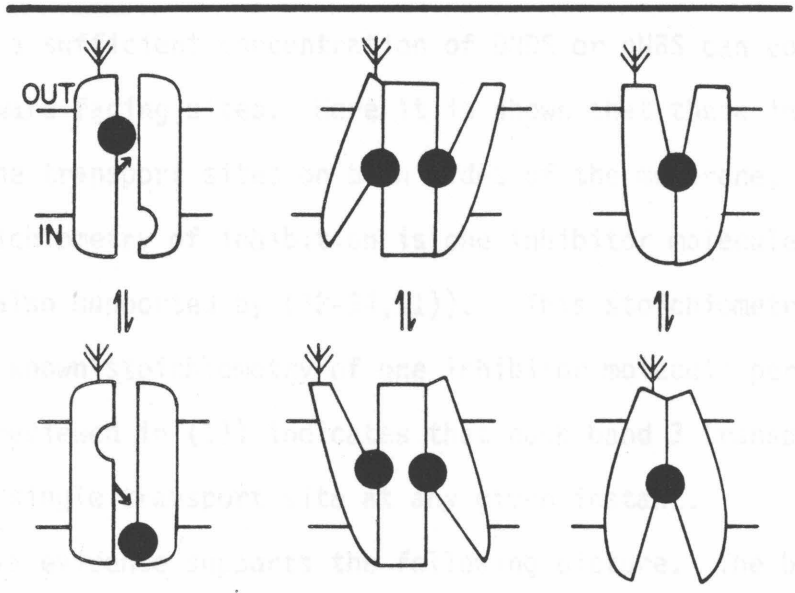
the inhibitor-bound outward-facing conformation. A number of kinetic experiments have previously suggested that a transmembrane gradient of substrate can cause partial (13,14,16) or complete (15) recruitment of transport sites. However, recruitment can only be directly demonstrated by resolving the binding of substrate to the inward- and outward-facing transport sites. Here the first direct observation of transport site recruitment is presented; inhibitors that bind only to the outward-facing site also recruit the inward-facing sites away from the internal compartment.

This result distinguishes between different classes of mechanistic models for band 3-catalyzed anion exchange. In general, these models can be placed in one of three categories: fixed site models (1,35,36) simultaneous transport models (1,37), and alternate transport models (1,2-7,9,10). In fixed-site models, substrate anion migrates between two or more fixed binding sites that are exposed to opposite sides of the membrane (Fig. 5). In simultaneous transport models, two substrate anions bind to opposite sides of the transport unit and are simultaneously transported in opposite directions across the membrane (Fig. 5). A model in which the two anions are simultaneously transported by different band 3 monomers seems particularly attractive since the dimer is thought to be the smallest native form of the protein (1). However, both the fixed-site and simultaneous transport models dictate that inhibitors of the outward-facing transport sites will leave the inward-facing sites intact (Fig. 5). These models are excluded by the observation that DNDS and pNBS each recruit all transport sites to the inhibitor-bound outward-facing conformation, thereby inhibiting the inward-facing sites.

Figure 5

Three general models for band 3-catalyzed anion exchange. Shown for each model are a single transport unit. Upper two rows: a) chloride ion is translocated between fixed sites, the memory gate preserves the electroneutrality of the transport cycle, b) two chloride ions are simultaneously transported in opposite directions to preserve electroneutrality, c) chloride ion is alternately transported in opposite directions to preserve electroneutrality. Lower row: inhibitor occupies the outward-facing site; the inward-facing site is accessible (a,b) or inaccessible (c). These schematic drawings do not specify the number of band 3 monomers per transport unit, nor do they describe the mechanical form of any model; instead, they simply describe the conceptual form of each model.

FIXED SITES      SIMULTANEOUS TRANSPORT      ALTERNATE TRANSPORT



● = SUBSTRATE (Cl<sup>-</sup>)  
 ◐ = INHIBITOR (DNDS, pNBS)

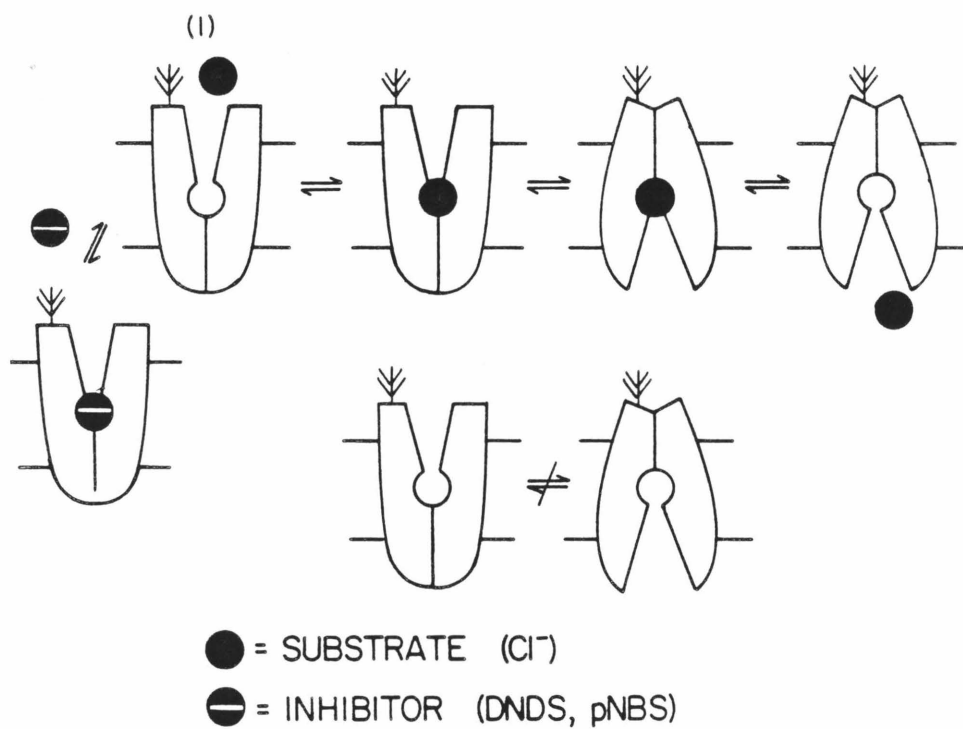
Alternate transport models propose that anion transport in opposite directions occurs in different or alternate steps in the transport cycle (Fig. 5). The simplest general model of the class can be termed the alternating site model (Fig. 6). A characteristic feature of this model is that the transport sites can all be recruited to one side of the membrane so that a sufficient concentration of DNDS or pNBS can completely eliminate the inward-facing sites. Here it is shown that these inhibitors inhibit all of the transport sites on both sides of the membrane, suggesting that the stoichiometry of inhibition is one inhibitor molecule per transport site (also supported by (32-34,11)). This stoichiometry, when coupled with the known stoichiometry of one inhibitor molecule per transport unit (reviewed in (1)) indicates that each band 3 transport unit possesses a single transport site at any given instant.

The available evidence supports the following picture. The band 3 transport unit is an alternating site transporter in which a single transport site is alternatively exposed to opposite sides of the membrane. The transport site can only reorient when it contains bound chloride; as a result, the transport cycle is electroneutral (1). In the presence of substrate chloride ion, a population of band 3 transport units reaches a kinetic steady state in which transport units are distributed among the inward- and outward-facing states. The inhibitors DNDS and pNBS bind to the outward-facing transport site and prevent translocation, thereby shifting the distribution of transport units toward the outward-facing state.

Certain fundamental characteristics of the alternating site mechanism in the band 3 system have yet to be elucidated. Two current

Figure 6

Schematic alternating site model observed for band 3. Starting at state (1), the empty outward-facing site can proceed to the right along the anion exchange pathway, or it can proceed to the left, where it is trapped by inhibitors. The lower pair of empty transport sites depict the negligibly slow transmembrane translocation of any empty transport site. These schematic drawings do not specify the number of band 3 monomers per transport unit, nor do they include non-transport chloride binding sites or describe any mechanical details of the model; instead, they simple describe the conceptual form of the model.

SCHEMATIC ALTERNATING SITE MODEL

models for the transport cycle fall within the alternating site category: the ping-pong model ((3); also discussed (1,4-7,9)) and the two-site ordered-sequential model (10). The transport cycle of the ping-pong model is essentially the same as in Fig. 6, while the transport cycle of the two-site ordered-sequential model is more complicated. In addition to the transport site, the latter model proposes a second anion binding site. This non-transport site is constrained to be NMR silent since  $^{35}\text{Cl}^-$  linebroadening experiments show no evidence of a site distinct from the transport site (11). Both sites move in concert through the transport cycle such that they retain the same transmembrane orientation. However, only one ion is transported by the two sites at each step; thus, the two-site ordered-sequential model is an alternating site model that cannot be resolved from the ping-pong model by the present results. Furthermore, other experiments designed to resolve these models have provided contradictory results (3,38,10). Thus, more work is needed to ascertain the details of the alternating site mechanism in the band 3 system.

## REFERENCES

1. Knauf, P. A. (1979) Curr. Topics in Membranes and Transport 12, 249-363.
2. Gunn, R. B. (1979) Membrane Transport in Biology 2, 59-79.
3. Gunn, R. B., and Frohlich, O. (1979) J. Gen. Physiol. 74, 351-374.
4. Rothstein, A., Ramjeesingh, M., and Grinstein, S. (1980) in Membrane Transport in Erythrocytes (Larsen, V. V., Ussing, H. H., and Wieth, J. O. ed.) Vol. 14, 329-344.
5. Passow, H., Kampmann, L., Fasold, H., Jennings, M., and Lepke, S. Ibid., 345-372.
6. Macara, I. G., and Cantley, L. C. (1981) Biochemistry 20, 5696-5701.
7. Wieth, J. O., and Bjerrum, P. J. (1982) J. Gen. Physiol. 79, 253-282.
8. Solomon, A. K., Chasan, B., Dix, J. A., Lukacovic, M. F., Toon, M. R., and Verkman, A. S. (1982) Biophys. J. 37, 215a.
9. Lowe, A. G., and Lambert A. (1983) Bioch. Biophys. Acta 694, 353-374.
10. Salhany, J. M., and Rauenbeuhler, P. B. (1983) J. Biol. Chem. 258, 245-249.
11. Falke, J. J., Pace, R. J., and Chan, S. I. (1984) J. Biol. Chem. 259, 6481-6491.
12. Dalmark, M. (1975) J. Physiol. 250, 39-64.
13. Knauf, P. A., Tarskis, T., Grinstein, S., Furuya, W. (1980) in Membrane Transport in Erythrocytes (Larsen, V. V., Ussing, H. H., and Wieth, J. O., eds.) Vol. 14, 389-408.
14. Jennings, M. L. Ibid., 450-466.
15. Jennings, M. L. (1982) J. Gen. Physiol. 79, 169-185.
16. Eidelman, O., and Cabantchik, Z. I. (1983) J. Memb. Biol. 71, 149-161.

17. Robinson, J. W., ed. (1974) Handbook of Spectroscopy, CRC Press, Cleveland, Ohio.
18. Steck, T. L. (1974) in Methods in Membrane Biology 2, 245-381.
19. DuPre, A. M., and Rothstein, A. (1981) Bioch. Biophys. Acta 646, 471-478.
20. Gunn, R. B., Dalmark, M., Tosteson, D. C., and Wieth, J. O. (1973) J. Gen. Physiol. 61, 185-200.
21. Forsén, S., and Lindman, B. (1981) Methods of Biochemical Analysis 27, 289-486.
22. Markwell, M.A., Haas, S. M., Bieber, L. L., and Tolbert, N. W. (1978) Analytical Bioch. 87, 206-210.
23. Lowry, O. H., Rosebrough, N. J., Farr, A. L., and Randall, R.J. (1951) J. Biol. Chem. 193, 265-275.
24. Yu, J., and Steck, T. L. (1975) J. Biol. Chem. 250, 9176-9184.
25. Pineric, L., Manery, J. F., Chandry, I. H., and Madapallimattan, G. (1975) Blood 45, 709-724.
26. Lux, S. E. (1979) Nature 281, 426-429.
27. Lieber, M. R., and Steck, T. L. (1982) J. Biol. Chem. 257, 11651-11659.
28. Lieber, M. R., and Steck, T. L. Ibid., 11660-11666.
29. Moore, R. B., and Mannery, J. F. (1981) Arch. Biochem. Biophys. 211, 179-191.
30. Chiancone, E., Norne, J.E., Forsén, S., Bonaventure, J., Bunori, M., Antonini, E., and Wyman, J. (1975) Eur. J. Bioch. 55, 385-390.
31. Tatsumi, N. (1981) Biochem. Biophys. Acta 641, 276-280.
32. Barzilay, M., and Cabantchik, Z. I. (1979) Memb. Bioch. 2, 297-322.
33. Frohlich, O. (1982) J. Memb. Biol. 65, 111-123.

34. Barzilay, M., and Cabantchik, Z. I. (1979) Memb. Bioch. 2, 255-296.
35. Mond, R. (1927) Pfluegers Arch. Gesamte Physiol. Menschen Tiere 217, 618-630.
36. Passow, H. (1969) Prog. Biophys. Mol. Biol. 19, 425-467.
37. Klingenberg, M. (1981) Nature 290, 449-454.
38. Gunn, R. B., and Frohlich, O. (1980) in Membrane Transport in Erythrocytes (Lassen, V. V., Ussing, H. H., and Wieth, J. O., eds.) Vol. 14, 431-449.
39. Falke, J. J., Pace, R. J., and Chan, S. I. (1984) J. Biol. Chem. 259, 6481-6491.

## FOOTNOTES

<sup>1</sup>When the exchange-averaged region extends throughout the sample, as for leaky ghosts, the quantities  $\sum_c n_c(X_iCl)$  and  $\sum_c n_c(Cl^-)$  can each be divided by the sample volume to yield macroscopic concentrations, and Equation 1 becomes Equation 2 in the previous paper (11).

<sup>2</sup>In less ideal systems, exchange averaging could occur which is not complete. Incomplete exchange averaging can lessen the contribution of a particular compartment to the observed linebroadening; however, that contribution could still be measurable, in which case the procedure used here to resolve the observed contributions from different compartments would still be successful.

CHAPTER V  
THE TRANSPORT SITE AND THE CHEMICAL  
EQUATION FOR TRANSPORT

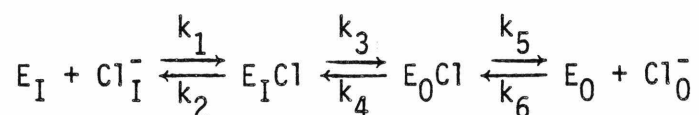
ABSTRACT

Although the recruitment studies of the previous chapter demonstrate that band 3 has a single functional transport site which is alternatively exposed to opposite sides of the membrane, such studies do not rule out the existence of a second anion binding site which is invisible to the  $^{35}\text{Cl}$  NMR technique. A second site has, in fact, been proposed to explain the self-inhibition of anion exchange that is known to occur at large anion concentrations. Yet the role, if any, of this postulated inhibitory site in the transport cycle is not known. Here the simplest one-site form of the alternating site model is tested to see if it can quantitatively fit the data. It is shown that: 1) when the  $[\text{Cl}^-]$ ,  $[\text{Br}^-]$  or pH is varied, the band 3 transport sites on both sides of the membrane behave like a homogeneous population of simple anion binding sites in  $^{35}\text{Cl}$  NMR experiments, and 2) when the  $[\text{Cl}^-]$  is varied, the outward-facing transport site behaves like a simple anion binding site. These results indicate that the postulated inhibitory site has no effect on chloride binding to the transport site. Instead, the results are quantitatively consistent with the ping-pong model [R. B. Gunn and O. Frolich (1979) J. Gen. Physiol. 74, 351-374], which states that the transport site is the only site involved in the transport cycle. Expressions are derived for the macroscopically observed characteristics of a ping-pong transporter: these characteristics are shown to be weighted averages of the microscopic properties of the inward- and outward-facing conformations of the transport site.

In addition to supporting the simplicity of the transport

mechanism, the high-pH titration curve for chloride binding to the transport site provides insight into the structure of the site. The macroscopically observed  $pK_A = 11.1 \pm 0.1$  in the leaky ghost system indicates that an arginine must provide the essential positive charge in the inward- or outward-facing conformation of the transport site, or in both conformations.

The results presented here allow the chemical equation for the chloride transport cycle to be written (Figure 5, p. 186):



The following chapter investigates the rate constants in this chemical equation.

## INTRODUCTION

Band 3 is a 95,000 dalton transmembrane protein that catalyzes the one-for-one exchange of two monovalent anions in opposite directions across the membrane of the human red cell. The physiological substrate anions of this protein are bicarbonate, produced by the hydration of carbon dioxide, and chloride. The passive exchange of these anions by band 3 is essential to the respiration of carbon dioxide; as a result, the band 3 anion transport system is the most heavily used ion transport pathway in typical vertebrate organisms (1,2).

I have been interested in obtaining a molecular picture of the ion transport event in band 3. A first step in the development of such a picture is the determination of the chemical and kinetic equations that describe the transport cycle; the present chapter focuses on the chemical equation. Some features of the transport cycle have already been established. One of the key findings is that band 3 is an alternating site transporter possessing a single transport site that is alternately exposed to opposite sides of the membrane. This site can only cross the membrane when it is occupied by substrate anion; thus, when a chloride gradient is imposed across the membrane, the transport site accumulates on the side of the membrane exposed to low chloride concentration (3). Recently,  $^{35}\text{Cl}$  NMR has been used to resolve band 3 transport sites on opposite sides of the membrane. Such experiments have confirmed the alternating site mechanism; the inhibitor 4,4'-dinitrostilbene-2,2'-disulfonate (DNDS), which binds exclusively to the outward-facing transport site, was observed to recruit the transport site exclusively to the outward-facing conformation (4).

Although there now exists a substantial body of evidence indicating

that band 3 possesses a single, alternating transport site, it is not yet possible to exclude the existence of other anion binding sites on the protein which do not transport anions but which may be involved in the transport cycle. For example, one or more inhibitory anion binding sites have been postulated to explain the inhibition of band 3 catalyzed anion exchange that is observed at sufficiently large anion concentrations (5-7). Thus, it is important to determine whether the transport cycle involves only the transport site or other sites as well. The simplest form of the alternating site mechanism, termed the ping-pong mechanism by Gunn and Frölich (8), proposes that the transport site is in fact the only site involved in the normal transport cycle.

The ping-pong model makes a set of predictions that are amenable to quantitative tests when  $^{35}\text{Cl}$  NMR is used to observe transport site behavior. These predictions involve the heterogeneity of the inward- and outward-facing transport sites. A variety of existing evidence is consistent with the idea that the two transport site orientations are structurally different: 1) substrate ions such as  $\text{Cl}^-$  and  $\text{Br}^-$  exhibit greater apparent affinities for the outward-facing sites than for inward-facing sites in transport saturation experiments (8), though such differences could be due to differences in translocation rate constants as well as differences in site structure (9), and 2) organo-anions that competitively inhibit substrate binding to the transport sites generally bind more tightly to the extracellular face of the protein, where they occupy the outward-facing transport site (9). Despite this evidence, which indicates that the structure of the transport site and/or its surroundings must change upon translocation, the ping-pong model predicts that the inward- and outward-facing transport sites

will together behave like a homogeneous population of transport sites in macroscopic experiments. In the present chapter I introduce  $^{35}\text{Cl}$  NMR data indicating that when the  $[\text{Cl}^-]$ ,  $[\text{Br}^-]$  or pH is varied, the inward- and outward-facing band 3 transport sites exhibit the macroscopic homogeneity required by the ping-pong model. Also, for a specific case, the data are shown to be sufficiently good to rule out a more complicated model. In short, the results are completely consistent with a transport cycle in which the transport site is the only important site. The kinetic equation for this transport cycle is the subject of the following chapter (10).

#### MATERIALS AND METHODS

All chemicals used were reagent grade or better; packed red cells were the kind gift of the Los Angeles Chapter of the American Red Cross.

All of the following procedures were carried out exactly as previously described in detail (2,4). Leaky red cell ghost membranes were prepared by osmotic lysis of intact red cells, followed by extensive washing to remove the cytoplasmic contents of the cells. The isolated membranes were stored at 4° C for no more than four days in 5 mM  $\text{NaH}_2\text{PO}_4$ , pH to 8 with NaOH, 130  $\mu\text{M}$  dithiothreitol and 10  $\mu\text{M}$  PMSF. Where appropriate, crushed ghosts or sonicated ghosts were made from leaky ghosts. NMR samples were made on ice by diluting the isolated membranes with an equal volume of ice cold 2 x NMR buffer and were assayed by  $^{35}\text{Cl}$  NMR the same day. The  $^{35}\text{Cl}^-$  linebroadening due to band 3 transport sites was isolated from the linebroadening due to other sites using DNDS, a competitive inhibitor of chloride binding to band 3 transport sites;

subtraction of the linebroadening of a membrane sample containing 1 mM DNDS from the linebroadening of an identical sample lacking DNDS yielded the transport site linebroadening. All linebroadenings were normalized to the same band 3 concentration by dividing each sample by its total ghost protein concentration, determined by Lowry protein analysis (11,12).

The pH-titration samples were prepared by incrementally adding 2 N NaOH or HCl to a sufficiently large volume of sonicated ghost membranes in NMR buffer on ice. When the pH reached a desired value, two aliquots were removed. DNDS in H<sub>2</sub>O was added to one of the samples, and the same volume of H<sub>2</sub>O to the other. This enabled determination of the transport site linebroadening at the desired pH as described above and, in complete detail, previously (2,4). The samples that resulted were virtually identical except with respect to pH and DNDS concentration, since the added acid or base only negligibly altered the chloride concentration and the sample volume.

#### THE <sup>35</sup>Cl NMR ASSAY

The work presented here examines the characteristics and mechanism of chloride transport by band 3 using a <sup>35</sup>Cl NMR technique. In Chapter III it was shown that <sup>35</sup>Cl NMR can be used to: 1) observe chloride binding to band 3 transport sites on red cell membranes without interference from other chloride binding sites (2), and 2) resolve the transport sites into two populations on opposite sides of the membrane (4). The <sup>35</sup>Cl NMR assay for chloride binding is based on the fact that the <sup>35</sup>Cl NMR spectral width of chloride in a macromolecular binding site is typically at least 10<sup>4</sup> times larger than the linewidth of chloride in solution. Because of the large

spectral width and relatively small concentration of bound chloride (in the present experiments  $[\text{total protein}]/[\text{total chloride}] < 10^{-3}$ ), the observed  $^{35}\text{Cl}$  NMR resonance is essentially that of solution chloride alone. However, when solution chloride samples macromolecular binding sites sufficiently rapidly, the sites can cause a measurable increase in the solution chloride linewidth. This increase in linewidth, or linebroadening, can be shown by a theoretical analysis to be linearly related to the concentration of chloride binding sites (2,13); moreover, this linear relationship has been experimentally verified for the sites on red cell membranes (Chapter III, (2)). It has also been shown that the linebroadening due to band 3 transport sites can be isolated from the linebroadening due to other chloride binding sites on red cell membranes using DNDS, an inhibitor of chloride binding to band 3 transport sites (Chapter III, (2)). In the present chapter the linebroadening of the solution chloride  $^{35}\text{Cl}$  NMR resonance is again used as an assay for chloride binding to band 3 transport sites.

The  $^{35}\text{Cl}^-$  linebroadening due to chloride binding sites contains a variety of information. Theoretical and experimental analysis indicates that the linebroadening ( $\delta$ ) due to a heterogeneous population of chloride binding sites is given by (2)

$$\delta = \sum_j \alpha_j \frac{[E_j\text{Cl}]}{[\text{Cl}^-]} \quad (1)$$

where the sum is over the different types of sites,  $\alpha_j$  is a constant characteristic of the  $j^{\text{th}}$  type of site,  $[E_j\text{Cl}]$  is the concentration of chloride bound to the  $j^{\text{th}}$  type of site, and  $[\text{Cl}^-]$  is the total or stoichiometric concentration of chloride in the sample. Equation 1 assumes that the bound chloride returns to solution before binding to

another site, and that the concentration of bound chloride is negligible relative to the total chloride concentration. The linebroadening due to the different sites is additive in Equation 1, and the contribution of the  $j^{\text{th}}$  type of site to the linebroadening is simply

$$\delta_j = \alpha_j \frac{[E_jCl]}{[Cl^-]} \quad (2)$$

which can be rewritten to yield

$$\delta_j = \frac{\alpha_j [E_j]_T}{K_{Dj}} \cdot \frac{[Cl^-]^{-1}}{[Cl^-]^{-1} + K_{Dj}^{-1}} \quad (3)$$

where  $[E_j]_T$  is the total or stoichiometric concentration of binding sites and  $K_{Dj}$  is the microscopic dissociation constant for chloride binding (2). Equation 2 indicates that the linebroadening is proportional to  $[E_jCl]/[Cl^-]$ , which is the fraction of total chloride that is bound to the  $j^{\text{th}}$  type of site; Equation 3 indicates that the linebroadening will yield a simple square hyperbola on a plot of linebroadening vs.  $[Cl^-]^{-1}$ . In both equations the quantity  $\alpha_j$  contains information that depends on the physical situation (2): when the exchange of chloride between the binding site and solution is sufficiently fast,  $\alpha_j$  depends on the characteristics of the  $j^{\text{th}}$  type of site; in contrast, when the exchange is sufficiently slow,  $\alpha_j$  depends only on the rate constant for dissociation of chloride from the  $j^{\text{th}}$  type of site. Thus, for sites in the slow exchange limit, the linebroadening can be used to study the dissociation of chloride from a chloride binding site. In short, the linebroadening provides considerable insight into the molecular events that occur at the transport site.

## THE PING-PONG MODEL

INTRODUCTION

The following discussion presents a mathematical treatment of the ping-pong model. In particular, the linebroadening due to the transport sites of a ping-pong transporter is examined as a function of varying: 1) chloride concentration, 2) inhibitor concentration, and 3) pH.

Definitions. The subscripts 0 and I are used to represent the outside (extracellular) and inside (intracellular) compartments, and symbols for ionic charges and concentration brackets are understood rather than expressly written. For instance,  $Cl_0$  and  $H_0$  denote the chloride and hydrogen concentrations in the outside compartment, respectively.

Conditions. Only leaky membranes are utilized here; thus, the following conditions hold:  $Cl_I = Cl_0 = Cl$  and  $H_I = H_0 = H$ . Also the concentration of chloride binding sites is negligible relative to the total (stoichiometric) chloride concentration, so the free and total chloride concentrations are essentially identical.

Fundamental characteristics of a ping-pong transporter. This model proposes that the transport unit has a single transport site that binds a chloride ion on one side of the membrane; only then is the site able to cross the membrane. I make the reasonable assumption that the distribution of outward- and inward-facing transport sites reaches a kinetic steady state before this experiment begins. (The chloride translocation time is  $\leq 2$  msec

per turnover at 0°C (19).) Under these conditions, the flux of binding sites from outside to inside must cancel the opposing flux, or

$$k_{0I}(E_0Cl) + k'_{0I}(E_0) = k_{I0}(E_I Cl) + k'_{I0}(E_I) \quad (4)$$

Here  $k_{xy}$  is the rate constant for the side x to side y translocation.  $E_x$  is the concentration of empty transport sites on side x, and  $E_x Cl$  is the concentration of occupied transport sites on side x. For a perfect ping-pong transporter the rate constants for empty site translocation are  $k_{0I} = k'_{I0} = 0$ . In this limit the transport site interconversion is described by the equilibrium  $E_0 Cl \rightleftharpoons E_I Cl$  and Equation 4 becomes

$$k_{0I} E_0 Cl = k_{I0} E_I Cl \quad (5)$$

For a ping-pong transporter, then, the distribution of bound chloride between the two sides of the membrane is determined solely by the rates of chloride translocation. This characteristic behavior of the ping-pong model has been previously described (8,9).

THE  $^{35}Cl^-$  LINEBROADENING DUE TO A PING-PONG TRANSPORTER: DEPENDENCE ON  $[Cl^-]^{-1}$

The microscopic dissociation constant for chloride binding to transport sites will be different on the two sides of the membrane if the inward- and outward-facing transport sites have different structures. However, the following discussion shows

that a ping-pong transporter will always exhibit a single macroscopic dissociation constant  $(\overline{K_D})$  for chloride binding in linebroadening experiments, even though the microscopic chloride dissociation constant may be different for the inward- and outward-facing sites.

Useful relationships and assumptions. Use will be made of the familiar expressions for  $K_{D_0}$ , the microscopic dissociation constant for chloride binding to the outward-facing transport site, and  $P_0$ , the fraction of these sites that contains bound chloride:

$$K_{D_0} = \frac{(E_0)(Cl_0)}{E_0Cl} \quad (6)$$

$$P_0 = \frac{E_0Cl}{N_0} = \frac{Cl_0}{Cl_0 + K_{D_0}} \quad (7)$$

where  $N_0$  is the total or stoichiometric concentration of outward-facing transport sites. Analogous expressions can be written for inward-facing transport sites. The validity of Equations 6 and 7 assumes that dissociation is the only significant pathway available to a bound chloride ion; thus, the dissociation rate must be sufficiently rapid compared to the translocation rate. This assumption is justified in the following chapter.

The concentration of occupied transport sites. In order to determine the linebroadening due to transport sites (or, in kinetic studies, the rate of transport), the concentration of the transport sites must be determined. This quantity can be derived by first

substituting Equation 7 into Equation 4 to yield

$$k_{OI}N_0P_0 = k_{IO}N_I P_I \quad (8)$$

Rearrangement of this expression yields the concentration of outward-facing transport sites:

$$N_0 = \left( \frac{k_{IO}}{k_{OI}} \right) \left( \frac{P_I}{P_0} \right) N \left/ \left( 1 + \frac{k_{IO}}{k_{OI}} \frac{P_I}{P_0} \right) \right. \quad (9)$$

where  $N = N_0 + N_I$  is the total concentration of occupied and unoccupied transport sites, irrespective of sidedness. Substitution of Equation 7 for  $N_0$  yields

$$E_0Cl = \left( \frac{k_{IO}}{k_{OI}} \right) (P_I) N \left/ \left( 1 + \frac{k_{IO}}{k_{OI}} \frac{P_I}{P_0} \right) \right. \quad (10)$$

Finally, substitution of Equation 7 for  $P_0$  and  $P_I$  under the condition  $Cl_0 = Cl_I = Cl$  yields the concentration of occupied outward-facing transport sites:

$$E_0Cl = \left( \frac{k_{IO}}{k_{OI}} \right) \left( \frac{Cl}{Cl + K_{D_I}} \right) N \left/ \left( 1 + \frac{k_{IO}}{k_{OI}} \frac{Cl + K_{D_0}}{Cl + K_{D_I}} \right) \right. \quad (11)$$

An expression for  $E_I Cl$  can be derived in an analogous way.

The transport site linebroadening. The total  $^{35}\text{Cl}^-$  linebroadening due to a heterogeneous population of independent binding sites is given by

$$\delta = \sum_j \alpha_j \left( \frac{E_j \text{Cl}}{\text{Cl}} \right) \quad (12)$$

where  $E_j \text{Cl}$  is the stoichiometric concentration of chloride bound to the  $j^{\text{th}}$  type of site, and  $\alpha_j$  is a constant characteristic of the  $j^{\text{th}}$  type of site. The  $\alpha_j$  of the transport site could be different in its inward- and outward-facing conformations; thus, the transport site linebroadening is

$$\delta = \alpha_0 \left( \frac{E_0 \text{Cl}}{\text{Cl}} \right) + \alpha_I \left( \frac{E_I \text{Cl}}{\text{Cl}} \right) \quad (13)$$

Substitution of Equation 11 for  $E_0 \text{Cl}$  and an analogous expression for  $E_I \text{Cl}$  followed by rearrangement yields the following simple expression for the transport site linebroadening:

$$\delta = \frac{N \bar{\alpha}}{\text{Cl} + \bar{K}_D} \quad (14)$$

where the macroscopically observed quantities  $\bar{\alpha}$  and  $\bar{K}_D$  are

$$\bar{\alpha} = \left( \frac{\alpha_0}{k_{0I}} + \frac{\alpha_I}{k_{I0}} \right) / \left( \frac{1}{k_{0I}} + \frac{1}{k_{I0}} \right) \quad (15)$$

$$\bar{K}_D = \left( \frac{K_{D0}}{k_{0I}} + \frac{K_{DI}}{k_{I0}} \right) / \left( \frac{1}{k_{0I}} + \frac{1}{k_{I0}} \right) \quad (16)$$

Multiplication and division of Equation 14 with  $(C1\overline{K_D})^{-1}$  finally yields

$$\delta = \frac{N\overline{\alpha}}{\overline{K_D}} \cdot \frac{C1^{-1}}{C1^{-1} + \overline{K_D}^{-1}} \quad (17)$$

Thus, the ping-pong model predicts that the transport sites will behave like a homogeneous class of sites in linebroadening experiments with the macroscopically observed quantities  $\overline{\alpha}$  and  $\overline{K_D}$  given by the weighted average of the microscopic constants for the inward- and outward-facing transport sites.

#### THE $^{35}\text{Cl}^-$ LINEBROADENING DUE TO A PING-PONG TRANSPORTER: EFFECTS OF REVERSIBLE INHIBITORS

The linebroadening due to the transport sites of a ping-pong transporter is a function of the concentration of inhibitors; here the form of this function is derived for different types of reversible inhibitors. Special attention is given to the reversible transport site inhibitors that I have examined using  $^{35}\text{Cl}$  NMR:  $\text{Br}^-$ ,  $\text{I}^-$ ,  $\text{HCO}_3^-$ ,  $\text{F}^-$  DNDS, and p-nitrobenzene sulfonate. The expressions that are derived are general results of the ping-pong model and are applicable to linebroadening or kinetic experiments in a variety of red cell membrane experiments.

Useful relationships and assumptions. Consider an inhibitor of the linebroadening due to transport sites: the most general case is that of the mixed inhibitor that can bind either to an empty (E) or occupied (ECl) transporter. Thus, for each side of

the membrane, two inhibitor constants are required to explain inhibitor (X) binding:

$$K_{X_0} = \frac{(E_0)(X)}{E_0X} \quad (18)$$

$$K'_{X_0} = \frac{(E_0C_1)(X)}{E_0C_1X} \quad (19)$$

Analogous expressions can be written for the inside compartment.

Here it will be assumed that when an inhibitor binds to a particular transporter, it completely eliminates the transport site linebroadening from that transporter but has no effect on other transporters. In this case the transport site linebroadening is given by

$$\delta = \delta(0)(1-P_x) \quad (20)$$

where  $\delta(0)$  is the transport site linebroadening in the absence of inhibitor, and  $P_x$  is the fraction of the band 3 population which is inhibited.

Dependence of the fractional inhibition on the inhibitor concentration. The fractional inhibition is simply the concentration of the band 3-inhibitor complex divided by the total band concentration:

$$P_x = \frac{E_0X + E_I X + E_0C_1X + E_I C_1X}{E_0 + E_I + E_0C_1 + E_I C_1 + E_0X + E_I X + E_0C_1X + E_I C_1X} \quad (21)$$

Using 1) the definitions of  $K_{D_0}$  (Equation 6),  $K_{X_0}$  (Equation 18),  $K'_{X_0}$  (Equation 19), 2) the corresponding definitions for the inside compartment, and 3) Equation 5, the fractional inhibition can be written as

$$P_X = \frac{\left\{ \frac{X_0}{K'_{X_0}} + \frac{X_I}{K'_{X_I}} \cdot \frac{k_{OI}}{k_{IO}} + \frac{X_0}{K_{X_0}} \cdot \frac{K_{D_0}}{Cl_0} + \frac{X_I}{K_{X_I}} \cdot \frac{K_{D_I}}{Cl_I} \cdot \frac{k_{OI}}{k_{IO}} \right\}}{1 + \frac{k_{OI}}{k_{IO}} + \frac{K_{D_0}}{Cl_0} + \frac{K_{D_I}}{Cl_I} \cdot \frac{k_{OI}}{k_{IO}} + \left\{ \right\}} \quad (22)$$

When  $X_0 = X_I = X$ , this expression reduces to the simple form

$$P_X = \frac{X}{X + \bar{K}_X} \quad (23)$$

where the macroscopically observed inhibitor constant is

$$\bar{K}_X = \frac{1 + \frac{k_{OI}}{k_{IO}} + \frac{K_{D_0}}{Cl_0} + \frac{K_{D_I}}{Cl_I} \cdot \frac{k_{OI}}{k_{IO}}}{\frac{1}{K'_{X_{OI}}} + \frac{1}{K'_{X_I}} \cdot \frac{k_{OI}}{k_{IO}} + \frac{1}{K_{X_0}} \cdot \frac{K_{D_0}}{Cl_0} + \frac{1}{K_{X_I}} \cdot \frac{K_{D_I}}{Cl_I} \cdot \frac{k_{OI}}{k_{IO}}} \quad (24)$$

and when  $Cl_0 = Cl_I = Cl$ , rearrangement yields

$$\bar{K}_X = \frac{\frac{K_{D_0}}{k_{OI}} + \frac{K_{D_I}}{k_{IO}} + Cl \left( \frac{1}{k_{OI}} + \frac{1}{k_{IO}} \right)}{\frac{K_{D_0}}{K_{X_0} k_{OI}} + \frac{K_{D_I}}{K_{X_I} k_{IO}} + Cl \left( \frac{1}{K'_{X_0} k_{OI}} + \frac{1}{K'_{X_I} k_{IO}} \right)} \quad (25)$$

This expression indicates that  $\overline{K_X}$  depends on all of the inhibitor's microscopic dissociation constants. Also present are the quantities  $Cl$ ,  $K_{D_0}$ ,  $K_{D_I}$ , and  $k_{XY}$  because 1) chloride binding can change the overall affinity of the transporter for the inhibitor, and 2) varying chloride concentration can change the distribution of transport sites across the membrane unless  $K_{D_0} = K_{D_I}$  (Equation 7).

Competing substrates. Inhibitors of this class act by binding to the transport site, thereby preventing chloride binding. Such inhibitors cannot bind to the site when it is occupied by chloride, so the microscopic dissociation constants  $K'_{X_I}$  and  $K'_{X_0}$  can be neglected ( $1/K'_{X_0} \cong 1/K'_{X_I} \cong 0$ , Equation 19). In this case  $\overline{K_X}$  becomes

$$\overline{K_X} = \left( \frac{K_{D_0}}{k_{O_I}} + \frac{K_{D_I}}{k_{I_0}} + Cl \left( \frac{1}{k_{O_I}} + \frac{1}{k_{I_0}} \right) \right) / \left( \frac{K_{D_0}}{K_{X_0} k_{O_I}} + \frac{K_{D_I}}{K_{X_I} k_{I_0}} \right) \quad (26)$$

This expression describes the macroscopically observed  $\overline{K_X}$  for competing substrates that bind to both the inward- and outward-facing transport sites. The inhibitors of this type that I have studied by  $^{35}Cl^-$  NMR are  $Br^-$  (Chapter V),  $I^-$ ,  $F^-$ , and  $HCO_3^-$  (Chapter III).

Side-specific inhibitors. A competitive inhibitor of chloride binding to the transport site that only binds to the outward-facing orientation ( $1/K_{X_I} \cong 0$ ) further simplifies Equation 26:

$$\overline{K_X} = K_{X_0} \left[ 1 + \frac{K_{D_I}}{K_{D_0}} \cdot \frac{k_{O_I}}{k_{I_0}} + \frac{Cl}{K_{D_0}} \left( 1 + \frac{k_{O_I}}{k_{I_0}} \right) \right] \quad (27)$$

This equation as well as Equation 26 predicts that the chloride dependence of  $\overline{K_X}$  will have the form

$$\overline{K_X} = C_1 + C_2Cl \quad (28)$$

as has been experimentally observed for DNDS by Fröhlich (20) and verified in Chapter VII. This experimental result suggests that the binding of chloride and DNDS are mutually exclusive since an inhibitor that can bind to a transporter containing chloride will give rise to a more complicated expression ( $1/K_X' > 0$ , Equation 25).

#### THE $^{35}Cl^-$ LINEBROADENING DUE TO A PING-PONG TRANSPORTER: EFFECTS OF pH

If the transport site contains a titratable positive charge that is required for chloride binding, then the linebroadening due to the site will be inhibited when the charge is removed by sufficiently high pH. As shown below, a ping-pong transporter will titrate at high pH with a single macroscopically observed  $\overline{pK_A}$ , even if the microscopic  $pK_A$  for the transport site is different on the two sides of the membrane. The expressions that are derived are general results of the ping-pong model and are applicable to linebroadening or kinetic experiments with any type of red cell membrane preparation.

Useful relationships and assumptions. Consider a ping-pong transporter with the following characteristics: 1) the transport site contains a titratable positive charge to which substrate

anion binds, and 2) neutralization of the transport site eliminates chloride binding.

In order to clarify the presentation, the transport site concentration on side x will be written  $E_xH$  for intact sites and  $E_x$  for base neutralized sites. Thus, the concentration of chloride bound to transport sites is now written  $E_xHCl$  instead of the previous terminology  $E_xCl$ . The chloride dissociation constant for the outward-facing transport site can therefore be written

$$K_{D0} = \frac{(E_0H)(Cl_0)}{E_0HCl} \quad (29)$$

where it is assumed, as for Equation 7, that dissociation is the only significant pathway available to the bound chloride ion. Thus, the dissociation rate must be very rapid compared to the transport rate; this assumption is justified in the following chapter (10). The proton dissociation constant can be written

$$K_{A0} = \frac{(E_0)(H)}{(E_0H)} \quad (30)$$

Analogous expressions can be written for the inward-facing transport sites; also in this terminology Equation 5 becomes

$$k_{0I}(E_0HCl) = k_{I0}(E_IHCl) \quad (31)$$

Since it is assumed that neutralization of a particular transport site eliminates the linebroadening due to that site but has no effect on other sites, the transport site linebroadening is given by

$$\delta = \delta(0)(1 - P_X) \quad (32)$$

where  $\delta(0)$  is the transport site linebroadening when high pH inhibition is negligible, and  $P_X$  is the fraction of transporters that have been inhibited by base titration.

Dependence of the fractional inhibition on pH. The fractional inhibition is simply the number of inhibited transporters divided by the total number of transporters, or

$$P_X = \frac{E_O + E_I}{E_O + E_{OH} + E_{OHC} + E_I + E_{IH} + E_{IHC}} \quad (33)$$

This expression can be rewritten using the definitions of  $K_{D_O}$ ,  $K_{D_I}$ ,  $K_{A_O}$ ,  $K_{A_I}$ , and Equation 31 as well as the condition  $H_O = H_I = H$  to yield

$$P_X = \frac{H^{-1}}{H^{-1} + \overline{K_A}} \quad (34)$$

where the macroscopically observed quantity  $\overline{K_A}$  is

$$\overline{K_A} = \frac{K_{A_O} \cdot \frac{K_{D_O}}{C_{I_O}} \cdot \frac{1}{k_{O_I}} + K_{A_I} \cdot \frac{K_{D_I}}{C_{I_I}} \cdot \frac{1}{k_{I_O}}}{\frac{1}{k_{O_I}} \left( 1 + \frac{K_{D_O}}{C_{I_O}} \right) + \frac{1}{k_{I_O}} \left( 1 + \frac{K_{D_I}}{C_{I_I}} \right)} \quad (35)$$

This expression simplifies when the condition  $Cl_0 = Cl_I = Cl$  holds:

$$\overline{K_A} = \left( K_{A_0} \cdot \frac{K_{D_0}}{k_{O_I}} + K_{A_I} \cdot \frac{K_{D_I}}{k_{I_0}} \right) / \left( \frac{K_{D_0}}{k_{O_I}} + \frac{K_{D_I}}{k_{I_0}} + Cl \left( \frac{1}{k_{O_I}} + \frac{1}{k_{I_0}} \right) \right) \quad (36)$$

Inasmuch as I have derived Equation 36 assuming that chloride binding is a competitive inhibitor of deprotonation (see "Assumptions"), it is expected that  $\overline{K_A}$  depends upon the chloride concentration; when the chloride concentration increases, deprotonation ( $\overline{K_A}$ ) decreases accordingly.

In order to obtain the predicted form of the titration curve, Equation 34 can be reexpressed in terms of the pH and  $pK_A (= -\log_{10} K_A)$ :

$$P_X = \frac{10^{pH}}{10^{pH} + 10^{pK_A}} \quad (37)$$

This result can be substituted into Equation 32 to yield the pH-dependence of the linebroadening due to a ping-pong transporter:

$$\delta = \delta(0) \left( 1 - \frac{10^{pH}}{10^{pH} + 10^{pK_A}} \right) \quad (38)$$

Thus, a ping-pong transporter has a simple base titration curve and a single macroscopically observed  $\overline{pK_A}$ .

## RESULTS

Leaky Ghosts: Linebroadening vs.  $[Cl^-]^{-1}$ . The ability of the  $^{35}Cl$  NMR technique to resolve band 3 transport sites on both sides of the membrane can be used to test models for the transport cycle. The membrane system used to observe simultaneously the inward- and outward-facing transport sites is the leaky ghost system, in which both orientations of the transport site make measurable contributions to the linebroadening because the membranes have large holes that allow the bulk solution chloride to rapidly sample sites in both the internal and external compartments. I have previously shown that the transport site linebroadening due to leaky ghosts is composed of approximately 60% outward-facing and 40% inward-facing linebroadening (4).

The contributions made to the linebroadening by the two transport site orientations are additive (Equations 1-3). Thus, if the two orientations are completely independent, a plot of linebroadening vs.  $[Cl^-]^{-1}$  for leaky ghost membranes will yield a sum of two square hyperbola, each for each orientation (Equation 3). However, the data obtained for leaky ghost membranes are well approximated by a single square hyperbola for which the best-fit macroscopic chloride dissociation constant is  $90 \pm 10$  mM (Figure 1). At first glance this macroscopic homogeneity appears to contradict a variety of evidence suggesting that the characteristics of the inward- and outward-facing transport sites are different (see Introduction).

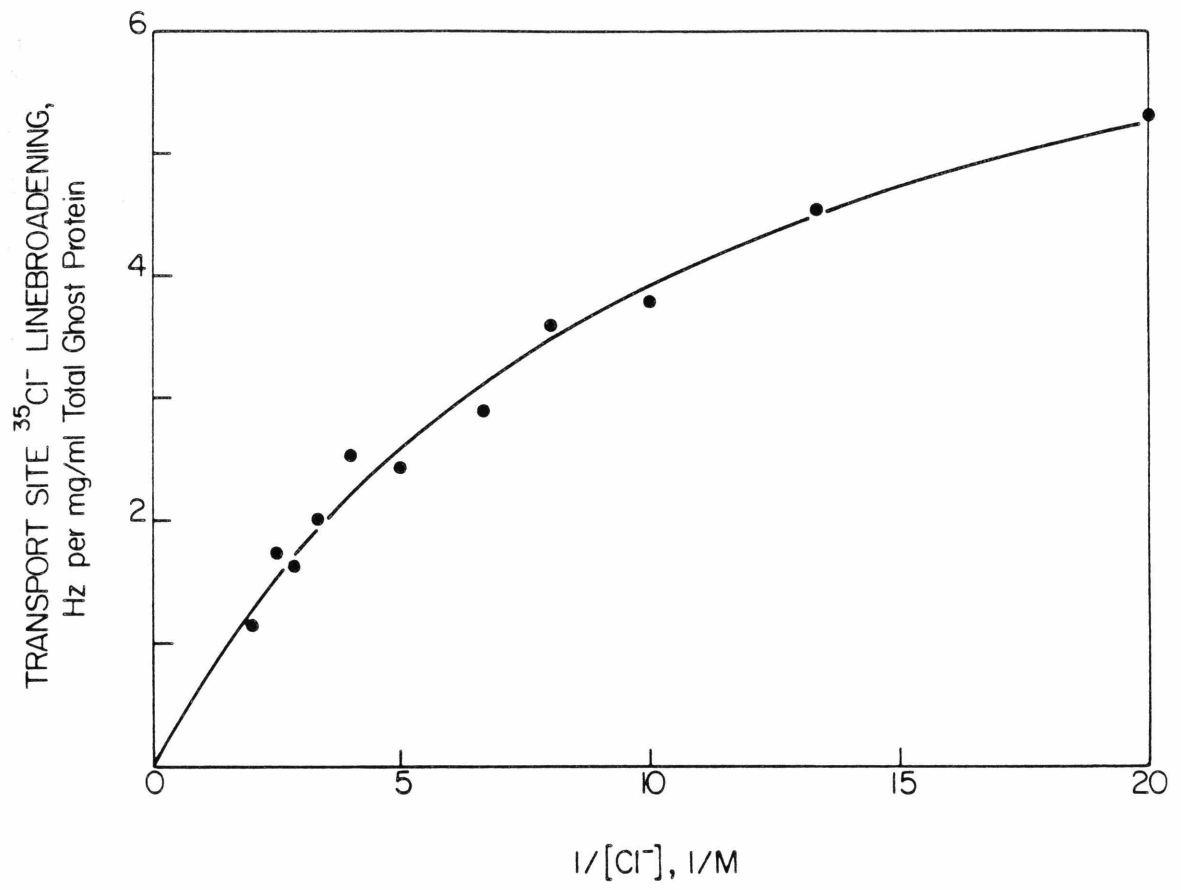
The ping-pong model can explain the observation of a single square hyperbola. For a ping-pong transporter, the steady-state transmembrane fluxes of occupied transport sites are equal for the two opposing directions (Equation 5):

Figure 1

The  $^{35}\text{Cl}^-$  linebroadening due to inward- and outward-facing band 3 transport sites. Shows the DNDS-sensitive linebroadening due to band 3 transport sites on leaky ghost membranes. The solid line curve is the nonlinear least-squares curve calculated for a classical binding site or a ping-pong transporter with a best-fit macroscopic  $K_D$  of  $90 \pm 10$  mM ( $y = Ax/(x + K_D^{-1})$ ). Each sample contained the indicated  $[\text{NH}_4\text{Cl}]$  as well as 7.5 mM  $\text{NaH}_2\text{PO}_4$ , 20%  $\text{D}_2\text{O}$ , pH to 8.0 with  $\text{NH}_4\text{OH}$ . Sufficient citric acid (pH to 8.0 with  $\text{NaOH}$ ) was added to bring the ionic strength up to that of the sample containing the highest  $[\text{NH}_4\text{Cl}] = 500$  mM. Spectral parameters: 8.8 MHz, 3°C and standard assay parameters (see text).

NOTE: There is no Equation Number 39 in this thesis.

Joseph Falke



$$k_{I0}[E_I C1] = k_{0I}[E_0 C1] \quad (40)$$

Here I have used  $[E_x C1]$  to denote the concentration of occupied transport sites on side  $x$ , and  $k_{xy}$  to denote the rate constant for translocation from side  $x$  to side  $y$ . Thus, the distribution of occupied transport sites  $[E_0 C1]/[E_I C1]$  is governed by the ratio of the translocation rate constants ( $k_{I0}/k_{0I}$ ). This constraint on the occupied site distribution leads to a well-defined averaging of the microscopic constants of the inward- and outward-facing sites so that the linebroadening due to transport sites on both sides of the membrane is given by (Equation 17):

$$\delta = \frac{\bar{\alpha}[E]_T}{\bar{K}_D} \cdot \frac{[C1]^{-1}}{[C1^{-}]^{-1} + \bar{K}_D^{-1}} \quad (41)$$

where  $[E]_T$  is the total concentration of band 3 transport units, and  $\bar{\alpha}$  and  $\bar{K}_D$  are macroscopically observed constants defined by (Equations 15,16):

$$\bar{\alpha} = \alpha_I \omega_I + \alpha_0 \omega_0$$

and

$$\bar{K}_D = K_{D_I} \omega_I + K_{D_0} \omega_0 \quad (42)$$

These macroscopic constants are weighted averages of the corresponding microscopic constants for the inward (subscript I)- or outward (subscript 0)-facing transport sites. The weighting factors in these averages are (Equations 15,16)

$$\omega_I = \frac{\tau_{I0}}{\tau_{I0} + \tau_{0I}}, \quad \omega_0 = \frac{\tau_{0I}}{\tau_{I0} + \tau_{0I}} \quad (43)$$

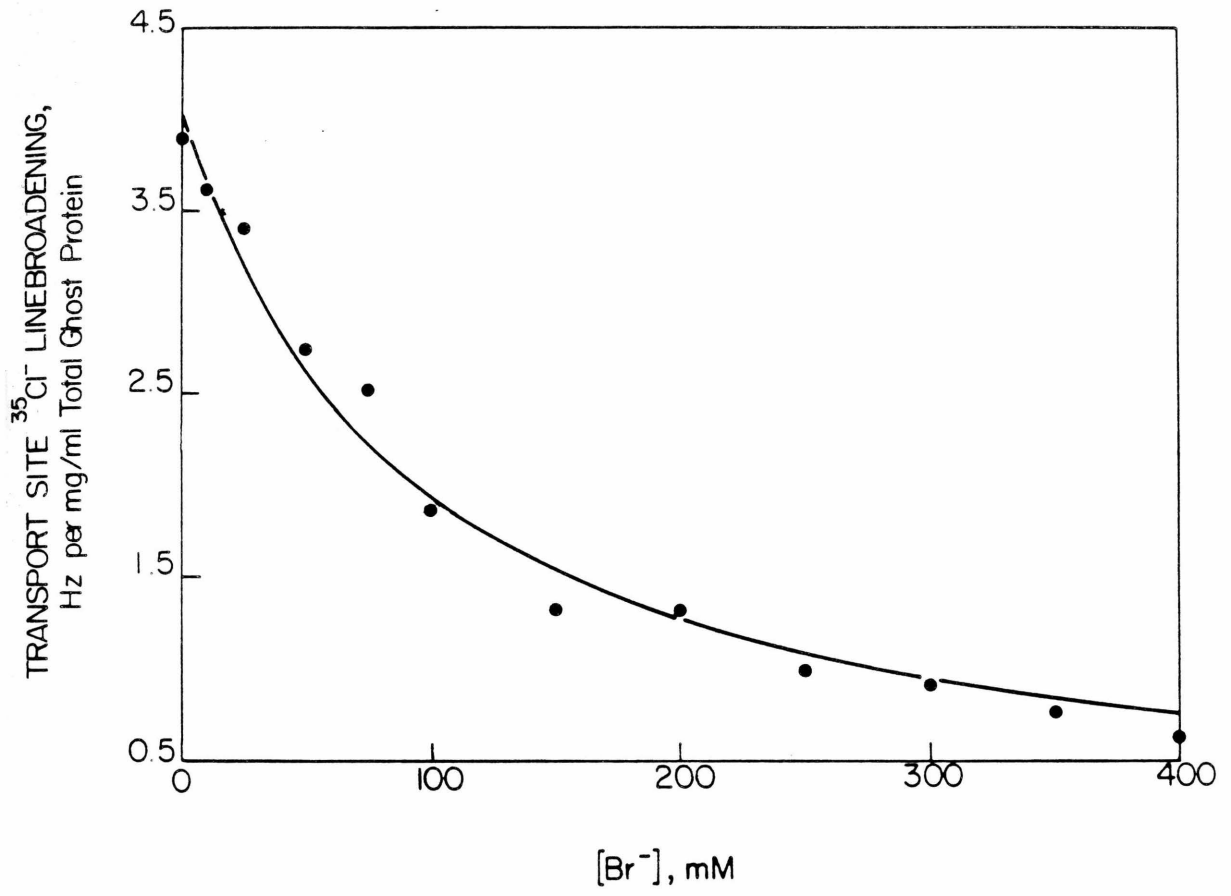
where the quantities  $\tau_{xy}$  are the inverse rate constants for the x to y translocation ( $\tau_{xy} = 1/k_{xy}$ ). The form of the weighting factors confirms the idea that the averaging is due to the special transport site distribution defined by Equation 40; assuming that the vast majority of transport sites are facing either side x or side y rather than actively undergoing translocation at any given point in time,  $\omega_x$  is simply the fraction of occupied sites found on side x (Equation 40).

Thus, the ping-pong mechanism couples the inward- and outward-facing transport site populations in such a way that the macroscopic characteristics of these sites appear to stem from a homogeneous population. This idea can be tested further by examining the macroscopic behavior of transport sites in the presence of varying bromide concentration or pH.

Leaky Ghosts: Linebroadening vs.  $[\text{Br}^-]$ . Bromide can be transported across the membrane in both directions by band 3 (8); thus, it must bind to both orientations of the transport site. Bromide binding is also known to competitively inhibit chloride binding to the transport site (6). Consistent with this picture is the observation that bromide completely inhibits the linebroadening due to band 3 transport sites on both sides of leaky ghost membranes (Figure 2). However, despite the fact that the characteristics of the inward- and outward-facing transport sites appear to be different (see Introduction), a plot of linebroadening vs.  $[\text{Br}^-]$  (Figure 2) for leaky ghost membranes is well approximated by a curve drawn for a homogeneous population of sites, where the macroscopic inhibitor constant for bromide is  $90 \pm 10$  mM in the presence of 100 mM chloride. Completely analogous results have been obtained for fluoride, iodide and bicarbonate, which are also competitive inhibitors

Figure 2

The effect of Br<sup>-</sup> on the <sup>35</sup>Cl<sup>-</sup> linebroadening due to inward- and outward-facing band 3 transport sites. Shown is a titration with Br<sup>-</sup> of the DNDS-sensitive linebroadening due to band 3 transport sites. The solid line is a nonlinear least-squares curve calculated for a classical binding site or a ping-pong transporter with a best-fit macroscopic K<sub>D</sub> of 90 ± 10 mM ( $y = A(1 - x/(x + K_D))$ ). Each sample contained the indicated concentration of NaBr, as well as 100 mM NaCl, 2.5 mM NaH<sub>2</sub>PO<sub>4</sub>, 20% D<sub>2</sub>O, pH to 8.0 with NaOH. Spectral parameters: 8.8 MHz, 3°C and standard assay parameters (see text).



that bind to both orientations of the transport site (2,6).

The macroscopic transport site homogeneity observed in experiments with competitive inhibitors is predicted by the ping-pong model. For a ping-pong transporter, the transport site linebroadening due to the inward- and outward-facing transport sites is (Equations 20,23)

$$\delta = \delta(0) \left( 1 - \frac{[X]}{[X] + \overline{K}_X} \right) \quad (44)$$

where  $\delta(0)$  is the transport site linebroadening in the absence of inhibitor,  $[X]$  is the inhibitor concentration, and  $\overline{K}_X$  is defined by (Equation 26)

$$\overline{K}_X = \frac{K_{D_I} \omega_I + K_{D_O} \omega_0 + [Cl^-]}{(K_{D_I}/K_{X_I}) \omega_I + (K_{D_O}/K_{X_O}) \omega_0} \quad (45)$$

The macroscopic quantity  $\overline{K}_X$  is a weighted average of the microscopic constants  $K_{X_I}$  and  $K_{X_O}$  for inhibitor binding to the inward- and outward-facing site, respectively. This average is more complicated than that for simple chloride binding (Equations 41,42) because for an inhibitor that competes with chloride for binding, the macroscopic inhibitor constant is a function of the chloride concentration. However, it is clear that macroscopic homogeneity remains a characteristic feature of the behavior of transport sites in the presence of competitive inhibitors.

Leaky Ghosts: Linebroadening vs. pH. Band 3-catalyzed chloride transport is inhibited at  $\text{pH} > 11$  in a reversible fashion (14), suggesting that the transport site contains at least one essential positive charge necessary for substrate binding. In the present experiments the pH-dependence of the transport site linebroadening is studied using sonicated leaky ghost membranes which, like the leaky ghost system, enable observation of the linebroadening of both inward- and outward-facing transport sites (4). Leaky ghosts are not used because at  $\text{pH} > 10$  such membranes spontaneously break up to form vesicles (15) which, if sealed, would hide the intravesicular transport sites (4). The transport site linebroadening due to sonicated ghosts is inhibited by high pH (Figure 3); this inhibition is not due to simple denaturation of the protein since the inhibition is removed by back-titration with acid (Table I). The base titration is well approximated by a titration curve drawn for a homogeneous population of sites that have a macroscopic  $\overline{\text{pK}}_A = 11.1 \pm 0.1$  in the presence of 250 mM chloride (Figure 3).

The behavior of the transport site in this base titration is another example of the macroscopic homogeneity predicted by the ping-pong model. For a ping-pong transporter the base titration of the transport site linebroadening is described by (Equation 38)

$$\delta = \delta(0) \left( 1 - \frac{10^{\text{pH}}}{10^{\text{pH}} + 10^{\overline{\text{pK}}_A}} \right) \quad (46)$$

where  $\delta(0)$  is the linebroadening when the essential positive charge is intact ( $\text{pH} \ll \overline{\text{pK}}_A$ ), and the macroscopically observed  $\overline{\text{pK}}_A$  is

Figure 3

The effect of pH on the  $^{35}\text{Cl}^-$  linebroadening due to inward- and outward-facing band 3 transport sites. Shown is a base titration of the DNDS-sensitive linebroadening due to band 3 transport sites. The solid line is a nonlinear least-squares curve generated for a classical binding site or a ping-pong transporter with a best-fit macroscopic  $\text{pK}_A$  of  $11.1 \pm 0.1$ . The samples contained 250 mM NaCl, 2.5 mM  $\text{NaH}_2\text{PO}_4$ , 20%  $\text{D}_2\text{O}$ , pH adjusted to the indicated value with NaOH or HCl. Spectral parameters: 8.8 MHz, 3°C and standard assay parameters.

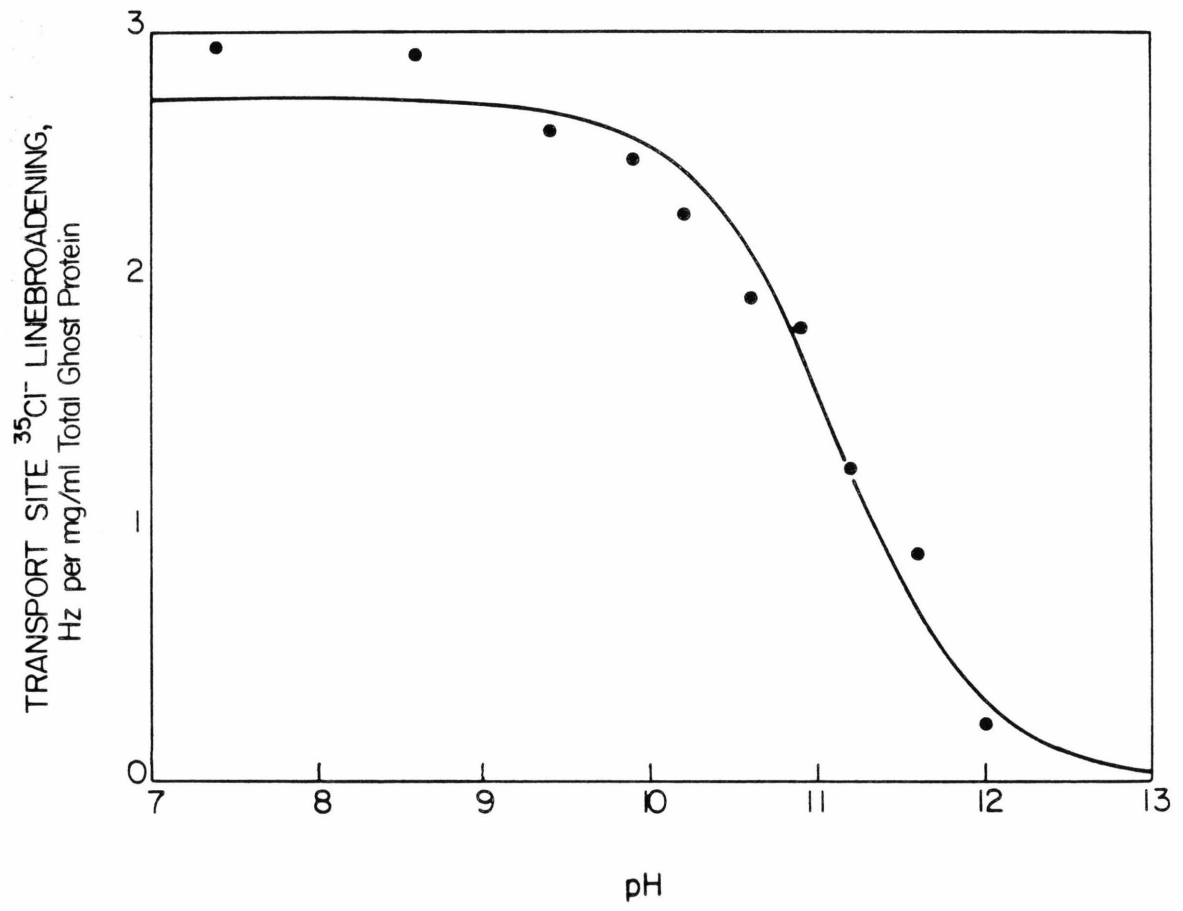


Table I. Reversibility of the High pH Inhibition of Transport Site  
Linebroadening in the Sonicated Ghost System

Treatment	$^{35}\text{Cl}^-$ Linebroadening Due to Sonicated Ghosts		$^{35}\text{Cl}^-$ Linebroadening Due to Band 3 Transport Sites
	A (No DNDS)	B (1 mM DNDS)	A - B
	Hz per mg/ml total membrane protein		
None (pH 8.0)	7.1 ± .3	4.2 ± .1	2.9
pH 12.2, then pH 8.0	7.3 ± .3	5.6 ± .3	2.7

(Equation 36)

$$\overline{pK_A} = \log_{10} \frac{K_{D_I} \omega_I + K_{D_O} \omega_O + [Cl^-]}{K_{A_I} K_{D_I} \omega_I + K_{A_O} K_{D_O} \omega_O} \quad (47)$$

Thus, the macroscopic titration of a transport site positive charge necessary for chloride binding is described by the quantity  $\overline{pK_A}$ , which is a weighted average of the microscopic quantities  $pK_{A_I}$  and  $pK_{A_O}$  for the inward- and outward-facing transport sites, respectively. The average is more complicated than that for simple chloride binding (Equations 41,42) because it is assumed that chloride binding protects the transport site from deprotonation; as a result, the  $\overline{pK_A}$  depends on the chloride concentration.

The measured  $\overline{pK_A}$  also provides some insight into the identity of the essential positive charge in the transport site. The observed value of  $\overline{pK_A} = 11.1 \pm 0.1$  is sufficiently large to suggest that one or both of the transport site conformations contains an essential arginine residue and no essential lysine residues. However, this value is significantly less than the value of 12.0 obtained for the outward-facing transport site in kinetic experiments at the same chloride concentration (250 mM chloride (14)). Since the macroscopic quantity  $\overline{pK_A}$  is an average of the microscopic  $pK_A$ 's of the two orientations of the transport site (Equation 47), it follows that the inward-facing site must satisfy  $pK_{A_I} < \overline{pK_A} = 11.1 \pm 0.1$ . These results are completely consistent with the previous conclusion that the positive charge in the outward-facing transport site is provided by arginine (1,9), but no conclusion can be made concerning the identity of the inward-facing positive charge, which could be an arginine or lysine. The macroscopic

homogeneity observed for the base titration is, however, consistent with the ping-pong model.

Crushed Ghosts: Dissociation of Chloride from the Outward-Facing Transport Site. For a classical binding site, the rate constant for dissociation of substrate from the site is independent of the substrate concentration. This rate constant can be studied for chloride dissociation from the outward-facing transport site of band 3 because this site is in the slow exchange limit where the linebroadening is a function of the rate constant for chloride dissociation (see following chapter (10)). Here the dependence of the macroscopically observed rate constant for chloride dissociation from the outward-facing transport site will be examined as a test of models for the transport cycle.

In order to specifically monitor the linebroadening due to the outward-facing transport site, crushed ghost membranes have proven particularly useful. These membranes, which are prepared from leaky ghost membranes, are permanently collapsed by large centripetal forces experienced during centrifugation. After crushing, the membranes give rise to a transport site linebroadening composed solely of the contribution from the outward-facing sites. The linebroadening due to inward-facing transport sites is not observed because the intracellular compartment makes a negligible contribution to the  $^{35}\text{Cl}$  NMR resonance, both due to the slowness of exchange between the intracellular and extracellular compartments and to the relatively small size of the intracellular compartment (4).

The linebroadening due to the outward-facing transport site has been shown to be in the slow exchange limit using crushed ghosts and

also right-side-out vesicles (see following chapter (10)); as a result, the factor  $\alpha_j$  in the linebroadening (Equations 2,3) is given by (2)

$$\alpha_j = \overline{k_{OFF}}/\pi \quad (48)$$

Here  $\overline{k_{OFF}}$  is an average over all of the outward-facing transport sites of the microscopic chloride dissociation constant  $k_{OFF}$ , which is defined for a single outward-facing transport site ( $E_0$ ) by the reaction



Thus,  $\overline{k_{OFF}}$  is a macroscopic rather than a microscopic quantity whenever heterogeneity exists in  $k_{OFF}$ . For a classical chloride binding site  $\overline{k_{OFF}} = k_{OFF}$  is a constant that is independent of the chloride concentration. In such a case  $\alpha_j$  is also a constant (Equation 2), and a square hyperbola is observed on a plot of linebroadening vs.  $[Cl^-]^{-1}$  (Equation 3). For crushed ghost membranes, a plot of transport site linebroadening vs.  $[Cl^-]^{-1}$  is well approximated by a square hyperbola, indicating that the outward-facing transport site behaves like a classical chloride binding site.

This classical behavior is predicted by the ping-pong model, for which the linebroadening due to outward-facing transport sites is given by (Equations 13,15-17)

$$\delta_0 = \frac{\overline{k_{OFF}}[E]_T}{\pi \overline{K_D}} \cdot \frac{\tau_{OI}}{\tau_{OI} + \tau_{IO}} \cdot \frac{[Cl^-]^{-1}}{[Cl^-]^{-1} + \overline{K_D}} \quad (50)$$

where  $\overline{k_{OFF}}$  is the average off-rate constant for the outward-facing transport site.  $[E]_T$  is the total concentration of band 3 transport

units,  $\overline{K_D}$  is the macroscopic chloride dissociation constant (Equation 42), and  $\tau_{xy}$  is the inverse of the rate constant for the translocation of the chloride-transport site complex from side x to side y (Equation 43).

In contrast to the ping-pong model, certain other models are inconsistent with the classical behavior of the outward-facing transport site, as can be illustrated by an examination of the two-site ordered sequential model (16). This model proposes that the transport domain of band 3 contains two transport sites that move together through the transport cycle, although only one of the sites can carry an anion during transmembrane translocation. When the two sites are in the outward-facing conformation it is proposed that at least one of the sites must be occupied. Consider an anion bound to one of the two outward-facing sites: this anion may have originated from the internal compartment, via a translocation, or from the outside compartment. In either case it is proposed that the anion cannot leave the site until a second anion is bound to the other outward-facing site. Thus, for the two-site ordered sequential model, the macroscopic rate constant for chloride dissociation from one of the two outward-facing sites ( $\overline{k_{OFF}}$ ) is a function of the occupancy of the other site, and thus of the chloride concentration as well (21).

To be specific, I now consider a particular case of the two-site ordered sequential model. It is assumed that:

- 1) one of the two sites is a NMR-visible site, generally termed the transport site, which has a chloride dissociation constant of  $\overline{K_D} = 80$  mM as measured by  $^{35}\text{Cl}$  NMR (2) or by saturation of chloride exchange (6,17), while
- 2) the other site is NMR-invisible and corresponds to the proposed modifier site, which has a chloride dissociation constant of  $\overline{K_D} = 340$  mM

as estimated by chloride self-inhibition in kinetic experiments (6). These assumptions are consistent with the previous proposal that the modifier site is one of the two sites in the transport domain of the two-site ordered sequential model (16). In Figure 4, it is shown that the best-fit curve resulting from these assumptions deviates from the curve for a classical chloride binding site. The deviation is particularly marked at low chloride concentration, where the linebroadening is smaller than that due to a classical site. This relative decrease in the linebroadening at low chloride concentration is due to a decrease in the occupancy of the NMR-invisible site, which causes  $\overline{k_{OFF}}$  for the NMR-visible site to decrease, thereby reducing the linebroadening parameter  $\alpha_j$  for the latter site (21). It is clear that the best-fit curve generated for a classical chloride binding site or for the ping-pong model provides a better fit to the data than the best-fit curve generated for the particular two-site ordered sequential model considered here (Figure 4). Thus, the data strongly disfavor any model in which  $\overline{k_{OFF}}$  for the outward-facing transport site is proposed to vary in the range  $25 \text{ mM} \leq [\text{Cl}^-] \leq 200 \text{ mM}$ .

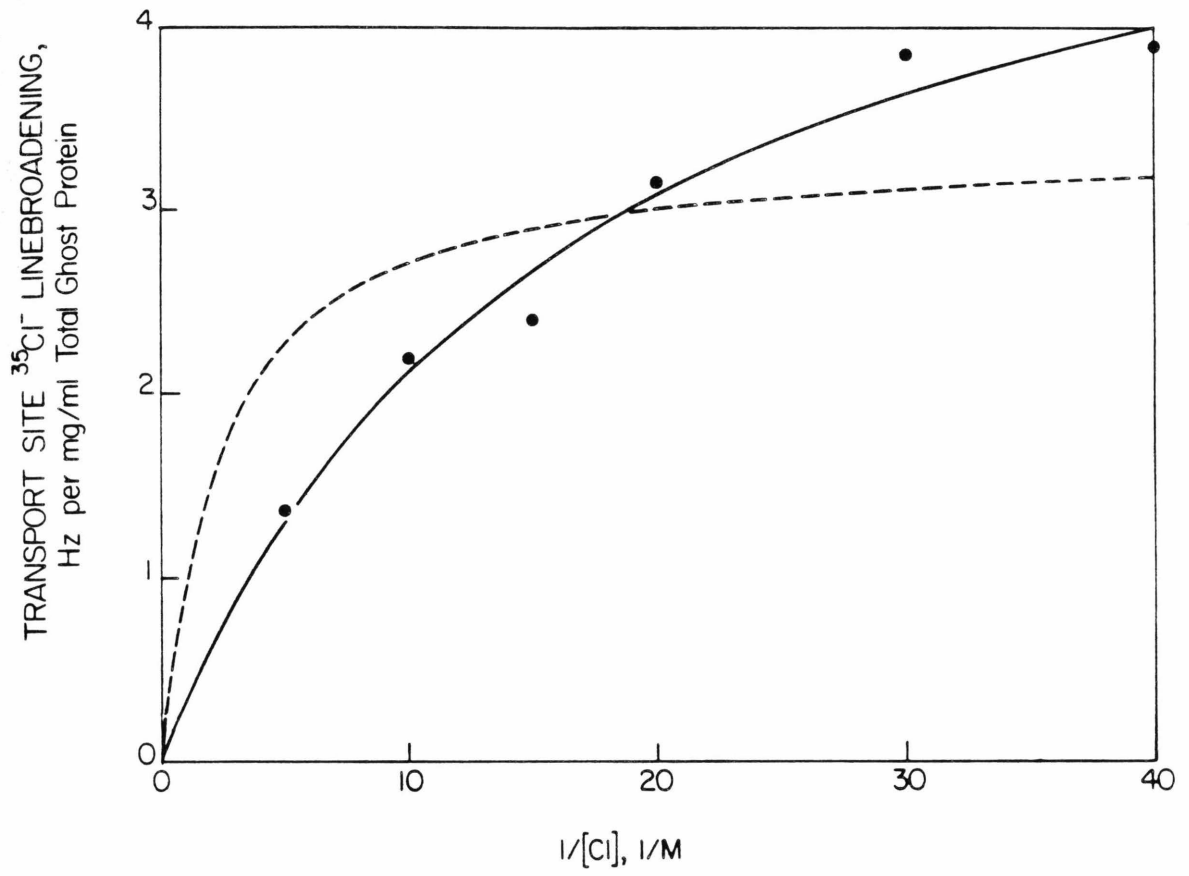
## DISCUSSION

In general, previously published mechanistic studies of band 3 using kinetic techniques have yielded results that are completely consistent with a ping-pong mechanism (reviewed in (1,9,18); for an exception see (16)). Despite this pre-existing strong body of evidence in favor of the ping-pong model, it still appears useful to test the mechanism using independent approaches; thus, I have employed  $^{35}\text{Cl}$  NMR

Figure 4

The  $^{35}\text{Cl}^-$  linebroadening due to outward-facing band 3 transport sites.

The DNDS-sensitive linebroadening due to band 3 transport sites was determined using crushed ghost membranes. The solid curve is the nonlinear least-squares best-fit curve for a classical binding site or a ping-pong transporter with a macroscopic  $K_D$  of  $60 \pm 10$  mM ( $y = Ax/(x + K_D^{-1})$ ). The dashed curve is the nonlinear least-squares best-fit curve for a special case of the two-site ordered sequential model, assuming that the transport site  $K_D = 80$  mM and the second site  $K_D = 340$  mM. Experimental details exactly as in Figure 1 legend, except that the ionic strength was brought to 200 mM, the highest  $[\text{NH}_4\text{Cl}]$  used here.

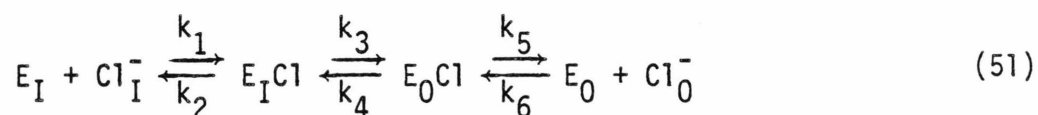


to examine the transport mechanism. The  $^{35}\text{Cl}$  NMR technique circumvents several difficulties of technique or interpretation that have been encountered previously: 1) chloride is a rapidly transported physiological anion that must be transported via the physiological band 3 mechanism; thus the possible significance of competing mechanisms that could become important for slowly transported, nonphysiological substrates is minimized, 2) the membrane systems utilized here are leaky; thus potential complications due to transmembrane ionic, electrical and pH gradients are nonexistent, and 3) the modifier effect is not observed in studies of chloride binding to band 3; thus complications due to this effect are avoided.

The ability of the  $^{35}\text{Cl}$  NMR technique to resolve band 3 transport sites on opposite sides of the membrane has made possible several tests of the mechanism of chloride transport, and in each case the ping-pong model is completely consistent with the data. For instance, the ping-pong model predicts that a population of transport sites will be distributed among the inward- and outward-facing conformations unless they are all recruited to one conformation by appropriate experimental conditions. The  $^{35}\text{Cl}$  NMR technique has confirmed the existence of both transport site conformations in the unperturbed system; also, the technique has allowed observation of transport site recruitment to the outward-facing conformation by DNDS (4). The present application of  $^{35}\text{Cl}$  NMR focuses on the characteristics of the mixed population of inward- and outward-facing transport sites. The ping-pong model predicts that the microscopic characteristics of the inward- and outward-facing conformations will be averaged due to the special way that a steady state population of

transport sites is distributed between the inward- and outward-facing states; as a result the inward- and outward-facing transport sites will together appear to be a homogeneous population in macroscopic experiments. Such macroscopic homogeneity is indeed observed; the transport sites exhibit a single affinity for chloride or bromide, studied here, as well as for fluoride, iodide and bicarbonate (2). Similarly, the transport sites exhibit a single  $pK_A$  for titration with base. Thus, the ping-pong model is both qualitatively and quantitatively consistent with all of the available  $^{35}\text{Cl}$  NMR evidence.

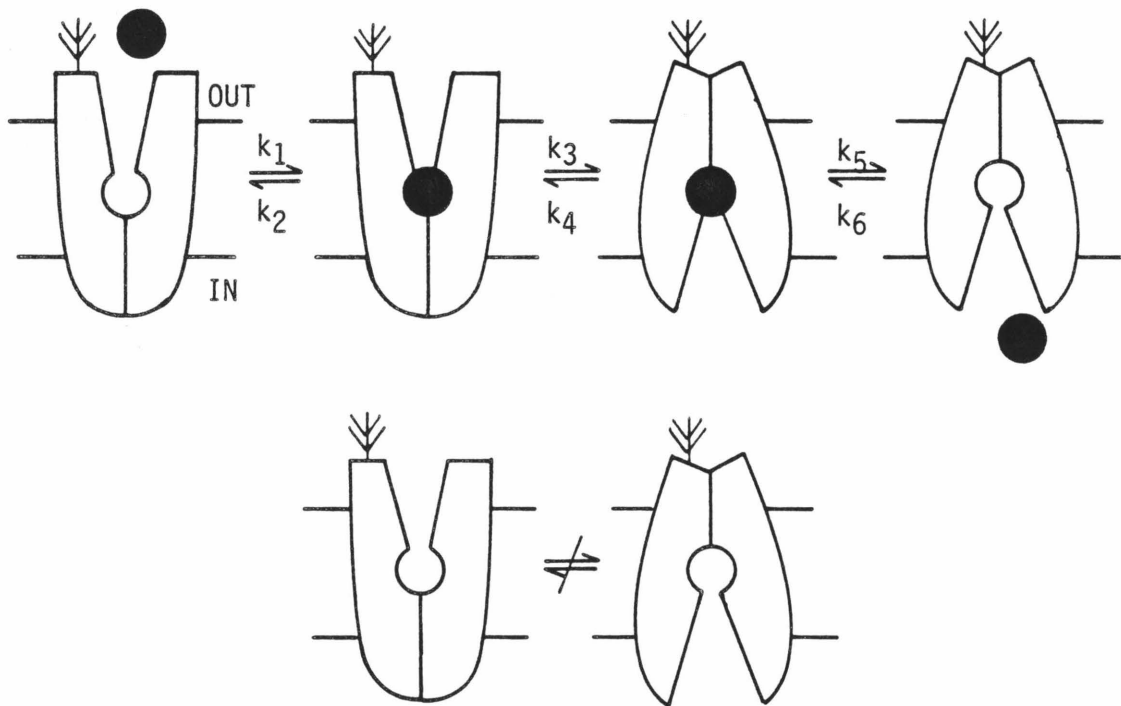
The conclusion that band 3 is a ping-pong transporter allows the chemical equation of the anion transport cycle to be specified. For a ping-pong transporter, the simplest possible chemical equation for chloride self-exchange is:



where E represents the band 3 transport site, and the subscripts I and O represent the inside and outside compartments. As already discussed, this chemical equation is consistent with a range of kinetic and  $^{35}\text{Cl}$  NMR results. This chemical equation also contains the fundamental features of the ping-pong transport cycle; the transport unit has a single transport site that is alternately exposed to opposite sides of the membrane, and the site can only reorient when it contains bound anion. These and other fundamental features of the band 3 transport cycle are further discussed in the following chapter, which focuses on the rate constants  $k_1$ - $k_6$  in the transport cycle.

Figure 5

Schematic ping-pong chemical equation. Shown is the simplest form of an alternating site transporter: the ping-pong transport cycle involves only one chloride binding site. This lone transport site is alternately exposed to opposite sides of the membrane. These schematic drawings do not describe any mechanical details of the model; instead they simply describe its conceptual form.



REFERENCES

1. Macara, I. G., and Cantley, L. C. (1983) Cell Memb. Meth. and Rev. 1, 41-87.
2. Falke, J. J., Pace, R. J., and Chan, S. I. (1984) J. Biol. Chem. 259, 6472-6480.
3. Jennings, M. L. (1982) J. Gen. Physiol. 79, 169-185.
4. Falke, J. J., Pace, R. J., and Chan, S. I. (1984) J. Biol. Chem. 259, 6481-6491.
5. Cass, A., and Dalmark, M. (1973) Nature New Biol. 244, 47-49.
6. Dalmark, M. (1976) J. Gen. Physiol. 67, 223-234.
7. Knauf, P. A., Law, F. Y., Tarshis, T., and Furuya, W. (1984) J. Gen. Physiol. 83, 683-701.
8. Gunn, R. B., and Frölich, O. (1979) J. Gen. Physiol. 74, 351-374.
9. Knauf, P. A. (1979) Curr. Top. Memb. Transp. 12, 249-363.
10. Falke, J. J. and Chan, S. I. (1984) J. Biol. Chem., submitted (a).
11. Lowry, O. H., Rosebrough, N. J., Farr, A. L., and Randall, R. J. (1951) J. Biol. Chem. 193, 265-275.
12. Markwell, M. A., Haas, S. M., Bieber, L. L., and Tolbert, N. E. (1978) Anal. Bioch. 87, 206-210.
13. Forsén, S., and Lindman, B. (1981) Meth. Bioch. Anal. 27, 289-486.
14. Wieth, J. O., and Bjerrum, P. J. (1982) J. Gen. Physiol. 79, 253-282.
15. Steck, T. L. (1974) Meth. Memb. Biol. 2, 245-281.
16. Salhany, J. M., and Rauenbeuhler, P. B. (1983) J. Biol. Chem. 258, 245-249.
17. Brazy, P. C., and Gunn, R. B. (1976) J. Gen. Physiol. 68, 583-599.

18. Gunn, R. B., and Frölich, O. (1982) Chloride Transport in Biological Membranes (J. A. Zadunaisky, ed.) Academic Press, New York.
19. Frölich, O., and Gunn, R. B. (1981) Adv. Physiol. Sci. 6, 275-280.
20. Frölich, O. (1982) J. Memb. Biol. 65, 111-123.
21. Falke, J. J. and Chan, S. I. (1984) J. Biol. Chem., submitted (b).

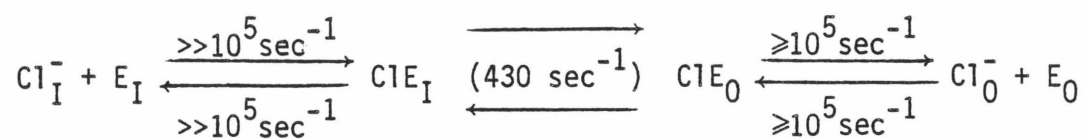
CHAPTER VI  
THE TRANSPORT SITE AND THE KINETIC  
EQUATION FOR TRANSPORT

ABSTRACT

The one-for-one exchange of two chloride ions across the red cell membrane by band 3 can be decomposed into two fundamental types of steps: 1) the binding and dissociation of chloride at the transport site, and 2) the translocation of bound chloride across the membrane. It has been widely assumed that translocation is rate-limiting in the transport cycle so that chloride binding can be described by a simple dissociation constant ( $K_D = k_{OFF}/k_{ON}$ ) rather than by a Michaelis-Menten constant ( $K_M = (k_{OFF} + k_{TRANSLLOCATION})/k_{ON}$ ). The  $^{35}\text{Cl}$  NMR and  $^{37}\text{Cl}$  NMR results presented here indicate that chloride dissociation from the inward-facing transport site satisfies  $k_{OFF} \gg (1.8 \pm .4) \times 10^5 \text{ sec}^{-1}$ ; similarly, chloride dissociation from the outward-facing transport site satisfies  $k_{OFF} \geq (4.2 \pm .5) \times 10^5 \text{ sec}^{-1}$  (both values for  $3^\circ \text{C}$ ). These rate constants specify the rates of both chloride binding and dissociation at the transport site when the site approaches saturation with chloride. Since these rates are at least two orders of magnitude faster than the known turnover rate for the saturated chloride transport cycle ( $430 \text{ sec}^{-1}$  at  $0^\circ \text{C}$ ), the rate-limiting step in the saturated transport cycle is a translocation step rather than a binding or dissociation step. Using these results, it is now possible to describe many features of the kinetic equation for the ping-pong chloride transport cycle. This transport cycle is composed of two transport half-reactions, each transporting a single chloride ion in opposite directions across the membrane. Assuming that the rates of the two opposing translocation steps differ by no more than two orders of magnitude, then the rate-limiting step in each saturated half-transport

reaction is the translocation step.

In summary, the data of this and previous chapters largely determine the chemical and kinetic equations for the band 3 transport cycle. For chloride transport these equations can be written (Figure 4, p. 213 ):



The following chapter begins an investigation of the structure of the transport domain.

## INTRODUCTION

Band 3, which catalyzes the one-for-one exchange of monovalent anions across the red cell membrane, is one of a wide variety of transport proteins found in biological systems. These proteins, despite their diversity, must share certain important features due to their similar functions. In particular, any transport protein that possesses transport site(s) must also possess a transport cycle that can be decomposed into at least three fundamental events: 1) binding of substrate to the transport site(s), 2) translocation of bound substrate across the membrane, and 3) dissociation of substrate from the transport site. The relative rates of binding, translocation, and dissociation are particularly important because they largely determine the nature of the transport cycle. In many discussions of transport proteins, it is assumed that binding and dissociation of substrates are rapid relative to translocation. This assumption appears reasonable, and it greatly simplifies mathematical models. However, it is impossible to rule out a priori a scheme in which binding or dissociation is rate-limiting in the transport cycle. In fact, transport proteins may contain channels leading to transport sites in the interior of the membrane (1), and the diffusion of substrate through such channels could in principle be quite slow.

Substrate channels have been proposed to exist in the band 3 transport unit (1), so it is particularly fortunate that in this system  $^{35}\text{Cl}$  and  $^{37}\text{Cl}$  NMR can be used to investigate the migration of substrate chloride ion between the transport site and the bulk solution (2,3). The physical basis of the NMR technique is the large difference in the spectral widths of bound and free chloride; the spectral width

of chloride bound to a macromolecule is typically  $\geq 10^4$  times larger than the spectral width of solution chloride. As a result, when solution chloride visits a macromolecular binding site sufficiently rapidly, the solution chloride NMR resonance can be measurably broadened. When broadening (termed the linebroadening) is observed, it contains information on the rate of chloride migration between the binding site and the bulk solution, in addition to information on the structure and motions of the site (2,3). The present chapter focuses on both the inward- and outward facing conformations of the band 3 transport site. For each conformation a lower limit is placed on the rate of chloride exchange between the site and the solution. The resulting lower limits are very rapid compared to the known turnover rate of the chloride transport cycle; thus, the rate-limiting step in the transport cycle is the translocation of bound chloride across the membrane rather than a binding or dissociation step. It should be emphasized that this result is independent of any model for the transport cycle; however, a wide variety of existing evidence suggests that anion transport by band 3 proceeds via a ping-pong mechanism ((4), reviewed in (5,6,7); also see the immediately preceding chapter (8)). Thus, a kinetic equation is presented for a ping-pong model of the chloride transport cycle; it is now possible to describe many of the interesting rates in this kinetic equation.

#### MATERIALS AND METHODS

Reagents. Freshly outdated human blood (packed red cells) was a kind gift of the Los Angeles Chapter of the American Red Cross. Human carbonic anhydrase B (HCAB) was from Sigma. All other chemicals were reagent grade or better, as previously described (3,9).

NMR Samples Containing Red Cell Membranes. NMR samples of leaky red cell ghosts (3), sonicated ghosts (9), crushed ghosts (9), and sealed right-side-out vesicles (ROV (9)) were prepared on ice exactly as previously described using 10 mm sample tubes. In order to determine the  $^{35}\text{Cl}^-$  or  $^{37}\text{Cl}^-$  linebroadening due to band 3 transport sites, the same volume of  $\text{H}_2\text{O}$  or DNDS stock solution was added to identical samples. The transport site linebroadening is given by the linebroadening inhibited by 1 mM DNDS and is also termed the DNDS-sensitive linebroadening (3).

$^{35}\text{Cl}$ ,  $^{37}\text{Cl}$  NMR Spectroscopy. Spectra were obtained at  $3^\circ\text{C}$  on a JEOL FX-90Q spectrometer ( $^{35}\text{Cl} = 8.8\text{ MHz}$ ,  $^{37}\text{Cl} = 7.3\text{ MHz}$ ). The standard spectral parameters used in acquisition of the  $^{37}\text{Cl}^-$  spectra were the same as those previously described for  $^{35}\text{Cl}^-$  (3), except that more pulses (5,000-10,000) were used due to the lower sensitivity of  $^{37}\text{Cl}$  NMR spectroscopy for natural abundance chloride. All spectra that were used to determine a single  $^{35}\text{Cl}^-/^{37}\text{Cl}^-$  linebroadening ratio were accumulated consecutively without interruption, using the same number of pulses for both  $^{35}\text{Cl}^-$  and  $^{37}\text{Cl}^-$  spectra. The linebroadening ratios were determined by obtaining  $^{35}\text{Cl}^-$  spectra, then  $^{37}\text{Cl}^-$  spectra (or vice versa), for the same set of six samples: three with 1 mM DNDS and three without 1 mM DNDS.

NMR Sample Analysis. Total membrane protein was determined for NMR samples using the modified (10) Lowry protein assay (11).  $^{35}\text{Cl}^-$  and  $^{37}\text{Cl}^-$  linebroadenings were normalized to 1 mg/ml total membrane protein as previously described (3).

Calculation of the  $^{35}\text{Cl}^-/^{37}\text{Cl}^-$  Linebroadening Ratio. The linebroadenings for each set of three identical samples were averaged to

yield the mean linebroadening with or without 1 mM DNDS. Then the transport site linebroadening (DNDS-sensitive linebroadening (3)) and the low-affinity site linebroadening (DNDS-insensitive linebroadening (3)) were calculated by subtraction of the average linebroadenings for samples with and without 1 mM DNDS. Finally, the transport site or low-affinity site  $^{35}\text{Cl}^-/^{37}\text{Cl}^-$  linebroadening ratio was calculated from the transport site  $^{35}\text{Cl}^-$  and  $^{37}\text{Cl}^-$  linebroadenings or from the low-affinity site  $^{35}\text{Cl}^-$  and  $^{37}\text{Cl}^-$  linebroadenings, respectively.

Statistics. For each membrane system the  $^{35}\text{Cl}^-/^{37}\text{Cl}^-$  linebroadening ratio was determined three or more times from separate experiments using different membrane batches. These linebroadening ratios were then averaged and are presented as means  $\pm$  one standard deviation.

## RESULTS

The Kinetic Information Contained in the  $^{35}\text{Cl}^-$  or  $^{37}\text{Cl}^-$  Linebroadening. The exchange of chloride between a binding site and solution can be slow, intermediate, or rapid on the chloride NMR timescale. For slow exchange the  $^{35}\text{Cl}^-$  or  $^{37}\text{Cl}^-$  linebroadening exactly specifies the exchange rate, while for intermediate and rapid exchange the linebroadening places a lower limit on the exchange rate.

In the slow exchange case the kinetics of both binding to and dissociation from a site can be precisely quantitated. The slow exchange case occurs when the lifetime of chloride in the site is much longer than the NMR timescale defined by the transverse relaxation time ( $T_2$ ) of chloride in the site (the same condition must be satisfied by all three of the chloride NMR transitions). Satisfaction of this condition

guarantees that a single binding event is sufficient to completely dephase the transverse magnetization contributed by a solution chloride ion. In this limit the  $^{35}\text{Cl}^-$  or  $^{37}\text{Cl}^-$  linebroadening is given by (Chapter II)

$$\delta \left\{ \begin{array}{l} = \\ < \\ \ll \end{array} \right\} k_{\text{OFF}} p_{\text{B}} / \pi \quad \begin{array}{l} \text{slow exchange} \\ \text{intermediate exchange} \\ \text{rapid exchange} \end{array} \quad (1)$$

where  $k_{\text{OFF}}$  is the rate constant for chloride dissociation from the site and  $p_{\text{B}} = ([\text{EC1}]/[\text{Cl}^-]_{\text{T}})$  is the fraction of the total chloride that is bound to the site. The equality in Equation 1 holds only when the linebroadening is due to single binding events. In the intermediate and rapid exchange cases, the linebroadening is due to multiple visits by each solution chloride ion to binding sites; thus, the linebroadening yields a lower limit on the exchange rate and the equality changes to one of the indicated conditions.

Equation 1 can be further specified at limiting total chloride concentrations, assuming that the stoichiometric concentration of sites ( $[\text{E}]_{\text{T}}$ ) and the chloride dissociation constant ( $K_{\text{D}} = k_{\text{OFF}}/k_{\text{ON}}$ ) are known. When the site is far from saturation ( $[\text{Cl}^-]_{\text{T}} \ll K_{\text{D}}$ ), the binding reaction controls the exchange rate and the linebroadening becomes (Chapter II)

$$\delta \left\{ \begin{array}{l} = \\ < \\ \ll \end{array} \right\} [\text{E}]_{\text{T}} k_{\text{ON}} / \pi \quad \begin{array}{l} \text{slow exchange} \\ \text{intermediate exchange} \\ \text{rapid exchange} \end{array} \quad (2)$$

or, when  $[\text{Cl}^-]_{\text{T}} \ll K_{\text{D}}$ , the dissociation reaction controls the exchange rate and the linebroadening becomes (Chapter II)

$$\delta \begin{cases} = \\ < \\ \ll \end{cases} \frac{[E]_T k_{OFF}}{[Cl^-]_T \pi} \begin{array}{l} \text{slow exchange} \\ \text{intermediate exchange} \\ \text{rapid exchange} \end{array} \quad (3)$$

Thus, the  $^{35}Cl^-$  or  $^{37}Cl^-$  linebroadening at the very least can be used to place lower limits on  $k_{ON}$  and  $k_{OFF}$ , while under the most favorable conditions these rate constants can be specified exactly.

The maximum amount of kinetic information can be obtained from the  $^{35}Cl^-$  or  $^{37}Cl^-$  linebroadening only when a site has been classified as a slow, intermediate or rapid exchange site. This classification becomes possible when the  $^{35}Cl^-/^{37}Cl^-$  linebroadening ratio is known. For a site in the slow exchange limit, the linebroadening is determined solely by the rate of chloride exchange between the site and solution. This rate is essentially the same for  $^{35}Cl^-$  and  $^{37}Cl^-$  because the kinetic isotope effect is negligible for such relatively heavy ions. As a result, the  $^{35}Cl^-/^{37}Cl^-$  linebroadening ratio is unity (Chapter II):

$$^{35}\delta/^{37}\delta \begin{cases} = 1 \\ >1, < 1.6 \\ = 1.6 \end{cases} \begin{array}{l} \text{slow exchange} \\ \text{intermediate exchange} \\ \text{rapid exchange} \end{array} \quad (4)$$

In the rapid exchange limit, the linebroadening is independent of the rate of chloride exchange but does depend on the characteristics of the site and on the nuclear electric quadrupole moment. The quadrupole moments of the  $^{35}Cl$  and  $^{37}Cl$  nuclei are known and are significantly different such that the square of their ratio, which determines the linebroadening ratio, is 1.6. The intermediate exchange case falls between the extremes of slow and rapid exchange; in this event  $1 < ^{35}\delta/^{37}\delta < 1.6$  (Equation 4).

In short, a combination of  $^{35}\text{Cl}$  NMR and  $^{37}\text{Cl}$  NMR can yield a significant amount of information on the kinetics of chloride exchange between a binding site and solution; moreover, this information is difficult to obtain by any other means.

The kinetics of chloride binding and dissociation at the band 3 transport site as revealed by the  $^{35}\text{Cl}^-$  linebroadening. The  $^{35}\text{Cl}^-$  linebroadening due to band 3 transport sites can be resolved into two components that arise from the inward- and outward-facing sites, respectively (9). Each component can be used to determine the lower limit on the rate of binding and dissociation events at the transport site, using the relationship  $k_{\text{OFF}} \geq \pi\delta/p_B$  (Equation 1).

For the outward-facing transport site,  $^{35}\delta = 1.6 \pm .2$  Hz (Table I). Calculation of the fraction of total chloride bound to the outward-facing transport site ( $p_B$ ) requires knowledge of both 1) the distribution of transport sites between the inward- and outward-facing conformations, and 2) the microscopic chloride dissociation constant for the outward-facing transport site. Neither of these quantities is presently known; however, an upper limit can be placed on  $p_B$  since there is at most one occupied outward-facing transport site per band 3 monomer. Thus,  $p_B \geq 1.2 \times 10^{-5}$  (Table 1). Use of this value in Equation 1 yields  $k_{\text{OFF}} \geq (4.2 \pm .5) \times 10^5 \text{ sec}^{-1}$  (at  $3^\circ \text{C}$ ), which is equivalent to the lower limit on the rate of chloride dissociation from the saturated outward-facing transport site. Since chloride binding and dissociation are assumed to have reached kinetic steady state, the rate of binding events at the saturated outward-facing transport site must also equal  $k_{\text{OFF}}$  and therefore must satisfy the same condition (on-rate)  $\geq (4.2 \pm .5)$

Table I. The Lower Limit on  $k_{OFF}$  for Chloride Dissociation from the Band 3 Transport Site

<u>Outward-Facing Transport Site</u>	<u>Inward-Facing Transport Site</u>
$k_{OFF} \geq \pi\delta/p_B$	
$\delta = 1.6 \pm .2 \text{ Hz}^a$	$\delta = 0.7 \pm .2 \text{ Hz}^a$
[Band 3] = 3.0 $\mu\text{M}$ (monomer)	[Band 3] = 3.0 $\mu\text{M}$
$[\text{Cl}^-]_T = 250 \text{ mM}$	$[\text{Cl}^-]_T = 250 \text{ mM}$
$p_B \leq [\text{band 3 monomer}]/[\text{Cl}^-]_T$ $= 1.2 \times 10^{-5}{}^b$	$p_B \leq 1.2 \times 10^{-5}{}^b$
$k_{OFF} \geq (4.2 \pm .5) \times 10^5 \text{ sec}^{-1}$	$k_{OFF} \geq (1.8 \pm .4) \times 10^5 \text{ sec}^{-1}$

<sup>a</sup>For 1 mg/ml total ghost protein, 3° C, 8.8 MHz (3,9)

<sup>b</sup>Assuming 1 transport site per band 3 monomer

$\times 10 \text{ sec}^{-1}$  (at  $3^\circ \text{ C}$ ). In contrast, the turnover rate of the band 3 catalyzed chloride transport cycle is only  $430 \text{ sec}^{-1}$  at  $0^\circ \text{ C}$  and saturating chloride concentration (12); thus, the chloride binding and dissociation reactions at the saturated outward-facing transport site are each at least two orders of magnitude too fast to be rate-limiting in the transport cycle.

For the inward-facing transport site  $^{35}\delta = 0.7 \pm .2 \text{ Hz}$ , and the same calculation outlined for the outward-facing transport site yields the lower limit for the  $k_{\text{OFF}}$  of this site (Table I). The result,  $k_{\text{OFF}} \geq (1.8 \pm .4) \times 10^5 \text{ sec}^{-1}$ , indicates that the rates of chloride binding and dissociation at the saturated inward-facing transport site are again at least two orders of magnitude faster than the turnover rate. Thus, the rate-limiting step in the chloride transport cycle is not a binding or dissociation event at either the inward- or outward-facing band 3 transport site.

The kinetics of chloride binding and dissociation at the band 3 transport site as revealed by the  $^{35}\text{Cl}^-/^{37}\text{Cl}^-$  linebroadening ratio.  
An examination of the  $^{35}\text{Cl}^-/^{37}\text{Cl}^-$  linebroadening ratio for the inward- and outward-facing transport sites further specifies the rates of chloride exchange between the sites and solution. Moreover, the linebroadening ratio indicates whether or not the transport site linebroadening is

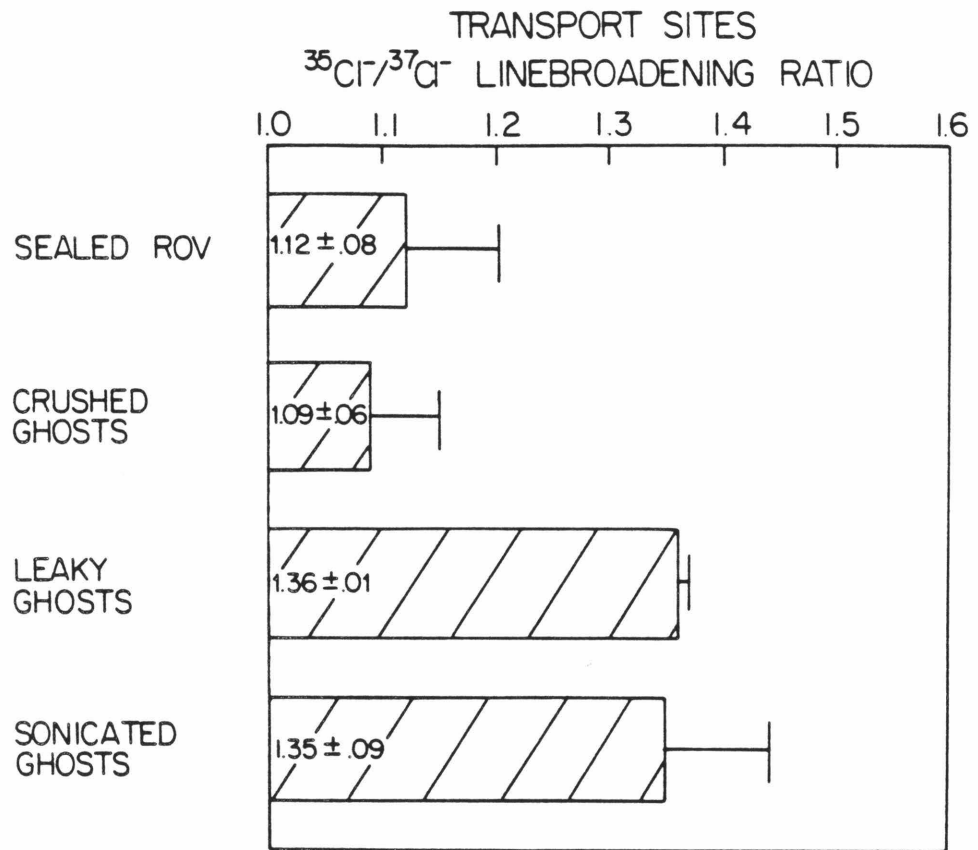
sensitive to changes in the exchange rate.

The outward-facing transport site can be selectively observed using crushed ghosts and sealed right-side-out vesicles (ROV (9)). This site exhibits a linebroadening ratio of 1.09-1.12 (Figure 1) which places the site in or near the slow exchange limit; that is, the transverse magnetization due to a bound  $^{35}\text{Cl}^-$  or  $^{37}\text{Cl}^-$  is completely dephased on a timescale rapid compared to the amount of time spent by the ion in the site ( $1/k_{\text{OFF}}$ ). The linebroadening due to a slowly exchanging site is sensitive to changes in  $k_{\text{ON}}$  and  $k_{\text{OFF}}$  (Equation 1); as a result, specific tests of the band 3 transport mechanism are possible (see the immediately preceding chapter (8)). In the slow exchange limit the exchange rate can be exactly specified from the linebroadening, assuming that the occupied site concentration is known (Equation 1). However, as discussed above, only an upper limit can be placed on the occupied site concentration. Use of this upper limit in the expression  $k_{\text{OFF}} = \pi\delta/p_B$  yields the same condition that was already determined (Table I):  $k_{\text{OFF}} \geq (4.2 \pm .5) \times 10^5 \text{ sec}^{-1}$ . This is simply a restatement of the previous conclusion that the chloride binding and dissociation events at the outward-facing transport site are at least two orders of magnitude too fast to be rate-limiting in the transport cycle.

An alternative explanation for the slow exchange transport site seen in the crushed ghost and ROV systems is that the observed transport site linebroadening might be leaking out from the internal compartment, which slowly exchanges chloride with the external compartment. However, this explanation is ruled out by two pieces of evidence: 1) the linebroadening ratio for the low-affinity sites on leaky or sonicated

Figure 1

Comparison of the  $^{35}\text{Cl}^-/^{37}\text{Cl}^-$  linebroadening ratio of inward- and outward-facing band 3 transport sites. The linebroadening ratio of outward-facing transport sites (sealed ROV, crushed ghosts) is compared with the linebroadening ratio of both inward- and outward-facing transport sites (leaky ghosts, sonicated ghosts). All samples contained 1-2 mg/ml total membrane protein and 250 mM  $\text{NaH}_2\text{PO}_4$ , pH to 8.0 with NaOH,  $\text{NH}_4\text{OH}$ ; the sealed ROV also contained 100  $\mu\text{M}$   $\text{MgSO}_4$ . Spectra were obtained at 8.8 MHz ( $^{35}\text{Cl}^-$ ) or 7.3 MHz ( $^{37}\text{Cl}^-$ ) at 3°C.

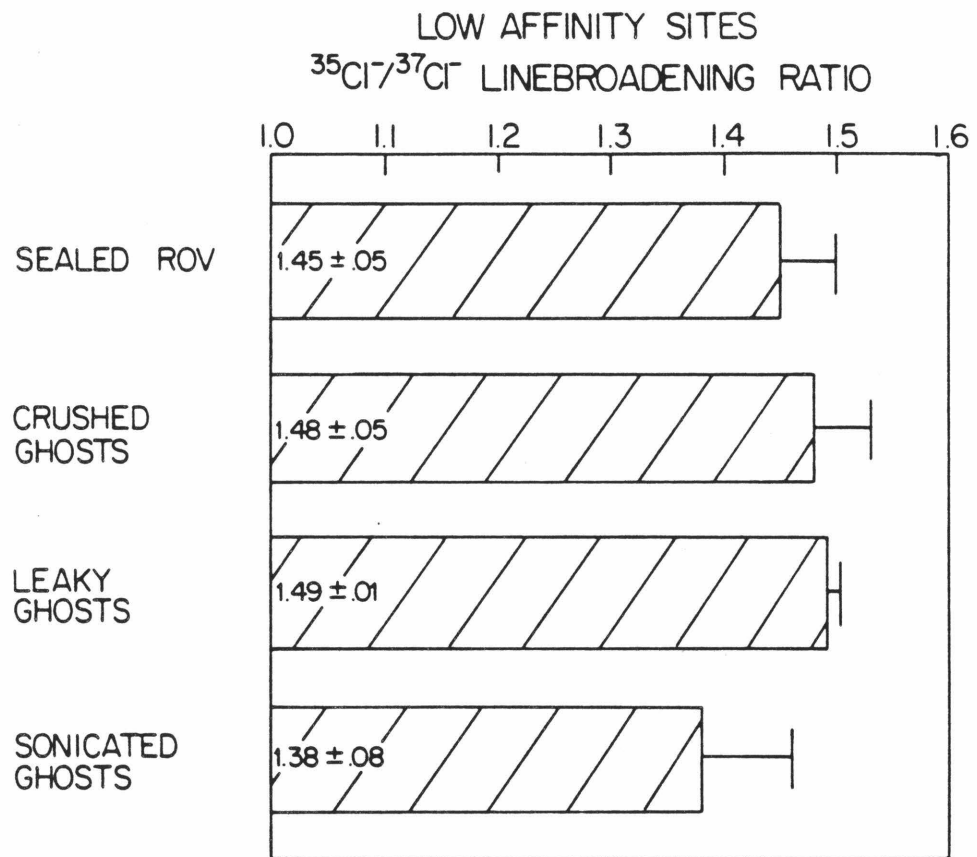


ghosts is not significantly larger than the linebroadening ratio for the low affinity sites on crushed ghosts or ROV (Figure 2), and 2) the outward-facing transport sites are also observed in the intact red cell system, where linebroadening due to internal sites cannot leak into the external compartment.

Both inward-facing transport sites and outward-facing transport sites are observed in the leaky ghost and sonicated ghost systems (9), and in these systems the  $^{35}\text{Cl}^-/^{37}\text{Cl}^-$  linebroadening ratio increases significantly relative to the isolated outward-facing transport site (Figure 1). Thus, the inward-facing transport sites are significantly closer to the rapid exchange limit than are the outward-facing transport sites. This analysis is supported by the linebroadening ratio calculated for the isolated inward-facing transport sites; subtraction of the linebroadening due to the outward-facing transport sites (crushed ghosts, ROV) from the linebroadening due to both inward- and outward-facing transport sites (leaky ghosts, sonicated ghosts) yields the linebroadening due to inward-facing transport sites. (The linebroadenings used in the present calculation are those used to generate Figure 1.) According to this calculation, the inward-facing transport sites exhibit a  $^{35}\text{Cl}^-/^{37}\text{Cl}^-$  linebroadening ratio of  $2.3 \pm .6$ , which is larger than the largest possible value of 1.6 for the rapid exchange limit. However, the uncertainty in the measured ratio is large due to the subtraction, so that the ratio is not statistically different from 1.6. This result, as well as the increase in the linebroadening ratio observed when the inward-facing transport sites are added to the outward-facing sites (Figure 1), together indicate that the inward-facing transport sites

Figure 2

Comparison of the  $^{35}\text{Cl}^-/^{37}\text{Cl}^-$  linebroadening ratio of inward- and outward-facing low-affinity sites. The linebroadening ratio of outward-facing low-affinity sites (sealed ROV, crushed ghosts) is compared with the linebroadening ratio of both inward- and outward-facing low affinity sites (leaky ghosts, sonicated ghosts). Sample compositions and spectra were as in Figure 1.



are in or near the rapid exchange limit. It follows that 1) the linebroadening due to the inward-facing transport sites is independent of moderate changes in  $k_{ON}$  or  $k_{OFF}$ , and 2) the expression  $k_{OFF} \gg \pi\delta/p_B$  (Equation 1) can be used to place a strong condition on the exchange rate for the inward-facing sites. Using the lower limit obtained from the  $^{35}\text{Cl}$  linebroadening (Table I), the exchange rate becomes  $k_{OFF} \gg (1.8 \pm .4) \times 10^5 \text{ sec}^{-1}$ . Thus, the chloride binding and dissociation events at the saturated inward-facing transport site must be more than two orders of magnitude faster than the turnover rate of the chloride transport cycle.

The  $^{35}\text{Cl}/^{37}\text{Cl}$  linebroadening ratio for the low-affinity chloride binding sites. Little is known about the low-affinity chloride binding sites on red cell membranes revealed by  $^{35}\text{Cl}$  NMR; their function is undetermined and it is not known whether they are a homogeneous or heterogeneous class of sites. These sites, which are distributed between both sides of the membrane (9), exhibit a macroscopic linebroadening ratio of 1.38-1.49 (Figure 2). No significant difference is observed between the linebroadening ratio for outward-facing low-affinity sites (crushed ghosts, ROV) and the linebroadening ratio for both inward- and outward-facing low-affinity sites (leaky ghosts, sonicated ghosts, Figure 2). At the present time it is not possible to determine whether the observed linebroadening ratios are due to a homogeneous class of intermediate exchange sites or to heterogeneous classes of slow, intermediate, and/or rapid exchange sites. Moreover, since nothing is known about the number of low-affinity sites, it is not possible to place any limits on the rate of chloride exchange between these sites and solution.

Positive controls for the  $^{35}\text{Cl}^-/^{37}\text{Cl}^-$  linebroadening ratio. Human carbonic anhydrase B possesses a chloride binding site that has previously been shown to be in or near the slow exchange limit by the temperature dependence of the  $^{35}\text{Cl}^-$  linebroadening (13). In the present experiments the HCAB site exhibits a linebroadening ratio of  $1.10 \pm .04$  (Figure 3), thereby confirming the previous conclusion that this site approximates the slow exchange limit.

The linewidth ( $\Delta$ ) of the solution chloride  $^{35}\text{Cl}^-$  or  $^{37}\text{Cl}^-$  resonance is dominated by quadrupole effects; thus, the ratio of these linewidths should approach  $^{35}\Delta/^{37}\Delta = 1.6$ . In the present experiments the observed ratio is  $1.49 \pm .01$  (Figure 3), which is near the theoretically predicted value. Most significantly, these positive controls indicate that the slow and rapid exchange limits are easily resolved experimentally (Figure 3).

#### DISCUSSION

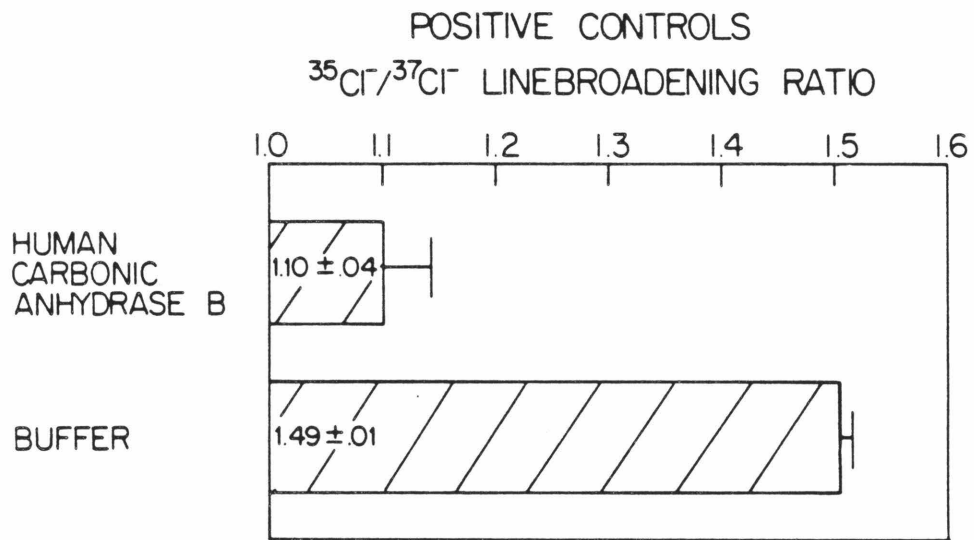
The  $^{35}\text{Cl}$  and  $^{37}\text{Cl}$  NMR data presented here yield the rates of chloride binding and dissociation at both the inward-facing ( $E_I$ ) and outward-facing ( $E_O$ ) band 3 transport sites:



where the indicated values are the number of events per saturated transport site per second at  $3^\circ \text{C}$  (or, equivalently,  $k_{\text{OFF}}$  for chloride dissociation from the site). The chloride binding and dissociation events at both orientations of the saturated transport site are at least two

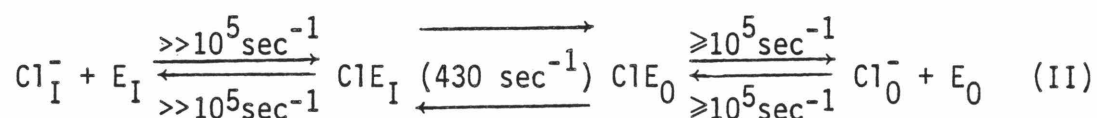
Figure 3

Comparison of the  $^{35}\text{Cl}^-/^{37}\text{Cl}^-$  linewidth ratio and the  $^{35}\text{Cl}^-/^{37}\text{Cl}^-$  linebroadening ratio of positive controls. The linewidth ratio of buffer-only samples (250 mM  $\text{NH}_4\text{Cl}$ , 20%  $\text{D}_2\text{O}$ , 5 mM  $\text{NaH}_2\text{PO}_4$ , pH to 8.0 with  $\text{NaOH}$ ,  $\text{NH}_4\text{OH}$ ) is compared with the linebroadening ratio of human carbonic anhydrase B (1 mg/ml in 500 mM  $\text{NaCl}$ , 20%  $\text{D}_2\text{O}$ , 10 mM  $\text{NaH}_2\text{PO}_4$ , pH 7.4 with  $\text{NaOH}$ ). Spectra were as in Figure 1.



orders of magnitude faster than the turnover rate of the saturated chloride transport cycle ( $430 \text{ sec}^{-1}$  at  $0^\circ \text{ C}$  (12)); thus, the rate-limiting step in the transport cycle is the translocation of bound chloride rather than chloride binding or dissociation. It should be emphasized that this conclusion is not dependent on any model for the transport mechanism.

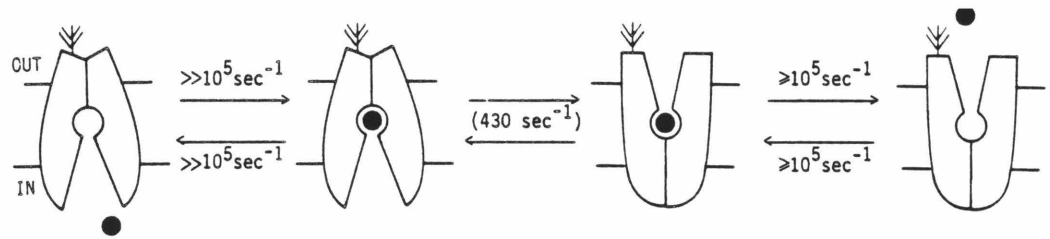
The ping-pong model is now generally accepted as an accurate description of the band 3 transport cycle (4), reviewed in (5,6,7); see also the immediately preceding chapter (8)). The chloride binding and dissociation rates determined here allow the kinetic equation for a ping-pong transport cycle to be described for the first time:

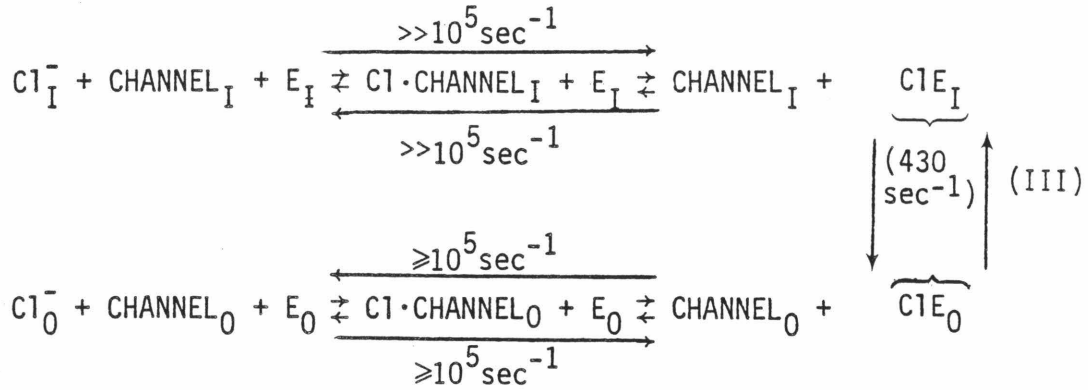


where the translocation of bound chloride is shown to be the rate-limiting step. There are two directions of translocation, and it is not known whether translocation in one direction is sufficiently slow to completely control the turnover rate. However, assuming that the two translocation rates are within two orders of magnitude of each other, the translocation step is rate limiting in both of the half-reactions in the transport cycle (Equation II). The kinetic equation is made still more complete by inclusion of channel migration steps for both orientations of the transport site, since recent results indicate that both internal and external solution chloride must migrate through substrate channels to reach the transport site (1):

Figure 4

Schematic ping-pong kinetic equation. Shown is the ping-pong transport cycle, where the indicated rates are the number of events  $\text{sec}^{-1}$  at each transport site. These schematic drawings do not describe any mechanical details of the transport cycle; instead they simply describe its conceptual form.





As indicated by the kinetic equation, the journey by chloride from solution to the transport site can be decomposed into the fundamental steps of 1) channel migration and 2) binding; note that the rates of chloride binding and dissociation presented here describe the entire journey. The last major undetermined feature of the kinetic equation is the ratio of the in-to-out and out-to-in translocation rate constants. For a ping-pong transporter this ratio partly determines the macroscopically observed dissociation constants of the inward- and outward-facing transport sites, as well as the distribution of transport sites between these two conformations. Thus, more work is still needed to completely specify the kinetic equation for the band 3 transport cycle.

REFERENCES

1. Falke, J. J., and Chan, S. I. (1984) Biophys. J. 45, 91-92.
2. Forsén, S., and Lindman, B. (1981) Meth. Bioch. Anal. 27, 289-486.
3. Falke, J. J., Pace, R. J., and Chan, S. I. (1984) J. Biol. Chem. 259, 6472-6480.
4. Gunn, R. B., and Frölich, O. (1979) J. Gen. Physiol. 74, 351-374.
5. Knauf, P. A. (1979) Curr. Top. Memb. Transp. 12, 249-363.
6. Gunn, R. B., and Frölich, O. (1982) Chloride Transport in Biological Membranes (J. A. Zadunaisky, ed.) Academic Press, New York.
7. Macara, I. G., and Cantley, L. C. (1983) Cell Memb. Meth. and Rev. 1, 41-87.
8. Falke, J. J., and Chan, S. I., (1984) J. Biol Chem., submitted.
9. Falke, J. J., Pace, R. J., and Chan, S. I. (1984) J. Biol. Chem. 259, 6481-6491.
10. Markwell, M. A., Haas, S. M., Bieber, L. L., and Tolbert, N. E. (1978) Anal. Bioch. 81, 206-210.
11. Lowry, O. H., Rosebrough, N. J., Farr, A. L., and Randall, R. J. (1951) J. Biol. Chem. 193, 265-275.
12. Frölich, O., and Gunn, R. B. (1981) Adv. Physiol. Sci. 6, 275-280.
13. Ward, R. L., and Cull, M. D. (1972) Arch. Bioch. Biophys. 150, 436-439.

CHAPTER VII

INHIBITORS OF TRANSPORT

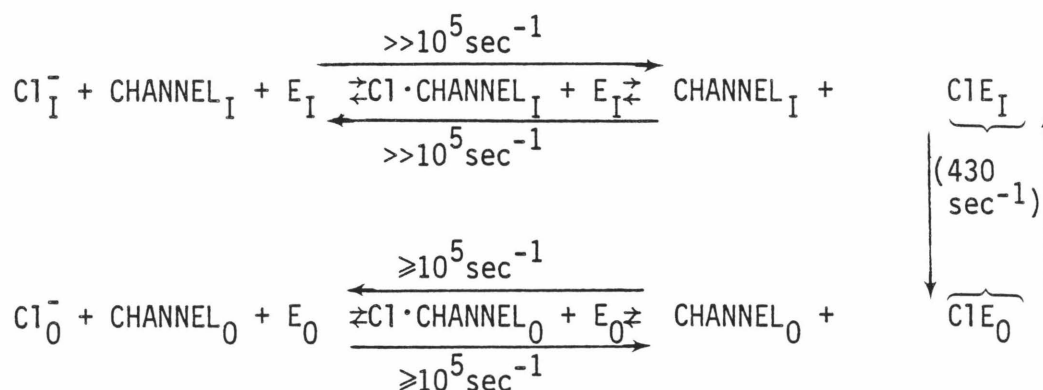
- A. TRANSPORT SITE INHIBITORS
- B. CHANNEL BLOCKERS
- C. TRANSLOCATION INHIBITORS

ABSTRACT

Several important features of the structure of band 3 can be ascertained by understanding how inhibitors of anion transport interrupt the transport cycle. The  $^{35}\text{Cl}$  NMR technique monitors both the migration of chloride to the vicinity of the transport site and binding to the site; thus, the technique can be used to determine whether an inhibitor blocks one of these two steps in the transport cycle. Such a study is conducted in the present chapter to examine the mechanism of inhibition of three different band 3 inhibitors. First, the arginine-specific reagent phenylglyoxal (PG) is shown to inhibit the transport site linebroadening; moreover, the inhibitory covalent reaction is slowed when the site is protected by bound chloride or DNDS, indicating that PG covalently modifies an essential arginine in the transport site itself. Second, the arginine-specific reagent 1,2-cyclohexanedione (CHD) also inhibits the transport site linebroadening, but in this case the inhibitory covalent reaction is unaffected by chloride and DNDS, indicating that CHD inhibits the migration of chloride to the transport site rather than binding to the site. Third, the reversible anion niflumic acid leaves chloride migration and binding to the transport site intact, and similarly leaves the distribution of transport sites between the inward- and outward-facing conformations unchanged; therefore, this inhibitor must slow the translocation step in both the (in  $\rightarrow$  out) and (out  $\rightarrow$  in) half-turnovers of the transport cycle. These results reveal the existence of at least three distinct types of transport inhibitors: 1) transport site inhibitors such as PG that occupy the transport site and prevent chloride binding,

- 2) channel blockers such as CHD that leave the transport site intact but block a channel leading from the transport site to solution, and  
 3) translocation inhibitors that leave the transport site and channel intact but slow the translocation of bound chloride across the membrane.

These data provide direct evidence for a substrate channel leading from the transport site to the solution so that the chemical and kinetic equations for the transport cycle can now be written more completely (Figure 5, p. 238):



Such substrate channels may be a general feature of membrane proteins.

The data also verify (recall the pH-dependence in Chapter V) that the positive charge in the transport site is provided by one or more arginine residues in at least one of the transport site conformations. The following chapter further investigates the structure of the transport site.

## INTRODUCTION

Band 3 is an integral membrane protein which catalyzes the exchange of anions across the red cell membrane. Each band 3 monomer possesses a single transport site which is alternately exposed to opposite sides of the membrane (Chapters IV, V). This transport site contains at least one essential arginine residue that provides the positive charge necessary for anion binding (Chapter V, also (1,2)). Here it is confirmed by  $^{35}\text{Cl}$  NMR that this essential arginine can be covalently modified with the arginine-specific reagent phenylglyoxal (PG), so that the PG-modified transport site no longer binds chloride. In addition, two new types of anion transport inhibitors are described: 1,2-cyclohexanedione (CHD) slows the exchange of chloride between the transport site and solution, while niflumic acid (NIF) leaves chloride migration and binding to the site intact but inhibits the translocation of bound chloride across the membrane. The results indicate that there are at least three distinct types of inhibitors of band 3: 1) transport site inhibitors that occupy the transport site and prevent chloride binding, 2) channel blockers that leave the transport site intact but block a channel leading from solution to the transport site, and 3) translocation inhibitors that leave the transport site and channel intact but slow the translocation of bound chloride across the membrane. These results provide the first evidence for the existence of a substrate channel leading from the transport site to the solution.

## MATERIALS AND METHODS

Reagents. 4,4'-Dinitrostilbene-2,2'-disulfonate (DNDS) was purified as described (3). Phenylglyoxal (PG, Aldrich), 1,2-cyclohexanedione (CHD, Aldrich) and niflumic acid (NIF, Squibb and Sons) were used without further purification.

Membrane preparation. Intact red cells (4), sealed right-side-out vesicles (ROV, (4)), leaky red cell ghosts (ghosts, (3)), and sonicated ghosts (4) were prepared exactly as previously described.

NMR sample preparation. The membranes from one of the above preparations were used to make NMR samples exactly as previously described (3). All samples were prepared on ice the same day that the ghost preparation and  $^{35}\text{Cl}$  NMR were performed. In order to determine the  $^{35}\text{Cl}^-$  linebroadening due to band 3 transport sites, the same volume of  $\text{H}_2\text{O}$  or DNDS stock solution was added to identical samples. The transport site linebroadening is given by the linebroadening inhibited by 1 mM DNDS and is also termed the DNDS-sensitive linebroadening (3).

$^{35}\text{Cl}$  NMR spectroscopy. Spectra were obtained at  $3^\circ\text{C}$  on a JEOL EX-90Q spectrometer ( $^{35}\text{Cl}$  = 8.8 MHz). The standard spectral parameters used in acquisition were the same as those previously described (3).

NMR sample analysis. Total membrane protein was determined for NMR samples using the modified (5) Lowry protein assay (6).

$^{35}\text{Cl}^-$  linebroadenings were normalized to 1 mg/ml total membrane protein as previously described (3).

Statistics. All averages are given as the mean  $\pm$  one standard deviation for  $n \geq 3$ .

## RESULTS

The  $^{35}\text{Cl}$  NMR technique. The mechanism by which anion transport inhibition occurs can be identified by using  $^{35}\text{Cl}$  NMR to monitor 1) the migration of chloride between the solution and the transport site, and 2) the binding of chloride to the transport site. It will be helpful to review the technique in order to explain its application to the present problem. Recently it has been shown that  $^{35}\text{Cl}$  NMR provides a sensitive assay for chloride binding to band 3 transport sites on both sides of the red cell membrane (3,4). The physical basis of this technique is the large  $^{35}\text{Cl}$  NMR spectral width of chloride in a macromolecular binding site; the bound chloride spectral width is typically at least  $\geq 10^4$  times larger than the linewidth of chloride in solution. As a result, when solution chloride samples a binding site sufficiently rapidly, the site can cause measurable broadening of the solution chloride linewidth. This increase in linewidth, or linebroadening, contains information on the structure and motions of the site and on the rate of chloride migration between the site and solution (3,4). The  $^{35}\text{Cl}^-$  linebroadening due to a heterogeneous population of chloride binding sites is given by (4)

$$\delta = \sum_j \frac{\alpha_j [E_j]_T}{K_{D_j}} \frac{[Cl^-]^{-1}}{[Cl^-]^{-1} + K_{D_j}^{-1}} \quad (1)$$

where the sum is over the different types of sites  $E_j$ ,  $\alpha_j$  is a constant characteristic of the  $j$ 'th type of site,  $K_{D_j}$  is the chloride dissociation constant of the  $j$ 'th type of site, and  $[E_j]_T$  is the total concentration of the  $j$ 'th type of site. Equation 1 assumes that the bound chloride returns to solution before binding to another site and that the bound chloride concentration is negligible relative to the total chloride concentration. In the red cell membrane system, multiple types of chloride binding sites are observed (3). The additive contribution of the transport site to the total red cell membrane linebroadening can be determined using DNDS, an anionic reversible inhibitor of the transport site, to identify the transport site linebroadening. For a homogeneous class of sites the linebroadening becomes (3)

$$\delta_j = \frac{\alpha_j [E_j]_T [Cl^-]^{-1}}{K_{D_j} [Cl^-]^{-1} + K_{D_j}^{-1}} \quad (2)$$

Equation 2 indicates that a high-affinity site ( $K_{D_j} \leq [Cl^-]$ ) gives rise to a square hyperbola on a plot of  $^{35}Cl^-$  linebroadening vs.  $[Cl^-]^{-1}$ , while a low-affinity site ( $K_{D_j} \gg [Cl^-]^{-1}$ ) gives rise to a straight line of zero slope. This type of plot can be used to monitor band 3 transport sites, which are high-affinity sites and give rise to a characteristic square hyperbola. The effect

of an inhibitor on this square hyperbola reveals whether the inhibitor a) decreases the linebroadening due to the site, or b) leaves the linebroadening due to the site intact but alters the affinity of the site for chloride, or c) has no effect on the site nor on the exchange of chloride between the site and solution.

Inhibitors that decrease the linebroadening due to the site can in principle act in one of three ways. An inhibitor that reduces chloride binding to the site (decrease in  $[E_j]_T$  or increase in  $K_{D_j}$ , Equation (2)) can be recognized because the binding of the inhibitor is dependent on the chloride concentration, such that chloride binding disfavors inhibitor binding, and vice-versa. In contrast, an inhibitor that slows the exchange of chloride between the site and solution (decrease in  $\alpha_j$ , Equation (2)) need not interact with the site; in this case inhibitor binding is completely independent of the chloride concentration. Finally, an inhibitor could alter the structure of the site (decrease in  $\alpha_j$  caused by a decrease in the electric field gradient at the site or by an increase in the motion of the site (Chapter II)) without altering chloride binding or migration to the site; however such a constrained structural change is highly unlikely. Thus, in practice, there are only two general classes of linebroadening inhibitors that need be considered: 1) inhibitors that reduce chloride binding to the site, recognized by their competition with chloride for binding; and 2) inhibitors that

slow the exchange of chloride between the site and solution, recognized by their lack of dependence on the chloride concentration. Both classes of linebroadening inhibitors have been identified in the band 3 system.

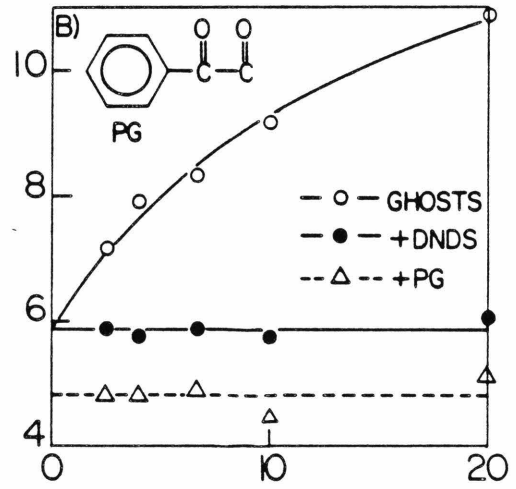
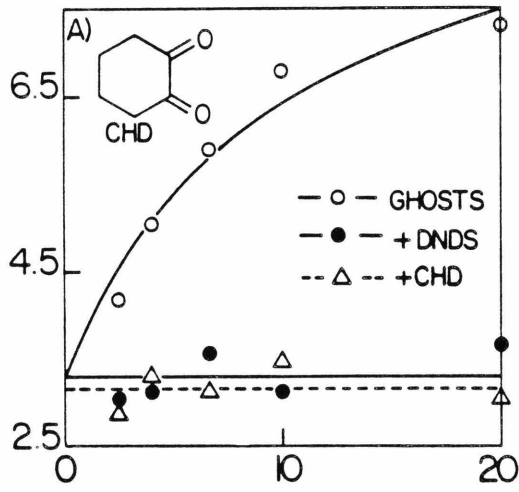
Linebroadening inhibitors: phenylglyoxal is a transport site inhibitor and 1,2-cyclohexanedione is a channel blocker. The arginine-specific reagents phenylglyoxal (PG) and 1,2-cyclohexanedione (CHD) have both been shown to be inhibitors of band 3 catalyzed anion exchange (1,2). Figure 1 indicates that CHD and PG also inhibit the  $^{35}\text{Cl}^-$  NMR linebroadening of ghost membranes. The modified membranes give rise to linebroadening which is similar to that observed for unmodified membrane samples containing the band 3 inhibitor DNDS (Figure 1). We have previously shown that DNDS inhibits the characteristic square hyperbola (Figure 1, Equation 1) due to chloride binding to band 3 transport sites ( $K_D = 80 \text{ mM}$  (3)). Thus, CHD and PG both inhibit the linebroadening due to band 3 transport sites (Figure 1). In addition, PG appears to inhibit some of the linebroadening due to low-affinity ( $K_D \gg 0.5 \text{ M}$ , (3)) chloride binding sites that remain in the presence of DNDS (Figure 1).

The inhibition of the transport site linebroadening by PG stems from transport site destruction: PG is known to covalently modify arginine residue(s) in the transport site (2). This essential arginine is less available for modification when the transport site is occupied with substrate chloride ion or with the inhibitor DNDS. Thus, the reaction of the transport site with PG

Figure 1Inhibition of transport site linebroadening by DNDS, CHD, and PG.

Leaky ghost membranes ((3), 3 parts) were diluted with buffer (2 parts) to yield 100 mM boric acid, pH to 8.0 with NaOH, with or without a) 100 mM CHD or b) 30 mM PG. The resulting suspensions were incubated at 37°C for 1 hr. [Subsequently, the membranes in (b) were washed to remove excess PG by three cycles of pelleting (48,000 xg/15 min), aspiration of the supernatant, and resuspension in 83 mM boric acid, pH to 8.0 with NaOH. The washed membranes were then sonicated (4)]. Finally, the membrane suspensions (5 parts) were diluted with buffer (1 part) to yield X mM NaCl, ionic strength = (400 - X) mM Na citrate, pH 8.0, with a) 83 mM or b) 70 mM borate, and 2) 7% or b) 17% D<sub>2</sub>O, pH 8.0. Where indicated, DNDS was added to 1 mM.

$^{35}\text{Cl}^-$  LINEBROADENING,  
Hz per mg/ml Total Membrane Protein



$1/[\text{Cl}^-]$ , 1/MOLAR

is slowed in the presence of chloride or DNDS (Figure 2, also (1,2)).

In the case of CHD, the inhibition of the transport site linebroadening is not due to simple modification of the transport site since the site is not protected from CHD by the presence of chloride or DNDS (Figure 2). Moreover, the linebroadening inhibition is not due to denaturation of band 3 since a) incubation of ghost membranes with 10 mM 1,4-cyclohexanedione (instead of 1,2-cyclohexanedione) at 37°C for 1 hr inhibits the transport site linebroadening only 17%; and b) the inhibition by CHD is  $46 \pm 2\%$  reversible (by overnight incubation at 4°C in 200 mM  $\text{NH}_2\text{OH}\cdot\text{HCl}$ , pH to 8.0 with NaOH, followed by incubation at 37°C for 1-3 hours and subsequent washing in NMR buffer). Instead, the observed loss of transport site linebroadening is due to decreased accessibility of transport sites to solution chloride ions. Since the linebroadening of both the inward and outward facing transport sites is inhibited by CHD (Figure 1), the transport site is inaccessible to solution chloride at both surfaces of the modified membranes. When the exchange of chloride between transport sites and solution is sufficiently slow, the constant  $\alpha_i$  (Equation 1) becomes zero for the transport sites. As a result the transport site linebroadening disappears even when the transport site remains intact.

Niflumic acid leaves the linebroadening intact and is a translocation inhibitor. Like PG and CHD, niflumic acid is known to inhibit anion transport. However, NIF has no effect on the transport site linebroadening (Figure 3). This negative result is not

Figure 2

The effect of chloride and DNDS on the rate of transport site line-broadening inhibition. Leaky ghost membranes ((3), 3 parts) were diluted with buffer (2 parts) to yield 81 mM boric acid, pH to 8.0 with NaOH + 200  $\mu$ M DNDS, and 14 mM CHD (left column) or 15 mM PG (right column). The resulting suspension was incubated at 37°C for the indicated time before removal to ice. Then the membranes (except for those in the upper left graph) were washed and sonicated as above where the washing buffer also contained 250 mM NaCl and 20% D<sub>2</sub>O. The transport site linebroadening was isolated using the DNDS-subtraction procedure (3). The data were fit with linear least-squares best-fit straight lines.

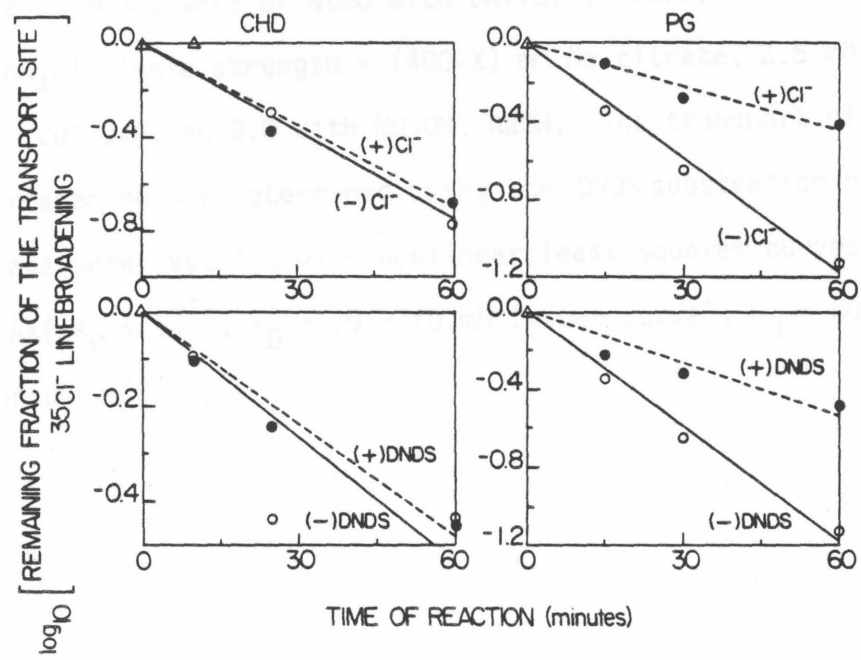
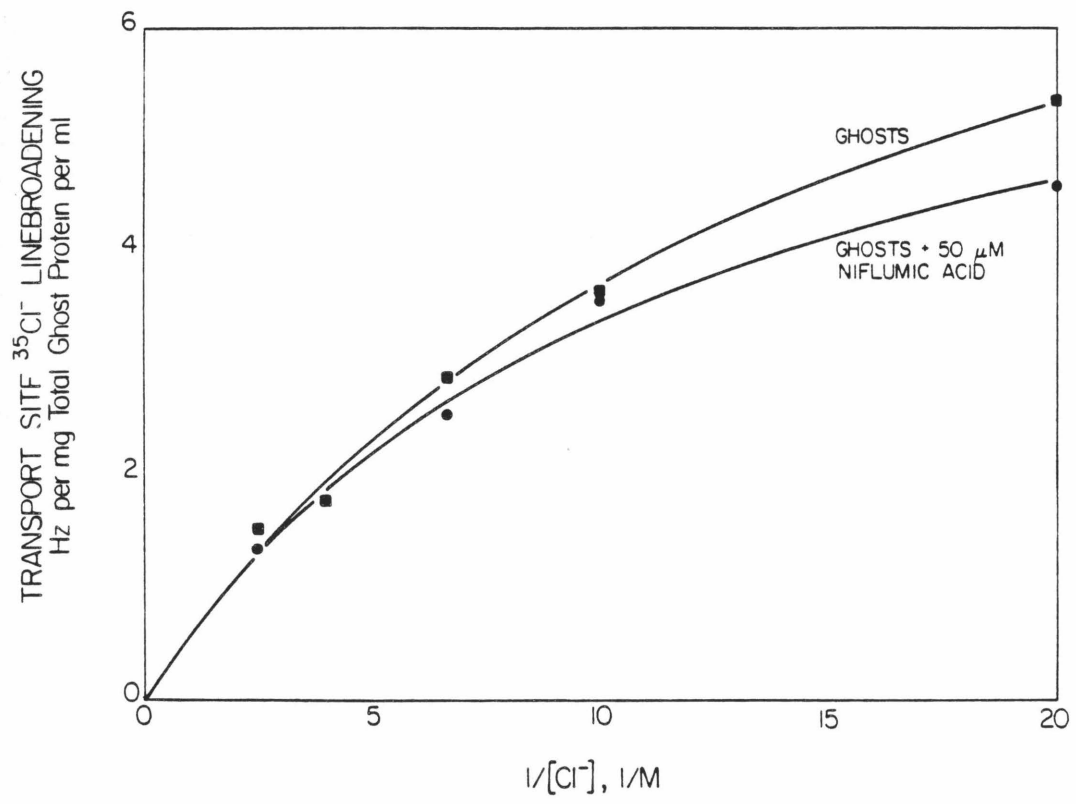


Figure 3

NIF leaves the transport linebroadening intact. Leaky ghost membranes (1 part) were diluted with buffer (1 part) on ice to yield X mM  $\text{NH}_4\text{Cl}$ , ionic strength = (400-X) mM Na citrate, 2.5 mM  $\text{NaH}_2\text{PO}_4$ , 20%  $\text{D}_2\text{O}$ , pH 8.0 with  $\text{NH}_4\text{OH}$ ,  $\text{NaOH}$ . The transport site linebroadening was determined using the DNDS substration procedure. The data were best fit with nonlinear least squares curves ( $y = Ax(xK_D + 1)^{-1}$ ,  $K_D = 70 \pm 10$  mM (upper curve),  $K_D = 80 \pm 10$  mM (lower curve)).



the result of artifactual destruction of the NIF binding site, since NIF restores the transport site linebroadening that is inhibited by DNDS, which indicates that NIF competes with DNDS for binding to band 3 (Figure 4). NIF does not affect the distribution of transport sites between the two surfaces of the membrane, since Table I indicates that the linebroadening due to outward-facing transport sites (intact red cells, ROV, crushed ghosts -- see Chapter IV) is unchanged by NIF; similarly the linebroadening due to both inward- and outward-facing transport sites (sonicated ghosts -- see Chapter IV) is unaffected by NIF. These results are consistent with the conclusion that NIF leaves chloride binding and migration to the inward- and outward-facing band 3 transport sites intact, and also does not recruit sites to one side of the membrane. The lack of recruitment indicates that transport inhibition by NIF is due to slowing of the translocation of bound chloride in both the in  $\rightarrow$  out and out  $\rightarrow$  in directions, since recruitment would occur if one translocation was affected more than the other (Chapter V).

#### DISCUSSION

All of the available evidence is consistent with the following model. The transport site of band 3 contains an essential arginine residue(s). This arginine reacts readily with the planar PG molecule. Nonplanar inhibitors are not able to interact with the transport site (7); thus, CHD cannot reach the arginine(s) there. However,

Figure 4

NIF restores the transport site linebroadening inhibited by DNDS.

Leaky ghost membranes (1 part) were diluted with buffer (1 part) on ice to yield 250 mM  $\text{NH}_4\text{Cl}$ , 5 mM  $\text{Na H}_2\text{PO}_4$ , 20%  $\text{D}_2\text{O}$ , pH 8.0 with  $\text{NH}_4\text{OH}$ ,  $\text{NaOH}$ . The transport site linebroadening was determined using the DNDS subtraction procedure. The data were best fit with a nonlinear least-squares curve (lower curve:  $y = Ax(x + K_D)^{-1}$ , apparent  $K_D = 4.4 \pm 0.7$  mM) or with a linear least-squares straight line (upper curve).

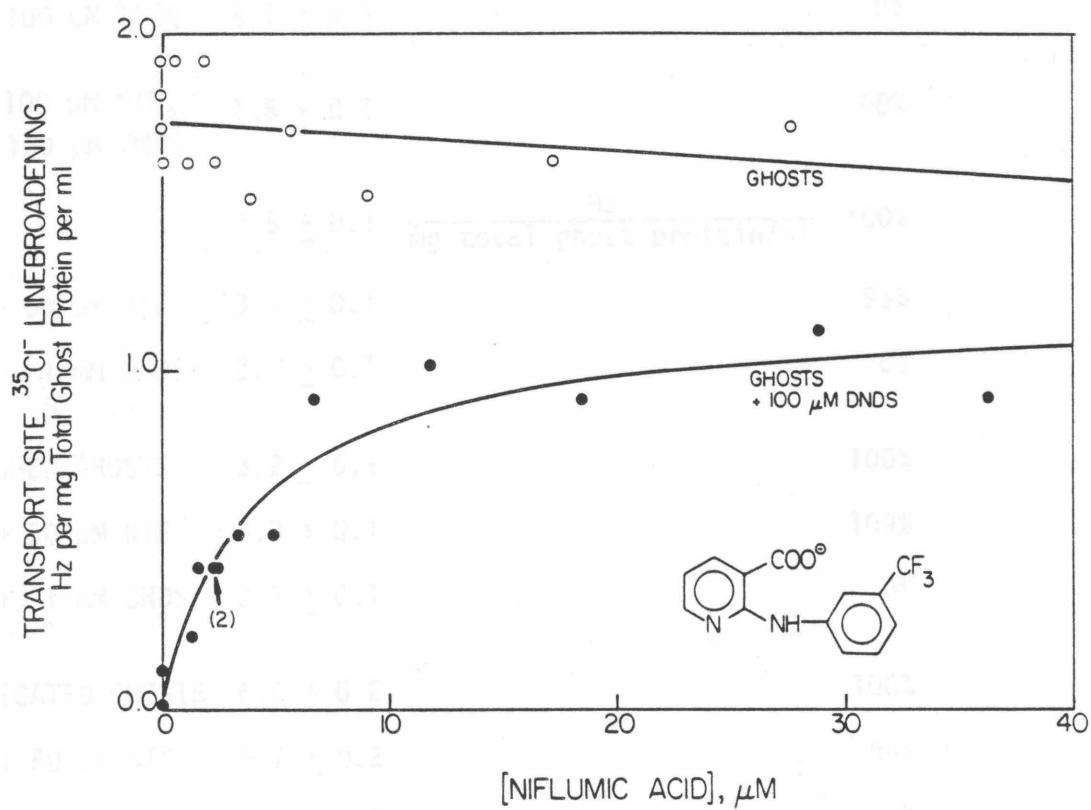


Table I

Niflumic Acid Does Not Significantly Alter  
The Transmembrane Distribution of Transport Sites

	Total $^{35}\text{Cl}^-$ Linebroadening	Transport Site Linebroadening <sup>a</sup>
Intact Cells	$2.1 \pm 0.1 \times 10^{-9}$ Hz per cell/ml	100%
+100 $\mu\text{M}$ Nif	$2.1 \pm 0.1$	100%
+100 $\mu\text{M}$ DNDS	$1.0 \pm 0.1$	0%
+100 $\mu\text{M}$ NIF, 100 $\mu\text{M}$ DNDS	$1.5 \pm 0.1$	60%
ROV	$3.5 \pm 0.1$ $\frac{\text{Hz}}{\text{mg total ghost protein/ml}}$	100%
+ 50 $\mu\text{M}$ NIF	$3.4 \pm 0.1$	93%
+ 1 mM DNDS	$2.1 \pm 0.1$	0%
CRUSHED GHOSTS	$3.2 \pm 0.1$	100%
+ 50 $\mu\text{M}$ NIF	$3.3 \pm 0.1$	109%
+ 1 mM DNDS	$2.1 \pm 0.1$	0%
SONICATED GHOSTS	$6.0 \pm 0.2$	100%
+ 50 $\mu\text{M}$ NIF	$5.7 \pm 0.2$	84%
+ 1 mM DNDS	$4.1 \pm 0.1$	0%

a) Calculated as the fraction of the DNDS sensitive linebroadening that remains intact.

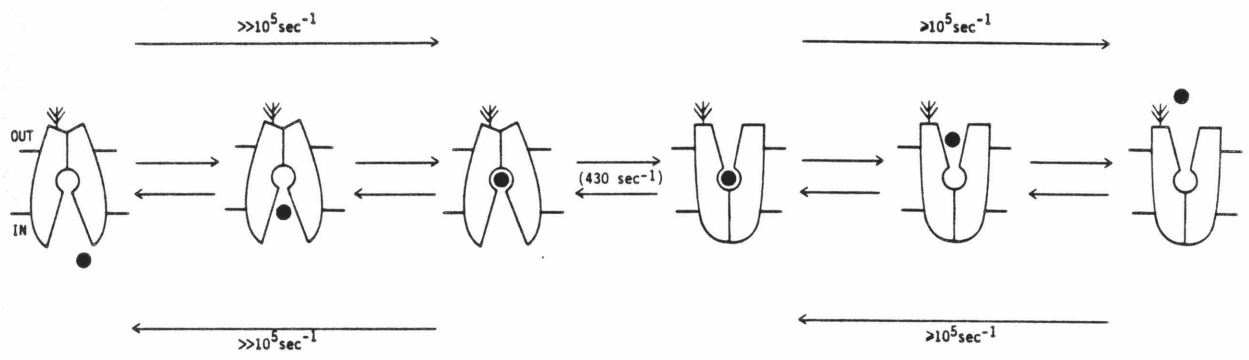
other essential arginines are found in ion channels of undetermined length which lead from both the inner and outer solutions to the interior of the protein where the transport machinery resides. These channel arginines provide positive charges that facilitate the diffusion of anions through the channels. The water-soluble CHD molecule can react with the channel arginines to block movement of anions between binding sites and solution. In contrast, the less water-soluble PG is less likely to be found in aqueous channels; thus, PG inhibits the transport site preferentially. NIF does not occupy either the transport site or the channel, but it binds near the transport site and thereby competes for binding with DNDS, a transport site inhibitor. The bound NIF raises the formation free energy of the intermediate state that occurs during the translocation of the transport site from one side of the membrane to the other. Thus the translocation is slowed by approximately the same factor in both directions, and the distribution of sites across the membrane is not significantly affected.

This model emphasizes the fact that channels can play an essential role even in proteins that do not form membrane pores. Substrate channels could be quite common in proteins, since certain enzymatic processes are most efficient in a low dielectric environment, as is found in the interior of a protein. Moreover, substrate channels could be important control elements, since channels are known to exhibit substrate specificity and can be opened or closed at appropriate times. Future structural studies will hopefully lead to an increased understanding of substrate channels in proteins.

Figure 5

Schematic ping-pong kinetic equation, including channel migration.

Shown is the ping-pong transport cycle, where the indicated rates are given as events  $\text{sec}^{-1}$  at a single transport site. These schematic drawings do not describe any mechanical details of the transport cycle; instead they simply describe its conceptual form.



## REFERENCES

1. Wieth, J. D., Bjerrum, P. J. and Borders, C. L. (1982) J. Gen. Physiol. 79, 283-312.
2. Zaki, L. (1983) Bioch. Biophys. Res. Comm. 110, 616-624.
3. Falke, J. J., Pace, R. J. and Chan, S. I. (1984) J. Biol. Chem. 259, 6472-6480.
4. Falke, J. J., Pace, R. J., and Chan, S. I. (1984) J. Biol. Chem. 259, 6481-6491.
5. Markwell, M. A., Haas, S. M., Bieber, L. L. and Tolbert, N.E. (1978) Anal. Bioch. 87, 206-210.
6. Lowry, O. H., Rosebrough, N. J., Farr, A. L. and Randall, R. J. (1951) J. Biol. Chem. 193, 265-275.
7. Knauf, P. A. (1979) Curr. Top. Memb. Transp. 12, 249-363.

CHAPTER VIII  
PROTEOLYTIC DISSECTION OF THE TRANSPORT SITE

ABSTRACT

Band 3 possesses two distinct structural and functional domains: 1) a 52 kDa transport domain that catalyzes the one-for-one exchange of anions across the membrane, and 2) a 40 kDa cytoskeletal domain that provides the attachment point on the membrane for the red cell cytoskeleton. The present chapter is a search for the minimal structure containing the intact chloride binding machinery, including both the transport site and the substrate channel leading to the transport site. The strategy employed begins with the removal of nonessential portions of the transport domain by proteolysis and/or stripping (Figure 1, p. 246); then the transport site  $^{35}\text{Cl}$  linebroadening is monitored for changes. The results indicate that removal of nonintegral red cell membrane proteins by high pH and high salt stripping steps, or removal of the band 3 cytoskeletal domain by trypsinization followed by stripping, each leave chloride binding to the transport site intact; thus, the transport site is structurally isolated from the nonintegral proteins and the transport domain. Similarly, cleavage of the transport domain into 17 kDa and 35kDa fragments by chymotrypsin leaves chloride binding to the transport site intact; thus, even though each of these fragments contains residues known to be in the vicinity of the transport site, the cleavage that separates the fragments has no effect on transport site structure, possibly because the two fragments remain associated in the membrane following the cleavage. More extensive cleavage of the transport domain is produced by papain, which is used to reduce the integral red cell membrane proteins to their transmembrane segments. The papain reaction followed by stripping removes approximately 60%

of the extramembrane portion of the transport domain and produces a mixture of small fragments primarily in the range 3-7 kDa, with the most predominant size being approximately 5 kDa. This extensive cleavage damages, but does not destroy, chloride binding to the transport site; thus, the transport site is composed of residues from one or more of the papain-generated fragments. In short, the results presented here are completely consistent with a picture in which 1) the transport site is buried in the membrane where it is protected from proteolysis, 2) the transmembrane segments that surround the transport site are held together by strong attractive forces within the bilayer, and 3) the transport site is accessed by solution chloride via an anion channel leading from the transport site to the solution. A significant feature of this picture is that the minimal structure containing the transport site is composed solely of transmembrane segments.

## INTRODUCTION

The band 3 protein of red cell membranes is a 95 kDa transmembrane protein composed of a single polypeptide chain. The protein exists as a dimer and tetramer in the membrane reviewed in (1), but each monomer appears to act as an independent unit in both the anion transport and cytoskeletal functions of band 3 (1-3). The anion transport reaction catalyzed by band 3 is the one-for-one exchange of chloride and bicarbonate: this reaction is central to the respiration of CO<sub>2</sub>. As a result, band 3 is the most heavily used ion transport protein in typical vertebrate animals (4). Band 3 also serves as the attachment point on the membrane for the red cell cytoskeleton (5,6); however, the distinct transport and cytoskeletal functions are associated with different structural domains of the monomer. Proteolysis with trypsin separates these domains and produces both 1) a 52 kDa membrane-bound transport domain that can still catalyze anion exchange (7) and 2) a 40 kDa water-soluble cytoplasmic domain that still binds the cytoskeletal protein ankyrin (8).

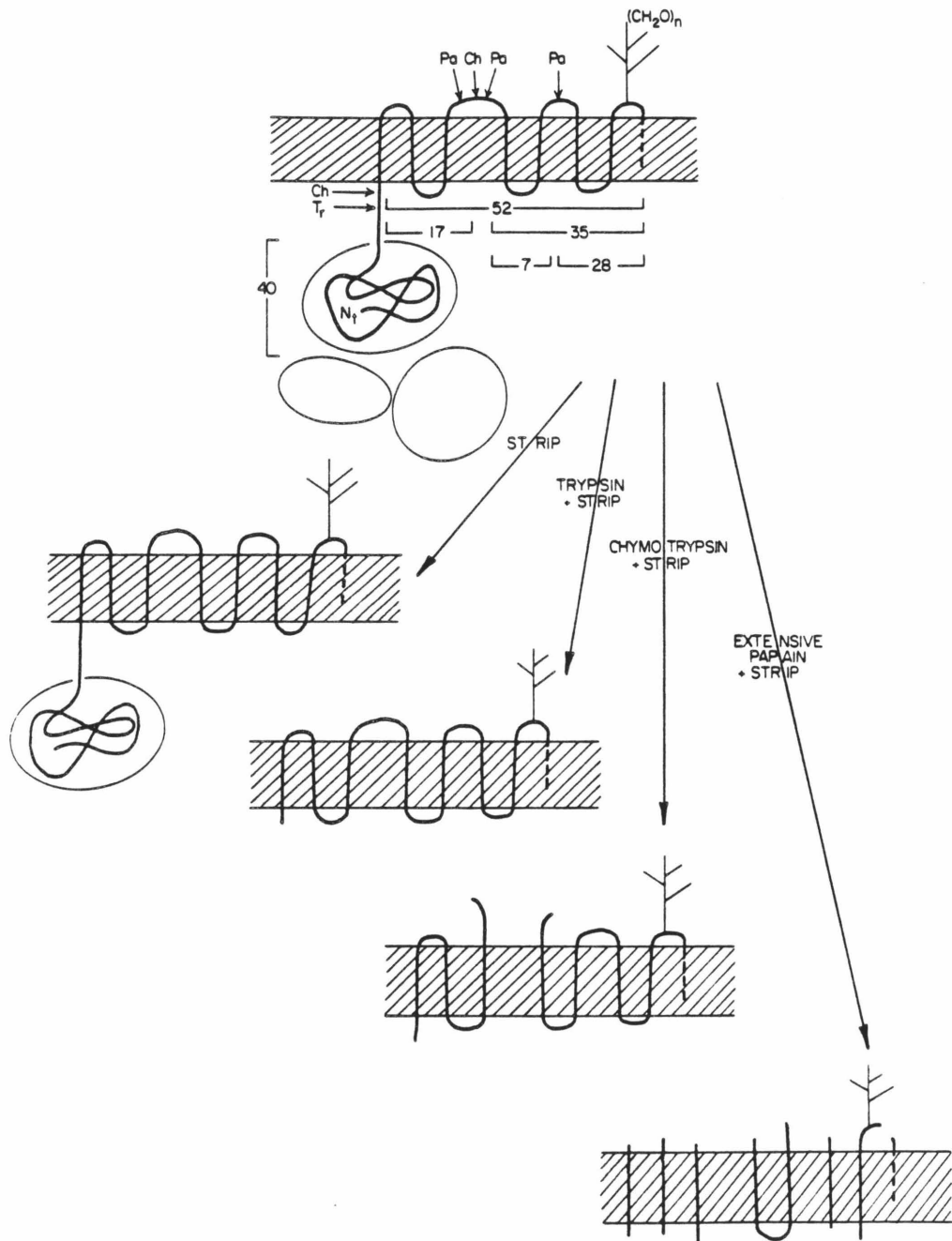
The present study focuses on the transport domain. The structure of this domain could be quite complicated since the transport domain contains at least seven different transmembrane segments. Proteolytic studies have played an important role in the development of the current picture of the transmembrane folding pattern of band 3: proteolytic cleavage sites relevant to the present work are indicated in Figure 1. Intracellular trypsin (9,10) or chymotrypsin (9,11) remove the cytoplasmic domain from the transport domain, while extracellular chymotrypsin (9,11,12) or papain (13) produce cleavages within

the transport domain (Figure 1). Recently, about five of the trans-membrane segments have been generated by proteolysis; extensive cleavage of both sides of the membrane with the nonspecific protease pepsin produced a mixture of small fragments, each large enough to span the membrane (14).

The transport domain contains a single transport site that is alternately exposed to opposite sides of the membrane during the transport cycle (1,15). This transport site is known to contain one or more essential arginine residues (16-18), but the location of these residues within the primary structure of the transport domain has not yet been determined. Chemical crosslinking and labeling studies indicate that multiple regions of the transport domain's primary structure are in close proximity to the transport site. In particular, the fragments that are generated by extracellular chymotrypsin or papain can be covalently crosslinked by 4,4'-diisothiocyanodihydrostilbene-2,2'-disulfonate ( $H_2DIDS$ ), an anionic inhibitor that binds reversibly to the transport site before reacting covalently at two lysine residues in the vicinity of the transport site (19,20). Similarly, 4,4'-diisothiocyanostilbene-2-2'-disulfonate ( $DIDS$  (21)), 4-isothiocyanobenzenesulfonate ( $ITCBS$ (22)), 3,5-diiodo-4-isothiocyanobenzenesulfonate ( $DIOITCBS$  (23)), and dinitrofluorobenzene ( $DNFB$  (24)) all irreversibly inhibit transport by covalently attaching to the 17 kDa chymotryptic fragment (Fig. 1), while phenylglyoxal ( $PG$  (24)), pyridoxal-5-phosphate ( $PDP$  (26)), and reductive methylation of lysine all irreversibly inhibit transport by covalently attaching to the 35 kDa chymotryptic fragment (Figure 1). In addition, inhibitors that attach to the 17 kDa fragment ( $ITCBS$  and  $DNFB$ ), as well as inhibitors that attach to the 35 kDa fragment ( $PG$ ,

Figure 1

Summary of the stripping and proteolytic treatments employed. Shown is the current model for the transmembrane structure of the transport domain of band 3. Also shown is the cytoplasmic domain of band 3 (circled), as well as cytoplasmic proteins nonintegrally associated with the membrane. The proteolytic cleavage sites indicated by the arrows are for trypsin (Tr), chymotrypsin (Ch), and papain (Pa).



PDP, and reductive methylation, each has been shown to overlap the binding site for the stilbenedisulfonates, which are known to occupy the transport site (1,2). Thus, it is likely that the structure of the transport site has contributions from multiple regions within the primary structure.

The present study investigates the location of the transport site within the transport domain. The strategy of this search is straightforward: first, a nonessential protein or peptide is removed from the transport domain by stripping away nonintegral proteins from the membrane or by proteolysis of the membrane; then  $^{35}\text{Cl}$  NMR is used to ascertain whether the transport site can still bind chloride. The results indicate that the transport site remains fully intact following 1) removal of nonintegral red cell membrane proteins by high pH stripping, or 2) removal of the band 3 cytoplasmic domain by trypsin or chymotrypsin, or 3) cleavage of the band 3 transport domain by chymotrypsin. It is also shown that extensive proteolysis on both sides of the membrane with the nonspecific protease papain produces a mixture of small fragments of appropriate size to be transmembrane segments. Chloride binding to the transport site is still observed for these membrane-bound fragments; thus, the transport site is buried within the membrane where it is protected from proteolysis, and the site is composed of residues from one or more of the papain-generated transmembrane segments.

#### MATERIAL AND METHODS

Reagents. Freshly outdated human blood (packed red cells) was

a kind gift of the Los Angeles Chapter of the American Red Cross. Used without further purification were: trypsin and  $\alpha$ -chymotrypsin (Worthington), papain (Calbiochem), H<sub>2</sub>DIDS (Molecular Probes), phenylglyoxal (Aldrich), SDS (specially pure from BHD Chemicals), acrylamide, bisacrylamide, temed, and ammonium persulfate (electrophoresis grade from Biorad), urea (ultra-pure from Schwarz/Mann) and glycine (ammonia-free from Sigma). Electrophoresis calibration proteins were from Pharmacia (LMW calibration kit), Boehringer Mannheim (aprotinin), and Sigma (insulin A).

H<sub>2</sub>DIDS Labeling of Red Cells. Where appropriate, intact red cells labeled with H<sub>2</sub>DIDS, as well as unlabeled control cells, were prepared from intact red cells. First, red cells were washed 3 times in PBS, with simultaneous removal of the buffy coat (4). Then cells to be labeled and control cells were incubated  $\pm$  20  $\mu$ M H<sub>2</sub>DIDS in PBS, 37° C/ 1 hr, followed by two washes in PBS + 0.2% BSA, and one wash in PBS before undertaking the standard ghost prep.

Preparation of Ghost Membranes. Leaky isolated red cell membranes, or ghosts, were prepared and stored exactly as previously described (4). Unless otherwise indicated, all further manipulations of membranes were on ice, all subsequent washes of ghost membranes or modified ghost membranes were 20 Krpm (48,000 x g<sub>max</sub>)/15 min in a Sorvall SS-34 rotor, 0° C, and in all washes the pellet was diluted to < 1/10 original concentration.

Phenylglyoxal Labeling of Ghost Membranes. Where appropriate, the pellet from the ghost prep was diluted to 3/5 original concentration and incubated in 20 mM PG  $\pm$  2 mM DNDS in 80 mM boric acid, pH to 8.0

with NaOH, 37° C/30 min. The ghosts were then washed twice in 5P8 (thus, a total of four washes in 5P8 before proteolysis--see below).

Proteolysis of Ghost Membranes. Unlabeled ghosts, or ghosts labeled with H<sub>2</sub>DIDS or phenylglyoxal, were washed twice in 5P8. The resulting pellet was resuspended in >10 vol of a control solution or a protease-containing solution and incubated as appropriate: trypsin ( $\pm$  30  $\mu$ g/ml, 40 mM NaCl, 5P8, 0° C/1 hr), chymotrypsin ( $\pm$  100  $\mu$ g/ml, 5P8, 23° C/45 min), and papain ( $\pm$  10 mg/ml, 50 mM Na acetate pH 5.2 with acetic, 4 mM cysteine-HCl pH 5.2 with NaOH, 37° C/1 hr--with vortexing every 5 min to prevent excessive aggregation of membranes). The protease was then removed by washing once in 5P8 containing the protease inhibitor PMSF (100  $\mu$ g/mol). The papain-treated membranes sometimes form a dense pellet that is difficult to resuspend to homogeneity by vortexing; in such cases the pellet was resuspended by repeatedly passing the suspension through a pasteur pipet.

High pH Stripping of Ghost Membranes. Ghosts or modified ghosts prepared as above were stripped of nonintegral proteins or proteolytic fragments by exposure to high pH at low ionic strength. Membranes were washed once in 5P8, once in H<sub>2</sub>O, once in 10 mM NaOH, and again in H<sub>2</sub>O. The pH was then lowered by immediately performing the high-salt wash.

High-Salt Washing of Ghost Membranes. Proteins or proteolytic fragments that adhere to the membrane via salt bridges were eluted from the membrane by high-salt washes. Ghosts or modified ghosts were washed once in 250 mM NH<sub>4</sub>Cl, 5P8, pH to 8.0 with NaOH, NH<sub>4</sub>OH, then once in 100 mM NH<sub>4</sub>Cl, 5P8, pH to 8.0 with NaOH, NH<sub>4</sub>OH.

NMR Sample Preparation. The pellet from each of the above preparations was resuspended in 100 mM  $\text{NH}_4\text{Cl}$ , 5P8, pH to 8.0 with NaOH,  $\text{NH}_4\text{OH}$ , to a volume equal to the original volume of ghosts used to make that sample. An exception was made for papain-treated membranes, which were resuspended to 1/4 of their original volume to counteract the decrease in the transport site  $^{35}\text{Cl}^-$  linebroadening caused by papain. The resulting suspensions were sonicated to disrupt sealed vesicles, crushed ghosts, or aggregates of ghosts (15); then the membranes were aliquoted and NMR samples were prepared exactly as previously described (4). In order to determine the  $^{35}\text{Cl}^-$  linebroadening due to band 3 transport sites, the same volume of  $\text{H}_2\text{O}$  or DNDS stock solution was added to identical samples. The transport site linebroadening is given by the linebroadening inhibited by 1 mM DNDS and is also termed the DNDS-sensitive linebroadening (4). All samples were prepared from red cells the same day that they were used for  $^{35}\text{Cl}$  NMR.

$^{35}\text{Cl}$  NMR Spectroscopy. Spectra were obtained at 3° C on a JEOL EX-90Q spectrometer ( $^{35}\text{Cl} = 8.8$  MHz). The standard spectral parameters were the same as those previously described (4), except that 200 dummy scans were performed immediately before the acquisition scans in order to ensure equilibration of sample temperature to that of the probe; this equilibration minimizes the experimental error in linebroadening determinations.

NMR Sample Analysis.  $^{35}\text{Cl}^-$  linebroadenings from different samples were corrected for differences in band 3 concentration by normalizing to the same cholesterol concentration, since the ratio of band 3/cholesterol must be the same for membranes made from the same batch

of red cells. To determine cholesterol, the membrane lipids were first extracted by adding 1 ml of sample (0.2 - 0.4 mg cholesterol) to 19 ml 2:1  $\text{CHCl}_3$ :MeOH and vortexing until mixed. The protein precipitate was removed by suction filtration, and 2 ml  $\text{H}_2\text{O}$  was added to the filtrate, with vortexing to ensure equilibration of soluble components between the newly forming organic and aqueous phases. A particular volume (typically 12 ml) of the organic phase was removed using a separatory funnel and placed in a hot water bath to boil off the solvent. Then the lipids were dissolved in 5 ml  $\text{CHCl}_3$  and the Liebermann-Buchard reaction was performed to determine cholesterol as previously described (27).

Preparation of Electrophoresis Samples. Membranes or modified membranes prepared as above were washed in 5P8 and kept on ice. One vol membranes were then added to one vol Laemmli sample buffer (30% glycerol, 80 mM dithiothreitol, 4% SDS, 130 mM Tris base, 5 mg/100 bromophenol blue), vortexed, and incubated at  $100^\circ\text{C}/3\text{ min}$ . Where appropriate, membrane components were first separated into organophilic and organophobic fractions by extraction with 2:1  $\text{CHCl}_3$ :MeOH. One vol membranes (protein  $\geq 1\text{ mg/ml}$ ) were added to 20 vol 2:1  $\text{CHCl}_3$ :MeOH in a Corex (Sorvall) centrifuge tube, with vortexing. The organophobic components that precipitate were pelleted by spinning at 10 Krpm/30 min in a Sorvall SS-34 rotor. Being careful to save the pellet, the supernatant containing the organophilic components was poured into a clean tube and the solvent boiled off in a hot  $\text{H}_2\text{O}$  bath. The resulting organophobic and organophilic fractions were resolubilized in two vol 2% SDS, 1% BME, 8 M urea by vortexing and washing of the sides of the tubes with a Pasteur pipet; the resolubilization was aided by sonication for

> 30 min in a bath sonicator. The solubilized samples were then diluted with Laemmli sample buffer and heated as above. Membranes to be used for gel samples were stored < 1 day at 4° C or >1 day at -80° C. Following addition of Laemmli sample buffer the samples were stored at room temperature for no more than 2 days.

Electrophoresis. Two gel systems were employed for high- and low-molecular weight ranges. Both systems used the discontinuous buffer system of Laemmli (28). For the HMW gel, the stacking gel contained 4% (w/v) acrylamide and 0.053% bisacrylamide, and the separatory gel contained 10% acrylamide and 0.13% bisacrylamide. HMW gels were stained with coomassie blue as previously described (29). For the LMW gel, the stacking gel contained 9.6% acrylamide and 0.048% bisacrylamide, and the separatory gel contained 16% acrylamide, 0.5% bisacrylamide, 21.6% urea, and 13.3% glycerol (v/v). The LMW stacking and separatory solutions were filtered and copolymerized (30). LMW gels were silver-stained as previously described (31), except that gels were first fixed in 10% TCA, 40% MeOH for > 4 hr, and all solutions before the staining solution and after the reducing solution contained 40% MeOH to prevent gel swelling. Photographs and negatives were obtained using a Polaroid land camera and Type 55 Polaroid film. Molecular weights were determined from a standard plot of migration (relative to the leading edge of the stack) vs.  $\log_{10}$  MW for the following standard proteins: phosphorylase b (94 kDa), BSA (67 kDa), ovalbumin (43 kDa), carbonic anhydrase (30 kDa), soybean trypsin inhibitor (20.1 kDa), lactalbumin (14.4 kDa), aprotinin (6.5 kDa), and insulin A (2.3 kDa).

## RESULTS

Observation of Band 3 Transport Sites by  $^{35}\text{Cl}$  NMR. The minimal structure containing the intact band 3 transport site can be identified only if it is possible to monitor the intactness of the site. We have recently shown that  $^{35}\text{Cl}$  NMR provides a sensitive assay for chloride binding to band 3 transport sites on both sides of the red cell membrane (4,15). The physical basis of this technique is the large  $^{35}\text{Cl}$  NMR spectral width of chloride in a macromolecular binding site; the bound chloride spectral width is typically at least  $\geq 10^4$  times larger than the linewidth of chloride in solution. As a result, when solution chloride samples a binding site sufficiently rapidly, the site can cause measurable broadening of the solution chloride linewidth. This increase in linewidth, or linebroadening, contains information on the structure and motions of the site and on the rate of chloride migration between the site and solution (32,33). The  $^{35}\text{Cl}^-$  linebroadening due to a heterogeneous population of chloride binding sites is given by (4)

$$\delta = \sum_j \frac{\alpha_j [E_j]_T}{K_{Dj}} \frac{[\text{Cl}^-]^{-1}}{[\text{Cl}^-]^{-1} + K_{Dj}^{-1}} \quad (1)$$

where the sum is over the different types of sites  $E_j$ .  $\alpha_j$  is a constant characteristic of the  $j$ 'th type of site,  $K_{Dj}$  is the chloride dissociation constant of the  $j$ 'th type of site, and  $[E_j]_T$  is the total concentration of the  $j$ 'th type of site. Equation 1 assumes that the bound chloride returns to solution before binding to another site and that the bound chloride concentration is negligible relative to the total chloride

concentration. In the red cell membrane system, multiple types of chloride binding sites are observed (4). The additive contribution of the transport site to the total red cell membrane linebroadening can be determined using DNDS, an anionic reversible inhibitor of the transport site, to identify the transport site linebroadening. For a homogeneous class of sites the linebroadening becomes (4)

$$\delta_j = \frac{\alpha_j [E_j]_T}{K_{D_j}} \frac{[Cl^-]^{-1}}{[Cl^-]^{-1} + K_{D_j}^{-1}} \quad (2)$$

This equation indicates that a high-affinity site ( $K_{D_j} \leq [Cl^-]$ ) gives rise to a square hyperbola on a plot of  $^{35}Cl^-$  linebroadening vs.  $[Cl^-]^{-1}$ , while a low-affinity site ( $K_{D_j} \gg [Cl^-]$ ) gives rise to a straight line or zero slope. Thus,  $^{35}Cl^-$  linebroadening vs  $[Cl^-]^{-1}$  data can be used to study the effects of removal of nonintegral proteins and of proteolysis on the integrity of the transport site.

#### The Effect of Nonintegral Proteins on the Transport Site.

Isolated red cell membranes or ghosts possess a variety of protein constituents. It is generally assumed that the chloride transport unit is localized completely within band 3, but it is possible that another unidentified protein(s) could be required for the structural integrity of the transport unit. Several distinct classes of proteins exist in the ghost membrane system including (34): 1) transmembrane integral proteins such as band 3, glycophorin, the glucose transporter and the Na,K-ATPase, 2) nonintegral cytoskeletal proteins including spectrin, actin, bands 4.1 and 4.2, and ankyrin, and 3) nonintegral cytoplasmic proteins that bind to band 3 such as hemoglobin

and glyceraldehyde-3-phosphate dehydrogenase. The nonintegral proteins can easily be removed from the ghost membrane; thus, it is possible to test for interactions between these proteins and the transport site.

The two methods used here for the removal of nonintegral proteins are high-salt extraction and high-pH stripping. High-salt extraction disrupts ionic interactions and releases at least one protein--glyceraldehyde-3-phosphate dehydrogenase--from the membrane. High-pH stripping at low ionic strength removes virtually all of the nonintegral protein; the mechanism of this stripping involves generation of a negative surface charge on the proteins and the membrane, which at low ionic strength repels the nonintegral proteins from the membrane (35). The effects of high-salt extraction and high-pH stripping on the protein composition of ghost membranes are shown in Figure 2. SDS-polyacrylamide gel electrophoresis indicates that a large number of proteins exist in untreated ghost membranes and a high-salt wash removes glyceraldehyde-3-phosphate dehydrogenase, while high-pH stripping followed by a high-salt wash removes most of the bands and leaves band 3 as the major protein constituent (70% of the remaining protein (1)). In each case, band 3 migrates as a broad band due to heterogeneous glycosylation of the membrane-bound transport domain (36).

The effect of nonintegral protein removal on the  $^{35}\text{Cl}^-$  linebroadening due to the band 3 transport site is shown in Figure 3. Transport site linebroadening vs.  $[\text{Cl}^-]^{-1}$  data is shown for three types of sonicated ghost membranes: 1) control membranes (ghosts), 2) membranes extracted with high salt (washed ghosts), and 3) membranes stripped with high pH at low ionic strength then extracted with high

Figure 2

Removal of nonintegral red cell membrane proteins and removal of the band 3 cytoskeletal domain. Shown are the SDS-polyacrylamide gel electrophoresis patterns of (a,g) molecular weight markers, (b) ghosts, (c) ghosts washed in high salt, (d,e) ghosts stripped with high pH at low ionic strength, then washed in high salt, and (f) trypsinized ghosts stripped with high pH at low ionic strength, then washed in high salt. Lanes a-d and e-f were run on two different gels, respectively. The high-molecular weight gel system was as described in text.

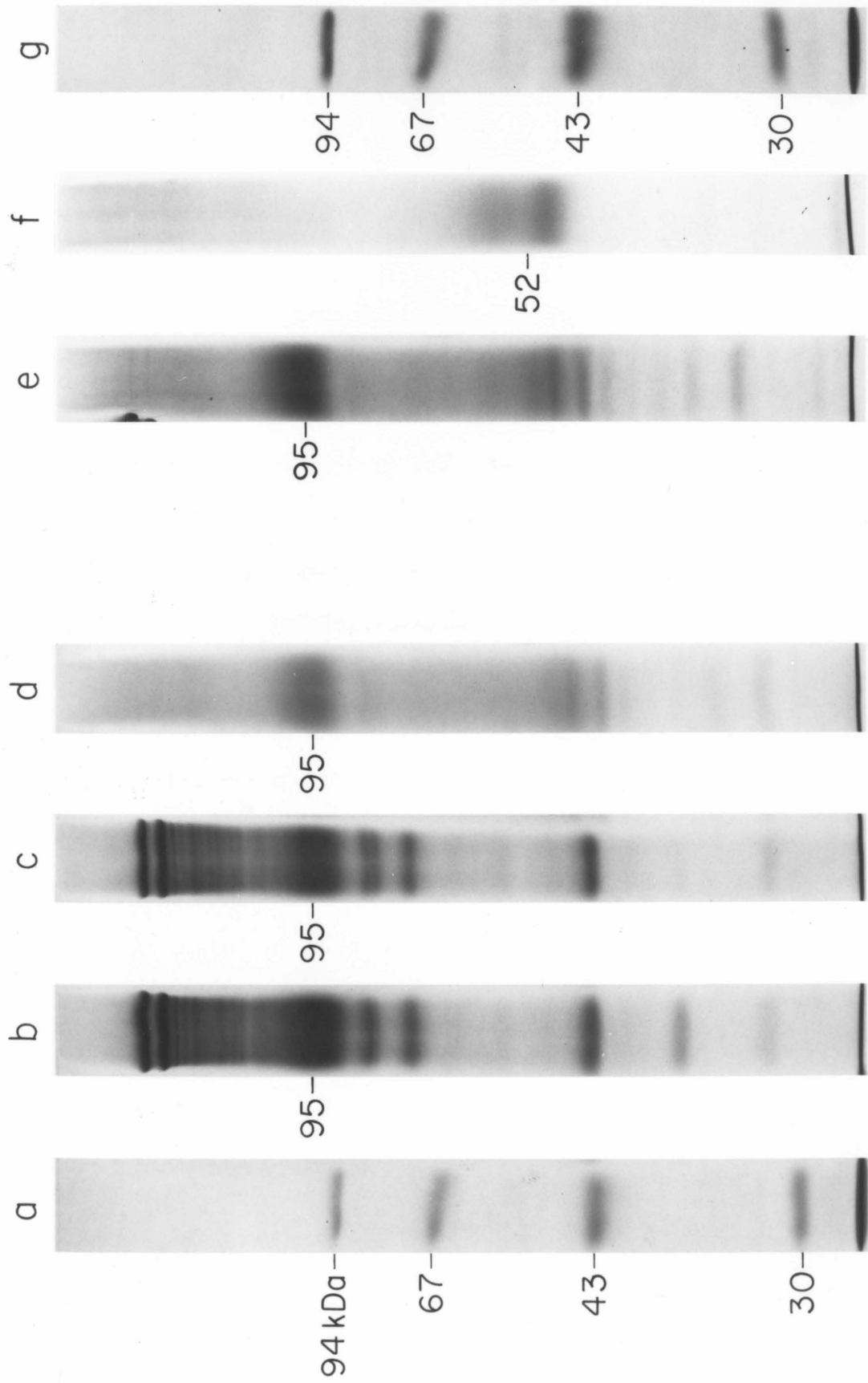
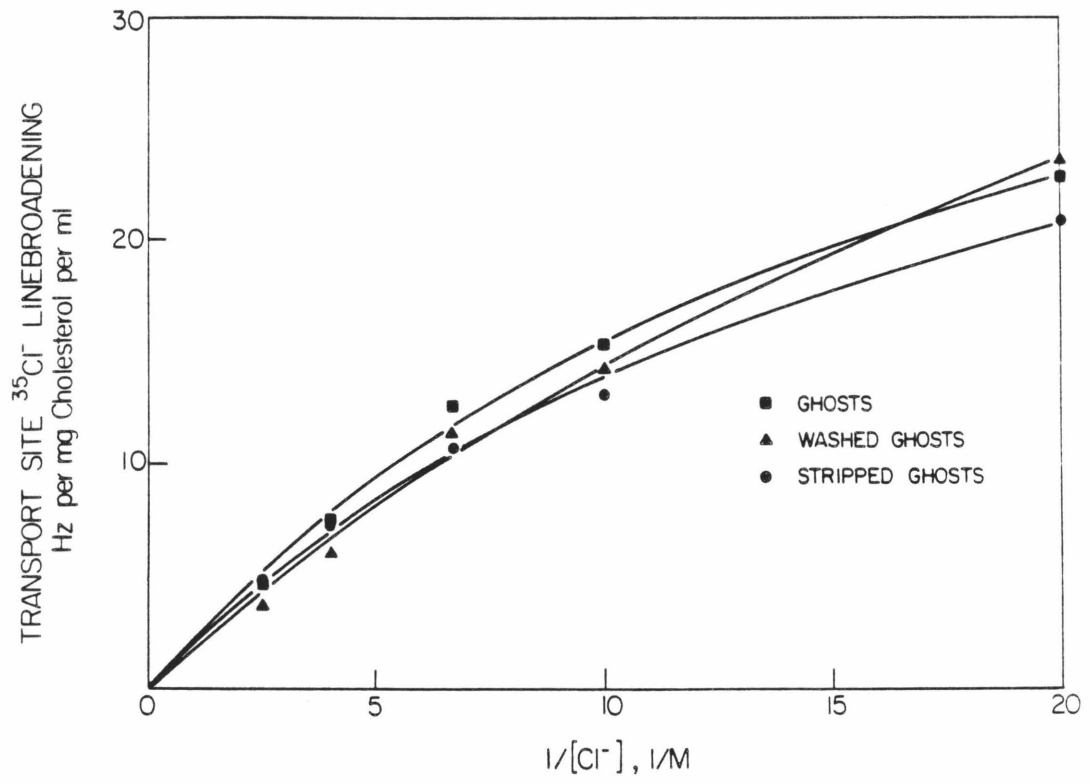


### Figure 3

The effect on band 3 transport sites of removal of nonintegral proteins. Shown is the  $^{35}\text{Cl}^-$  linebroadening due to band 3 transport sites on sonicated ghost membranes (ghosts), ghost membranes washed in high salt then sonicated (washed ghosts), and ghost membranes stripped with high pH at low ionic strength, then washed in high salt and sonicated (stripped ghosts). Samples contained  $x$  mM  $\text{NH}_4\text{Cl}$ , ionic strength to  $(400 - x)$  mM with Na citrate, 5 mM  $\text{NaH}_2\text{PO}_4$ , 20%  $\text{D}_2\text{O}$ , pH to 8 with NaOH and  $\text{NH}_4\text{OH}$ .  $^{35}\text{Cl}$  NMR spectra were obtained at 8.8 MHz and  $3^\circ\text{C}$ . The nonlinear least-squares best-fit curves ( $y = Ax/(1 + xK_D)$ , solid lines) yielded an average  $K_D = 50 \pm 15$  mM for chloride binding in the three cases.



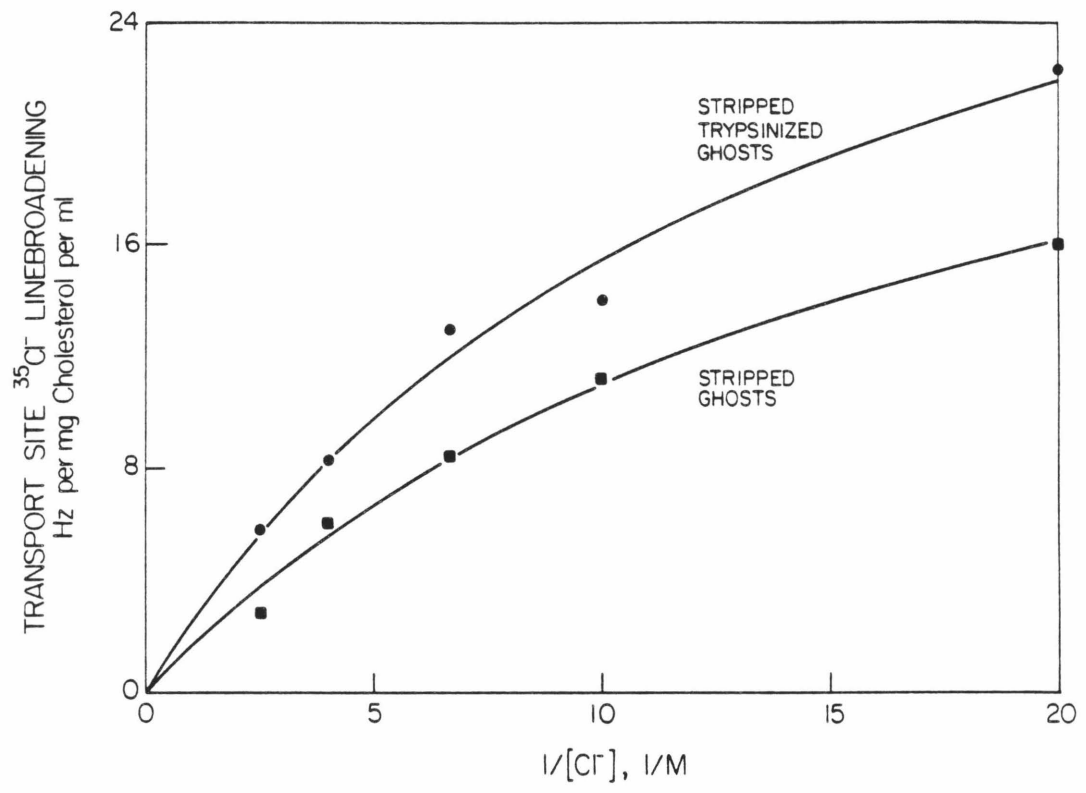
salt (stripped ghosts). These membrane samples correspond to the SDS-page lanes b-d in Figure 2, respectively. The data for these three cases are indistinguishable, and the average dissociation constant for chloride binding in the three cases is  $K_D = 50 \pm 15$  mM, which is within experimental error of the previously determined  $K_D = 80 \pm 20$  mM for chloride binding to band 3 transport sites on leaky ghost membranes (4). Thus, the nonintegral proteins have no measurable effect on the integrity of the transport site.

The Effect of the Cytoskeletal Domain on the Transport Site. The 40 kDa cytoskeletal domain of band 3 lies on the cytoplasmic surface of the membrane, where it binds the cytoskeletal protein ankyrin and other cytoplasmic proteins (34). Proteolysis can be used to quantitatively remove the cytoskeletal domain from the transport domain; thus, the proposal that the transport domain is structurally independent of the cytoskeletal domain can be easily tested. Trypsinization of leaky ghosts followed by stripping yields the 52 kDa transport domain, which migrates as a broad band due to heterogeneous glycosylation. A previously noted characteristic feature of this band is the higher staining intensity at its leading edge (13). In the present experiments the observation of this characteristic band confirms the removal of the cytoskeletal domain by trypsin (Figure 2, lane f).

The effect of removal of the cytoskeletal domain on the  $^{35}\text{Cl}^-$  linebroadening due to band 3 transport sites is shown in Figure 4. Transport site linebroadening vs.  $[\text{Cl}^-]^{-1}$  data is shown for two types of sonicated ghost membranes: 1) stripped ghosts, and 2) stripped trypsinized ghosts. These membrane samples correspond to the SDS-page

#### Figure 4

The effect on band 3 transport sites of removal of the cytoskeletal domain. Shown is the  $^{35}\text{Cl}^-$  linebroadening due to band 3 transport sites on ghost membranes (stripped ghosts) and trypsinized ghost membranes (stripped trypsinized ghosts). Both types of membranes were stripped with high pH at low ionic strength then washed in high salt and sonicated. Samples and  $^{35}\text{Cl}$  NMR spectra were as in Figure 3. The nonlinear least-squares best-fit curves ( $y = Ax(1 + xK_D)$ , solid lines) yielded  $K_D = 60 \pm 10$  mM and  $K_D = 70 \pm 10$  mM for chloride binding to transport sites on stripped ghosts and stripped trypsinized ghosts, respectively.



lanes e,f in Figure 2, respectively. The data indicate that removal of the cytoplasmic fragment does not inhibit the transport site linebroadening; instead, a slight increase (23%) in the transport site linebroadening is observed. It is not possible to specify the mechanism of this linebroadening increase; it could involve a small change in the structure of the band 3 transport domain, including a possible redistribution of the transport site between the inward- and outward-facing conformations, or an increase in the rate of chloride migration between the transport site and solution (4,33). The structure of the transport site is not significantly affected, however, since the chloride dissociation constant for the site is essentially the same with ( $K_D = 60 \pm 10$  mM) or without ( $K_D = 70 \pm 10$  mM) the cytoskeletal domain (Figure 4). These results are completely consistent with previous anion transport results, indicating that transport remains 50% (37) to 100% (7) intact following removal of the cytoskeletal domain with trypsin. Thus, the cytoskeletal domain is not essential for the structure of the transport site.

The Effect of Proteolytic Cleavage within the Transport Domain on the Transport Site. Treatment of leaky ghosts with chymotrypsin releases the cytoskeletal domain from the transport domain and also produces a second cleavage within the transport domain at the extracellular surface (Figure 1). Since it has just been shown that removal of the cytoskeletal domain leaves the transport site intact, chymotrypsin can be used to examine the effect of cleavage within the transport domain on the transport site.

Chymotryptic digestion of leaky ghosts produces 35 kDa and 17 kDa

fragments of the transport domain (Figure 1). The 35 kDa fragment gives rise to a broad band that is generally not observed on SDS-page gels due to heterogeneous glycosylation (38,39). In contrast, the 17 kDa fragment gives rise to a sharp band. In the present experiments observation of the characteristic band due to the 17 kDa fragment confirms the removal of the cytoskeletal domain and the internal cleavage of the transport domain (Figure 5, lane b).

The effect of the two chymotryptic cleavages on the  $^{35}\text{Cl}^-$  linebroadening due to band 3 transport sites is shown in Figure 6. Transport site linebroadening vs.  $[\text{Cl}^-]^{-1}$  data is shown for two types of sonicated ghost membranes: 1) stripped ghosts and 2) stripped chymotrypsinized ghosts, where the stripped chymotrypsinized membranes correspond to SDS-page lane b in Figure 5. The data indicate that removal of the cytoplasmic domain and cleavage of the transport domain into 17 kDa and 35 kDa fragments cause a slight increase ( $\sim 30\%$ ) in the transport site linebroadening. Since the same result is observed for the removal of the cytoplasmic domain alone (Figure 4), it can be concluded that the chymotryptic cleavage within the transport domain has no additional effect on the transport site linebroadening. The structure of the transport site is not significantly changed by the chymotryptic cleavages since the chloride dissociation constant of the control membranes ( $K_D = 80 \pm 10 \text{ mM}$ ) is essentially the same as that of the chymotrypsinized membranes ( $K_D = 70 \pm 2 \text{ mM}$ , Figure 6). These results are completely consistent with transport studies conducted on a similar system; extracellular chymotrypsin produces the same 35 kDa fragment as well as a 60 kDa fragment containing the

Figure 5

Cleavage of the band 3 transport domain by chymotrypsin and papain. Shown are the SDS-polyacrylamide gel electrophoresis patterns of (a,f) molecular weight markers, (b) chymotrypsinized ghost membranes, (c) papain-treated ghost membranes, (d) the precipitate from 2:1  $\text{CHCl}_3$  MeOH extraction of papain-treated ghost membranes, (e) the supernatant from same extraction of papain-treated ghost membranes, and (f) papain with its self-proteolysis fragments (10 mg/ml papain, 37° C/1hr). All membrane samples were stripped with high pH at low ionic strength and washed in high salt. Lanes a-b and c-g were run on two different gels, respectively. The low molecular weight gel system was as described in text.

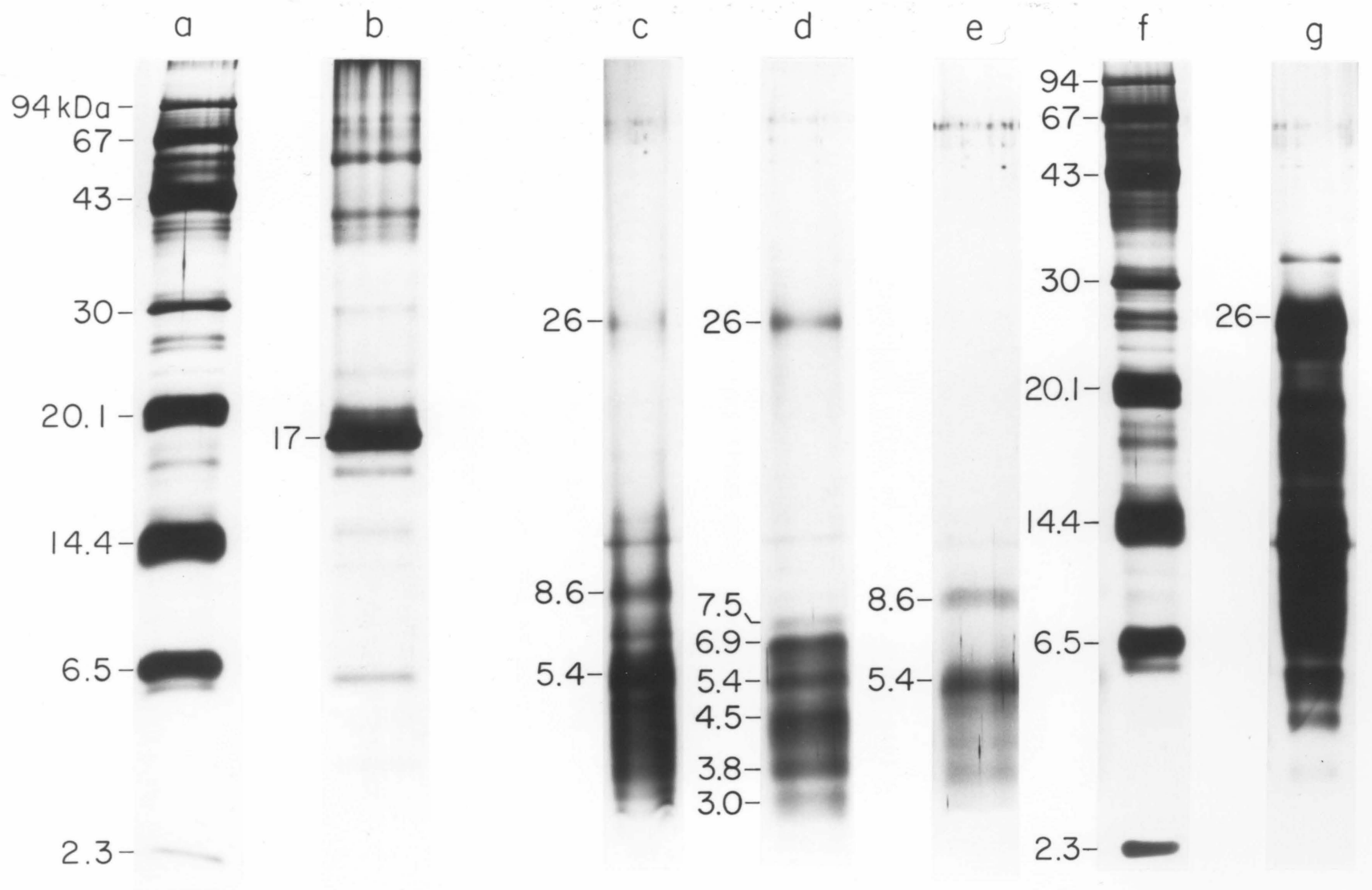
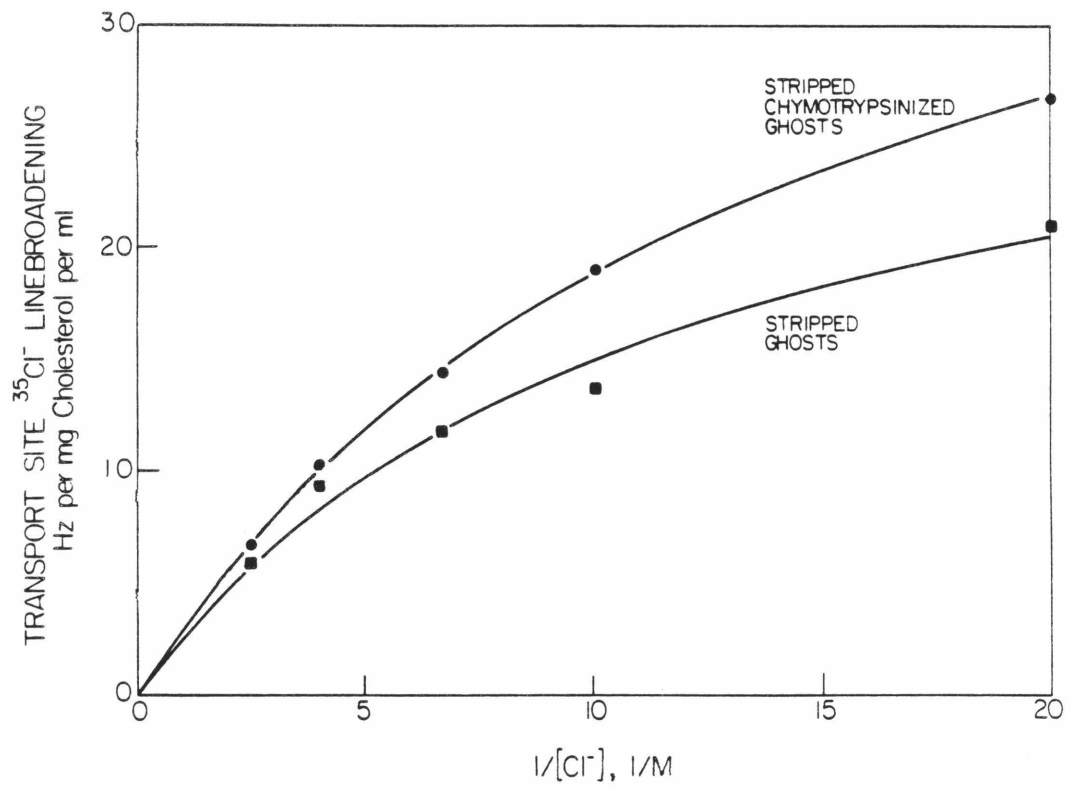


Figure 6

The effect on band 3 transport sites of chymotrypsin cleavage within the transport domain. Shown is the  $^{35}\text{Cl}^-$  linebroadening due to band 3 transport sites on ghost membranes (stripped ghosts) and chymotrypsinized ghost membranes (stripped chymotrypsinized ghosts). Both types of membranes were stripped with high pH at low ionic strength, then washed in high salt and sonicated. Samples and  $^{35}\text{Cl}$  NMR spectra were as in Figure 3. The nonlinear least-squares best-fit curves ( $y = Ax/(1 + xK_D)$ , solid lines) yielded  $K_D = 80 \pm 10$  mM and  $K_D = 70 \pm 2$  mM for chloride binding to the transport sites on stripped ghosts and stripped trypsinized ghosts, respectively.



cytoskeletal domain. Subsequent removal of the cytoskeletal domain with trypsin yields membranes containing 17 kDa and 35 kDa fragments of the transport domain (Figure 1); in this case transport remains 80% intact (7). Thus, the 17 kDa and 35 kDa fragments of the transport domain retain the transport site. By analogy with the stable association of the 60 kDa and 35 kDa products of external chymotrypsin, the 17 kDa and 35 kDa chymolytic fragments may remain associated in the membrane. Therefore, the transport site could be composed of residues from both fragments.

#### The Peptides Produced by Extensive Papain Digestion of Leaky Ghosts.

Recently it has been shown that extensive digestion of leaky ghost membranes with the nonspecific protease pepsin produces a mixture of fragments of the appropriate size to be transmembrane segments (the observed fragments are approximately 4 kDa (14)). Papain is also well-suited for generating transmembrane segments; this protein is one of the most nonspecific and active proteases known, the optimal pH of papain (pH 6.5) is considerably higher than that of pepsin (pH 3.0), and extensive extracellular papain treatment of intact red cells slows transport 75% (40) or 90% (41) but appears to leave the outward-facing transport site intact (41). Thus, papain is used in the present study to generate small transmembrane fragments from band 3 in a search for the minimal structure containing the band 3 transport site.

Extensive papain treatment (10 mg/ml papain, pH 6.5, 37° C/1 hr) followed by stripping yields the proteolytic fragments indicated in lane c of Figure 5. Nearly all (> 90%) of the resulting fragments are smaller than the molecular weight standard aprotinin (6.5 kDa) and larger than

the molecular weight standard insulin A (2.3 kDa). Thus, the range in apparent size of these fragments is approximately 3-7 kDa (Figure 5, lane c). The fragments are clearly a heterogeneous mixture, and the significant background staining observed below 5 kDa suggests that nonspecific proteolysis has resulted in heterogeneous copies of one or more fragments (Figure 5, lane c). However, superimposed on this background are fragments that give rise to discrete bands. These discrete fragments become more visible after the membrane samples are extracted with 2:1  $\text{CHCl}_3$ :MeOH to separate the peptides into two fractions that are soluble (organophilic) or insoluble (organophobic) in the organic solvent, respectively (Figure 5, lanes d,e). As least two organophilic fragments (5.4, 8.6 kDa) and seven organophobic fragments (3.0, 3.8, 4.5, 5.4, 6.9, 7.5, 26 kDa) are observed as discrete bands (Figure 5, lanes d,e). Excluding the 26 kDa fragment, which may be residual papain (see below), each of the other fragments is long enough to span the membrane only once or twice, assuming that a single  $\alpha$ -helical membrane-spanning segment must be at least 3 kDa (see Discussion). The relative intensities of the discrete bands in both the organophilic and organophobic fractions should not be used for quantitation since during the preparation of both fractions the fragments are precipitated and do not redissolve completely, so that differential resolubilization may occur.

Only two of the discrete fragments can be tentatively identified at the present time. The 26 kDa organophobic fragment appears to be residual papain, which comigrates with this fragment despite the fact that papain is known to be a 21 kDa polypeptide (42). No other

fragments comigrate with papain or the products of its self-proteolysis (Figure 5, lane g). The 8.6 kDa organophilic fragment may be identical to a fragment produced by extracellular cleavage by papain; the latter is known to be a 7.5 kDa polypeptide that is soluble in 2:1  $\text{CHCl}_3$ : MeOH (13). The discrete bands smaller than 8 kDa are all previously undescribed and could be fragments of any of the major integral ghost proteins: band 3 ( $1 \times 10^6$  copies per ghost (1,2)), glycophorin ( $5 \times 10^5$  copies per ghost (43)), or the glucose transporter (estimated  $3 \times 10^5$  copies per ghost (44)). Some of the observed fragments may contain two transmembrane segments; thus, the eight or more fragments observed in the range 3 - 8.6 kDa could include all seven or more of the band 3 transmembrane segments. It should be noted, however, that the single site of glycosylation on band 3 (45) may remain on one of the transmembrane segments. In this event, the broad band due to this heterogeneously glycosylated fragment would not be observed on SDS-page gels.

#### The Effect of Extensive Papain Digestion on the Transport Site.

It has just been shown that extensive papain digestion reduces all of the integral ghost proteins, including band 3, to small fragments protected by the membrane. In general, extensive proteolysis destroys band 3 catalyzed anion transport, as has been demonstrated for chymotrypsin (46), pronase (37), and to a lesser degree of inhibition, extracellular papain (41). A likely cause of such transport inhibition is blockage of bound chloride translocation across the membrane, since this translocation involves a conformational change that could require structural integrity throughout large regions of the transport domain. In contrast, the transport site itself could be localized within a small

region that is sterically protected, so that extensive digestion with a protease such as papain could leave the site relatively intact.

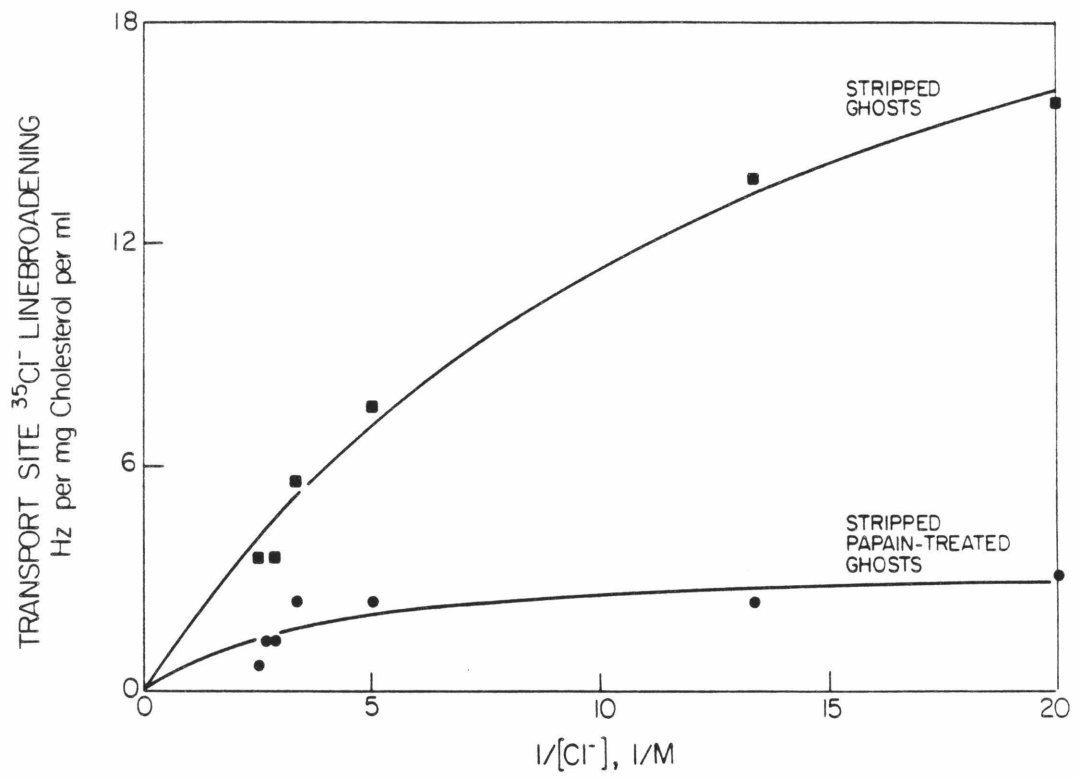
The effect of extensive papain digestion of the  $^{35}\text{Cl}^-$  linebroadening due to the transport site is shown in Figure 7, where the transport site linebroadening is identified by its sensitivity to DNDS (4). Transport site linebroadening vs.  $[\text{Cl}^-]^{-1}$  data is shown for two types of sonicated ghost membranes: 1) stripped ghosts and 2) stripped papain-treated ghosts. The stripped papain-treated ghosts correspond to SDS-page, lanes c-e in Figure 5. The papain treatment reduces the transport site linebroadening to <20% of its control value. Also, the linebroadening due to papain-treated transport sites approaches zero slope at lower  $[\text{Cl}^-]^{-1}$  than does the control linebroadening, indicating that the papain treatment reduces the affinity of the transport site for chloride (Equation 2, see below). Thus, the papain digestion significantly alters the structure of the transport site; however, a DNDS-sensitive site that could be a damaged transport site does remain after proteolysis.

Verification of the Identity of the Transport Site Following Extensive Papain Digestion. The DNDS-sensitive site produced by extensive papain digestion cannot be a priori identified as the transport site because the affinities of the two sites for chloride are significantly different. Thus, the relationship between the two sites must be further examined; here the effect of transport site inhibition on the papain-generated site is studied.

$\text{H}_2\text{DIDS}$  is a highly specific covalent inhibitor of the band 3 transport site. Under appropriate labeling conditions, one molecule of

Figure 7

The effect on band 3 transport sites of extensive papain cleavage of the transport domain. Shown is the  $^{35}\text{Cl}^-$  line-broadening due to band 3 transport sites on ghost membranes (stripped ghosts) and papain-treated ghost membranes (stripped papain-treated ghosts). Both types of membranes were stripped with high pH at low ionic strength, then washed in high salt and sonicated. Samples and  $^{35}\text{Cl}$  NMR spectra were as in Figure 3. The nonlinear least-squares best-fit curves ( $y = Ax/(1 + xK_D)$ , solid lines) yielded  $K_D = 70 \pm 10$  mM and  $K_D = 270 \pm 90$  mM for chloride binding to transport sites on stripped ghosts and stripped papain-treated ghosts, respectively.

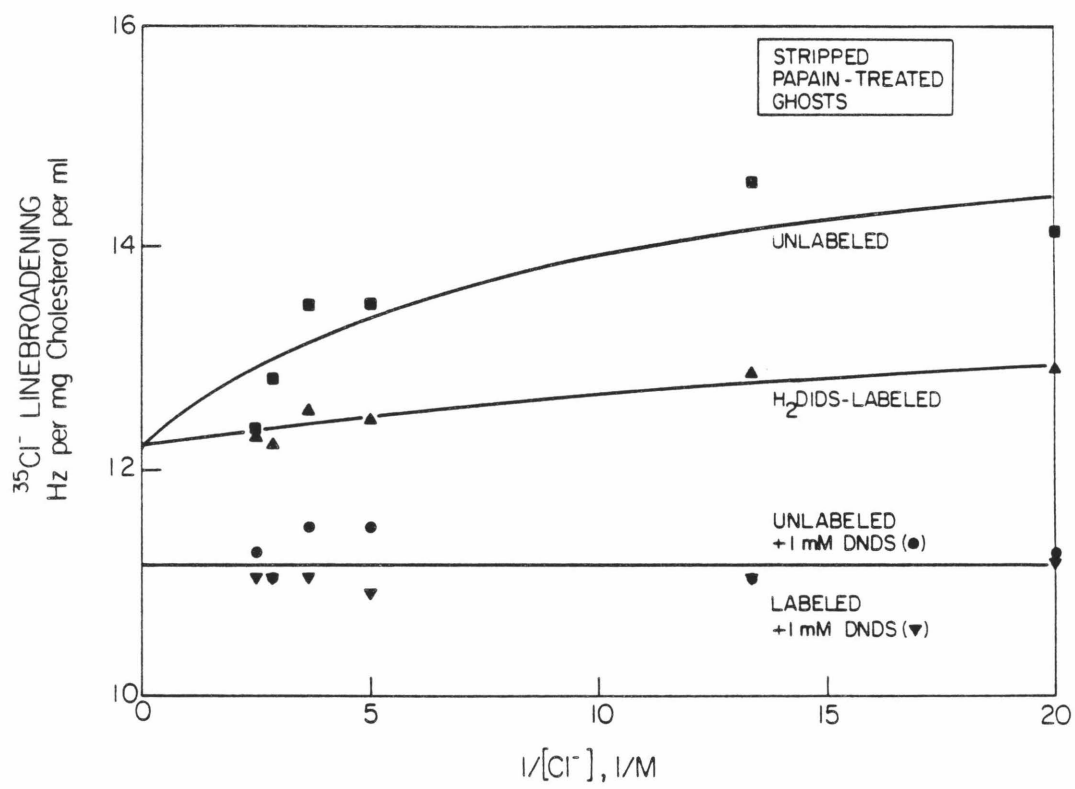


H<sub>2</sub>DIDS can be incorporated per band 3 monomer, with negligible labeling of other ghost proteins (2). The effect of H<sub>2</sub>DIDS transport site inhibition on the <sup>35</sup>Cl<sup>-</sup> linebroadening due to the papain-generated site is shown in Figure 8. Total linebroadening vs. [Cl<sup>-</sup>]<sup>-1</sup> data is shown for ghost membranes made from red cells labeled or unlabeled with H<sub>2</sub>DIDS, then digested with papain and stripped. The linebroadening due to the papain-generated site is inhibited by H<sub>2</sub>DIDS, although some positive slope is observed because the H<sub>2</sub>DIDS labeling was only 62% complete (as determined from residual transport site linebroadening of unproteolyzed ghosts). The linebroadenings due to both the unlabeled and labeled membranes are further inhibited, to the same final extent, by 1 mM DNDS (Figure 8). The results indicate that the papain-generated site is, in fact, the H<sub>2</sub>DIDS-sensitive transport site, and that DNDS inhibits both the transport site linebroadening and some linebroadening due to low-affinity (K<sub>D</sub> >> 400 mM) chloride binding sites as well.

Phenylglyoxal is an arginine-specific covalent inhibitor of the band 3 transport site that, like H<sub>2</sub>DIDS, can be used to test the identity of the papain-generated site. Phenylglyoxal labels band 3 at several sites in addition to the transport site (25,47); however, the transport site is protected against phenylglyoxal labeling by the presence of DNDS (18,25). The effect of phenylglyoxal inhibition of the transport site on the <sup>35</sup>Cl<sup>-</sup> linebroadening due to the papain-generated site is shown in Figure 9. Total linebroadening vs. [Cl<sup>-</sup>]<sup>-1</sup> data is shown for ghost membranes labeled with phenylglyoxal in the presence or absence of DNDS protection, then digested with papain and stripped. The linebroadening due to the papain-generated site is

Figure 8

The effect of H<sub>2</sub>DIDS on the papain-modified band 3 transport site. Shown is the <sup>35</sup>Cl<sup>-</sup> linebroadening from transport sites and low-affinity chloride binding sites on stripped papain-treated ghosts. Red cells were labeled or unlabeled with H<sub>2</sub>DIDS; then leaky ghost membranes were prepared and the ghosts were proteolyzed with papain, stripped with high pH at low ionic strength, washed in high salt and sonicated. Final samples were with or without 1 mM DNDS. Samples and <sup>35</sup>Cl NMR spectra were as in Figure 3. The nonlinear least-squares best-fit curve ( $y = A + Bx/(1 + xK_D)$ ) yielded  $K_D = 110 \pm 50$  mM for chloride binding to the papain-modified transport sites on unlabeled membranes (upper curve). The same function was used to best-fit the data for membranes labeled with H<sub>3</sub>DIDS (middle curve) since only 62% of the band 3 transport sites were actually inhibited by H<sub>2</sub>DIDS (see text). Only low-affinity sites ( $K_D \gg 400$  mM) remain on both labeled and unlabeled membranes in the presence of 1 mM DNDS (lower line); these data are fit by a straight line of zero slope.

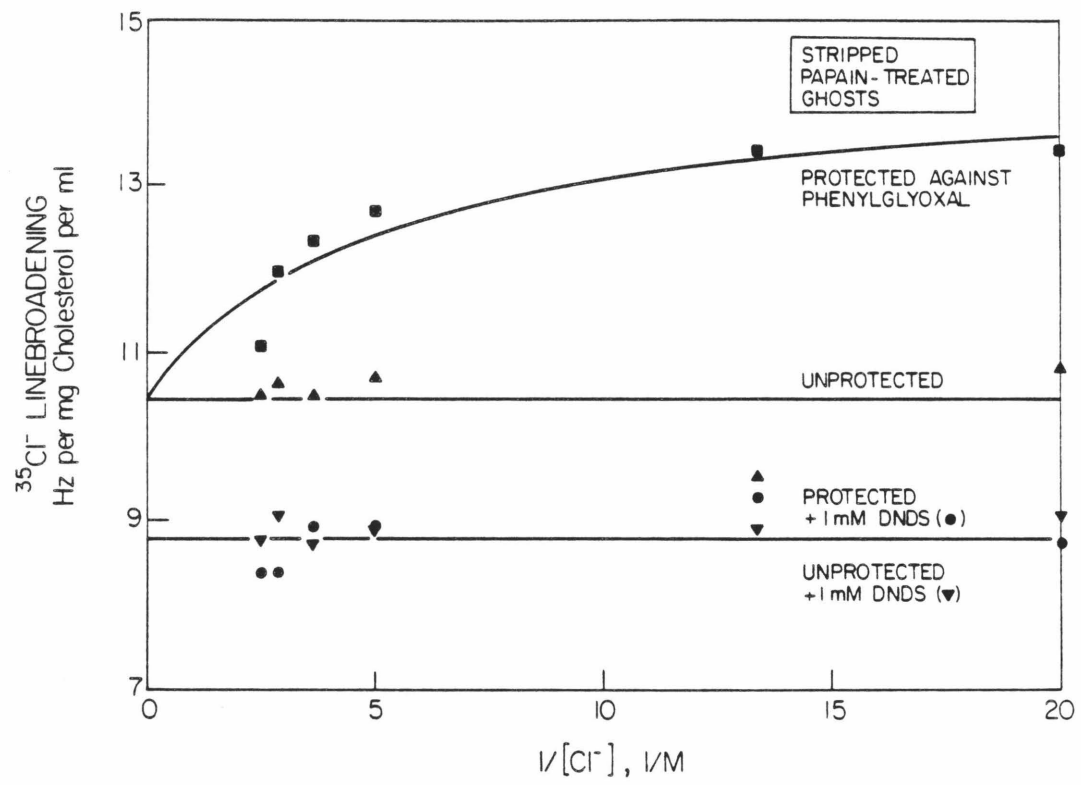


inhibited by phenylglyoxal, and DNDS protects the site against this phenylglyoxal inhibition. The linebroadenings due to both the protected and unprotected membranes are further inhibited to the same final extent by 1 mM DNDS (Figure 9). These results are completely consistent with those already described for H<sub>2</sub>DIDS; together, the phenylglyoxal and H<sub>2</sub>DIDS experiments indicate that 1) the band 3 transport site is damaged, but not destroyed by the papain cleavage, 2) the chloride dissociation constant for this papain-modified site is  $190 \pm 80$  mM (an average of the values derived from Figures 7, 8, 9), 3) approximately 2/3 of the DNDS-sensitive linebroadening stems from the transport site, and 4) the remaining 1/4 of the DNDS-sensitive linebroadening stems from low-affinity chloride binding sites ( $K_D \gg 400$  mM). Thus DNDS, which specifically inhibits the transport site linebroadening in the ghost membrane system, is no longer specific for the transport site after the papain digestion. Instead, the papain digestion appears to create new DNDS binding sites such that DNDS inhibits some of the low-affinity chloride binding sites in addition to the papain-modified transport site. In contrast, H<sub>2</sub>DIDS and phenylglyoxal, which are covalently attached before the papain digestion, specifically inhibit the papain-modified transport site.

The Effect of Nonintegral Protein Removal and Proteolysis on the Low-Affinity Chloride Binding Sites. The total <sup>35</sup>Cl<sup>-</sup> linebroadening due to leaky ghost membranes is composed of both transport site linebroadening and linebroadening due to low-affinity chloride binding sites ( $K_D \gg 400$  mM (4)). The nonintegral ghost proteins contribute to the low-affinity site linebroadening, since stripping removes 15% of the

Figure 9

The effect of phenylglyoxal on the papain-modified band 3 transport site. Shown is the  $^{35}\text{Cl}^-$  linebroadening from transport sites and low-affinity chloride binding sites on stripped papain-treated ghosts. Red cells were labeled with phenylglyoxal in the presence or absence of DNDS to protect the transport site from labeling; then leaky ghost membranes were prepared and the ghosts were proteolyzed with papain, stripped with high pH at low ionic strength, washed in high salt and sonicated. Final samples were with or without 1 mM DNDS. Samples and  $^{35}\text{Cl}$  NMR spectra were as in Figure 3. The nonlinear least-squares best-fit curve ( $y = A + Bx/(1 + xK_D)$ ) yielded  $K_D = 200 \pm 50$  mM for chloride binding to the papain-modified transport site that had been protected by DNDS from phenylglyoxal (protected, upper curve). Only low-affinity sites ( $K_D \gg 400$  mM) remain when the transport site is not protected by DNDS from phenylglyoxal (middle line); these data are fit with a linear least-squares straight line of zero slope. Similarly, only low-affinity sites remain on the protected and unprotected membranes in the presence of 1 mM DNDS (lower line); these data are again fit by a linear least-squares straight line of zero slope.



low-affinity site linebroadening (Table I). The integral proteins also contribute, since trypsin, chymotrypsin and papain remove an additional 17%, 4%, and 28% of the low-affinity site linebroadening, respectively (Table I). The identity and function of the low-affinity sites are unknown; however, since band 3 is the major polypeptide in ghost membranes, some or all of the low-affinity sites associated with integral proteins may be on band 3.

### DISCUSSION

$^{35}\text{Cl}$  NMR provides a powerful approach to the elucidation of the structure of the band 3 anion transport site. This technique enables study of two fundamental steps in the anion transport cycle: 1) migration of substrate chloride ion to the vicinity of the transport site, and 2) binding of chloride to the site. Since sealed vesicles are not needed for such studies, the  $^{35}\text{Cl}$  NMR technique yields easily quantified information concerning the intactness of the transport site. Thus, the  $^{35}\text{Cl}$  NMR technique can be used to determine the minimal structure containing the intact transport site, even if that minimal structure can no longer transport anions.

The results presented here indicate that the minimal structure containing the intact transport site includes neither the red cell nonintegral membrane proteins nor the band 3 cytoskeletal domain, since removal of these components from the transport domain leaves the transport site intact. Thus, no significant interaction occurs between the transport site and the cytoskeletal domain with its associated nonintegral proteins.

Table I. Effect of Nonintegral Protein Removal and Protease Treatment on Low-Affinity Chloride Binding Sites

TREATMENT	LOW-AFFINITY SITE $^{35}\text{Cl}^-$ LINEBROADENING <sup>a</sup>
(-)	100% <sup>b</sup>
High Salt Wash	104% <sup>b</sup>
High pH, Low Ionic Strength Stripping Followed by High Salt Wash	85% <sup>b</sup>
Trypsin in Both Compartments	68% <sup>c</sup>
Chymotrypsin in Both Compartments	81% <sup>c</sup>
Papain in Both Compartments	57% <sup>c,d</sup>

<sup>a</sup>Data from the same experiments used to generate Figures 3,4,6,9. The low-affinity site linebroadening is simply the DNDS-insensitive component of the linebroadening, except where indicated.

<sup>b</sup>Relative to unproteolyzed, unstripped sonicated ghost membranes.

<sup>c</sup>Relative to unproteolyzed, stripped sonicated ghost membranes.

<sup>d</sup>The low-affinity site linebroadening from papain-treated membranes is the phenylglyoxal-insensitive component of the linebroadening.

The transport site also remains intact when the transport domain is cleaved by chymotrypsin into 17 kDa and 35 kDa fragments, even though both fragments contain residues known to lie in the vicinity of the transport site (see Introduction). Thus, strong attractive forces must hold these fragments together after proteolysis; direct evidence for these attractive forces has been obtained in  $H_2DIDS$  cross-linking studies (19). These results remain completely consistent with the possibility that the transport site may be composed of residues from more than one region of the primary structure.

Data presented here also indicate that extensive proteolysis on both sides of the membrane by papain cleaves the integral red cell membrane proteins into a mixture composed primarily of small papain fragments in the range 3-7 kDa, where the most prominent size is approximately 5 kDa. These data suggest that extensive papain cleavage followed by stripping removes approximately 60% or more of that portion of the transport domain protruding from the membrane into the solution (assuming 7  $\alpha$ -helical transmembrane segments per 52 kDa transport domain (13), 3 kDa per 40 Å  $\alpha$ -helical transmembrane segment, and 5 kDa per average transmembrane segment produced by papain cleavage). Removal of the bulk of the extra-membrane material from the transport domain damages, but does not destroy, the transport site: thus, the transport site is composed of residues from one or more of the papain-generated fragments. These results are completely consistent with a picture in which 1) the transport site is buried near the center of the membrane, 2) the transmembrane segments that surround the transport site are held together by strong attractive forces

within the membrane itself, and 3) an anion channel leads from the transport site to the solution so that anions can visit the buried transport site. Such a picture explains both the protection of the transport site from proteolysis and the existence of channel-blocking inhibitors that interfere with exchange of chloride between the transport site and solution (48). The picture also explains the fluorescence energy transfer data of Rao, Reithmeier and Cantley (49), which show that the stilbenedisulfonate binding site is 34-42 Å from cysteine residues on the cytoskeletal domain. This distance is less than the thickness of the bilayer; thus, the stilbenedisulfonate binding site, including the transport site, is in the interior of the membrane. The picture appears physically reasonable: 1) the hydrophobic environment of the membrane interior would enhance the affinity of the transport site positive charge(s) for substrate anion, 2) the observation that the transmembrane translocation of bound chloride is the rate-limiting step in the transport cycle (50) is not inconsistent with the presence of anion channels leading to the transport site since anion migration through a transmembrane channel such as gramicidin is two orders of magnitude faster than the turnover rate of band 3 (2), 3) the reduction in the width of the anion permeability barrier due to anion channels leading to the transport site would not place an unreasonably large electric field across the region of the transport domain between channels, assuming that fixed charges on the transport domain exist to counteract the transmembrane electric field in the vicinity of the transport site, and 4) the presence of channels leading to the transport site simplifies the transport process by

shortening the distance over which the anion-transport site complex must be translocated.

The observation that proteolytic cleavage of the transport domain into transmembrane fragments does not destroy the transport site will greatly facilitate future structural studies of band 3, and a similar approach may be useful in a variety of systems involving transmembrane proteins (14). In the band 3 system, the ability to isolate the transmembrane segment(s) that are components of the transport site will greatly simplify both the identification of the essential residues in the transport site and the analysis of the associations between transmembrane segments that give rise to transport site structure.

REFERENCES

1. Macara, I. G. and Cantley, L. C. (1983) Cell Membr. 1, 41-87.
2. Knauf, P. A. (1979) Curr. Top. Memb. Transp. 12, 249-363.
3. Bennett, V. (1982) Bioch. Biophys. Acta 689, 475-484.
4. Falke, J. J., Pace, R. J. and Chan, S. I. (1984) J. Biol. Chem. 259, 6472-6480.
5. Bennett, V. and Stenbuck, P. J. (1979) Nature 280, 468-473.
6. Hargreaves, W. R., Giedd, K. N., Verkleij, A. and Branton, D. (1980) J. Biol. Chem. 255, 11965-11972.
7. Grinstein, S., Ship, S., and Rothstein, A. (1978) Bioch. Biophys. Acta 507, 294-304.
8. Bennett, V., and Starbuck, P. J. (1980) J. Biol. Chem. 255, 6424-6432.
9. Steck, T. L., Ramos, B. and Stapazor, E. (1976) Biochem. 15, 1154-1161.
10. Jenkins, R. E. and Tanner, M. J. A. (1977) Bioch. J. 161, 139-147.
11. Drickamer, L. K. (1976) J. Biol. Chem. 251, 5115-5123.
12. Cabantchik, Z. I. and Rothstein, A. (1974) J. Memb. Biol. 15, 227-248.
13. Jennings, M. L., Lackey, M. A. and Denney, G. H. (1984) J. Biol. Chem. 259, 4652-4660.
14. Ramjessingh, M., Gaarn, A. and Rothstein, A. (1984) Bioch. Biophys. Acta 769, 381-389.
15. Falke, J. J., Pace, R. J. and Chan, S. I. (1984) J. Biol. Chem. 259, 6481-6491.

16. Wieth, J. O., Bjerrum, P. J. and Borders, C. L. (1982) J. Gen. Physiol. 79, 293-312.
17. Zaki, L. (1982) in Protides of the Biological Fluids (H. Peters, ed.) pp. 279-328, Pergamon Press, New York.
18. Falke, J. J. and Chan, S. I. (1984) Biophys. J. 45, 91-92.
19. Jennings, M. L. and Passow, H. (1978) Bioch. Biophys. Acta 554, 498-519.
20. Shami, Y., Rothstein, A. and Knauf, P. A. (1978) Bioch. Biophys. Acta 508, 357-363
21. Ramjeesingh, M., Gaarn, A. and Rothstein, A. (1979) Bioch. Biophys. Acta 599, 127-139.
22. Drickamer, K. (1977) J. Biol. Chem. 252, 6909-6917.
23. Mayby, W. J. and Findlay, J. B. C. (1982) Bioch. J. 205, 465-475.
24. Rudloff, V., Lepke, S. and Passow, H. (1983) FEBS Lett. 163, 14-21.
25. Bjerrum, P. J., Wieth, J. O. and Borders, C. L. (1983) J. Gen. Physiol. 81, 453-484.
26. Nanri, H., Mamasaki, N. and Minakami, S. (1983) J. Biol. Chem. 258, 5985-5989.
27. Stadtman, T. C. (1957) Meth. Eng. 3, 392-394.
28. Laemmli, U. K. (1970) Nature 227, 680-685.
29. Downer, N. W., Robinson, N. C. and Capaldi, R. A. (1976) Biochem. 15, 2930-2936.
30. Merle, P. and Kadenbach, B. (1980) Eur. J. Bioch. 105, 499-507.
31. Oakley, B. R., Kirsch, D. R. and Morris, R. (1980) Anal. Bioch. 105, 361-363.
32. Forsén, S. and Lindman, B. (1981) Meth. Bioch. Anal. 27, 289-486.

33. Falke, J. J. and Chan, S. I. (1984) J. Biol. Chem., submitted.
34. Heast, C. W. M. (1982) Bioch. Biophys. Acta 694, 331-352.
35. Steck, T. L. (1974) Meth. Memb. Biol. 2, 245-381.
36. Fukuda, M., Dell, A., Oates, J. E. and Fukuda, M. N. (1984) J. Biol. Chem. 259, 8260-8074.
37. Passow, H., Fasold, H., Lepke, S., Pring, M. and Schukman, B. (1977) in Membrane Toxicity (M. W. Miller and A. E. Shamoo, eds.) pp. 353-377, Plenum, New York.
38. Markowitz, S. and Marchesi, V. T. (1981) J. Biol. Chem. 356, 6463-6468.
39. Tsuji, T., Irimura, T. and Osawa, T. (1981) Carbohydrate Res. 92, 328-332.
40. Matsuyama, H., Kawano, Y. and Hamasaki, N. (1983) J. Biol. Chem. 258, 15376-15381.
41. Jennings, M. L. and Adams, M. F. (1981) Biochem. 20, 7118-7122.
42. Arnon, R. (1970) Meth. Eng. 19, 226-244.
43. Marchesi, V. T., Furthmayr, H. and Tomita, M. (1976) Ann. Rev. Bioch. 45, 667-698.
44. Jones, M. N. and Nickson, J. K. (1981) Bioch. Biophys. Acta 650, 1-20.
45. Drickamer, L. K. (1978) J. Biol. Chem. 253, 7242-7248.
46. DuPre, A. and Rothstein, A. (1981) Bioch. Biophys. Acta 646, 471-478.
47. Zaki, L. (1984) FEBS Lett. 169, 234-240.
48. Falke, J. J. and Chan, S. I., data to be published.

49. Rao, A., Martin, P. Reithmeier, R. A. F. and Cantley, L. C. (1979)  
Biochem. 18, 4505-4516.
50. Falke, J. J. and Chan, S. I. (1984) J. Biol. Chem., submitted.

CHAPTER IX  
CONCLUSIONS, AND A MODEL FOR  
THE ION TRANSLOCATION EVENT

## INTRODUCTION

The ability of  $^{35}\text{Cl}$  and  $^{37}\text{Cl}$  NMR to 1) directly monitor the migration of chloride between solution and the band 3 transport site and 2) directly study the binding of chloride to the site has enabled a new approach to the elucidation of the structure and mechanism of the band 3 anion transport unit. This approach complements the many kinetic studies conducted elsewhere, since kinetic studies monitor the operation of the full transport cycle but generally cannot resolve individual events such as chloride migration or binding. In this final chapter, the conclusions of the  $^{35}\text{Cl}$  and  $^{37}\text{Cl}$  NMR studies presented here are summarized. Then several models depicting the molecular details of the ion translocation event are discussed: these models can now be better analyzed in light of the newly formed conclusions.

## CONCLUSIONS OF THE PRESENT WORK

1.  $^{35}\text{Cl}$  NMR reveals two types of chloride binding sites on red cell membranes: a) low affinity binding sites associated with nonintegral and integral membrane proteins; and b) high affinity binding sites that are band 3 transport sites.
2. The low affinity sites and band 3 transport sites are each found on both sides of the membrane.

3. All of the band 3 transport sites on both sides of the membrane can be recruited to the outward-facing conformation.
4. The transport sites on both sides of the membrane behave like a homogeneous population in macroscopic experiments, indicating that any differences in the microscopic characteristics of the inward- and outward-facing transport sites are averaged by the transport cycle.
5. These results are qualitatively and quantitatively consistent with the ping-pong model, in which the transport unit contains a single transport site that is alternately exposed to one side of the membrane then the other, and can only 'cross' the membrane when occupied with substrate chloride.
6. The chloride binding and dissociation events at both the inward- and outward-facing transport sites are fast: the rate of binding and dissociation events at the inward-facing transport site is  $\gg 10^5$  events per sec at  $0^\circ\text{C}$ , and the corresponding rate at the outward-facing site is  $\geq 10^5$  events per sec.
7. The rate limiting step in the chloride transport cycle is the translocation of the chloride transport site complex across the membrane. Assuming

that the rate constants for the (in → out) and (out → in) translocations differ by no more than a factor of  $10^2$ , the translocation step is rate limiting in both the (in → out) and (out → in) half turnovers of the transport cycle.

8. The transport site contains essential arginine in the inward- or the outward-facing conformation, or in both conformations.
9. Chloride binding to the transport site can be inhibited by occupation of the site with a competing substrate or an inhibitor.
10. The transport site is buried in the membrane and is reached by a substrate channel leading from the solution to the site.
11. The exchange of chloride between the transport site and solution can be slowed by an inhibitor that blocks the substrate channel.
12. The translocation of the chloride transport site complex across the membrane can be slowed by an inhibitor that binds to the transport unit without affecting either chloride binding to the site or the distribution of sites across the membrane.

13. Structurally, the transport site remains intact when the nonintegral red cell membrane proteins or the cytoskeletal domain of band 3 are removed.
14. The transport site is composed of residues from one or more membrane-spanning peptides produced by cleavage of band 3 with papain.
15. Assuming that multiple transmembrane segments are required for transport site and substrate channel structure, the membrane-spanning peptides produced by papain are held together by strong associative forces between the peptides.

#### COMPARISON OF MODELS FOR THE ION TRANSLOCATION EVENT

The choice of models to be discussed. Historically, a large number of models for the band 3-catalyzed anion transport cycle have been described in the literature. However, the experimental conclusions presented here and elsewhere indicate that the transport cycle possesses a ping-pong mechanism, thus only ping-pong models need be considered. The following discussion treats four different ping-pong models that each describe the molecular details of the ion translocation event. Three of the models are shown to be implausible; in contrast, the previously undescribed fourth model is consistent with all of the available evidence. This new model also illustrates several concepts that may be of general importance in membrane protein systems.

Large scale conformational change. The ion translocation event must involve a conformational change within the monomeric band 3 transport unit, and the first type of model proposes that this conformational change significantly alters the macroscopic structure of the monomer. However this large scale conformational change would involve volume changes and translation of entire regions of the monomer that would be slow to occur, and such macroscopic rearrangements are inconsistent with two observations: 1) the macroscopic rearrangement of a particular monomer would sterically affect the other monomers in the same multimer, but the monomers in band 3 dimers and tetramers do not interact during the transport cycle (1); and 2) the turnover rate of the transport cycle is very rapid for physiological substrates ( $> 5 \times 10^4 \text{ sec}^{-1}$  for chloride at  $37^\circ\text{C}$  (2)). Thus the recently developed models for the translocation event involve conformational changes on a smaller scale.

The anionic gate. This model proposed microscopic conformational changes that can easily explain the rapid turnover rate. The anionic gate is a small, flexible barrier that is found in the transport site together with two positive charges (Figure 2a (1)). Initially the gate is salt-bridged to one of the positive charges, thereby blocking access to one solution compartment. The transport cycle begins when a substrate anion binds to the positive charge in this salt-bridge, so that the anionic gate is free to swing away and salt-bridge to the second positive charge. However this proposed substrate binding step is implausible, since the positive

Figure 1

A model for ion translocation involving a large scale conformational change. This representation of the ping-pong transport cycle depicts a conformational change affecting large regions of the band 3 monomer. Note that this diagram has been used throughout this thesis as a purely schematic illustration, and is not intended to imply support for a conformational change of this magnitude.

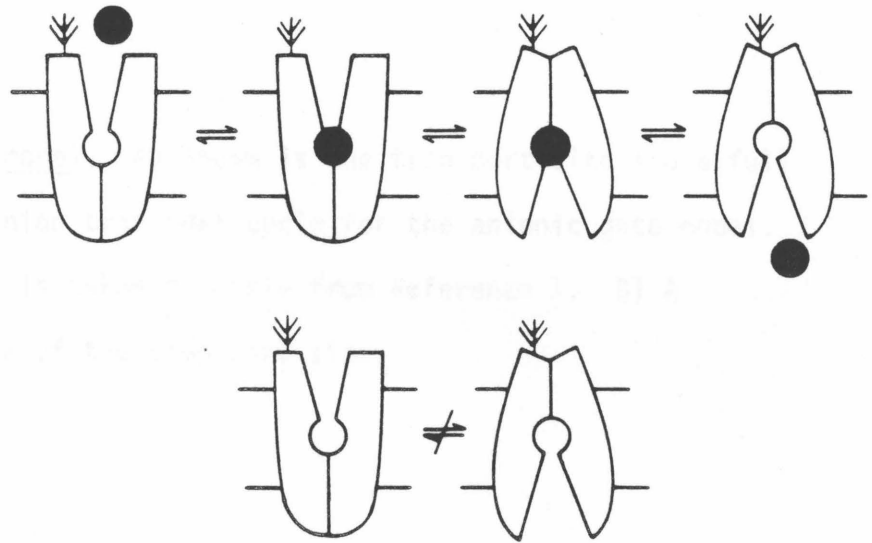
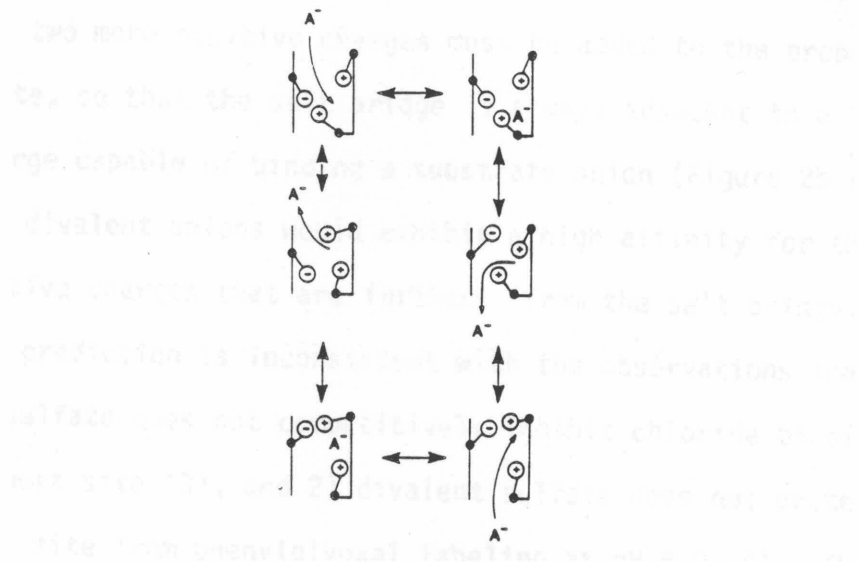


Figure 2

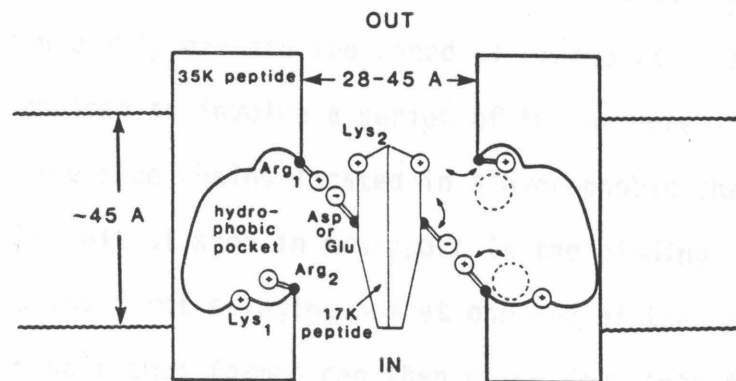
The anionic gate model. A) Shown is the transport site and a full turnover of the anion transport cycle for the anionic gate model.

This illustration is taken directly from Reference 1. B) A more detailed view of the transport site.

A



B

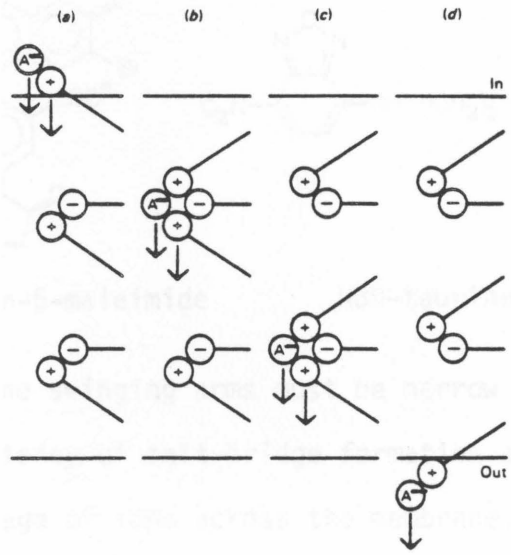


charge in a salt-bridge would have very little affinity for substrate anion. Thus two more positive charges must be added to the proposed transport site, so that the salt bridge is always adjacent to a positive charge capable of binding a substrate anion (Figure 2b (1)). In this case divalent anions would exhibit a high affinity for the pair of positive charges that are farthest from the salt bridge; however this prediction is inconsistent with the observations that 1) divalent sulfate does not competitively inhibit chloride binding to the transport site (3), and 2) divalent sulfate does not protect the transport site from phenylglyoxal labeling at pH 8.0 (4). Thus another model is examined that again involves the microscopic swinging of charged groups, but also accounts for the observed specificity for monovalent anions.

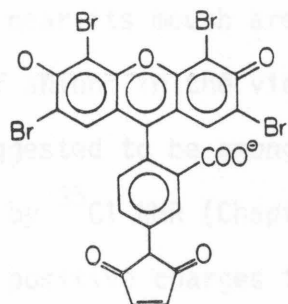
The swinging arm model. This model, which was published by Brock, Tanner and Kempf (5) and developed independently in the Chan laboratory by R. J. Pace, again involves microscopic conformational changes that can easily explain the speed of transport. The transport machinery is proposed to involve a series of two or more flexible arginine or lysine side chains located in a hydrophobic channel (Figure 3). The initial step in transport is the binding of a monovalent anion to the first swinging arm at one end of the channel: the neutral ion pair thus formed can then swing down into the hydrophobic interior, where the anion is passed to the next swinging arm that lies waiting, salt-bridged to a negative charge. As the

Figure 3

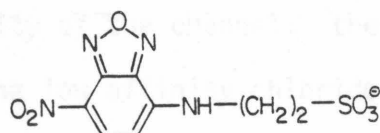
The swinging arm model. Shown is a set of three swinging arms executing a half-turnover of the transport cycle. The anion is indicated by  $A^-$ ; the flexible side chains of arginine or lysine are indicated by the positive charges; and the side chains of aspartate or glutamate are indicated by negative charges. This diagram is taken directly from reference 5, and is essentially the same as a model developed in the Chan laboratory by R. J. Pace.



translocation continues, the anion is passed between successive swinging arms until it is released at the other end of the channel. This model can successfully explain many of the features of the transport cycle, but it is inconsistent with a series of results obtained with the following large organic substrate and inhibitor molecules:



eosin-5-maleimide



NBD-taurine

The channel containing the swinging arms must be narrow in order to 1) maximize the efficiency of salt-bridge formation and 2) prevent nonspecific leakage of ions across the membrane. Since the physiological substrate anions are relatively small, it is expected that large organoanions such as NBD-taurine would not be transported: however this molecule is known to be a substrate of the one-for-one anion exchange system (6,7). Similarly, although eosin-5-maleimide occupies the outward-facing transport site, it is expected that this large molecule could not be transported through the narrow channel; yet partial translocation does occur since  $\text{Cs}^+$  applied to the intracellular side of the membrane is able to significantly quench the eosin fluorescence (1). Thus a new model has been developed which can accommodate both large

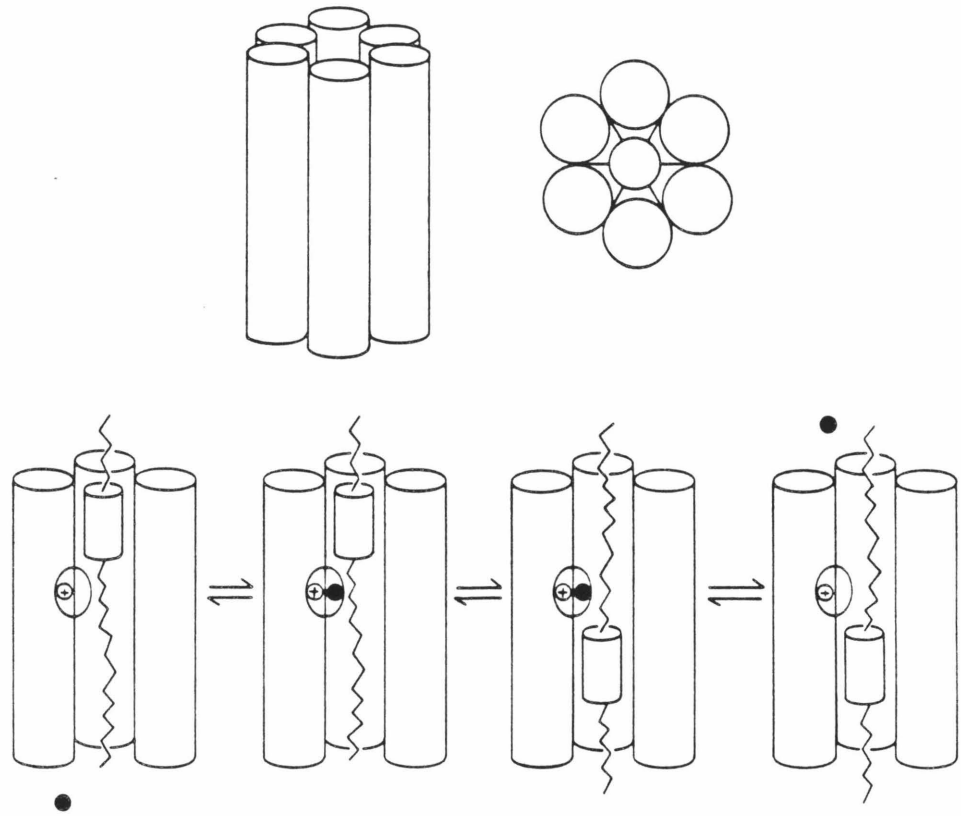
and small substrates and inhibitors.

The hydrophobic barrier model. This previously undescribed model proposes that the transport domain consists of a channel surrounded by six or more membrane-spanning  $\alpha$ -helical rods that are tightly associated within the membrane (Figure 4). Outside of the channel near its mouth are positive charges that increase the activity of anions in the vicinity of the channel: these charges are suggested to be among the low affinity chloride binding sites observed by  $^{35}\text{Cl}$  NMR (Chapter III). Inside the channel are 1) one or more positive charges that facilitate anion movement through the channel, 2) a transport site that is composed of a single positively charged arginine residue lying in a hydrophobic cleft between two transmembrane helices, and 3) a hydrophobic barrier that consists of a helical hydrophobic region flanked by two random coil regions. Initially the hydrophobic barrier cannot migrate past the charged site, but neutralization of the site by a monovalent anion allows barrier migration to occur so that the site becomes newly exposed to the opposite solution. This rate-determining barrier migration step accounts for: 1) the rapid turnover rate, since the conformational change is on a small scale, 2) the observed transport of large organoanions, since these molecules could intercalate into the transport site cleft where they would not prevent barrier migration, and 3) the known discrepancy between the transport rates of monovalent anions and the much slower transport rates of divalent anions (8), since neutralization of the single

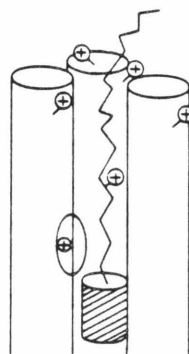
Figure 4

The hydrophobic barrier model. Shown is a schematic representation of the structure of a band 3 monomer. The channel forming  $\alpha$ -helices surround the hydrophobic barrier, which may be a smaller helix such as a  $3_{10}$  helix. The ion translocation event occurs when substrate anion neutralizes the charge in the transport site so that the hydrophobic barrier can move past the site. Also shown are 1) the positive charges near the mouth of the channel that increase the activity of anions in the vicinity of the channel, 2) the positive charges inside the channel that facilitate migration of an anion within the channel, and 3) the single positively charged arginine residue in the transport site.

## HYDROPHOBIC BARRIER MODEL



## POSITIVE CHARGES



transport site arginine is a prerequisite for barrier migration.

Another feature of anion transport consistent with barrier migration is the large temperature dependence of the turnover rate: for chloride this rate is  $430 \text{ sec}^{-1}$  at  $0^\circ\text{C}$  and  $> 5 \times 10^4 \text{ sec}^{-1}$  at  $37^\circ\text{C}$  (2,8), corresponding to an activation enthalpy of approximately 30 kcal/mol. Essentially the same activation enthalpy has been obtained for all substrates examined (Table 1). A simple explanation for this value is that it represents the electrostatic free energy required to place the hydrophobic barrier in front of the transport site, where the arginine-anion electric dipole lies. This picture is quantitatively reasonable, since the observed activation enthalpy is roughly 1/3 of the electrostatic free energy required to move a dipole from water to an organic solvent, as would be expected for the movement of a third hydrophobic helix (the barrier) in front of the two helices that define the transport site cleft. An alternative explanation for the size and similarity of the activation enthalpies is that the observed temperature dependence stems from expansion of the channel as the channel-forming helices are heated. This expansion would allow the barrier to migrate more freely, thus speeding translocation. In contrast to the activation enthalpies, the transport rates of the different substrates vary widely over a range spanning four orders of magnitude (Table 1). These differences can be explained by steric interactions: if the bound substrate projects into the channel, or if substrate binding changes the packing of the channel forming

TABLE 1

## TRANSPORT DATA FOR DIFFERENT ANIONS

	Apparent Transport Site $K_D(0^\circ\text{C})$	$V_{\max}$ Relative to $\text{Cl}^-(0^\circ\text{C})^a$	Ref.	Activation Energy	Ref.
$\text{Cl}^-$	80 mM	1	8	$33^b$ kcal/mole	10,11
$\text{HCO}_3^-$	16	1.01	8	$27^c$	12
$\text{F}^-$	88	0.07	8	?	
$\text{Br}^-$	32	0.15	8	$37^b$	10
$\text{I}^-$	16	0.004	8	26	10
$\text{SCN}^-$	$\sim 10$	$\sim 0.034$	8	29	10
$\text{SO}_4^{=}, \text{H}^+$	30	$< 0.0001$	8	32	13,4
NBD-Taurine		0.0002	6	$21-40^b$	6

a) Calculated from rate at nonsaturating substrate concentrations

b) Arrhenius plot is biphasic

c) Calculated from only two points at  $0^\circ\text{C}$ ,  $38^\circ\text{C}$ .

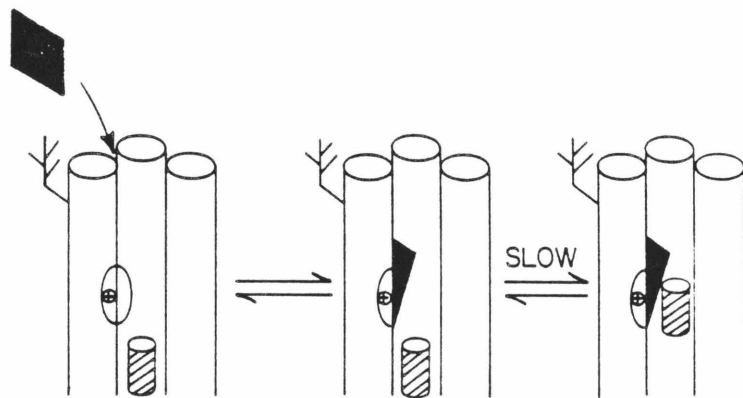
helices, the migration of the hydrophobic barrier would be slowed. Thus different substrates are proposed to yield significantly different steric effects upon binding.

The hydrophobic barrier model also successfully explains each of the known types of anion transport inhibition. Transport site inhibitors - including the stilbene disulfonates - have been extensively studied: the required planarity of these molecules is consistent with the idea that the transport site to which they bind is intercalated between two transmembrane helices. For example, the covalently bound inhibitor 4-benzamido-4'-isothiocyanostilbene-2,2'-disulfonate (BIDS) has been shown to have low mobility and to lie in a hydrophobic environment within the membrane (1). When bound, a large transport site inhibitor like BIDS projects into the channel and sterically prevents full translocation of the barrier: the resulting incomplete translocation locks the inhibitor into the site and partially exposes the inhibitor to the opposite solution compartment (Figure 5). Thus it is observed (9,1) that the binding of a reversible inhibitor such as 4,4'-dibenzamidostilbene-2,2'-disulfonate (DBDS) begins with rapid binding to a low affinity site (proposed to be binding to the transport site), followed by slow binding to a high affinity site (proposed to be locking of the inhibitor into a place by barrier migration over the site). Such partial translocation between the outward- and inward-facing conformations has, as mentioned above, been observed for the fluorescent inhibitor eosin-5-maleimide (1). It should be

Figure 5

Transport site inhibitors and the hydrophobic barrier model. Shown is the rapid binding of a stilbene disulfonate to the outward-facing transport site, followed by the slow migration of the barrier over the site. The bound inhibitor projects into the channel so that the overlying barrier locks the inhibitor into place, and the barrier can migrate no farther due to steric hindrance by the inhibitor.

## TRANSPORT SITE INHIBITORS



 = DISULFONIC STILBENES,  
PHENYLGLYOXAL

noted that the successful partial translocation of such a large molecule is completely consistent with the idea that the occupied transport site does not itself move during the translocation event.

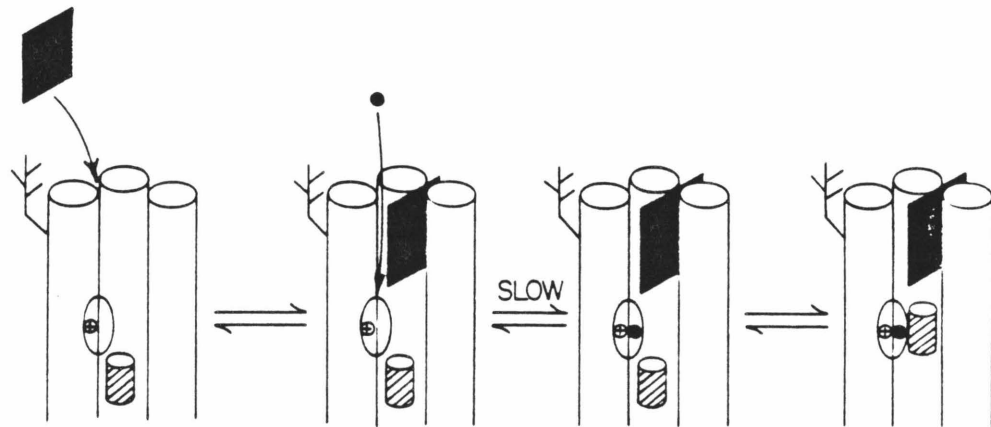
The channel blocking inhibitors are proposed to occupy a site within the channel, thereby slowing the migration of chloride between the site and solution (Figure 6). 1,2-Cyclohexanedione (CHD) eliminates the  $^{35}\text{Cl}^-$  linebroadening due to both the inward- and outward-facing conformations of the transport site (Chapter VII); thus access to the transport site is blocked on both sides of the membrane. This result is consistent with a picture in which a single molecule of inhibitor binds to the channel, such that the inhibitor blocks one mouth of the channel while the hydrophobic barrier blocks the other.

Translocation inhibitors are proposed to bind between two transmembrane helices, thereby altering the packing of the channel-forming helices which in turn cause steric hinderance of barrier migration (Figure 7). In contrast, the transport site and substrate channel are left relatively intact and remain accessible to substrate anion (Chapter VII). Like the transport site inhibitors, the translocation inhibitors contain flat, conjugated ring systems suitable for intercalation between hydrophobic helices. The binding site of the inhibitor need not be close to the point at which barrier migration is hindered, since a change in the helix packing at the binding site will affect the helix packing throughout the channel. Thus the hydrophobic barrier model provides a straightforward explanation for allosteric effects in the band 3 system. In summary,

Figure 6

Channel blockers and the hydrophobic barrier model. Shown is a channel blocking inhibitor that projects into the channel, thereby slowing the exchange of chloride between the transport site and solution. The hydrophobic barrier prevents access to the site from the solution in the opposite compartment, and the barrier cannot fully translocate across the membrane due to steric hindrance by the inhibitor.

## CHANNEL BLOCKERS

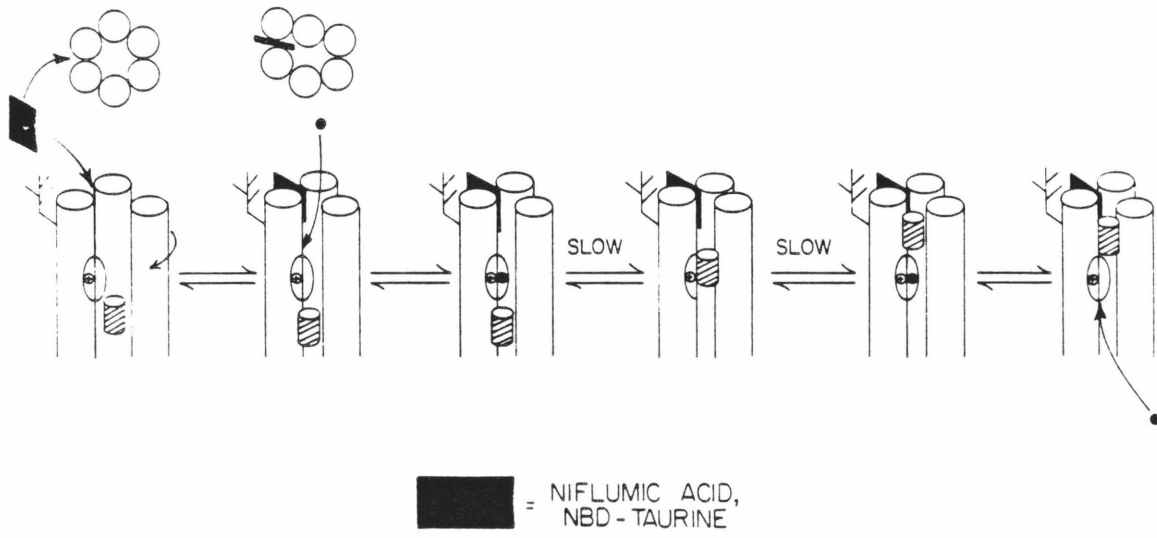


 = DIPYRIDAMOLE,  
1,2-CYCLOHEXANEDIONE

Figure 7

Translocation inhibitors and the hydrophobic barrier model. Shown is a translocation inhibitor that binds to between two of the channel-forming helices, thereby changing the packing of the helices and sterically slowing the migration of the hydrophobic barrier. The barrier can still slowly translocate between its inward- and outward-facing orientations, and anion can still migrate through the channel and bind to the site.

## TRANSLOCATION INHIBITORS



this model is consistent with all of the currently available experimental evidence.

Generalizable implications of the hydrophobic barrier model.

A sliding barrier model could have widespread applicability in transport systems, since such a model can easily explain the transport of both large and small substrates. The model also contains several characteristic features, some of which may be important for ion transport proteins in particular while others may be important for membrane proteins in general. It is proposed that ion transport proteins generally possess: 1) surface charges that increase substrate ion activity near the mouth of the substrate channel, 2) a substrate channel leading from the surface of the protein to the buried transport site so that simple diffusion is able to carry out part of the process of transmembrane translocation, 3) a transport site buried in the hydrophobic interior of the protein where the thermodynamic driving force for lessening of the transport site total charge is strong, and 4) a requirement for the neutralization of the transport site total charge by substrate binding that contributes to substrate specificity. Even more generally, transmembrane  $\alpha$ -helices are common structural components in nearly all current models describing the structure of membrane proteins. Thus it is proposed that membrane proteins typically have substrate and inhibitor binding sites lying between two adjacent helices; as a result, allosteric effects due to changes in helix packing are likely to be widespread in membrane protein systems.

Concluding remarks. It is hoped that the work presented in this thesis 1) sheds light on the ion translocation event in the band 3 system, 2) suggests concepts that may be of general interest in the study of membrane proteins, and 3) stimulates the development of new experiments. My ultimate goal is to further our understanding of biological systems, since an understanding of these systems on a molecular level reveals a combination of complexity and simplicity that can deepen our appreciation of the magic and beauty that constantly surround us.

REFERENCES

1. Macara, I. G. and Cantley, L. C. (1983) Cell Membr. 1, 41-87.
2. Frolich, O. and Gunn, R. E. (1981) Adv. Physiol. Sci. 6, 275-280.
3. Pace, R. J., personal communication.
4. Zaki, L. (1983) Bioch. Biophys. Res. Comm. 110, 616-624.
5. Brock, C. J., Tanner, M. J. A., and Kempf, C. (1983) Bioch. J. 213, 577-586.
6. Eidelman, O. and Cabantchik, Z. I. (1983) J. Membr. Biol. 71, 141-148.
7. Eidelman, O. and Cabantchik, Z. I. (1983) J. Membr. Biol. 71, 149-161.
8. Knauf, P. A. (1979) Curr. Top. Memb. Transp. 12, 249-363.
9. Verkman, A. S., Dix, J. A. and Solomon, A. K. (1983) Gen. Physiol. 81, 421-449.
10. Dalmark, M. and Wieth, J. O. (1972) J. Physiol. 224, 583-610.
11. Pralim, J. (1977) J. Gen. Physiol. 70, 283-306.
12. Lowe, A. G. and Lambert, A. (1973) Biochem. Biophys. Acta 694, 353-374.
13. Lepke, S. and Passow, H. (1971) J. Memb. Biol. 6, 158-182.
14. Schnell, K. F. (1972) Biochem. Biophys. Acta 282, 265-276.